DOCTORAL THESIS

Early Age Autogenous Deformation and Cracking of Cementitious Materials – Implications on Strengthening of Concrete Structures

Katalin Orosz

Structural Engineering

LULEÅ UNIVERSITY OF TECHNOLOGY

LULEÅ
UNIVERSITY
OF TECHNOLOGY

DOCTORAL THESIS

Early Age Autogenous Deformation and Cracking of Cementitious Materials – Implications on Strengthening of Concrete Structures

Katalin Orosz

Luleå University of Technology
Department of Civil, Environmental and Natural Resources Engineering
Division of Structural and Fire Engineering

Printed by Luleå University of Technology, Graphic Production 2017

ISSN 1402-1544
ISBN 978-91-7583-908-0 (print)
ISBN 978-91-7583-909-7 (pdf)

Luleå 2017

www.ltu.se

Academic thesis

For the Degree of Doctor of Philosophy (PhD) in Structural Engineering which, with the permission of the Technical Faculty Board at Luleå University of Technology, will be defended in public on:

Monday, June 19th, 2017, 13:00

in Room F1031 at the Luleå University of Technology.

Opponent:	Prof. Andrzej GARBACZ Warsaw University of Technology, Warsaw, Poland
Examining Committee:	Prof. Mirja ILLIKAINEN University of Oulu, Oulu, Finland
	Prof. Jeanette ORLOWSKY Technical University of Dortmund, Dortmund, Germany
	Prof. Anders ANSELL KTH Royal Institute of Technology, Stockholm, Sweden
Chairman, Principal Supervisor:	Prof. Andrzej CWIRZEN Luleå University of Technology
Assistant Supervisor:	Adj. Prof. Hans HEDLUND Luleå University of Technology and Skanska Sverige AB, Teknik

PREFACE

The PhD project presents results from two distinct research projects. The first one was titled "CFRP retrofitting of Concrete Structures", and was a joint project between the Technical University of Denmark and the Northern research Institute – Norut Narvik – in Narvik, Norway. The second project, "Effects of curing regime on the properties of young concrete", was a recent research project conducted at Luleå University of Technology.

This PhD thesis could not have been written without the support and encouragement I have received from countless people, both professionally and personally. First and foremost, I would like to thank my current principal supervisor, Prof. Andrzej Cwirzen and assistant supervisor, Adj. Prof. Hans Hedlund for guiding me and believing in me sometimes more than I did. Prof. Jan-Erik Jonasson should be credited for convincing me to continue with my young concrete project. Up to the point of my Licentiate thesis, I was carefully guided by Prof. Mats Emborg, Prof. Björn Täljsten, and Assoc. Prof. Thomas Blanksvärd. I am also grateful for the assistance I received while staying at Norut Narvik; in particular, Bård Antsen and Bjørnar Sand. Furthermore, I would like to thank the lab personnel at both universities for all the technical help I received.

A big thank you to all my colleagues and friends at the Division of Structural and Fire Engineering for the fantastic working environment and your continued friendship. Special thanks to Natalie, Mimis, Zsuzs, Magda, Abeer, and Andrea; you know who you are and I am seriously not good with words.

I greatly acknowledge the funding sources provided by the Swedish Road Administration (TRV), the Development Fund of the Swedish Construction Industry (SBUF), Skanska, the Norwegian Research Council, Sto Scandinavia, and the Elsa and Sven Thysell Foundation.

Above all, I'd like to thank my Family.

Katalin Orosz

Luleå, May 2017

SUMMARY

The most urgent need in concrete strengthening and repair works is long-term durability. Shrinkage compatibility between base concrete and strengthening material, and a general understanding of shrinkage mechanisms that serve as a foundation to predict cracking risk are a prerequisite for durable repairs in concrete structures. High performance cementitious materials are particularly prone to early-age shrinkage cracking while the tensile strength of the material is not fully developed yet. On the material side, improved tensile strain capacity of the strengthening material has the potential to mitigate macrocracking, but the material may still remain susceptible to shrinkage cracking. Cracking, beyond the immediate reduction in tensile capacity, increases the permeability of the strengthening or repair layer which may initiate a vicious cycle of cracking – corrosion, or freeze-thaw damage – more cracking – accelerated deterioration – spalling or delamination.

In the current work, first, the strengthening potential of high performance cementitious strengthening materials for concrete has been evaluated experimentally while placing particular focus on their tensile behavior (strengthening effect, tensile strain capacity, strain hardening, cracking pattern) because it is the tensile properties of the material that allow the material to resist (macro-) cracking. The repair potential of emerging new materials such as alkali activated materials (AAM) has also been looked into because they represent a major trend in current material development. However, the understanding and characterization of shrinkage mechanisms, and the prediction of the increased shrinkage cracking potential of high performance materials are severely underresearched. Therefore, in the continuation, autogenous shrinkage behavior of ordinary Portland cement concrete (OPC), Portland Composite cement Concrete (PCC) and alkali activated slag concrete (AASC) undergoing heat curing have been evaluated and modeled, with the intention to contribute to shrinkage and cracking risk predictions for high performance strengthening materials, whose shrinkage behavior has largely been uncharacterized. Focus of interest has been placed on the early age autogenous deformation behavior.

On the material front, the tensile ductility and strain hardening behavior of the strengthening material have been identified as the most important markers for excellent structural performance. Extensive testing of promising materials and material combinations has been performed, with an emphasis on the tensile characterization and cracking of these materials. The second part of the work started out as a standalone project with the aim to adjust a maturity concept based shrinkage prediction model for Portland composite cement concretes. However, in the experiments unsystematically occurring autogenous expansion has been found in both PCC and AASC.

Specific repair mortars have not been tested for shrinkage; however, the large amounts of slag or fly ash incorporated in them, the possible alkali activation, the refined pore structure, the significantly increased percentage of mesopores (particularly in AAM), the lack of internal restraint due to no coarse aggregates present, the larger paste volume, and the effects of possible heat curing all forecast significant issues with the autogenous deformation behavior of these materials. The expansion appears to be triggered by heat curing; however, the temperature gradients causing it are not necessarily large. Swelling has been observed even at ambient temperature in literature. In the experimental data presented here, the expansion in both PCC and AASC is of a magnitude that is non-negligible and has a potential to mitigate part of the shrinkage stresses, but currently cannot be predicted by autogenous shrinkage prediction models.

Keywords: concrete strengthening, strain hardening, microcracking, tensile behavior, shrinkage cracking, autogenous deformation, expansion, swelling, maturity concept

SAMMANFATTNING

Det mest akuta behovet av förstärknings- och reparationsarbeten av betong har att göra med långsiktig beständighet. Krympkompatibilitet mellan basbetong och förstärkningsmaterial och en allmän förståelse av krympningens mekanismer, som utgör grunden för att förutsäga sprickrisker, är en förutsättning för hållbara reparationer av betongkonstruktioner. Högpresterande cementmaterial är särskilt utsatta för krympsprickor vid tidig ålder då materialets draghållfasthet ännu inte är fullt utvecklad. På materialsidan har en förbättrad deformationsförmåga hos förstärkningsmaterialet potential att reducera makrosprickor, men materialet kan fortfarande vara känsligt för krympsprickor. Upprickning orsakar, utöver den omedelbara minskningen av draghållfasthet, en ökning av permeabiliteten hos det förstärkande eller reparerande skiktet som kan initiera en ond cirkel av sprickbildning – korrosion eller skador av frysning och upptining – mer sprickbildning – accelererad nedbrytning – spjälkning eller delaminering.

I det aktuella arbetet har förstärkningspotentialen för högpresterande cementbaserade förstärkningsmaterial utvärderats experimentellt. Fokus har lagts på beteendet i dragriktningen (förstärkningseffekt, töjningsförmåga, töjningshårdnande, sprickbildning), eftersom det är dessa egenskaper som ger materialet förmågan att motstå (makro)sprickbildning. Reparationspotentialen hos nyutvecklade material som alkaliaktiverade material (AAM) har också undersökts eftersom de är viktiga exempel på trender i materialutvecklingen. Emellertid saknas till stor del forskning om förståelse och karaktärisering av mekanismer för krympning och den ökade risken för krympsprickor hos högpresterande material. Följaktligen utvärderas och modelleras i fortsättningen autogena krympningsbeteenden hos vanlig Portlandcementbetong (OPC), Portland kompositcementbetong (PCC) och alkaliaktiverad slaggbetong (AASC), som genomgår värmehärdning. Avsikten är att bidra till krympnings och sprickriskprogoser för högpresterande bindemedel, vars krympningsbeteende i stor utsträckning har varit okategoriserade. Fokus har lagts på det autogena deformationsbeteendet vid tidig ålder.

På materialsidan har töjningsförmågan och de töjningshårdnande egenskaperna hos förstärkningsmaterialet identifierats som de viktigaste markörerna för det strukturella beteendet hos materialet. Omfattande testning av lovande

material och materialkombinationer har utförts, med tonvikt på beteende i dragriktningen och sprickbildning hos dessa material. Den andra delen av arbetet startade som ett fristående projekt med målet att anpassa en mognadsbaserad modell för krympningsberäkning för betonger av portlandkompositcement. I experimenten har emellertid osystematiskt förekommande autogen expansion hittats i både PCC och AASC.

Specifika reparationsbruk har inte testats för krympning. Emellertid kan problem med det autogena deformationsbeteendet förutspås hos dessa material på grund av de stora mängderna slagg eller flygaska som finns i dessa, den möjliga alkaliska aktiveringen, den fina porstrukturen, den signifikant ökade andelen mesoporer (särskilt i AAM), bristen på inre tvång på grund av att grövre ballast saknas, den högre pastavolymen och effekterna av möjlig värmehärdning. Expansionen verkar utlösas av värmehärdning. Emellertid är temperaturgradienterna som orsakar det inte nödvändigtvis stora. I litteraturen har svällning observerats även vid rumstemperatur. I de experimentella data som presenteras här är expansionen för både PCC och AASC av en storlek som inte kan försummas och har en potential att mildra en del av krympspänningarna, men expansionen kan för närvarande inte förutspås av autogena krympningsmodeller.

Nyckelord: betongförstärkning, töjningshårdnande, mikrouppsprickning, dragbeteende, krympsprickor, autogen deformation, expansion, mognadskoncept

CONTENTS

NOTATION AND SYMBOLS

$E_{Lt,}$ E_{Tt} – Young´s modulus of the grid in longintudinal (0°)/transversal (90°) direction; tested value

$f_{Lt,}$ f_{Tt} – ultimate stress in the grid in longitudinal/transversal direction; tested value

$\varepsilon_{Lt,}$ ε_{Tt} – strain at failure in the grid, longitudinal/transversal direction; tested value

$E_{Lm,}$ E_{Tm} – Young´s modulus of the pure carbon fiber in longintudinal/transversal direction; manufacturer-given

$f_{Lm,}$ f_{Tm} – ultimate stress in the pure carbon fiber in longitudinal/transversal direction; manufacturer-given

$\varepsilon_{Lm,}$ ε_{Tm} – strain at failure in the pure carbon fiber, longitudinal/transversal direction; manufacturer-given

E_c – Young's modulus of concrete

f_{cc} – compressive strength of concrete

f_{ct} – tensile strength of concrete

f_y – yield strength of steel

σ_{cc} – first cracking stress of concrete/mortar

σ_{pc} – post-cracking stress of concrete/mortar

ε_{cc} – tensile strain capacity of concrete

ε_{su} – tensile strain capacity of steel

ε_{FRP} – tensile strain capacity of FRP

ε_{tot} – free-, or fully coupled total deformation (AD+TD)

ε_{SH} or AD – autogenous deformation

ε_T or TD – thermal deformation

α or CTE – thermal expansion/contraction coefficient

$\beta_{ST}(T)$ – temperature sensitivity factor, or the "temperature effect on autogenous shrinkage"

$T_c^{max}(t)$ – maximum temperature in the concrete sample up to time "t"

$a_0 \ldots b_2$, T_1, T_2 – fitting parameters in the employed shrinkage model

β_{s0} – relative time development or time distribution of autogenous shrinkage

t_e – equivalent time, maturity, or concrete age

t – time after mixing

t_{start} – start time of autogenous shrinkage specified in real time after mixing
t_{s0} – curvature parameter in the shrinkage model
η_{SH} – curvature parameter in the shrinkage model

ACRONYMS AND SHORT DEFINITIONS

OPC stands for Ordinary Portland cement Concrete – any Concrete made with Type I cement.

SCM refers to supplementary cementitious materials such as fly ash, granulated blast furnace slag, limestone, and silica fume.

PCC, Portland Composite cement Concrete is concrete made with Type II cement. Type II cements use fractions of SCMs or pozzolans to replace part of the clinker. PCC performs better against sulfate or chloride attacks.

AAM is an umbrella term for Alkali Activated Materials; paste, mortar, or concrete that are made by "activating" a wide range of aluminosilicate precursor materials (slag, fly ash, metakaolin etc.) with a strongly alkaline solution to produce a hardened binder, offering a more sustainable alternative to Portland cement binders.

GGBS - ground granulated blast furnace slag

AAS – alkali activated slag, a particular instance of AAM in which the latent hydraulic properties of GGBS are activated with an alkali component

AASC – alkali activated slag concrete

AD or autogenous deformation (contraction or expansion) is the dimensional change of a cementitious material caused by chemical shrinkage in a sealed environment; i.e., without moisture exchange to the environment.

C-S-H: calcium-silicate-hydrate gel in concrete

C-(A)-S-H: calcium aluminosilicate hydrates, or partially aluminum replaced C-S-H gel, similar but not identical to the C-S-H gel observed in OPC/PCC, exhibiting nanocrystallinity. There are differences to C-S-H in terms of, e.g., atomic packing density and porosity.

N-A-S-H: fully polymerized, amorphous gel phase observed in geopolymers. N stands for sodium (Na).

AD swelling – autogenous expansion; a term often used in literature

TD stands for thermal deformation.

CTE, the coefficient of thermal expansion (or contraction) is often used interchangeably with TDC – thermal dilation coefficient in literature

PMM and **PMC** stand for polymer-modified mortar or concrete, often referred to as "polymer concrete"; a cement mortar, or concrete, in which part of the Portland cement has been replaced by polymeric admixtures. These mortars/concretes harden faster than ordinary mixes; they can have significantly higher compressive strength, and modulus of elasticity. Creep is lower and resistance to freezing/thawing cycles is enhanced.

FRP refers to fiber-reinforced polymer. It is a composite material, which consists of a polymeric matrix reinforced with glass-, carbon-, or aramid fibers. For structural engineering applications, the matrix is typically epoxy. **AFRP**, **GFRP**, and **CFRP** denote aramid-, glass-, or carbon fiber-reinforced polymers, respectively.

AR-glass: alkali-resistant glass (fiber, or textile)

PVA, polyvinyl-alcohol fibers are high-performance reinforcement fibers for concrete and mortar. They are unique in their ability to create a molecular (hydrogen) bond with cement during hydration.

FRC and **FRM** are general terms describing different types of fiber-reinforced concrete, and fiber-reinforced mortar. The short, discrete, and randomly oriented fibers increase the structural integrity. Fibers include steel, glass, synthetic, and natural fibers, among others.

TRM and **TRC** refer to textile-reinforced mortar, or concrete. The "textile" is typically alkali-resistant glass, or carbon textile, aligned in the direction of the principal stresses for maximum efficiency. The textile is only partially penetrated by the mortar phase. Technically, it is more correct to use the term "mortar" rather than "concrete", because in TRC there are no coarse aggregates. The maximum grain size is normally 1mm or less.

MBC refers to mineral-based composite. It consists of a polymer-modified mortar phase (binder) and a stiff CFRP grid (reinforcement). The surface of the concrete structure is first roughened by sandblasting or other means, such as jackhammers, grinding, hydro-jet blasting, needle gunning. Then, a surface primer is applied on the roughened surface to reduce moisture transport from the polymer-modified mortar to the base concrete. This is followed by the application of the first layer of mortar. A CFRP grid is placed on the mortar and covered by a second layer of mortar.

SFRC, steel fiber-reinforced concrete is the most commonly used fiber-reinforced concrete. Steel fibers are added to enhance tensile strength, first cracking strength, toughness, and energy absorption capacity. After first cracking, it exhibits tension-softening behaviour, i.e., a decaying load capacity.

Strain hardening, or "plastic hardening" is the contribution of a cementitious matrix to the load-deformation response of a structural member. It is more accurate to refer to the mechanism as *pseudo strain hardening*, differentiating it from the "real" strain hardening observed in metals. The pseudo strain-hardening behaviour in SHCCs is achieved by the sequential development of matrix multiple cracking. In metals however, it is based on dislocation micromechanics in the plastic deformation regime.

HPFRCC denotes high-performance fiber-reinforced cementitious composite. HPFRCCs exhibit excellent overall "high performance" tensile behaviour. Since the term is too general, HPFRCCs have been renamed to SHCC (strain-hardening cementitious composite) lately. Their distinctive feature of is the high ultimate tensile strain capacity up to 6%. This *pseudo*-ductility is achieved by the sequential multiple cracking of the matrix while undergoing strain-hardening behaviour after first cracking.

ECC, engineered cementitious composite, is a major subclass of SHCC. The design principle ECCs is based on micromechanics and fracture mechanics. ECC uses randomly oriented, short (8-12mm) polymeric fibers (typically, PVA, or polypropylene) in low amounts (less than 2 vol. %), or in certain cases, hybrid fibers, and high volumes of fly ash. It can be tailored to suit particular structural needs (low shrinkage mixes, high early age strength, etc.), or application methods (sprayable). **PVA-ECC** is the most typical form of ECC. It contains PVA fibers up to 2 vol. %. **R-ECC** refers to an ECC member with internal steel reinforcement (bars or welded grids). **TR-ECC** stands for textile-reinforced ECC. The textile is similar to that in textile-reinforced concrete.

WST, wedge-splitting test, is a well-established test method to perform stable fracture mechanics tests on brittle or quasi-brittle materials. Compared to a uniaxial tensile test, WST also provides information on the softening part of the load-deformation curve after peak load. It does not ensure a uniform tensile stress field since there is bending in the specimen.

COD stands for crack opening displacement; here specifically in the wedge-splitting test. In the WST (above), a specimen with a starter slit on top is being split into two halves, by means of a rigid steel wedge that is pressed down vertically. The COD is the opening of the crack, measured at the top of the starter slit.

LIST OF TABLES AND FIGURES

Figures

Tables

1 INTRODUCTION

1.1 Background and motivation

Much of the built environment consists of concrete, which is the single most widely used construction material. With the volume of buildings and infrastructure built from concrete worldwide, in recent years, there has been a great deal of research aimed at improving the durability of concrete structures.

It is well-known that concrete is a brittle material which results in cracking when the tensile stresses exceed the tensile strength of the material, which is generally only about 10% of the compressive strength. ***Cracking in concrete*** can be a consequence of shrinkage, thermal contraction, large differential temperatures within the concrete body, external or internal restraints, too large deformations, or applied loads. One of the most common reasons for cracking is *shrinkage*. Concrete is particularly prone to cracking at a very young age. Early-age cracking due to shrinkage (Figure 1-1) can present a significant problem in concrete because the tensile strength of the material is still developing while volume changes are already taking place due to the combined effect of heat of hydration, the binder hydrating, and the outer surfaces drying out. Restrained volume changes in concrete will drive tensile stress development.

Figure 1-1: Plastic shrinkage cracking of concrete (concretenetwork.com)

Beyond it being unsightly, the cracking of concrete may severely affect the durability performance and service life of structures since it contributes to the corrosion of the reinforcement, it aggravates freeze-thaw cycles resulting in quick deterioration, and facilitates alkali-aggregate reactivity. Severe cracking often calls for costly measures to fix. As a result, research aiming at the prevention of shrinkage cracking and predicting early-age cracking risk has been on the rise (Holt 2001, Yuan and Wan 2002, Bentur and Kovler 2003, Holt and Leivo 2004, Cusson and Hoogeveen 2008, Tongaroonsri 2009).

One way to restore damaged or deteriorated concrete to extend its service life is ***repairing*** it by a casting a bonded overlay on top. This involves removal of the damaged top layer of the concrete and replacing it with a new repair layer. A similar technique to this is often used for ***strengthening*** concrete structures (Figure 1-2) in cases when the load capacity needs to be increased due to increased demands, unexpected loading conditions (blast explosions, earthquakes), or changes in utilization. Steel fiber reinforced concrete, textile reinforced concrete (TRC), high performance concrete (HPC) or specific, tailored repair materials are often used for this purpose. Cementitious binders can also be used in combination with a fiber reinforced polymer (FRP) component. Such strengthening systems are applied on the roughened concrete substrate in a several mm thick layer where the FRP component is embedded into the strengthening mortar (Blanksvärd 2007, 2009, Täljsten and Blanksvärd 2007, Blanksvärd et al. 2008).

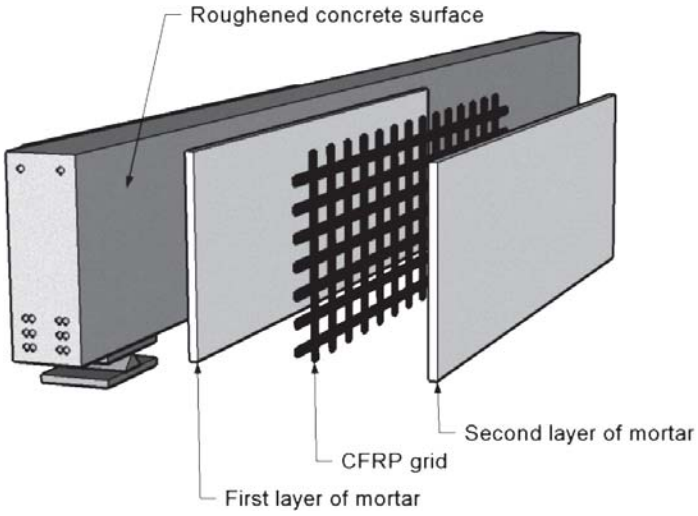

Figure 1-2: Shear strengthening of a concrete beam (Blanksvärd et al. 2009)

The most urgent need in concrete strengthening and repair works is ***long-term durability*** (Bentz et al. 2015). The success of such an overlay type strengthening system hinges on good ***compatibility*** with the base concrete, in terms of elastic moduli, bond strength, diffusion properties, chemical compatibility, thermal expansion coefficients, etc. (Vaysburd et al. 2014, Courard et al. 2015), the ***integrity*** of the old substrate, proper surface preparation, and moisture saturation levels (Garbacz et al. 2013, Bissonnette et al. 2014).

As (Vaysburd et al. 2014) suggest, an ideal way to approach concrete repairs is to think in terms of a three-phase system (Figure 1-3). The long-term durability will depend on the properties of both the substrate and the repair material, and the transition phase (interface) between the two.

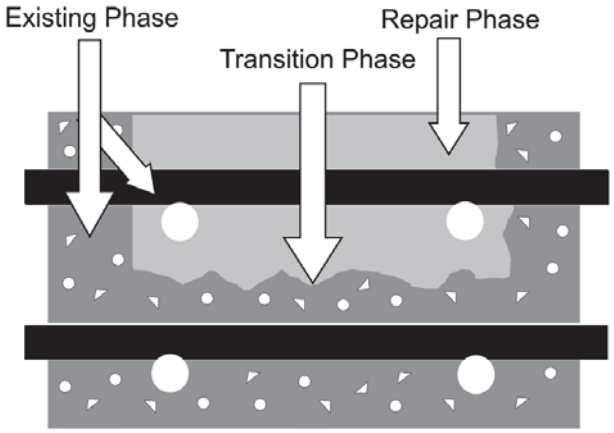

Figure 1-3: Three phase system, a prerequisite for monolithic action in concrete repairs (Vaysburd et al. 2014)

Incompatibility between the base concrete and the strengthening/repair material can ruin the system, resulting in debonding or spalling especially if the load is applied parallel to the bond line. One particularly important aspect of compatibility is shrinkage compatibility because restrained shrinkage develops in the relatively large paste of the repair mortar volume, due to the absence of coarse aggregates. The newly cast repair or strengthening layer has a tendency to shrink at a high rate, while the base concrete acts as a rigid foundation that restrains these movements. The differential movements cause tensile stresses in the repair- or strengthening material and compressive stresses in the base concrete (Figure 1-4) that may cause the repair layer to crack; in the worst case, already in the pre-loaded state, rendering it useless as a strengthening material, and prone to degradation. If

stresses continue to accumulate as the shrinkage builds up and the tensile strength or the interfacial bond strength is exceeded, interface delamination between the repair material and the base concrete occurs.

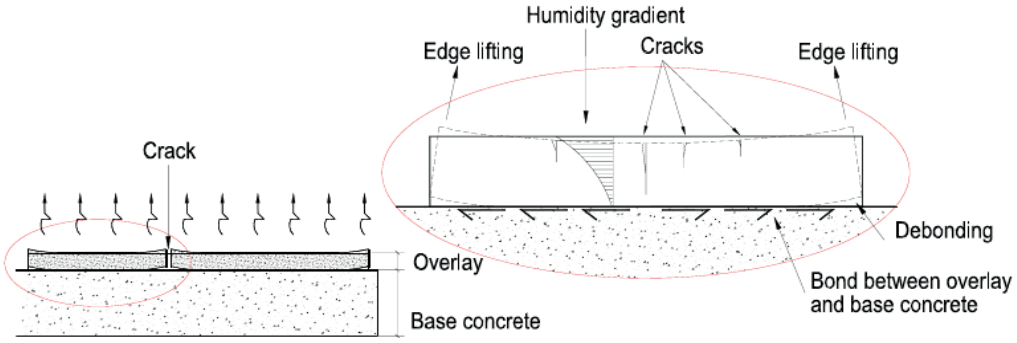

Figure 1-4: Critical effects of shrinkage for bonded overlays, inducing cracks and edge-lifting (Blanksvärd 2009)

Generally speaking, ***shrinkage incompatibility*** is more associated with cement based mortars, since shrinkage happens in the cement phase, while the polymer modified mortars show better compatibility, and epoxy resin mortars (that consist of a resin, a hardener, and aggregates) have shown to have the best shrinkage compatibility with the base concrete (Hassan et al. 2001).

Yet, the quantification and, particularly, the ***prediction of the development of shrinkage***, and/or ***evaluating cracking risk*** in high performance repair mortars appears to be a major gap in research; with shrinkage data rarely available, and most often limited to drying shrinkage. In some high performance repair materials, there are certain ways to reduce, or mitigate some of the shrinkage. These include shrinkage reducing admixtures (SRA), internal curing by means of lightweight aggregates (LWA), or the use of chopped fibers. Fibers are added to achieve better mechanical performance, with shrinkage- and cracking reduction being a favorable side effect. Several of the best performing repair mortars incorporate short, chopped fibers (polyvinyl alcohol, or sometimes, polyethylene) which are added in order to enhance the *tensile strain capacity* and force the material to exhibit tensile strain hardening accompanied by multiple cracking with controlled, tight crack widths (Li et al. 2000, Wang and Li 2005, Li 2008, Sahmaran and Li 2010, Maalej 2012).

Materials with enhanced *deformation capacity* can resist shrinkage cracking: while they may develop numerous, very fine cracks, the crack widths are very tight; from a durability point of view, cracked engineered cementitious composites

(ECC) can still be treated as uncracked (Weimann and Li 2003). In a newly developed ECC mix with a tensile strain capacity of 2.5%, the measured drying shrinkage strain at 28 days was only 110-240 microstrains (less than 10% of the tensile strain capacity), while in traditional ECCs the 28-day drying shrinkage is around 1200 microstrains (Zhang et al. 2009). However, the required consistency and workability suitable for repair work require the use of large amounts of SCMs and different types of chemical admixtures (plasticizers, shrinkage reducing admixtures, retarders etc.) that are all known to influence the developing pore structure and make the shrinkage behavior more complex. Emerging new, clinker-free materials that are being evaluated with regard to their strengthening material potential (Torgal et al. 2015), such as alkali activated materials (AAM), where cement has been replaced by slag, fly ash, or metakaolin and the pozzolanic properties have been "activated" by a highly alkaline chemical activator solution, have likely very ***complex shrinkage behavior*** (Bernal and Provis 2014, Lee et al. 2014) due to microstructure and differences in the hydration processes and -products when compared to ordinary Portland cement binders.

Shrinkage can be divided into plastic-, chemical-, autogenous-, drying-, and carbonation shrinkage. Plastic shrinkage occurs in the fresh state, before the solid skeleton has been formed, and is highly dependent on the evaporation rate. Carbonation shrinkage is associated with calcium hydroxide ($Ca(OH)_2$) conversion into denser calcium carbonate ($CaCO_3$) after exposure to carbon dioxide present in the atmosphere. Drying shrinkage makes up the bulk of the total shrinkage, in normal strength concretes, and mortars. The main factors that influence drying shrinkage are the age at the beginning of drying, the relative humidity of the environment (that influences the rate of evaporation), and specimen size. ***Autogenous shrinkage*** is the dimensional change of a cementitious material caused by chemical shrinkage (Figure 1-5) in a sealed environment; i.e., without moisture exchange with the surroundings. Autogenous shrinkage is associated with internal water loss (self-desiccation) accompanying the hydration of the binder and it has generally been regarded as "insignificant" for ordinary concretes where the drying shrinkage plays the dominant role. However, it has shown to be a concern in high-strength, or high-performance concretes with a relatively low water-to-cement ratio.

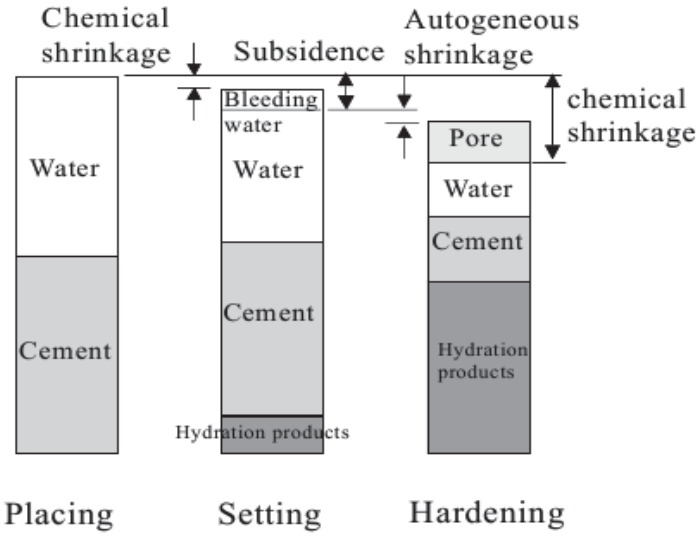

Figure 1-5: Definition of autogenous shrinkage (Tazawa et al. 2000, Mihashi and Leite 2004)

Shrinkage behavior that is fundamentally understood and predictable is essential to predicting and reducing cracking risk in concrete. Furthermore, as stated before, shrinkage compatibility (which assumes understanding of the shrinkage behavior of the overlay material) is a prerequisite to durable repairs and successful strengthening work. Finally, it is easy to see that an ideal strengthening/repair material needs to be "crack free" in its preloaded state. Crack free means that the shrinkage mechanisms have been understood and the material has been optimized to exhibit controlled shrinkage.

1.2 Aim, objectives, and research questions

The overall aim of the current PhD work has been twofold. First, the strengthening effect of an array of *cementitious systems* suitable for ***repair purposes*** is investigated, with particular attention to tensile strength- and strain capacity to create a robust and durable repair. Shrinkage performance, which is a prerequisite to good compatibility with the base substrate was not looked into directly, but identified as a research gap that needs to be addressed.

Second, the work aims to expand the basic understanding and knowledge on the ***early-age shrinkage deformation behavior*** of cementitious materials, ranging from *ordinary and composite Portland cement concretes* (OPC/PCC) to clicker-free

alkali-activated slag (AAS), in the hope that part of the findings (shrinkage mechanisms and their significance) can be generalized and extended to repair mortars that incorporate the same materials but in larger fractions and with larger paste volume. Only autogenous shrinkage is being focused on. The materials tested are partly determined by the project limitations (OPC/PCC), and partly chosen due to the recent shifting interest in the research of strengthening- and repair materials towards more sustainable, environmentally friendly solutions (alkali activated materials).

The following objectives have been set:

a) Characterize the strengthening effect and tensile behavior of a number of selected cementitious strengthening systems to create a high performance repair.

b) Contribute to a "database" of shrinkage data by performing extensive testing under specific, frequently occurring curing conditions that have been identified as relevant and not properly understood (variable heat curing).

c) Incorporate the effect of variable temperature heat curing into maturity concept-based shrinkage models for early age cracking risk prediction. If possible, generalize this model to cover mortars.

The following research questions have been identified:

RQ1. What materials are most suitable for strengthening concrete structures with bonded cementitious overlays for optimum structural performance?

RQ2. How does the ductility of the mortar influence the strength, strain capacity, and cracking behavior of the overlay? What are the impacts of the material choice on durability?

RQ3. How does temperature curing influence the development of autogenous shrinkage and the cracking risk in cementitious materials (OPC and AAS)? What are possible implications on durability and performance of strengthening systems based on Portland cement?

RQ4. Are maturity concept-based models suitable to predict autogenous deformation in cementitious materials? Could these models be used to predict cracking risk of repair systems based on Portland cement?

1.3 Scientific approach

The first major section of the thesis is a critical state-of-the-art report. The information has been structured in a comprehensive way, which led to finding gaps in the current understanding worth to look into. In the next step, the research questions were formulated, and an experimental program was built up around them.

The objectives were, to a large extent, approached experimentally, providing an extensive experimental test program which has been performed during the current work. As part of the experimental program focused on tensile (and, to a minor extent, fracture) characterization of repair systems with particular interest in the post-peak behavior, two different test setups had to be developed (adapted); a direct tensile test on dogbone-shaped samples and a wedge-splitting test. Shrinkage tests were performed independently in the framework of a separate project. The shrinkage modeling served as evaluation of the experimentally obtained data on OPC.

1.4 Limitations

1.4.1 Strengthening

In the two papers relevant for strengthening, typical – commercial – ***strengthening mortars*** and an ***ECC*** mix were tested. The testing was geared mainly at the performance as repair material in terms of load- and deformation capacity. The focus was placed on tensile behavior (strength, and deformation capacity) because the tensile properties are the set of parameters that characterize the ability of the material to withstand cracking, or prevent a crack from opening by bridging it. Dynamic loading, fatigue, freeze-thaw performance etc. were not covered. Shrinkage was covered, but at the time of writing, only on the state-of-the-art level; mainly identified as a gap in current (2013) understanding.

1.4.2 Shrinkage behavior

No shrinkage tests on repair mortars have been performed. The shrinkage tests that are included in the thesis were performed as part of another, separate project focusing on autogenous shrinkage in ***PCC***. The tests were then complimented with ***alkali activated slag***. The alkali activated materials of choice, for the shrinkage testing, were slag-based instead of fly ash. The AAS mixes were not developed by the author; instead, they were provided by a colleague at LTU. They have not been optimized for either shrinkage performance or strengthening purposes. This limitation was imposed by the project proposals – the work has been performed within the framework of two separate projects - and financial limitations. State-of-the-art knowledge on how the results obtained for concrete may or may not translate into mortar behavior has been discussed.

Drying, plastic, and carbonation shrinkage are beyond the scope of the current work. Research has been limited to autogenous deformation. Deformation measurement started at the earliest possible stage when the concrete could be demolded. This largely removed autogenous strain before setting time. If the concrete body is unrestrained, then (chemical) shrinkage before setting does not generate stresses and hence, does not contribute to the cracking risk.

Stress and strain development in hardening concrete is volume dependent. Heat development and heat generated stresses in mass concrete structures are more prominent. The heat gradient towards an outer surface also causes differential autogenous shrinkage across the mass concrete. The applicability of the findings is therefore limited to relatively thin structures, such as slabs, or concrete overlays; *potentially* to strengthening or repair overlays.

1.5 Structure of the thesis

The thesis is written in the format of an article thesis in which printed or reprinted journal papers are appended to a concise summary of the entire PhD work. The summary consists of Chapters 1 – 7.

Chapter 1 serves as a general introduction. It clarifies the objective, hypothesis, and research questions.

Chapter 2 aims to summarize previous work done on the research subject in a critical and concise manner.

Chapter 3 introduces the autogenous shrinkage model employed.

Chapter 4 presents an overview of the experimental program.

Chapter 5 summarizes the most important results from the experiments in a condensed format, followed by the analysis of the data.

Chapter 6 relates the findings of the current work to the aim of the research. It revisits and answers the research questions.

Chapter 7 concludes with recommendations for future research.

Chapter 8 lists all references.

1.6 Appended papers

Two papers have been selected from the Licentiate thesis, from the field of strengthening of concrete with externally bonded, cementitious strengthening systems. Furthermore, three papers are included to summarize the research carried out in the second half of the PhD studies, following the Licentiate thesis.

Paper One

Orosz K, Blanksvärd T, Täljsten B and Fischer G (2010) From material level to structural use of mineral-based composites—an overview. Advances in Civil Engineering Vol. 2010, Article ID 985843.

The paper presents an overview of materials and techniques for strengthening of concrete structures by means of externally bonded cementitious strengthening systems, from material level (interfacial bond, strain hardening, multiple cracking) to structural applications (full scale tests).

My contribution to the paper was planning the paper, writing the majority of the state-of-the-art part, performing and evaluating the uniaxial tensile- and wedge splitting tests, and writing the relevant parts of the paper.

Paper Two

Orosz K, Blanksvärd T, Täljsten B and Fischer G (2013) Crack development and deformation behaviour of CFRP-reinforced mortars. Nordic Concrete Research Vol. 48, 49–69.

Direct tensile testing on dogbone-shaped carbon fiber grid-reinforced mortars has been carried out with ultimate load capacity, crack patterns, deformation behavior, and ductility evaluated. The influence of the matrix ductility and strain-hardening quality on shifting the failure mode from brittle to "ductile" has been one of the most important conclusions drawn.

My contribution was performing and evaluating the tests, and writing the majority of the paper.

Paper Three

Orosz K, Hedlund H, and Cwirzen A. (2017) Effects of variable curing temperatures on autogenous deformation of blended cement concretes. Accepted for publication to the Journal of Construction & Building Materials.

Early-age concrete shrinkage tests have been performed on blended Portland cement based samples subjected to variable curing temperatures. The effects of the imposed temperature history on the autogenous deformation have been investigated.

My contribution was performing and evaluating the tests, and writing the paper.

Paper Four

Orosz K, Hedlund H, and Cwirzen A. (2017) Maturity concept vs. prediction of autogenous deformations. Submitted for publication to the Materials and Structures.

The study focuses on the applicability of a commonly used, maturity concept-based shrinkage model, developed for CEM I type binder to predict autogenous deformations of blended cement, CEM II type concretes.

I contributed with testing, analyzing the test results, modeling, and writing the paper.

Paper Five

Orosz K, Humad A, and Cwirzen A. (2017) Early-age autogenous deformation of heat-cured alkali activated blast furnace slag. Submitted for publication to the Journal of Advanced Concrete Technology.

Autogenous deformations developing in heat cured alkali activated slag (AAS) has been compared to the behavior of composite Portland Cement (CEM II) mixes.

My contributions were performing the shrinkage testing, evaluating the shrinkage results, evaluating the XRD tests together with the co-authors, and writing the paper.

1.7 Additional publications

Täljsten B, **Orosz K** and Blanksvärd T (2006) Strengthening of Concrete Beams in Shear with Mineral Based Composites – Laboratory tests and theory. In: Third International Conference on FRP Composites in Civil Engineering. Miami, USA.

Orosz K, Täljsten B and Fischer G (2007) CFRP strengthening with mineral based composites loaded in shear. In: Proceedings of the 8th International Symposium on Fiber Reinforced Polymer Reinforcement for Concrete Structures (FRPRCS-8). Patras, Greece.

Täljsten B, **Orosz K** and Fischer G (2007) Crack development in CFRP reinforced mortar - An experimental study. In: The First Asia-Pacific Conference on FRP in Structures. Hong Kong, China.

Orosz K (2013) Tensile behaviour of mineral-based composites. Luleå University of Technology, Department of Civil, Environmental and Natural Resources Engineering. *Licentiate Thesis.*

Orosz K, Fjellström P, Jonasson J-E, Emborg M and Hedlund H (2014) Evaluation of the Linear Logarithmic Creep Model. Nordic Concrete Research: Proceedings of the XXII Nordic Concrete Research Symposium. 50, 417–420.

Orosz K, Fjellström P, Jonasson J-E, Emborg M and Hedlund H (2014) Evaluation of Thermal Dilation and Autogenous Shrinkage at Sealed Conditions. Nordic Concrete Research: Proceedings of the XXII Nordic Concrete Research Symposia. 50, 299–302.

Orosz K (2014) Strengthening of Concrete with Carbon Fibre Reinforced Polymer (CFRP) Grids Bonded by Cementitious Binders. Nordic Concrete Research: Proceedings of the XXII Nordic Concrete Research Symposia. 50, 207–210.

2 STATE OF THE ART

2.1 Cracking and deterioration of Portland cement based systems

Over the last few decades, many advances in concrete technology have been made in order to comply with the ever increasing demands in terms of material performance. High performance concrete (HPC), ultra high performance concrete (UHPC); and many other high performance cementitious materials have been developed, offering improvements in compressive strength and higher strength-to-weight ratio. Despite their advantages, high performance concretes and mortars have been shown to be more susceptible to cracking, in particular, at early ages. While cracks may develop for a variety of reasons, the underlying reason is the inherently low tensile strength. Furthermore, when the material is very young, its tensile strength is not fully developed yet, while relatively large volume changes compared to ordinary Portland cement concrete are taking place due to shrinkage mechanisms.

Shrinkage induced cracking is of increasing concern because it can severely decrease concrete service life. A cracked structure is susceptible to chloride- and carbonation induced corrosion. Repeated freeze-thaw cycles with the water expanding in the cracks can contribute to rapid deterioration, such as surface scaling (Figure 2-1) of the concrete cover; e.g., (Control of Cracking in Concrete - State of the Art, 2006), especially in combination with aggressive environment (deicing salts, sulfates, etc.).

Figure 2-1: Surface scaling of concrete

Shrinkage is related to moisture loss to either evaporation, referred to as plastic shrinkage (before setting), drying shrinkage (after setting), or the hydration of the binder which generates autogenous shrinkage. Cracking in concrete can be a consequence of any of these or a combination of them, taking place in either the plastic/fresh or the hardened state. High autogenous shrinkage and restrained thermal deformations render a structure particularly susceptible to early age cracking.

Shrinkage takes place in two distinct stages. The definition of *early age* cracking varies depending on the purpose of the study; some authors define it as the first 24 hours after casting, e.g. (Holt 2001) while others use the term early age for up to a month (Yoshitake et al. 2012); followed by long-term shrinkage. For the purpose in this thesis, early age is defined as concrete that is no more than two weeks old.

During early age cracking, first internal microcracks form on the aggregate – mortar interface due to shrinkage stresses, which may extend and combine into macrocracks. Early-age shrinkage cracking can progress into damage accumulation across the entire structure (Li and Wang 2017).

2.2 Cracking of repair overlays and possible implications on durability

Cracking in a structural element, for obvious reasons (material discontinuity, softening), reduces the load capacity. Furthermore, a cracked surface layer allows water and other corrosives (chemicals, salts) to penetrate into the structure, eventually leading to reinforcement corrosion. Increased permeability leads to further corrosion and deterioration in a chain reaction-like manner; (Wang et al. 1997). The effects of cracking in an overlay type repair are magnified because there is a larger cracking potential due to a relatively large surface exposed to drying out, while simultaneously a repair layer is often thin enough to stop functioning as a barrier to environmental damage if cracked. For a durable repair, it is recommended to limit the cracking of the surface layer to within a threshold of 50-100 μm (Wang et al. 1997, Wang and Li 2005, Umbreen-Us-Sahar 2015) to keep the permeability low. From a durability point of view, certain repair materials, such as cracked engineered cementitious composites (ECC) can still be treated as uncracked (Weimann and Li 2003) even when fully cracked because of their

extremely tight crack widths. Crack widths as tight as 60 μm have been reported under uniaxial tensile load by (Sahmaran et al. 2009). The typical crack widths of ECC at crack saturation (fully microcracked, before localization) are around 80 μm (Li et al. 2002, Zhang and Leng 2008).

Direct correlation has been observed between material brittleness and shrinkage in alkali activated slag mortars by (Duran Atics et al. 2009). It is assumed that the higher shrinkage leads to significant microcracking in the matrix. The formation of cracks, if the crack widths are not kept controlled, leads to increased permeability and quick deterioration of the material. In contrast, in PVA-reinforced fly ash-based geopolymers, crack widths nearly as tight as in ECC, ranging from 70-120 μm (loaded) have been reported by, e.g., (Nematollahi et al. 2015a).

2.3 Cementitious overlay strengthening systems

2.3.1 Materials

The following section is mostly a condensed extract from the Licentiate thesis published in 2013, where strengthening systems have been looked into and compared in great detail. The information presented here is selective to the context defined by the Introduction.

Strengthening systems for concrete that employ inorganic, cementitious binders can consist either of a standalone matrix, often reinforced with short fibers, or an FRP (fiber reinforced polymer) component embedded into a cementitious matrix. An example to the first one is ***engineered cementitious composites*** (ECC) which is a micromechanically tailored (Li et al. 2001, Wang and Li 2003, Zhou 2011) fine-grained mortar with flowable consistency, intended both as standalone material and for durable repairs in situations where the deformation capacity (tensile ductility) and/or tensile strain hardening behavior are important. The *tensile strain hardening behavior* (Figure 2-2) is accompanied by very fine microcracking throughout the matrix. Up to 2%, oiled PVA fibers are responsible for the strain capacity. Oiling is necessary to lessen the interfacial bond between fibers and matrix so that a pullout response take place instead of fiber breakage – PVA has a low modulus of elasticity. The tensile strain capacity can clearly been linked to a reduction in shrinkage cracking. Since the strain capacity of a typical ECC is in the 3-6% range, it appears reasonable to prioritize ECC as a repair layer because it is able to accommodate shrinkage deformations by forming very fine, multiple cracks

without localized failure. This was illustrated by (Li and Li 2011) on high early strength ECC which had a total shrinkage strain of less than 300 με, significantly lower than its tensile strain capacity of 3-6%. Furthermore, the fracture toughness of the matrix is also tailored. Too high fracture toughness can adversely affect the strain hardening behavior and tensile ductility since high fracture toughness means that significantly more energy is necessary for new cracks to propagate, which works against the sequential microcracking of the matrix.

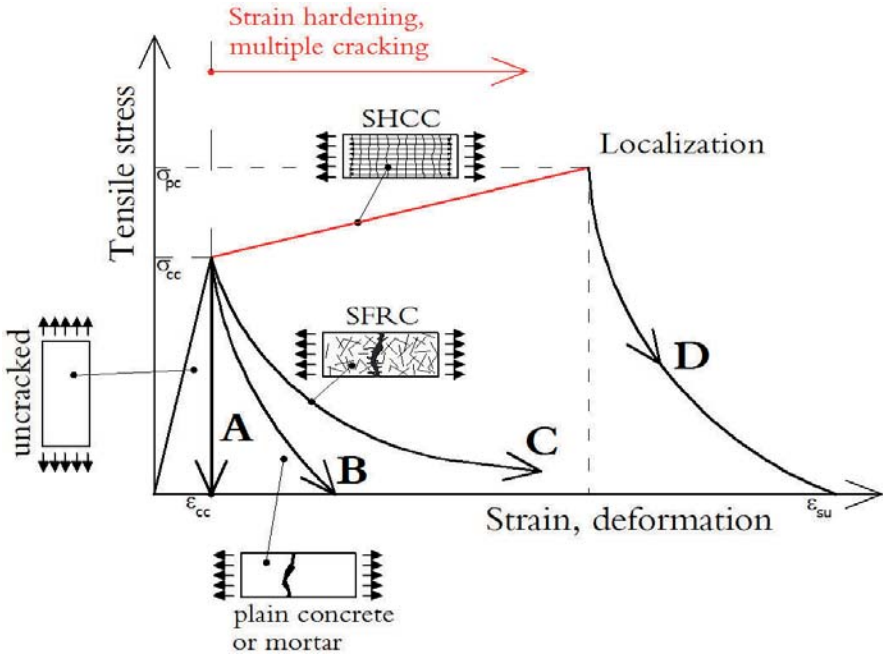

Figure 2-2: Definition of (A) brittle- [glass], (B) quasibrittle- [concrete and conventional mortars], (C) strain softening- [steel fiber reinforced concrete], and (D) strain hardening behavior [strain hardening cementitious composites] under tensile load (Fischer and Li 2002, Matsumoto and Mihashi 2003)

ECCs use very high fractions of cement per volume. In recent years, considerable amount of efforts have been made to lower the CO2 emission that is associated with cement production. Environmentally friendly alternatives that do not compromise the strain hardening behavior and tensile ductility of ECCs are desirable. Partial replacement of cement by SCMs has resulted in "green ECC" (Yang 2008). The most recent research has been increasingly focusing on replacing cement entirely, without compromising the high performance nature of ECC. Recently, strain-hardening fly ash-based ***geopolymers*** have been developed (Shaikh 2013b, Ohno and Li 2014, Nematollahi et al. 2015a, 2015b, 2016, 2017, Choi et

al. 2016, Shaikh and Zammar 2017) that use a fraction of chopped polymeric fibers comparable to that in ECC (up to 2% by volume). These new materials exhibit tensile strain capacity similar to that of ECC. However, other properties are either not practical or optimized yet (low to moderate compressive strength) or not well investigated/understood (durability). These studies, however, did not investigate either the applicability of these new composites for strengthening/repair purposes or the shrinkage behavior; instead, all are strictly focused on material characterization (compressive/tensile strength, tensile strain hardening, deflection hardening, and microcracking). Yet, these materials hold a promise as strengthening materials: as (Li et al. 2000, 2000) emphasized, the ductility of a material can be identified as one of the most important parameters that translate into actual structural performance. This statement could be extended into strengthening applications because the ductility of the strengthening material would prevent unpredictable, sudden failure. Additionally, it renders the repair/strengthening more durable and sustainable by keeping tight crack widths.

An example to the second approach is ***textile reinforced concrete*** (TRC), which comprises of a very fine-grained, optimized, often polymer-modified matrix and one or more directed layers of technical fabric or textile (Häußler-Combe et al. 2004). The textile filaments are aligned to the direction of the tensile stresses. Usually high-modulus FRP (AR-glass, PBO, or carbon) is used for reinforcement. Low modulus fibers can also be used, such as polyethylene. Despite the fiber choice, similarly to ECC, TRC exhibits tensile strain hardening (Colombo et al. 2012). Mix designs with partial replacement of cement by silica fume or fly ash exhibit better bond strength between the textile and the binder because of the denser microstructure (Mobasher et al. 2004). The matrix is able to penetrate the textiles to some extent, and since there is no textiles are not impregnated but consist of individual filaments, the degree of penetration is a major influencing parameter determining the strength of the TRC system as the load transfer relies on the fiber surface in contact with the cement phase (Jesse et al. 2008, Contamine et al. 2010).

ECC has also been combined with technical textiles or fabrics, and stiff carbon grids. A hybrid carbon-glass textile was used by (Dai et al. 2009) where the ECC matrix provided ductile behavior, despite the textile being brittle, due to the matrix being able to redistribute stresses and compensate for fiber breakage. Another strengthening system, in the past often referred to as ***mineral based***

composites (MBC) employs a polymer-modified mortar and a stiff carbon fiber grid (Blanksvärd 2007, 2009). Both components being quasibrittle, the resulting system if an efficient and proven strengthening system, however, failure is sudden, often accompanied by spalling of the strengthening layer.

Figure 2-3 presents one particular way of grouping cementitious materials, to map possible base substrate- and strengthening material combinations. The conventional approach focuses predominantly on material strength (compressive strength). The greater the *ductility* of the strengthening material, the greater its stress-bridging ability is. Ideal repair materials would, therefore, appear in the top half – top right corner of Figure 2-3. The reasoning is that minimizing the repair layer cracking (which is achieved by the increased ductility) would likely correlate with a lessened risk of interfacial delamination on the surface between the old concrete and the new layer.

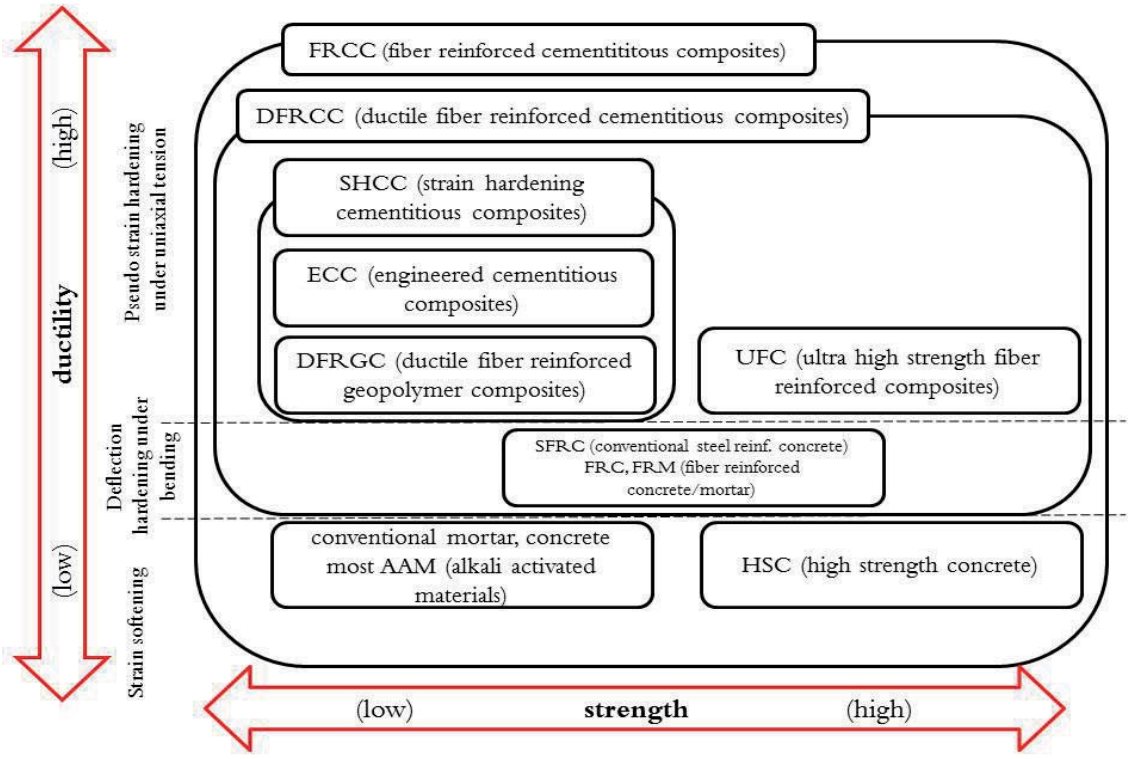

Figure 2-3: Classification of cementitious materials based on their ductility and strength. Based on (Matsumoto and Mihashi 2003, Rokugo et al. 2009), expanded by the author

2.3.2 Bond strength

As stated before, the success of strengthening hinges on the bond strength on the interface between the concrete substrate and the strengthening layer. Other possible failure modes, such as slippage in the plane of the technical fabric embedded in the mortar phase are not discussed here further; however, they have been elaborated on in the Licentiate thesis and in Paper 1.

Bond to the concrete surface is usually enhanced by means of surface roughening and applying a primer (bond coating). As long as the base substrate and the strengthening layer form a monolithic unit, the deformations remain compatible. If the autogenous and drying shrinkage of the high performance matrix are excessive, this leads to shrinkage severely restrained by the old concrete substrate which can lead to cracking in the strengthening layer. In extreme cases, bond can fail on the interface and the strengthening layer may debond from the surface; in particular if the concrete surface is weak, which is common in deteriorated structures.

Debonding has occurred in alkali activated slag mixes where the apparent incompatibility can sometimes be unrelated to shrinkage properties. Shrinkage compatibility is just one aspect of compatibility, albeit a very important one. Compatibility with the base concrete must be sufficient in terms of thermal-, chemical-, elastic moduli-, absorption-, diffusion properties compatibility, chemical compatibility also. In a recent study where the potential of alkali activated materials as repair material was evaluated (Kramar et al. 2016), it was found that the slag-based mortar tested delaminated from the concrete surface during curing, rendering it unsuitable as a strengthening material due to insufficient bond strength, albeit it had the lowest shrinkage among all mixes. The likely causes have been identified as chemical incompatibility due to either too low levels of soluble silica, or a chemical reaction between the calcium hydroxide rich substrate reacting with the AAS.

2.4 Shrinkage behavior of cementitious materials

Since shrinkage has been identified as a major factor that influences compatibility in repair or strengthening applications, the shrinkage behavior of cementitious materials is described more in detail. Due to the vastness of information available, only autogenous shrinkage behavior is considered further on.

2.4.1 Autogenous deformation in OPC

Autogenous shrinkage (AS) is the dimensional change of cementitious material caused by chemical shrinkage (Figure 1-5) in a sealed environment; i.e., without moisture exchange to the surroundings. The total volume of the products of the hydration process is lesser than the initial volume of water and cement; this results in a volume reduction. After initial set, without water being supplied from the environment, self-desiccation, or internal drying of the paste occurs due to the pressure in the capillary pores dropping as a consequence of internal water consumption by the hydration process (Persson 1997, Tazawa et al. 2000, Holt 2001). Since by this stage the solid skeleton has already formed, the paste resists the deformation. Internal cracking may develop because of the limited deformation capacity of the hardening concrete. Factors known to have an effect on the AS at early ages are the water-to-cement (w/c) ratio, the fraction of supplementary cementitious materials (SCMs), the internal restraint from aggregates, fibers (if any), chemical admixtures, and curing conditions.

With the recent increased use of high early strength-, high performance-, and/or blended binder concretes, with low water/cement ratio the AS makes up for a substantially larger part of the total shrinkage (Emborg 1989, Bjøntegaard 1999, Hedlund 2000, Cusson and Hoogeveen 2008). It is significant enough to induce micro- or macro cracking due to the increased paste volume and higher binder content per unit volume. In a high performance concrete sample, AS reached 250 microstrains by 24 hours of age (Cusson and Hoogeveen 2008) – this presents a significant cracking risk if movements are restrained.

Typically, autogenous deformation (AD) manifests as shrinkage. Recent research, however, has reported on cases where a substantial autogenous expansion or "AD swelling", as commonly referred to, has occurred. Autogenous expansion in early age concrete/mortar typically – but not always – takes place in heat-cured samples, after the cooling down stage. Earlier studies (Bjøntegaard 1999) showed that the natural cooling down phase from temperatures exceeding 50^{0}C was characterized by a reduced rate of AS and was followed by autogenous expansion. The expansion started between 3-4 days of age and was attributed to "thermally induced" shock of the deformation. The autogenous deformation in this study was backcalculated by offsetting the total deformation assuming a constant thermal coefficient (CTE) of $10x10^{-6}$ $1/^{o}$C which did not account for the *nonlinearity of the CTE* at early ages (see Chapter 5.4). Both the rate and the starting point of

swelling appear to vary with the cooling down rate. Even when the same curing path is used up to the peak temperature (60^0C below), different rates of the cooling down will result in entirely different autogenous behavior for several days afterwards; see "60" vs. "60-cool" below. The autogenous deformation behavior has also shown to be unsystematic where contraction and expansion do not show a clear correlation with the curing paths/levels; e.g., "40" and "60" will expand but "47" will experience monotonous shrinkage.

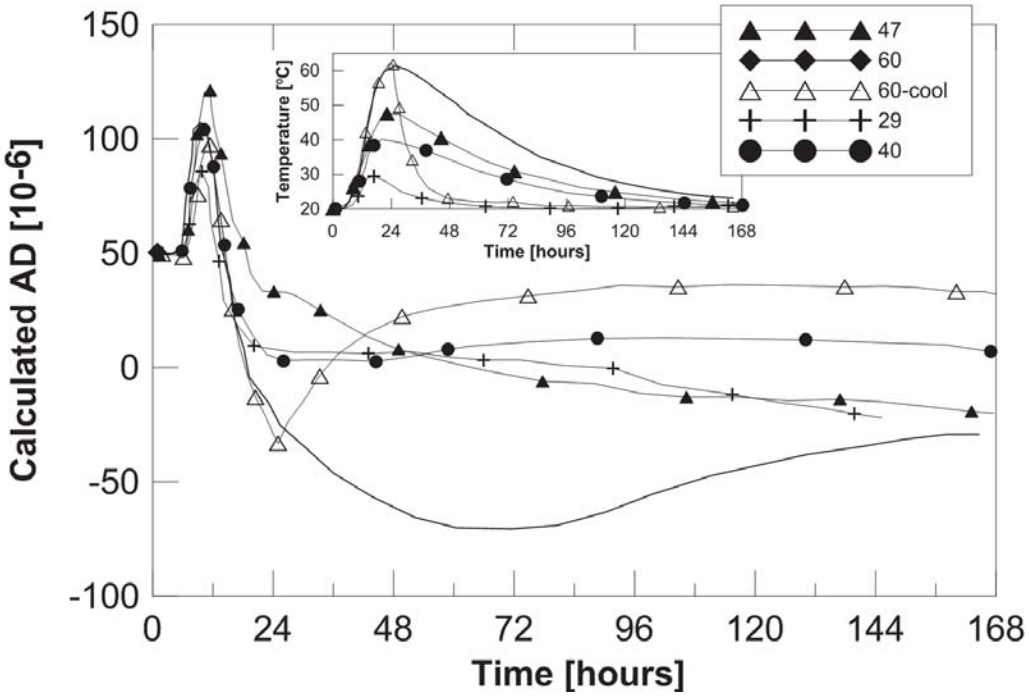

Figure 2-4: Temperature histories and unsystematic (backcalculated) autogenous behavior. Data from (Bjøntegaard 1999)

Furthermore, the author also showed that regardless of the choice of more "realistic" TDC values, the unsystematic tendencies observed in the autogenous deformation did not improve substantially.

Recently, slow expansion of over 10 days in fly ash concretes (Figure 2-5) was observed (Klausen 2016). The onset of swelling about coincided with the maximum temperature and continued throughout the cooling down phase. Swelling is prominent when $\Delta T \leq 20°C$, regardless of fly ash content (listed in Table 2-1). The Type I OPC reference sample, however, exhibited swelling after undergoing a 30°C temperature change.

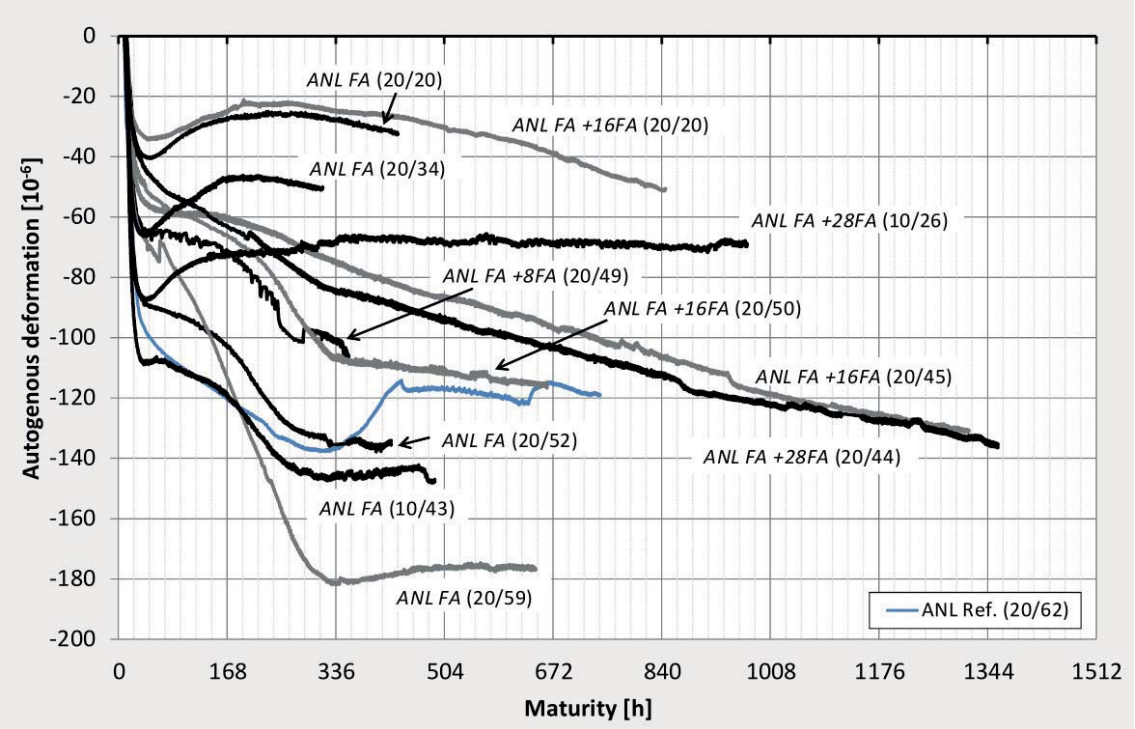

Figure 2-5: Autogenous expansion in fly ash mixes by (Klausen 2016)

	ANL Ref. [kg/m3]	*ANL FA* [kg/m3]	*ANL FA +8FA* [kg/m3]	*ANL FA +16FA* [kg/m3]	*ANL FA +28FA* [kg/m3]
Cement*	372.3	365.3	324.1	284.3	229.8
FA_{cem}	0.0	60.6	53.8	47.2	38.1
FA_{added}	0.0	0.0	36.0	71.1	118.5
Silica	18.6	18.3	18.0	17.6	17.4

Table 2-1: Fly ash (FA) content in the mixes, from (Klausen 2016)

AD swelling in OPC concrete with 50% fly ash, w/c 0.30, under 20°C isothermal conditions has been reported by others (Termkhajornkit et al. 2005). The expansion occurred well after the concrete has cooled down; the temperature in the sample did not reach 25°C at any point (Figure 2-6a). The swelling was prominent at around day five and lasted for another 7-8 days. The authors attributed the swelling to a possible ettringite formation. No swelling was observed in mixes with only 25% fly ash.

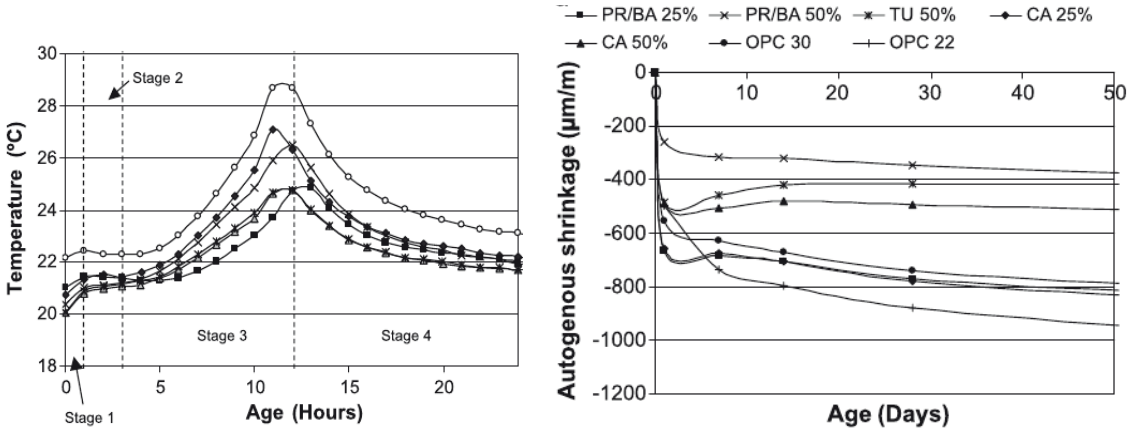

(a) **(b)**

Figure 2-6: (a) temperature histories, and (b) autogenous deformations, as observed by (Termkhajornkit et al. 2005). *PR/BA, TU, and CA are different kinds of fly ash*

AD swelling was also observed by (Maruyama and Teramoto 2011) in both OPC cement paste and OPC with 30% and 45% blast furnace slag (Figure 2-7). In that case, the curing temperature of 60°C was applied 50 hours after casting. The AD swelling was observed for the entire duration of the cooling down phase. A smaller but steady swelling was also observed in the OPC sample cured at 40°C. The same authors observed autogenous expansion in OPC mixed with 10% *silica fume* so consistently, beginning during the cooling off period that they concluded that the "gradual expansive behavior under temperature descending period is an intrinsic property" of the paste tested (Maruyama and Teramoto 2013).

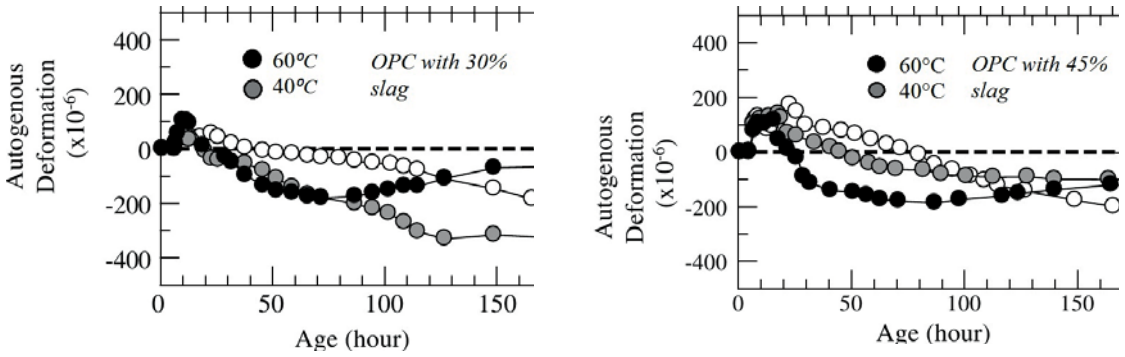

(a) **(b)**

Figure 2-7: Autogenous expansion observed by (Maruyama and Teramoto 2011)*; (a) OPC with 30% slag, (b) OPC with 45% slag; w/c 0.40*

Heating-cooling curing regime has been observed to cause AD swelling during the cooling off phase, lasting until the temperature levels off (Viviani et al. 2007). Finally, AD swelling has been also linked to possible ettringite formation in mixes made with coarser cements by (Bentz et al. 2001).

Despite the fact that the expansion has been observed worldwide, sometimes sporadically, but often across several mixes/curing paths, the exact variables causing it have not been identified in full. Most literature tackles the phenomenon on an experimental level, if at all. Often, it appears to occur in certain mixes or under certain curing conditions where it is not expected to appear by logic, and it may not appear in cases where it is expected based on the rest of the tests; e.g., the "47" sample in Figure 2-4. Considering that the parameters causing it are unclear, currently, no models incorporating the phenomenon exist.

2.4.2 Shrinkage in alkali activated materials

Alkali activation means that the latent pozzolanic properties of a cement-free binder, *typically* ground granulated blast furnace slag (GGBS) or fly ash (FA) or a combination thereof, are "activated" by a highly alkaline solution. In a high calcium system, alkali activation renders the aluminosilicate content of the slag into a reactive form that, with the available water and the alkali and calcium ions, produce primarily calcium silicate hydrates (C–S–H) and calcium-aluminosilicate hydrates (C–A–S–H). Since the gel contains a certain amount of sodium (Na), it is often referred to as (C–(N)–A–S–H). The C-S-H has a lower Ca/Si ratio than the corresponding phase in OPC (Gruskovnjak 2006). The exact type of gel that forms ranges from predominantly OPC-like C–S–H phases to fully polymerized N-A–S–H type gels and depends on the calcium- and magnesium content of the system, the type and pH of the activator, and the curing conditions (Fernández-Jiménez et al. 2003, Lodeiro et al. 2009, Garcia-Lodeiro et al. 2011, Puertas et al. 2011, Bernal and Provis 2014). Alkali activated materials with a predominantly N-A-S-H gel are commonly referred to as geopolymers, characterized by the presence of zeolites; e.g., (Provis and Van Deventer 2009). Other precursors, such as metakaolin (Vasconcelos et al. 2011, Chen et al. 2016), or pulverized rockwool and glass wool (Yliniemi et al. 2016) have been also used successfully to create new, innovative AAMs.

Research on shrinkage behavior of alkali-activated materials (AAM) is, at its current stage, not comparable to the vast amount of information available on OPC.

This is partly due to the fact that the mechanisms that cause shrinkage in OPC and AAM are different due to the differences in hydration process, the reactions that take place, and the hydration products. Widespread industrial adoption, commercial scale production, and standardization of design procedures employing AAM, however, have been hindered by the lack of long-term performance/durability data and the limited understanding of shrinkage behavior and the driving mechanisms behind shrinkage.

Research focusing specifically on *autogenous shrinkage* in alkali-activated materials is limited to a very small number of studies. The driving mechanism behind the autogenous shrinkage in AAS is not clarified. Considering the range of phases that can form in alkali-activated materials, the shrinkage mechanisms - both the autogenous and the drying shrinkage behavior - are expected to be *more complex* than those in OPC. Both autogenous and drying shrinkage in AAS have shown to exceed that of comparable strength OPC (Collins and Sanjayan 2000, Neto et al. 2008, Cartwright et al. 2015); up to seven times larger (Bakharev et al. 2000). Autogenous shrinkage increases with the addition of more slag and sodium silicate (Lee et al. 2014); more slag results in reduced total porosity and a denser microstructure (Lee et al. 2014). Different activators generate coarser or finer capillary porosity (Haha et al. 2011) which is expected to have an impact on the shrinkage behavior. Furthermore, recently, alkali resistant glass, carbon, and even PVC fibers have been successfully incorporated into alkali-activated binders (Funke et al. 2016, Vilaplana et al. 2016). The addition of carbon fibers up to 1 mass % reduced (drying) shrinkage by up to about 60% depending on fiber length (Vilaplana et al. 2016). The available information on the applicability of basalt fibers is contradictory; according to (Funke et al. 2016), the basalt degraded in the high pH environment, while they have been used successfully by others (Timakul et al. 2016). Finally, autogenous shrinkage in AAS has shown strong correlation with brittleness. It was found by (Duran Atics et al. 2009) that sodium silicate activated slag was more brittle than sodium carbonate activated slag. It was hypothesized that the higher shrinkage would cause microcracking in the matrix, leading to a reduction in tensile capacity. Sodium carbonate was recommended as an activator because the use of it would result in comparable or lower shrinkage than OPC.

References about autogenous expansion are scarce. One notable reference has been identified in which slow and long-lasting expansion was found both in the

reference OPC mix and in AAS mixes, with and without shrinkage-reducing admixtures (Figure 2-8).

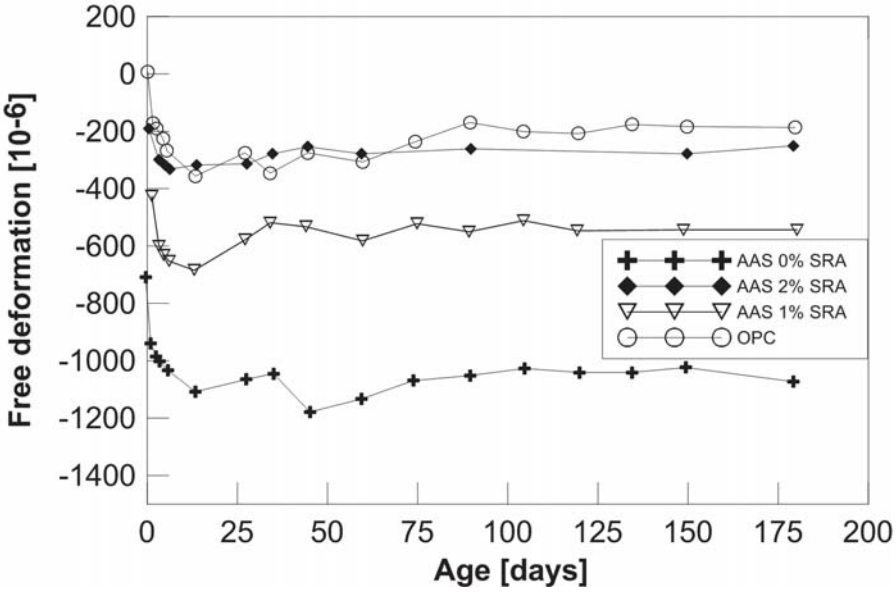

Figure 2-8: Free deformation in waterglass-activated slag mortars and OPC; data from (Palacios and Puertas 2007)

3 MODELING OF AUTOGENOUS SHRINKAGE IN YOUNG CONCRETE

When starting out with the experimental work, one of the main objectives was to incorporate the effects of variable temperature curing into the "HH model" (described below) to describe the development of autogenous deformation in young concrete in a way that can be used by industry for cracking risk prediction for current mixes (blended cement mix designs, and possibly future binders employing large fractions of SCM).

3.1 Decoupling deformations

During hydration, fully coupled autogenous deformation (AD) and thermal deformation (TD) are recorded as free deformations; Eq. 1 and Eq. 2.

$$\varepsilon_{tot} = \varepsilon_{SH} + \varepsilon_{T} \quad (1)$$

$$\varepsilon_{T} = \alpha \cdot \Delta T \quad (2)$$

Where ε_{tot} is the total deformation, ε_T is the thermal dilation, ε_{SH} is the autogenous deformation, α is the coefficient of thermal expansion (CTE) and ΔT is the temperature change. For a robust model capable to describe any conceivable temperature history and to calculate shrinkage-induced stresses in the concrete, it is fundamental to determine the relative importance of both AD and TD, and to be able to model satisfactorily both (Bjøntegaard 1999).

The maturity concept assumes a time shift from real time to "concrete age". The equivalent age or concrete age can be calculated from compressive strength data for each individual concrete mix. It has been used to compare autogenous shrinkage of different temperatures where the rate of the hydration is different since higher temperature accelerates hydration.

One of the most widely used shrinkage prediction models developed by Hedlund (Hedlund 2000) in 1999 (Eqs. 3—6) has repeatedly proven to work well

for normal- and high strength ordinary Portland cement concretes, but has recently been shown to be inaccurate for certain newer types of blended cements containing fly ash (Fjellström 2013, Orosz et al. 2014). This model, further referred to as "HH model", is based on an ultimate reference autogenous shrinkage (Eq. 3) which is determined based purely on w/c and altered to account for the temperature effects (Eq. 4.). The effects of heat curing are incorporated into a factor denoted as $\beta_{ST}(T)$ *temperature sensitivity factor* (Eq. 5.) or the "temperature effect on autogenous shrinkage" (Hedlund 2000). This expression accounts for the temperature in the sample in relation to the maximum temperature in the sample, up to the time of interest. It does not, however, account for how long that has been kept at a certain level. In essence, it accounts for the amplitude of temperature (T) but not the duration of it.

The following equations are used:

$$\varepsilon_{ref} = (-0.65 + 1.3 \cdot (w/c)) \cdot 10^{-3} \quad (3)$$

$$\varepsilon_{SH} = \varepsilon_{ref} \cdot \beta_{s0}(t_e) \cdot \beta_{ST}(T) \quad (4)$$

$$\beta_{ST}(T) = a_0 + a_1 \cdot \left(1 - \exp\left[-T_c^{max}(t)/T_1\right]^{b_1}\right) + a_2 \cdot \left(1 - \exp\left[-T_c^{max}(t)/T_2\right]^{b_2}\right) \quad (5)$$

$$\beta_{s0}(t_e) = \exp\left(-\left[t_{s0}/(t_e - t_{start})\right]^{\eta_{SH}}\right) \quad (6)$$

where ε_{ref} [-] = reference ultimate shrinkage, a fitting parameter determined by the least square method; ε_{SH} [-] = autogenous shrinkage; $\beta_{ST}(T)$ [-] = temperature sensitivity factor; $T_c^{max}(t)$ [°C] = maximum temperature in the concrete sample up to time t; t [s, h or d] = real time specified as time after mixing; a_0 [-], a_1 [-], a_2 [-], b_1 [-], b_2 [-], T_1 [°C], T_2 [°C] = fitting parameters; β_{s0} [-] = relative time development or time distribution of autogenous shrinkage; t_e [s, h or d] = equivalent time of maturity; t_{start} [s, h or d] = start time of autogenous shrinkage specified in real time after mixing; t_{s0} [s, h or d] and η_{SH} [-]= curvature parameter; a fitting parameter determined by least square method.

3.2 Temperature sensitivity factor

It is well-known that deformation measurements recorded on samples that undergo heat curing at isothermal temperature levels are larger than the deformations of a sample that is stored at a chosen ambient temperature. In earlier models, the absolute magnitude of curing temperature has been accounted for, but not the duration or gradient of the heat curing. This is very clearly represented in the so-called temperature sensitivity factor (Figure 3-1) incorporated into the model used in this thesis, where it can be seen that for a certain isothermal temperature level, the temperature sensitivity factor is unequivocally defined. Whether a sample is being cured at 50°C for one day or one week would result in the exact same $\beta_{ST}(T)$ factor. Whether a sample has been heated up to that temperature "instantaneously" or over the course of five days is not incorporated into the model either – which, considering that the importance of the first few days into the curing is well-known, may be considered one of the decisive parameters that is ignored.

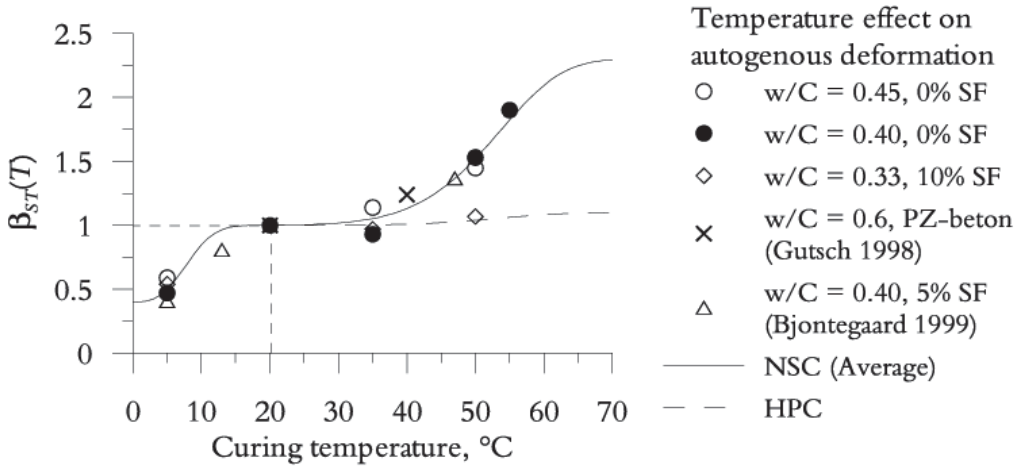

Figure 3-1: Temperature sensitivity factor as a function of isothermal curing temperature (Hedlund 2000)

3.3 Gaps in current knowledge

There are several other shrinkage prediction models; with the major driving forces contributing to AS having been identified as the surface tension, capillary depression, and capillary tension. The Tazawa and Miyazawa prediction model developed in 1997 takes into consideration both w/c ratio and cement type (Long

et al. 2011). Another model, referred to as the CEB-FIP model relates the AS to the compressive strength, cement type, and concrete age, but it is only applicable to normal strength concretes. It has also been shown to underestimate shrinkage, (Long et al. 2011).

Despite the earliest observations of autogenous expansion dating back to the late 90s, (Bjøntegaard 1999), to the author's knowledge, no current model taking into account the possibility of autogenous expansion exists.

Another significant gap in knowledge is the incorporation of variable temperature levels into prediction models. There is no clear agreement whether the maturity concept can be applied to describe AD development under variable temperature curing conditions, which is a prerequisite to successful decoupling of AD and TD. It was suggested that the maturity concept based on effective age could be used by addition of a temperature-correcting factor, (Hedlund and Jonasson 2000). It should be possible to separate AD and TD in cement pastes, based on the maturity concept, by offsetting the total deformation by thermal deformation part (TD) as long as the temperature range is between 10^0C and 40^0C, (Turcry et al. 2002). In contrast, others indicate that the maturity concept is unsuitable, (Bjøntegaard 1999, Jensen and Hansen 1999). Early models (Emborg 1989, Hedlund 2000) took into account the effect of curing temperature as the maximum curing temperature only. However, according to new data, the AD development rate and its magnitude are strongly dependent on the curing temperature history, (Bjøntegaard 1999, Jensen and Hansen 1999, Bjøntegaard and Sellevold 2001, Hai and Zhu 2009, Klausen 2016).

A further difficulty is that the AD behavior has been found to be unsystematic, even when assuming realistic CTEs; see Figure 2-4. Others also emphasized that higher temperature does not necessarily lead to higher AS (Lura et al. 2001). Therefore, AD in a real structure cannot be predicted from isothermal test results alone because the deformation depends on the specific imposed temperature history.

4 EXPERIMENTAL PROGRAM

This section briefly summarizes the choice and design of the test specimens and procedures for both the strengthening work and the shrinkage testing.

4.1 Tensile characterization of strengthening materials

4.1.1 Materials

The reader is referred to Papers 1 and 2 or, alternatively, to the Licentiate thesis (Orosz 2013) for a significantly more detailed description.

As stated in Chapter 1, the first half of the work presented in the thesis dealt with strengthening work. Two test series have been carried out on the components of what had been referred to as "Mineral Based Composites" at LTU (Blanksvärd 2007, 2009).

Mainly the same materials were used for the two test series (albeit not in all/the exact same combinations); a CFRP grid with two different grid spacing and fiber amounts in each direction ("medium" and "small" grid), and as binder/matrix, quasibrittle (commercial) mortars and a strain hardening engineered cementitious composite (ECC). Grids with different spacing and fiber amount per direction, placed in "strong" (favorable) and "weak" (rotated) directions in relation to the direction of the loading have been tested. Detailed material data on the FRP component can be found in Papers 1 and 2.

Only the ECC composition is given here in Table 4-1. The ECC is a flowable paste with large amounts of fly ash (of unidentified chemical composition), and 10mm long, chopped, randomly mixed in PVA fibers (1% by weight, or 2% by volume).

Fraction	wt%
Type I cement	22
Fly ash	44
Sand (<0.15mm)	8
Quartz powder 100/22	8
Water	18
Superplasticizer (Melflux)	0.02
Oiled PVA fibers	1

Table 4-1: Mix composition of ECC

4.1.2 Test setup

The first test series was ***uniaxial tensile tests*** carried out on large size dogbone specimens (Figure 4-1) cast out of strengthening mortar, with a stiff, 2D CFRP grid placed in the midplane. The bare strengthening material was tested in an optimized setup with custom-made, double-hinged clamps to avoid bending of the sample.

The uniaxial tests, while providing information on the *strain hardening behavior and the* tensile strength (but not the other two, important parameters of the post-peak behavior; the shape of the softening curve, and the fracture energy) are known to be very sensitive for brittle or quasi-brittle materials. It is difficult to ensure that cracking will happen in the prescribed (and monitored) test field, preferably in the middle of the web of a dogbone specimen. There is a high risk of cracks initiating where the web meets the bulk end of the specimen. Research by (Naaman and Reinhardt 1995) has indicated that this risk exists even if the transition between the test field and the bulk end is gradual (a concave arch).

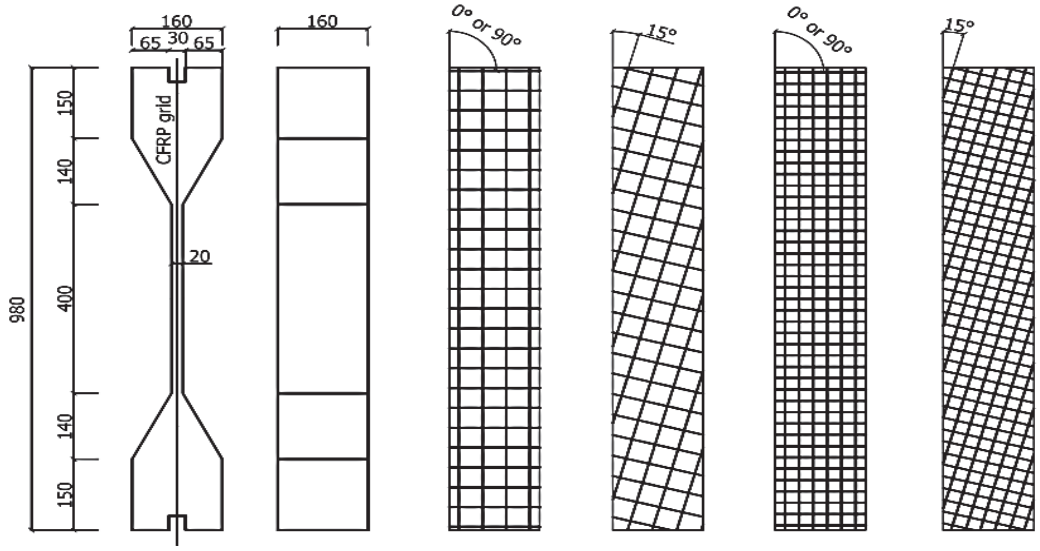

Figure 4-1: Dogbone samples with reinforcement configuration: (a) sample top view; (b) sample side view; (c)-(d): "medium grid" (referring to grid spacing) configurations; (e)-(f): "small grid" configurations

The second test series was an upscaled version of the ***wedge splitting tests*** (WST) used in fracture mechanics. The toughness of concrete is usually evaluated by means of the post-failure behaviour in tension, governed by the stress versus crack width relation (σ-w), the *tension softening behaviour*. It is a basic property of the concrete described by the (a) tensile strength, (b) the shape of the softening curve, and (c) the fracture energy, which corresponds to the area under the stress versus crack width curve (Hillerborg et al. 1976). Knowledge of these parameters enables estimations of shear capacity and brittleness in compression and tension. While the WST is not a direct tensile test, it *can* provide valuable data on the tensile *and* fracture behaviour. The WST, originally introduced by (Linsbauer and Tschegg 1986), and improved by (Brühwiler and H. 1990) is a fracture mechanics test method, that has proven to be suitable for obtaining both *splitting* tensile strength and an estimation of the fracture energy. The most prevalent advantage it offers over uniaxial tensile tests is its stability; it always results in stable crack propagation (Østergaard et al. 2004). This is due to the low amount of elastic energy stored in the specimen compared with the energy consumed by crack propagation.

The pre-notched WST samples (Figure 4-2) were reinforced with the same strengthening material on both sides, then split into two halves to capture the first

cracking load, peak load, tensile strain hardening behavior (if any), and post-peak behavior (strain softening) until failure. Fracture energy was also calculated.

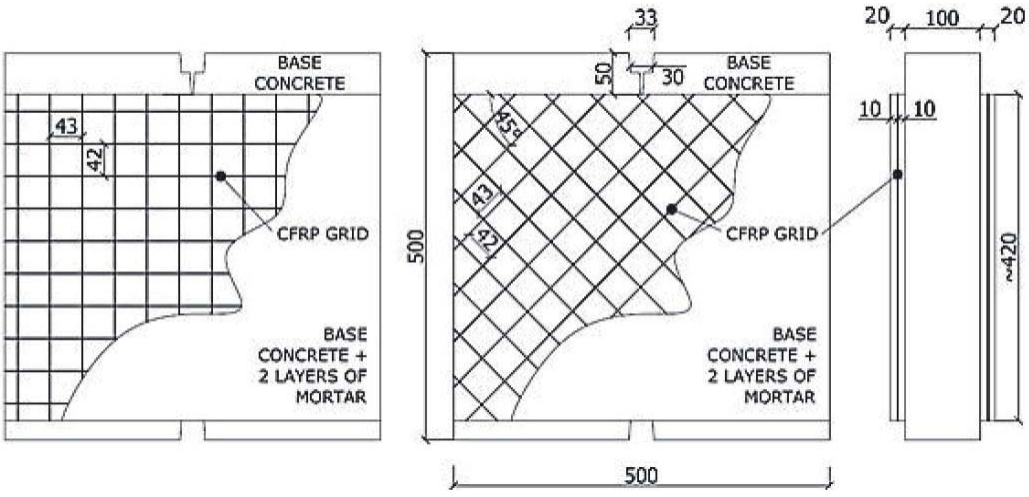

Figure 4-2: WST specimens with grids placed in "strong" and "weak" directions

The WST setup has its inherent limitations. The main drawback compared to uniaxial tests is that it does not create a uniform tensile field because the specimen undergoes bending simultaneously. Furthermore, an inverse analysis needs to be performed in order to obtain the tensile properties. However, even without performing the inverse analysis, the test setup can be used to characterize fracture energy, which is directly proportional to the area under the load-CMOD curve.

4.1.3 Methods

The dogbone setup has simply been upscaled based on literature recommendations. The length of the test field was set to the longest possible to ensure a high cracking potential, but short enough so that demolding the samples would not break them at their weakest. Self-centering anchor clamps (fixtures) have been developed and manufactured to ensure an even loading in pure tension. A detailed description of the design of the anchor clamps is found in Paper 2.

The WST setup was purely experimental. Existing loading devices and setup were used in a creative way. As stated earlier, the goal was purely to assess post-peak behavior depending on mortar quality (quasibrittle vs. "ductile" mortars) and grid orientation (behavior of grid joints); not the tensile capacity per se.

Both test series were run displacement controlled. DIC measurements (ARAMIS) completed the recorded load-deformation data to visualize strain fields and quantify cracking patterns, crack development over time, crack density, and crack widths up to failure. Inverse analysis for the WST has not been performed as it was not necessary for the intended outcome.

4.2 Autogenous deformation behavior of PCC and AAS – materials

4.2.1 Materials

The autogenous deformation behavior in both ordinary (OPC) and composite Portland cement concrete (PCC) and alkali activated slag concrete (AASC) was investigated in the second half of the PhD studies. The samples were prepared with a blended, Type II/A type cement ("BAS" concrete) and Type I cement ("ANL"). ANLFA is a control mix in which 30% of the ANL cement has been replaced by fly ash. The alkali activated slag mixes are denoted as SC10, SS10, and SS14, where SC is activated by 10% sodium carbonate, while SS10 and SS14 are activated by 10% and 14% sodium silicate solution (alkali modulus 1.00), respectively. The following mix designs have been prepared (Table 4-2).

Fraction [kg/m^3]/mix	SC10	SS10	SS14	BAS 0.38	BAS 0.55	ANL 0.55	ANLFA 0.38
fly ash	–	–	–	–	–	–	126
slag	450	450	450	–	–	–	–
0/4	1332	1332	1332	–	–	–	–
4/8	331	331	331	–	–	–	–
water, eff.	202.5	202.5	202.5	179	198	187	168
cement	–	–	–	470	360	340	294
0/8	–	–	–	975	1067	1072	928
8/16	–	–	–	790	733	398	844
16/27	–	–	–	–	–	401	–
activator	10% SC	10% SS	14% SS	–	–	–	–
alkali modulus		1.00	1.00	–	–	–	–
pH of activator	11.2	13.7	13.7	–	–	–	–
28-day cube strength [MPa]	46	42	77	70	45	45	52

Table 4-2: Mix designs. Alkali activated slag (SC10 – SS14), OPC (ANL and ANLFA), and PCC (BAS) concretes

The most important physical and chemical properties of the binders are tabulated in Table 4-3.

Property/amount	**BAS**	**ANL**	**slag**	**fly ash***
Blaine-fineness	450 m^2/kg	310 m^2/kg	500 m^2/kg	N/A
Setting time	150 min	160 min	N/A	N/A
Compact density	3000 kg/m^3	3200 kg/m^3	2950 kg/m^3	N/A
CaO	55.4%	64.1%	48.9%	5.9%
SiO_2	24.0%	22.4%	24.2%	47.6%
Al_2O_3	6.7%	3.7%	7.9%	23.3%
Fe_2O_3	N/A	4.5%	0.8%	5.3%
MgO	2.8%	1.2-1.5%	6.6%	1.5%
K_2O	1.3%	N/A	1%	1.2%
SO_3	3.4%	2.4%	2.5%	N/A
TiO_2	N/A	N/A	6%	1.2%
MnO	N/A	N/A	1.2%	0.05%
Water-soluble Cr^{6+}	<2 ppm	<2 ppm	N/A	N/A
C_3A	5.2%	2.1	N/A	N/A
C_3S	N/A	48%	N/A	N/A
C_2S	N/A	28%	N/A	N/A
C4AF	N/A	13.8%	N/A	N/A

Table 4-3: Physical and chemical properties of the binders

**Not available at the time of writing Papers 3-5.*

4.2.2 Test setup

The test setup was adopted from (Hedlund 2000). Concrete and alkali activated slag concrete cylinder samples (Ø=80mm, h=300mm) were cast in pairs; one sample cured at ambient temperature, and one undergoing a certain forced path of heat curing that mimics "realistic" curing conditions. The curing consisted of an isothermal plateau at 35^0C, resp. 50^0C for a preset time (1, 3, and 5 days, depending on temperature level), then a cooling down part at a steady rate, followed by isothermal curing at ambient temperature (20^0C). The general test setup is pictured in Figure 4-3.

The temperature paths varied depending on materials. For PCC, different temperature levels were tested (Figure 4-4), while for AASC, only one temperature path (50^0C for 3 days, referred to as 50-3D) was employed to compare the behavior of PCC vs. AASC. This was a limitation imposed due to both time constraints and financing of the AASC part of the testing.

Figure 4-3: Free deformations test setup

All samples were demolded 8 hours after casting. A pair of symmetrically mounted linear variable differential transformers (LVDTs) of the type Schaevitz type 010 MRH was used to record the deformations over a time period of two weeks. The two-week duration of the tests was chosen as suitable based on earlier tests (Hedlund 2000, Fjellström 2013). Temperatures (ambient-, water bath-, and in the center of the samples) were recorded with thermocuples.

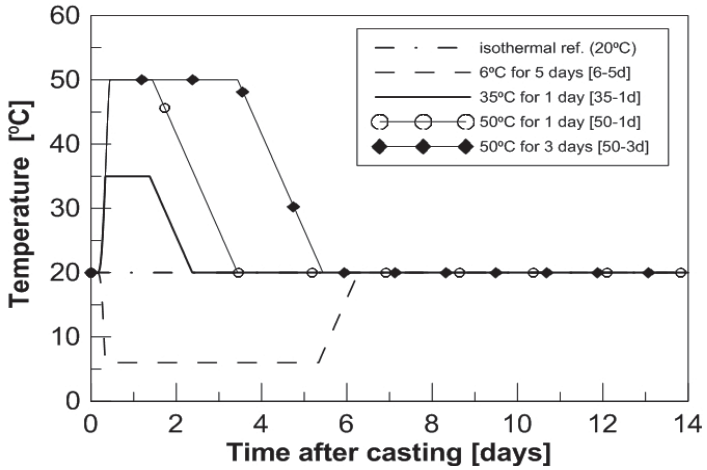

Figure 4-4: Forced temperature paths

After mounting the LVDTs, the deformations were zeroed at 8.5 hours, and the samples were sealed in a waterproof metal encasing lowered in a heated/cooled water bath to record coupled autogenous shrinkage and thermal deformations.

4.2.3 Methods

The coupled free deformations were analyzed both as total deformation (Papers 3 and 5) and – for PCC - as decoupled autogenous and thermal deformations, using a convenient shrinkage model (Paper 4).

The shrinkage model (Hedlund 2000), described in Chapter 3 uses a constant thermal expansion/contraction coefficient (CTE) where the CTE is actually one of the fitting parameters calculated within a reasonable, given range for *hardened* concrete. Beyond this, manual decoupling was also attempted, where a range of different CTEs were assumed based on literature. Decoupling has only been attempted for the PCC samples because the kind of information necessary to perform such decoupling (real time – equivalent time conversion and knowledge of early-age CTE development) for AASC, at the time of research, was largely unknown.

5 RESULTS AND ANALYSIS

5.1 Tensile behavior

An extract of the results from the tensile characterization of the strengthening materials are dealt with, in a comprehensive form, together below. Full results are presented in the appended papers.

Strain hardening behavior in uniaxial tension has been obtained with all mortars; however, the plots of the quasibrittle mortars are jagged (Figure 5-1), indicating the rupture of subsequent grid tows at each drop, while the use of ECC results in an immediate redistribution of stresses which is indicated by the lack of drops in load capacity as the grid tows rupture. Best performance, in terms of ductility, has been achieved with the medium grid rotated crosswise.

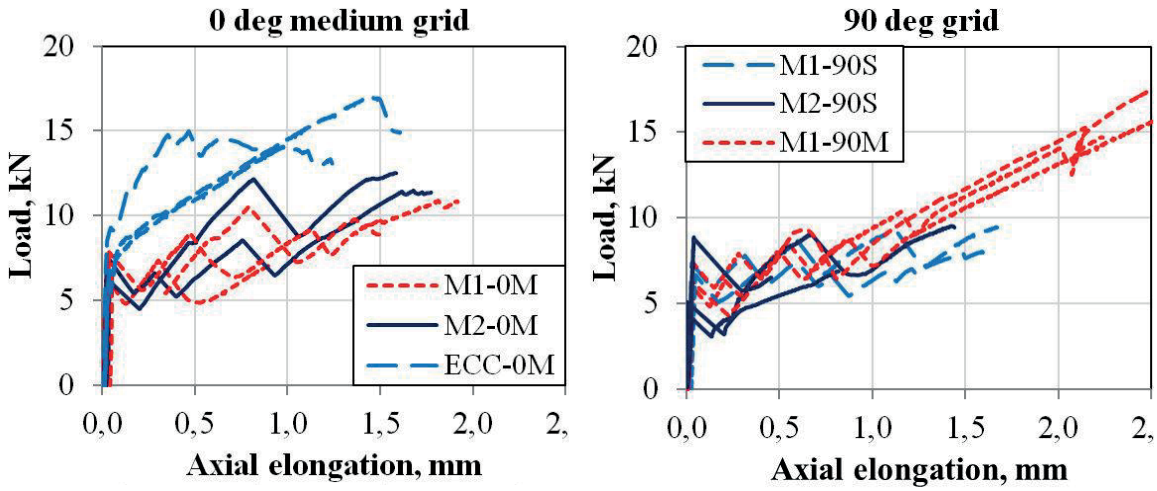

Figure 5-1: Load-axial elongation plots for (a) effect of strain hardening matrix with medium grid in strong direction; (b) the effect of grid spacing: crosswise rotated grids with quasibrittle matrices M1 and M2, small grid S, medium grid M.

Crack patterns have been monitored with DIC (Digital Imaging Correlation) method (Figure 5-2). Both the grid spacing and the mortar quality had an influence on the cracking pattern. More evenly distributed cracking patterns were obtained

with the "small" grid and the ECC. The crack widths of the ECC specimens are very small, ranging from 0.08 mm to 0.50 mm vs. crack widths for the quasibrittle mortars between 0.20 mm to 1 mm, depending on exact material combination/grid orientation.

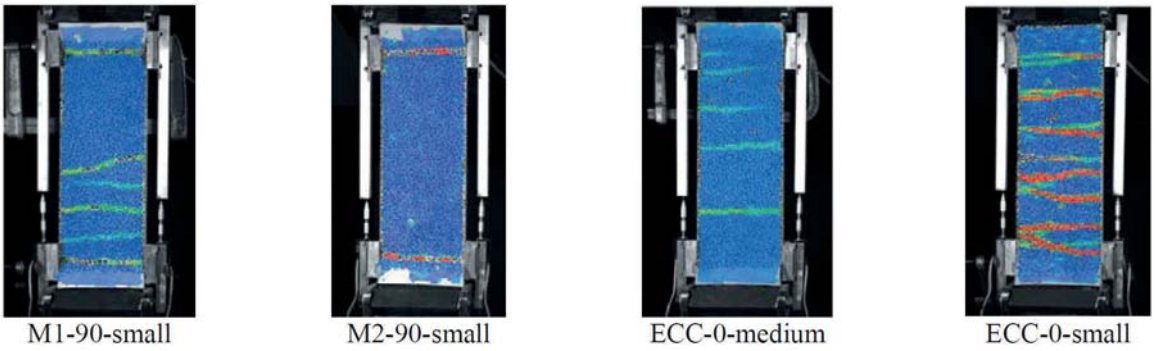

Figure 5-2: DIC strain images: crack patterns illustrating the mean number of cracks at failure. Quasibrittle (M1, M2) vs. strain hardening mortars (ECC).

The primary results from the WST tests (Figure 5-3) reveal tensile strain hardening behavior only with the grids being placed in the "strong" direction (PMM-0 and ECC-0). No hardening was observed with grids rotated in a 45^0 direction (PMM-45 and ECC-45).

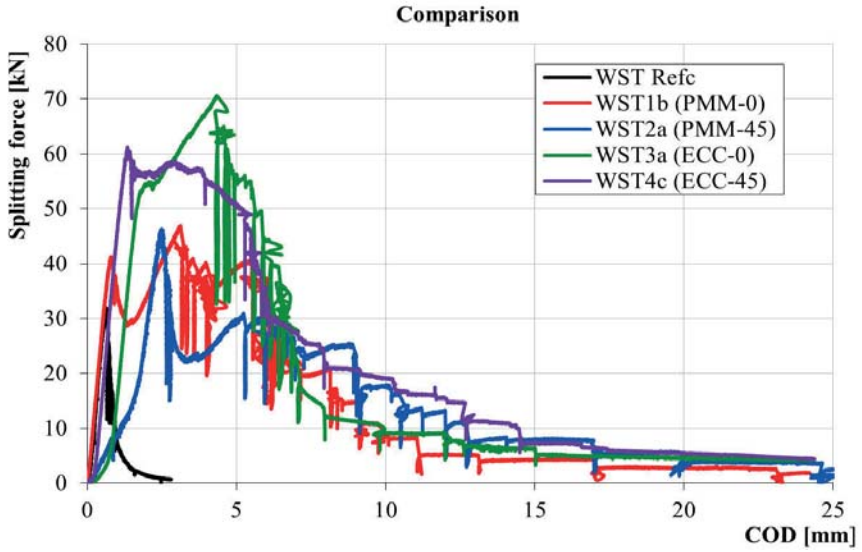

Figure 5-3: COD (crack opening displacement) - splitting force relationships for quasibrittle mortars (PMM) and ECC; with FRP grids placed in "strong" direction (0) and rotated in a weak 45^0 angle (45)

The lower load capacity and/or drops in load capacity were attributed to shear failure due to the very limited deformation capacity of the stiff grid intersections (Figure 5-4a). The ECC was able to counteract the large drops in load capacity (ECC-45); however, no hardening could be achieved with the grid rotated into its most vulnerable position. Furthermore, spalling of the mortar was observed in some of the samples with the quasibrittle mortar (Figure 5-4b). The ECC had the ability to redistribute stresses as the grid tows (or intersections) were gradually failing. This is in line with the findings presented in e.g. (Dai et al. 2009).

(a) **(b)** **(c)**

Figure 5-4: (a) shear deformation of the grid intersections, (b) spalling of the mortar, and (c) multiple cracking of the ECC matrix

The strongest combination, both in terms of load capacity, and exhibiting the most pronounced strain hardening was the sample (WST3a) analogous to the ECC-0M in the "dogbone" tests; the combination of ECC with the medium grid placed in its "strong" position. Peak splitting loads were increased by 30-110% compared to the unstrengthened plain concrete reference sample, while the calculated fracture energy was 7-11 times that of the reference sample; the lower values correspond to the quasibrittle matrices, while the top of the range was achieved by using ECC as binder.

5.2 Autogenous deformation and modeling

Autogenous deformations have been evaluated in two distinct ways. First, the total deformations were split into thermal and autogenous part either by the employed model, or manually, by assuming a range of CTEs. Further, in the free deformation plots the deformations are still fully coupled (AD+TD); however, certain conclusions regarding the autogenous part can be drawn simply by the logic that at the stages of the curing when the temperatures are stabilized and kept constant, the deformation that is visible must be purely autogenous in nature.

5.3 Free deformations in PCC and AASC

Detailed results for every concrete mix and temperature level can be found in Paper 3. For AASC results, the reader is referred to Paper 5. Here only a comprehensive summary is given.

For PCC, the following trends have been observed, as illustrated on the lower w/c PCC mix (Figure 5-6):

5.3.1 Autogenous shrinkage

It is known that AAS has a relatively long dormant period compared to OPC (*Figure 5-5*), with a peak in adiabatic heat development at around 16 hours (Gruskovnjak 2006). Therefore, the forced steering (determined based on calorimetric tests performed on the PCC w/b 0.38 mix) caused a temperature rise in the AAS at a faster rate than its own natural adiabatic heat development would have progressed. This *may* have contributed to accelerated hydration early on and, subsequently, larger deformations in the AAS.

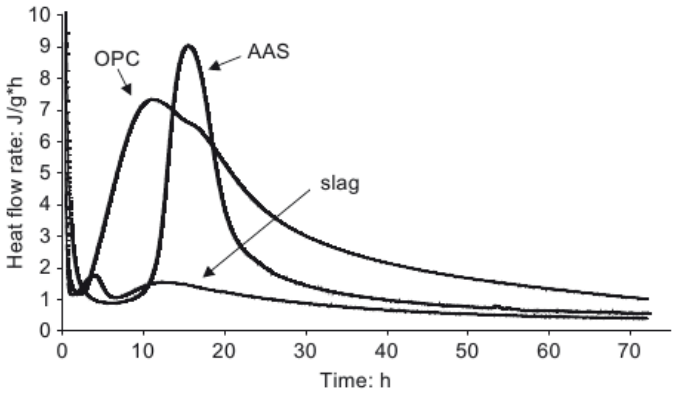

Figure 5-5: Heat flow calorimetry for AAS, OPC, and slag without activator, from (Gruskovnjak 2006).

5.3.2 Autogenous expansion

Autogenous expansion can be identified for certain curing temperature paths when both the heat curing at constant temperatures and the cooling down stage have finished. After the times marked as $\Delta T=0$ the samples are kept at ambient temperature; therefore, the deformation observed is autogenous in nature since there is no thermal component present. Past this point, strict shrinkage was observed only in the sample that underwent cooling down (marked as w/c 0.38 6-5D). The two 50^0C temperature levels resulted in distinct, non-negligible *swelling* (Figure 5-6). The lower curing temperature level (35^0C) resulted in marginal expansion that lies within measurement error. As it can be seen from the behavior of the 50-1D and 50-3D samples, during the duration of the tests, the expansion has not leveled off. Both the presence of autogenous expansion following a heat-curing regime and the stage at which it occurs (past cooling down, beginning likely already during cooling down) are in line with current literature, e.g., (Bjøntegaard 1999, Bjøntegaard and Sellevold 2001, Klausen 2016). It appears that higher temperatures are more likely to cause this type of expansion. One study (Maruyama and Teramoto 2013) concludes that "the general expansive behavior under temperature descending period is an intrinsic property" of the cement pastes they tested. The paste was prepared using a low heat Portland cement premixed with 10% silica fume.

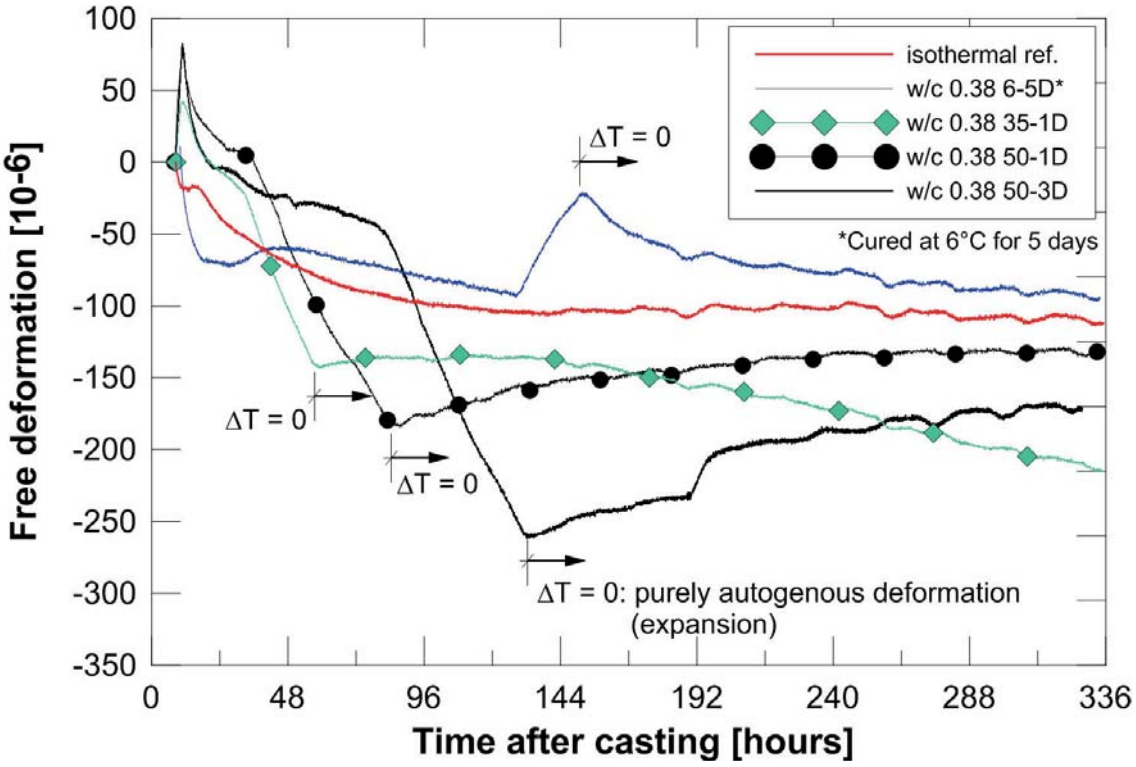

Figure 5-6: Effects of curing temperature on w/c 0.38 concrete, comparison

From the free deformation plots, it is difficult to draw conclusions about when exactly the expansion begins. Most literature would agree that the expansion is likely to begin already during cooling down. The reasons have been hypothesized as thermal "shock" on the deformation (Bjøntegaard 1999), or possible ettringite formation, e.g., (Termkhajornkit et al. 2005). It has not been clearly established whether this expansion has to do with the rate of the cooling down because only one rate has been employed, but it can be said that *if* the swelling has to do with condensation water reabsorption into the sample (a small amount of condensation water developing within the air space between the sample and the waterproof encasing due to rapid cooling down), then the rate of cooling down may certainly have an impact. In (Bjøntegaard 1999), a comparison between applying the same curing temperature (60^0C) but a different cooling down rate can be found. Both curing paths resulted in expansion. However, in the (derived) autogenous deformation of the sample cooled down at a much faster rate, a clear inflection point could be observed where shrinkage turned into a distinct expansive stage, while gradual cooling down resulted in swelling beginning slowly about halfway into the cooling down stage, as it was illustrated in Figure 2-4.

5.3.3 "Thermal shock" of the deformation

A couple more conclusions can be drawn from the free deformation plots, as further elaborated in Paper 3. First, cold curing (6-5D) appears to have triggered some kind of expansive behavior early into the curing; also shown in Figure 5-9. No explanation to this phenomenon has been found in literature. It would require further research to say with certainty whether this expansion is the result of an "extreme" thermal shock (the sample being cooled down at a very steep rate compared to the regular cooling down rate following heat curing), or whether some kind of expansive hydration product is forming suddenly in larger amounts, such as ettringite.

5.3.4 Nonlinear nature of early-age CTE

The second obvious conclusion is that the proportional temperature changes during the cooling down stages produce non-proportional thermal jumps. By thermal jump, the coupled (AD+TD) deformations during the cooling down stage are understood. Naturally, the thermal jumps still have an autogenous component. However, by comparing the shrinkage rates, for example, right before the thermal jump and the expansion rates right after for both 50-1D vs. 50-3D, it can be deduced that the thermal coefficient CTE appears to vary significantly over time, depending on the curing regime imposed. This finding is also consistent with the state-of-the-art; it is well-documented, albeit inconsistently, that the CTE of young concrete varies due to different internal RH, hydration products/stages of hydration, and possibly different pore systems developing as a result of different curing regimes; e.g., (Cusson and Hoogeveen 2006, Sellevold and Bjøntegaard 2006, Grasley and Lange 2007). The development of the CTE for the specific mixes and curing paths in the testing program has not been investigated. However, in Paper 3, some conclusions regarding the "implicit" CTE have been formulated.

5.3.5 Unsystematic shrinkage/expansion behavior

Furthermore, it can be seen that the development of shrinkage/expansion is unsystematic. For example, curing at 35^0C (35-1D) results in larger shrinkage *by 14 days* than curing at 50^0C (either 50-1D or 50-3D). Cold curing appears to induce an initial expansion (Figure 5-9) when common sense dictates that the rate of hydration and the associated shrinkage should slow down.

The faster rate of shrinkage compared to the isothermally cured reference sample is has been also observed by (Maruyama and Teramoto 2013). The authors

published a study in which they observed an increased magnitude of autogenous shrinkage in silica fume cement paste samples undergoing cooling down shortly after mixing, followed by a larger increase at higher temperature histories. The authors attributed the larger deformations to possible cracking within the concrete, and warned that this behavior may "pose problems for winter construction".

5.3.6 Expansive products

Within the framework of this PhD, no XRD analysis was performed to confirm the presence of expansive products in PPC, such as ettringite. However, XRD analysis has been performed in the second phase of the testing, when the same test setup was extended to alkali activated slag concrete samples. The substantial expansion in AASC prompted the need to look into hydration (and geopolymerization) products in AASC. Morphologically, similar free deformation curves have been obtained for AASC, but with both the contraction part and the expansive parts much more pronounced, as illustrated below in Figure 5-7 (Paper 5 contains the full results).

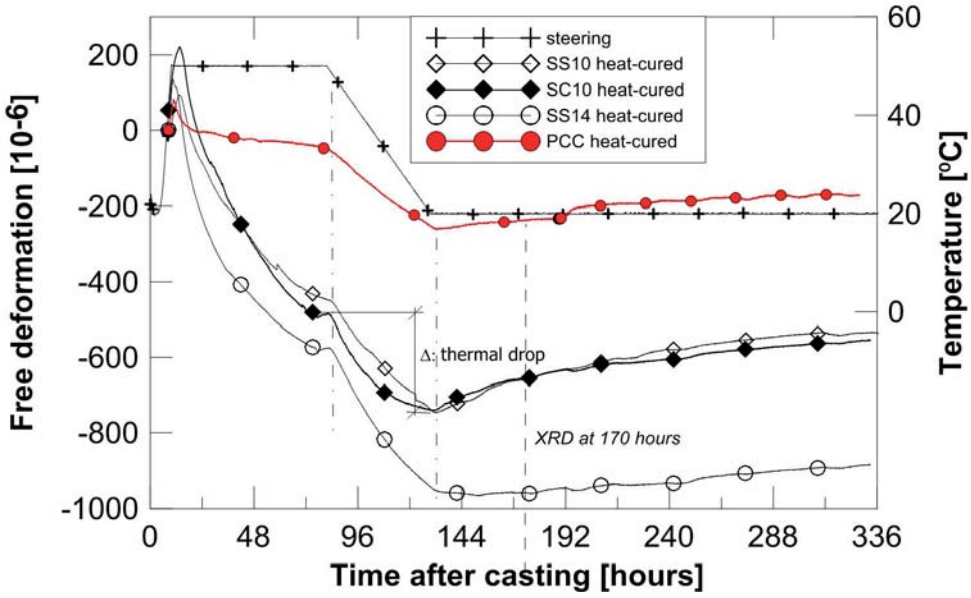

Figure 5-7: Free deformation in PCC vs. AASC, 50-3D temperature level, comparison

Here, PCC refers to the same BAS concrete sample with a w/c ratio of 0.38 as the "w/c 0.38 50-3D" sample in Figure 5-6. For AASC, no other temperature levels were tested.

XRD analysis on AAS has confirmed the presence of certain expansive products typical to AAS /AASC mixes. This, however, does not explain the reasons of expansion in PCC. X-ray diffractograms, with the analysis performed at ~170 hours after casting, are plotted in Figure 5-8. The main expansive product identified, present in all three AAS mixes is identified as hydrotalcite ($Mg_6Al_2(CO_3)(OH)16{\cdot}4(H_2O)$, which is a typical hydration product in AAS. It forms readily in the presence of available MgO as a function of the activator type and curing conditions; e.g., (Chen and Brouwers 2007, Haha et al. 2011, 2012, Gu et al. 2014, Ke et al. 2016, Ye and Radlinska 2016, Myers et al. 2017).

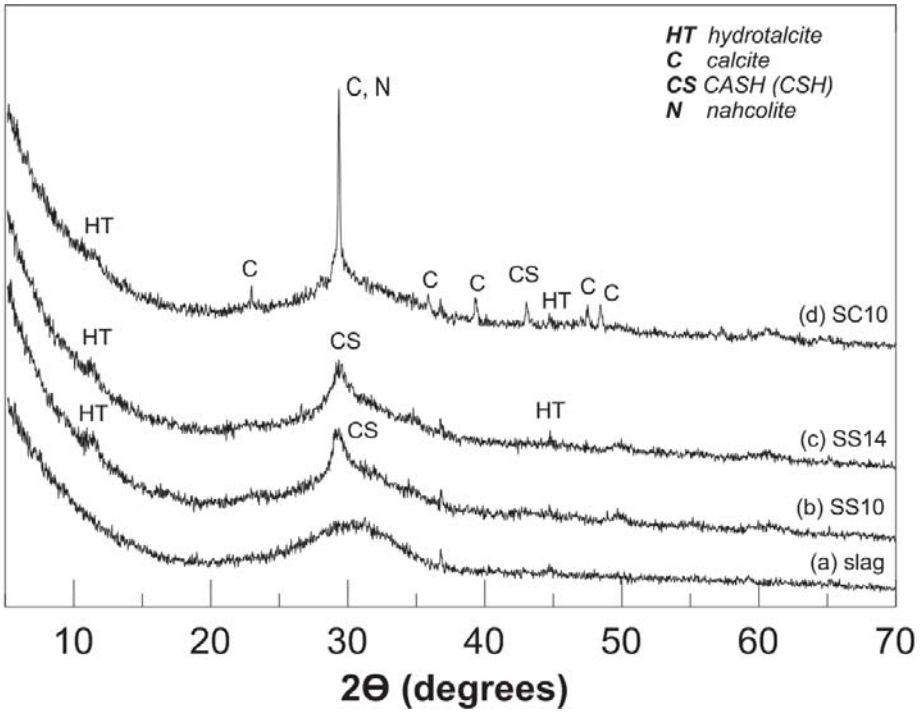

Figure 5-8: X-Ray diffractograms for AAS; (a) unreacted slag, (b) heat-cured SS10; (c) heat-cured SS14; (d) heat-cured SC10

The XRD analysis (more in detail in Paper 5) alone did not unequivocally clarify the differences in the *magnitude* of the observed expansion in the different AAS mixes. Further, it is only suspected that the hydration products causing the – compared to AAS, little – expansion in the PCC sample could be ettringite (Termkhajornkit et al. 2005) or possibly some brucite, although the MgO content of the cement is rather low to encourage brucite formation.

Another possible explanation for the expansion in the PCC sample is the amount of gypsum present in the binder. The SO_3 content of a Type II cement with less than 8% C_3A is generally limited to 3%. The BAS cement contains 5.2% C_3A and its gypsum content is marginally over the limit; 3.4%. Too much gypsum may cause expansion. It is also described in the US ASTM C 452 (ASTM 1995) that expansion in mortars between 24 hours and 14 days is measured when SO_3 is added to the cement in a fraction up to 7% (Advanced Concrete Technology, 2003).

5.4 Decoupled deformations

Modeling (using the Model described in Chapter 3) and decoupling of deformations are presented in Paper 4. An extract of the results is presented here.

Decoupling of deformations has only been performed for the PPC mixes. As mentioned before, decoupling as post-processing requires first a timescale conversion from real time to equivalent time/concrete age, which for AASC is not feasible at the time of writing. A further prerequisite is the knowledge of the development of the thermal coefficient which is expected to vary wildly for young AAS/AASC. Due to the fact that besides hydration, geopolymerization is also present, depending on the exact mix, activator type, and curing conditions, hydration products different to OPC are expected along with a different pore structure to form that further complicate the development of CTE.

Figure 5-9 through Figure 5-12 present the (graphical) results for the lower w/c concrete mix prepared with Type II/A BAS cement. For data on the w/c 0.55 concrete and fitting parameters, the Reader is redirected to Paper 4.

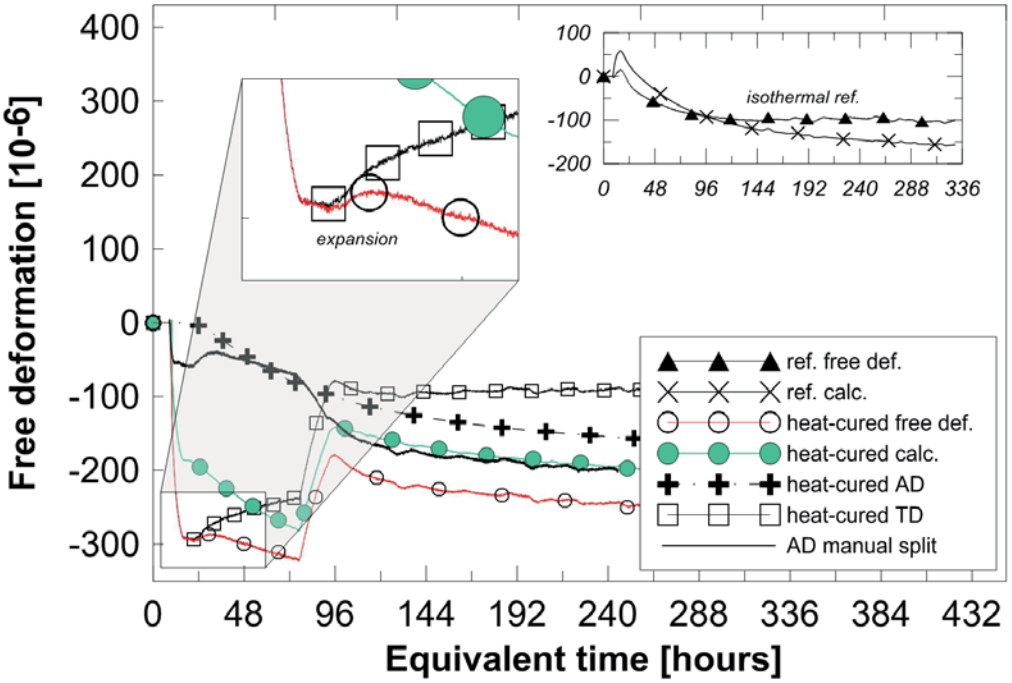

Figure 5-9: PCC w/c 0.38 cured at 6 ^{o}C for 5 days vs. reference sample

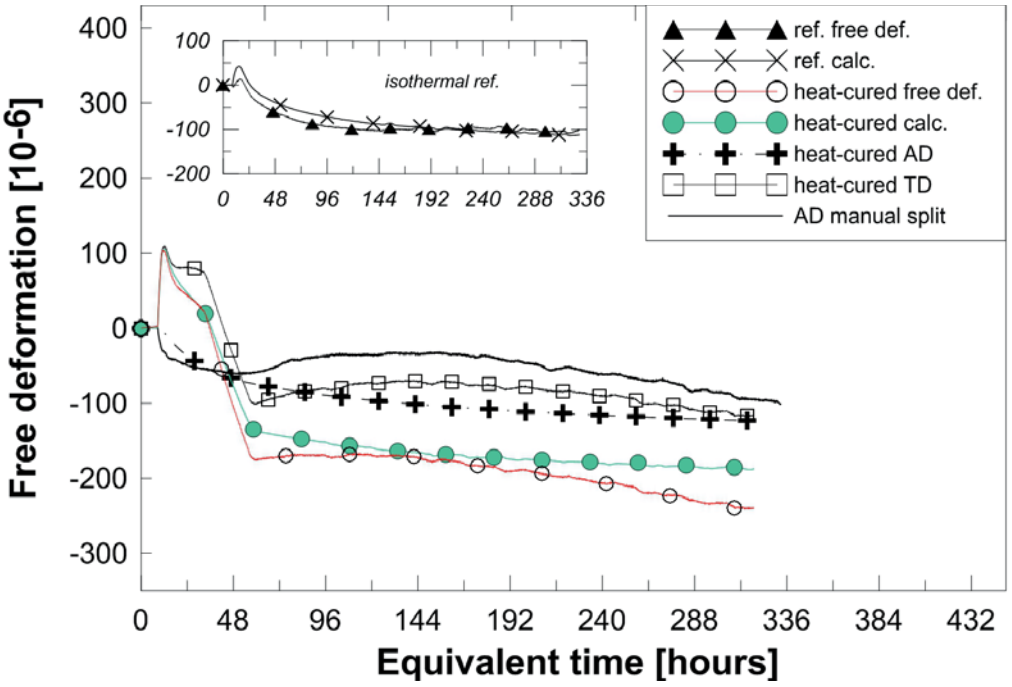

Figure 5-10: PCC w/c 0.38 cured at 35 ^{o}C for 1 day vs. reference sample

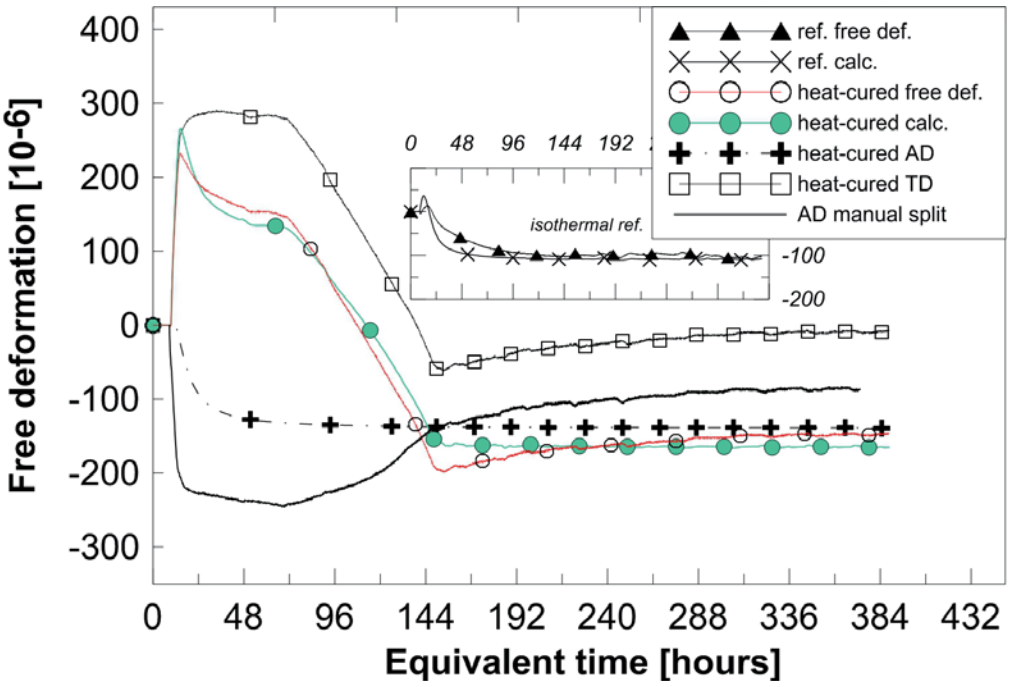

Figure 5-11: PCC w/c 0.38 cured at 50 ^{o}C for 1 day vs. reference sample

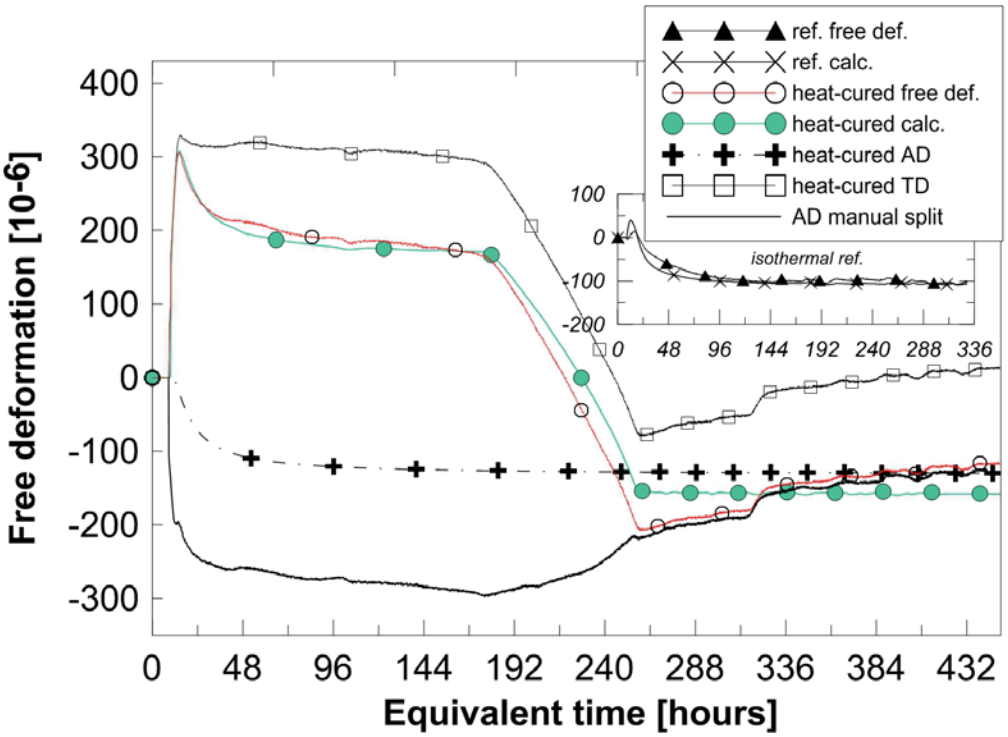

Figure 5-12: PCC w/c 0.38 cured at 50 ^{o}C for 3 days vs. reference sample

In the figures above, "free def." denotes the measured free deformations for both the heat-cured and the isothermally cured reference sample, as indicated; "calc." stands for the *best fitting* achieved with the HH model, for both samples. For the heat-cured sample, AD + TD splitting using the HH model was performed marked with "heat-cured AD" and "heat-cured TD", respectively. Finally, manual splitting (marked as "AD manual split") was performed by offsetting the recorded free deformation with ε_{TD}, assuming a constant CTE of 10×10^{-6} $1/^{0}$C.

All fitting has been performed on a sample-per-sample basis. Ideally, at least a pair of samples (heat-cured and isothermal reference sample) per mix and curing temperature level would be attempted with the same set of parameters, but this was not feasible so all fitting has been optimized fort the *heat-cured sample* only. From a practical point of view, mass fitting across all samples of the same mix, regardless of curing temperature level would be optimal to obtain a minimum number of fitting parameters to perform shrinkage- and cracking risk predictions with. In practice, however, no two samples of the same concrete mix have been possible to evaluate simultaneously.

As it can be seen from the results, for blended cement concretes, overall, even the "best fit" for autogenous deformation (AD) obtained with the HH model did not provide a satisfactory approximation to the recorded free deformations. The expansive stage cannot be adequately modeled because the core assumption of the model is that the deformation of a heat cured sample can be related to that of a reference sample (contraction) through two simple multiplication factors (Eq. 5.). As it can be seen from all reference sample plots in Figure 5-9 through Figure 5-12, apart from a small expansion due to heat of hydration in the very beginning, the deformation is always contraction through the entire range. From the manual splitting (marked as "AD manual split" in all plots), it can be deduced that the "AD manual split" and the behavior if the reference samples are simply not comparable in terms of shape. In the reference samples, the calculated AS ranges from being underestimated (w/c 0.55 50-1D in Paper 4) through good fit (e.g., Figure 5-12) to significantly overestimated (e.g., w/c 0.38 6-5D in Figure 5-9 and, most prominently, w/c 0.55 35-1D).

Depending on the exact temperature level, in some cases, the model gives an acceptable fit until about halfway into the cooling down stage. Best fit for this part is obtained for the 35 °C temperature level, while worst fit is obtained for both 6

°C samples that exhibit unexplained swelling right after having undergone cooling down from 20 °C to 6 °C at a steep rate. Past halfway into the cooling down is the part of the deformation path where several authors in literature have found that the autogenous expansion begins, as summarized in the state-of-the-art part of the thesis. Subsequently, this is the part where the HH model cannot approximate the lab data with an acceptable precision. Furthermore, the "AD manual split" curves reveal that autogenous expansion may, in fact, have begun earlier than in can be seen in the free deformation plots. The "AD manual split" results are more consistent with current literature that states that swelling begins already during cooling down, not after. According to this manual splitting, even the 35 °C sample swells significantly during cooling off. For all mixes, the swelling lasts for *several days* after the temperatures have already stabilized. It must be emphasized here that the "AD manual split" was still performed with an assumed constant CTE when it is known to be untrue. The development of CTE is heavily influenced by the internal RH of the sample (Sellevold and Bjøntegaard 2006). This is due to the fact that the CTE of water is about seven times higher in comparison with hardened concrete. In young concrete, CTE decreases sharply during the first hours after casting due to large amounts of free water from $20x10^{-6}$/°C to ~$7x10^{-6}$/°C at around the setting time (Cusson and Hoogeveen 2006, Loser et al. 2010, Chu et al. 2012). Thereafter, it slowly increases due to self-desiccation (Sellevold and Bjøntegaard 2006), converging to the value characteristic of hardened concrete, which is in the range of 9…12 $x10^{-6}$/°C. The reduction around setting time can be related to the fact that before setting, the free water is continuous while as a solid skeleton is being built up, this continuity is disrupted.

For a specific mix of interest and temperature path, CTE can be measured "stepwise", (Bjøntegaard 1999). During the intervals where the temperature is kept constant, only AD is recorded as a function of the entire temperature history leading up to that point. Conversely, when an "instantaneous" thermal load is applied in steps, ideally, pure TD can be measured. A similar method was applied also for mortars (Loukili et al. 2000) and pastes (Sellevold et al. 2005, Maruyama and Teramoto 2013).

Part of the sources of error in modeling is that the HH model employs a constant thermal expansion/contraction coefficient (CTE). CTE values for hardened concrete are published in literature, but data for early-age concrete are rather limited and inconsistent. For young concrete, *by now*, a vast number of

studies indicate that the CTE is highly nonlinear. This knowledge has not been implemented in the HH model. However, according to (Bjøntegaard 1999), calculated AD did not become more consistent and most importantly, the *swelling did not disappear* across multiple mixes when using more "realistic" CTE alone. This suggests that the anomalies introduced by assuming a constant CTE are only part of the problem. The core problem appears to be that swelling as a phenomenon is not accommodated by the model.

Not surprisingly, for the cooled down sample (Figure 5-9) the model can catch the rate of shrinkage after 96 hours (because the sample contracts at that stage), but underestimates it by about 50 microstrains. For all other samples, the expansion part cannot be modeled satisfactorily.

One of the known limitations of the HH model is that it only considers the w/c ratio as the primary influencing factor that determines the AS, which has been shown to underestimate the shrinkage and results in a large scatter for self-compacting concretes (Long et al. 2011). Perhaps Eq. 3 could be updated to incorporate SCM content and other factors that are known to influence autogenous shrinkage. The other known problem is that in the original HH model, shrinkage measurements were initiated at 24 hours of age. Before that, it is assumed that the concrete is plastic and no stresses are developing. In the current test series, the samples were demolded at 8 hours and the measurements zeroed (started) at 8.5 hours which age range has not been intended to be covered by the original model. Considering that a significant percentage of AS occurs in the first 1-2 days of age, this would partly explain the cases where the fit is unsatisfactory, both in terms of expansion due to hydration heat and the subsequent contraction part. This is the case for both w/c 6-5D and 50-1D samples, and the w/c 0.55 50-3D sample.

The errors in modeling manifest even more markedly when the backcalculated thermal deformations (TD) are evaluated. TD is obtained by simply offsetting the measured free deformation by the calculated AD. Naturally, this results in calculated TD that is inconsistent with the imposed temperature paths. In reality, samples are kept at isothermal ambient temperature once the heat curing part finished. However, the calculated TD during isothermal conditions is never a flat line as it should be. This is, however, simply an artifact due to the AD part not being approximated properly - however, it serves as an excellent visual checkpoint.

6 DISCUSSION AND CONCLUSIONS

6.1 Research questions and answers

In Chapter 1, the following research questions have been formulated:

RQ1. ***What materials are most suitable for strengthening concrete structures with cementitious strengthening systems (bonded overlays) for optimum structural performance?***

A1. Based on the experimental work performed in the framework of the Licentiate thesis (Papers 1 and 2), *strain hardening mortars* such as ECC have exhibited better performance than quasibrittle ones both in terms of deformation capacity and in their ability to reduce local stress concentrations in the grid joints, which is in line with the literature (Dai et al. 2009). The better performance is indicated by the finer and more evenly distributed cracks, as evidenced by DIC strain images (Paper 2) and the absence of large drops in load capacity when grid tows fail in a subsequent manner. Furthermore, the ECC samples exhibited significant tensile strain hardening behavior – the contribution of the ECC matrix over the load capacity of the embedded grid. ECC also prevented spalling of the mortar, in line with the existing literature, by e.g. (Lim and Li 1997, Kanda et al. 2003), in specimens where with the same grid orientation and size, spalling of the quasi-brittle mortar was observed in the wedge-splitting tests. It can also be said, based on the state-of-the-art performed that from a durability point of view – a prerequisite to long term structural performance – strain hardening materials hold a promise because their fully microcracked state is often characterized by such tight crack widths that, in terms of permeability, they can still be considered uncracked (Weimann and Li 2003).

Although only stiff grids have been tested, based on the state-of the-art, a *flexible technical fabric* would probably be an even more suitable material. A textile is thinner, it is easier to work with and apply since it does not have a residual curvature. The grid comes in rolls and it needs to be evened out and held in place

in order to stay positioned in the midplane of the strengthening layer. There are no fixed, brittle joints; therefore, the fabric allows for more deformation when loaded in an angle other than fiber direction.

Higher first cracking strength, strain hardening over the polymer-modified, quasibrittle mortar, smaller drops in load capacity after first cracking, and significantly higher fracture energy have also been shown in the wedge splitting tests. For in-depth information on the wedge-splitting tests, the reader is referred to the Licentiate thesis (Orosz 2013).

It has been established on the level of the state-of-the-art part of this thesis that certain alkali activated materials have a strengthening potential; in particular, fully geopolymerized, fly ash-based strain hardening mortars with small fractions of chopped PVA fibers; e.g., (Shaikh 2013a, Shaikh and Lu 2013, Shaikh et al. 2013, Ohno and Li 2014, Nematollahi et al. 2015a). However, to the author's knowledge, no actual strengthening applications with strain hardening fly ash based AAM have been studied yet. Only the current trends in material development can be identified. Metakaolin-based geopolymers have been tested for concrete retrofitting purposes, in combination with carbon fiber sheets by (Vasconcelos et al. 2011). Satisfactory adhesion on the concrete – geopolymer interface has been obtained; however, the adhesion strength between the geopolymer and the CFRP was low.

RQ2. ***How does the ductility of the mortar influence the strength, strain capacity, and cracking behavior of the overlay? What are the impacts of the material choice on durability?***

A2. Two test series have been conducted aiming to characterize the tensile behavior. First, uniaxial tests were carried out on upscaled dogbone samples, on the bare strengthening material (mortar + grid). The second test series, the wedge-splitting test targeted specifically the deformation capacity and fracture behavior. Both tests involved PMM (polymer-modified, quasibrittle) and ECC (engineered cementitious composite, strain hardening) mortars and CFRP grids of different geometry and fiber amount.

Both the dogbone and the wedge splitting tests resulted in specimens failing with FRP rupture in accordance with earlier results from (Blanksvärd, 2007), indicating that there is a *satisfactory bond* within the system, both on the concrete-

composite interface and within the mortar and the grid component. The *strengthening effect* of the ECC exceeded that of the PMM by up to 42% (WST), and up to 110% (direct tensile tests). *First cracking strength* was barely noticeably improved by the ECC (direct tensile tests); however, up to 33% increase has been achieved in the WST tests. Furthermore, the strain-hardening mortar has been found to enhance both the load bearing-, and the in particular, the deformation capacity. It has also been shown that the ECC mortar is capable to shift the overall behavior from brittle towards a *more ductile failure* (no spalling, no large drops in load capacity as the grid gradually fails). *Multiple cracking* was observed in all samples with ECC. Accordingly, the calculated fracture energy (WST tests) was significantly enhanced for the ECC samples. All these findings are in line with the state-of-the-art literature on ECC; e.g., (Li 1998, 2008, Fischer and Li 2002, Li et al. 2009).

Strain hardening could be shown in both tests. In the uniaxial tests, there was little improvement in the first cracking strength, regardless of the strengthening material composition. However, after first cracking, a significant strain hardening effect could be shown in case of the ECC mortars, while moderate to no hardening (depending on the exact mortar – grid combination) in the PMM specimens. It has been confirmed that replacing the PMM by ECC would result in strain hardening behavior. In the wedge-splitting tests, it could be observed that the strain hardening behavior was not only material-, but grid direction-dependent. Both mortars, with the grid placed in the "strong" direction (0°-grid orientation) exhibited hardening; with a distinct, steady hardening behavior (ECC) or with a drop in load capacity after first cracking, but "recovering" later (PMM). No hardening was observed when the grid was rotated in a 45° direction, regardless of mortar; furthermore, excessive shear deformations were observed at the grid intersections (where the grid could be seen – PMM). An extreme ductility could be observed – the tests were stopped because of the clip gauge measuring the COD reaching its limit (25 mm), not because of the actual failure of the samples.

RQ3. ***How does temperature curing influence the development of autogenous shrinkage and the cracking risk in cementitious materials (OPC and AAS)? What are possible implications on strengthening systems based on Portland cement?***

A3. As evidenced by the experimental data presented, significant autogenous expansion has been found in both PCC (Papers 3-4) and AAS (Paper 5) mixes. In

PCC, the expansion appears to correlate with the higher curing temperature level. Lower levels of curing temperature have not resulted in expansion beyond measurement precision.

It has been indirectly proven that different curing paths result in concrete with a different microstructure; likely with a different amount and distribution of gel-, meso-, and capillary pores and air voids. This, in turn, would affect both the magnitude and the rate of the contraction and the occurrence and magnitude of the expansion in the recorded free deformations. The observed differences in thermal coefficient support this assumption, since the temperature would affect the rate at which the different hydration products develop; e.g., (Turcry et al. 2002).

The decoupled autogenous deformation across different recipes and temperature levels has shown to be unsystematic; i.e., crossover effects could be observed where the higher temperature curing for a longer time did not necessarily result in higher shrinkage associated, as a function of the equivalent age, or concrete maturity. At higher temperature levels, as established in the state-of-the-art part of the Papers, a strong correlation between equivalent age and autogenous deformation showed to be questionable. This is not new; applicability of the maturity concept has been questioned by several authors since the late 90s and it has been found by several authors that temperature has an unsystematic effect on autogenous deformation; e.g., (Bjøntegaard 1999, Turcry et al. 2002). The microstructure is heavily affected by the curing temperature, particularly at early age exposure to high temperatures while the matrix is still developing.

Based on the initial results obtained with OPC/PCC, only one temperature level was tested for AAS. This provides a limited foundation to draw any kind of generalized statements about the autogenous deformation behavior of AAS undergoing heat curing. However, some conclusions can still be drawn in comparison to the behavior of the OPC/PCC samples. Both the shrinkage and the expansion are magnified in most AAS mixes compared to the OPC/PCC sample cured at the same temperature levels. As indicated in the state-of-the-art, the process and products of hydration are not the same in AAS as in OPC/PCC. While in a high calcium and moderate to high magnesium system, C-(A)-S-H dominant gel forms as opposed to a N-(A)-S-H-type gel (Bernal 2016), this gel has proven different chemical composition (lower C/Si, lower density etc.) and associated mechanical properties than the C-S-H in the OPC.

Considering the higher fraction of SCMs and larger paste volume in repair systems, it is expected that the anomalies regarding the applicability of the maturity concept would be magnified, especially if heat curing is involved. A generalized, maturity concept-based model to describe autogenous deformation in repair mortars, at the time of writing, appears to be a *very* ambitious goal. The underlying shrinkage/expansion mechanisms, their dependence on SCM content, the differences in pore structure and pore size distribution; the exact hydration products, and the effects of temperature gradients need to be addressed first before such a model can be constructed. While direct shrinkage testing has not been performed in repair mortars, it can be said that repair mortars lack coarse aggregates entirely, and their shrinkage behavior when it comes to autogenous shrinkage is largely unknown. It has been shown by several authors that the autogenous deformation of the binder does not necessarily correlate with that of concrete (Bjøntegaard 1999, Lura and Jensen 2005, Sellevold et al. 2005). Several effects skew the behavior in concrete. The first is the internal restraint the aggregates provide. The degree of restraint will also change as the concrete hardens because the stiffness off the aggregates remains constant while the stiffness of the paste builds up. Furthermore, the aggregates have a certain porosity and will store a small amount of water that provides "internal curing" by releasing some water as needed.

Not only experimental data regarding early age autogenous deformation of repair mortars is missing but modeling and cracking risk prediction in general. This could be down to the fact that researchers focusing on the tailoring of high performance repair materials are predominantly material scientists, not necessarily civil engineers. For OPC pastes, (Turcry et al. 2002) showed that the maturity concept is applicable if the temperatures are kept in the 10-40°C range. Outside this range, unsystematic results were obtained, in agreement with e.g. (Bjøntegaard 1999). This suggests that if heat curing is involved, the autogenous behavior of mortars and in particular, the even more obscure alkali activated materials would have to be approached with extreme caution due to the likely relative magnitude of the unsystematic deformations – compared to concrete.

Regarding early age cracking risk, the expansion of the magnitude obtained in the tests can be deemed as beneficial in terms of offsetting some part of the shrinkage stresses.

RQ4. ***Are maturity concept-based models suitable to predict autogenous deformation in cementitious materials? Could these models be used to predict cracking risk of repair systems based on Portland cement?***

A4. Based on the tests and modeling performed in this work, the maturity concept does not appear to be applicable to model heat cured OPC/PCC (or AAS), mainly due to the crossover effects observed. The autogenous deformation behavior of OPC/PCC has indicated that heat curing – in this thesis, at variable levels – results in unsystematic autogenous deformations: (1) the deformation will not necessarily be contraction, (2) crossover effects are observed (a sample cured at higher temperature may shrink less than a sample cured at lower temperature), (3) the occurrence and magnitude of the expansion appears to correlate with the curing temperature level and length (heat curing for a longer time, at a higher temperature level is more likely to induce expansion), however (4) the expansion could not be related to the SCM content (here: fly ash) of the binder.

In AAS undergoing the exact same heat curing path, both the contraction (shrinkage) and the expansion (swelling) were "magnified". This can be attributed partly to the fact that the AAS mixes had a maximum aggregate size of 8 mm while the OPC mixes, 16 mm – therefore, there is a *larger paste volume* undergoing autogenous deformation in the AAS. The SCM in the AAS was slag, not fly ash, and it is known that the hydration processes and -products in AAS differ from those in OPC, as elaborated in the state-of-the-art. Furthermore, since both the magnitude and development rate of AD showing strong temperature history dependence, e.g., (Bjøntegaard 1999, Jensen and Hansen 1999, Bjøntegaard and Sellevold 2001), and so does the development of the thermal coefficient (as shown experimentally, but not determined for every separate mix and temperature path), the temperature effects could not be separated unequivocally. Therefore, the autogenous deformation as such could not be derived from the coupled free deformations.

6.2 General conclusions

6.2.1 The influence of SCM content on the autogenous behavior

The SCM content of the mixes could not be unequivocally linked to the autogenous deformation behavior. The OPC/PCC test results did not prove that fly ash (alone) would be the (sole) reason behind the expansion. The ANLFA mix

with 30% fly ash did not shrink more than the BAS cement samples with only 16% fly ash. It was also expected that the identically cured ANLFA mix would exhibit nearly twice the expansion compared to the BAS mixes because of twice the fly ash content and the coarser cement (in literature, expansion has been associated with coarser cements (Bentz et al. 2001)); however, no expansion was detected for the ANLFA mix. The swelling in the BAS samples may be a consequence of the factory fly ash content being of perhaps different mineral composition than the fly ash that was used for the ANLFA mix.

6.2.2 Thermal coefficient

Another parameter that is largely unknown is the early-age development of the thermal expansion/contraction coefficient both for repair mortars and alkali activated materials. CTE is better documented for OPC and cement pastes, as a short survey in Section 5.4, but with the recent surge of large amounts of SCMs being incorporated in binders, there is still no universal "early age CTE database" that could be used for decoupling, especially because CTE itself is also a product of the particular curing path (internal RH, hydration products and differences in pore structure as a result of the curing path).

Since heat curing means that, regardless of the testing method, the recorded autogenous and thermal deformations are always fully coupled, without having a "proper" thermal coefficient, decoupling is fictitious at best. If an improper CTE is used, autogenous swelling might simply get overlooked. In extreme cases, it could even mean that preventive measures taken to reduce the assumed high shrinkage are inappropriate altogether, as (Viviani et al. 2007) warn.

Although calibration of the thermal coefficient has not been in the focus of this work (this would require another PhD project, since the thermal coefficient is also a product of the entire temperature history), it has been shown experimentally that different curing paths generate different thermal coefficients; likely because of the different development of hydration products and/or pore structure. Thermal coefficient decreases with increased porosity as shown by (Zeng et al. 2012) in cement pastes. The authors assumed that the decrease in thermal coefficient in pastes and mortars may be related to a dense shell in low Ca/Si C-S-H forming around air voids. Again, since the paste volume is larger in mortars and the pore water content (correlating with the degree of hydration) heavily influences the magnitude of the thermal coefficient at a given stage of hydration, one can deduce

that variations in the thermal coefficient are likely even larger in mortars than in concrete. The effects of the C-(A)-S-H in AAS, or even, C-(N)-(A)-S-H phases (depending on calcium content and activator) in AAMs could result in significantly different thermal coefficients in alkali activated materials.

As illustrated in Paper 5, the "thermal drop" in all AAS mixes, for the same curing path, was larger than that in PCC. At this point, it is impossible to determine whether the larger thermal drop is attributed to a larger thermal coefficient, because the entire deformation – including the thermal drop – consists of fully coupled autogenous and thermal deformations, and the rate of the autogenous shrinkage in the AAS is higher preceding the thermal drop, so it is possible that the thermal drop is more pronounced than in PCC predominantly because of the autogenous component being significantly larger. Since it is generally accepted that the hydration processes (at least the formation of the outer C-S-H) of alkali activated materials are accelerated compared to OPC (Gruskovnjak 2006), this in turn would mean accelerated self-desiccation, therefore a lower internal RH at the same stage, which would result in a potentially lower thermal coefficient, all else (porosity, thermal coefficients of the hydration products) being the same because the thermal coefficient is heavily influenced by the moisture content (Sellevold and Bjøntegaard 2004). *If* the thermal coefficient at the same stage of curing is indeed lower than in OPC, it would imply that the relative importance of using a "proper" thermal coefficient for decoupling deformations is lesser than in OPC. At the same time, the relative importance of understanding and quantifying *autogenous deformation* of AAS to optimize material performance and reduce early age cracking risk would be magnified.

7 FUTURE RESEARCH

7.1 Material development

For strengthening purposes, tailored alkali activated materials could be developed, once the shrinkage/expansion mechanism is understood and can be quantified. The feasibility studies that have been published on PVA fiber-reinforced alkali activated materials, e.g., (Ohno and Li 2014, Nematollahi et al. 2016) should be expanded and the newly developed materials evaluated for strengthening purposes; both in terms of strengthening effect, and regarding their bond behavior/compatibility with the base concrete. The tensile ductility and the strain hardening behavior – comparable to that of ECC – these materials exhibit are some of the most sought-after feature of high performance repair mortars. An important engineering aspect of AAS is that they have much denser microstructure than concrete; e.g., (Lee et al. 2014). Furthermore, as reviewed in Section 2.2, some of these materials have the potential to exhibit such controlled crack widths that, from a durability point of view, they can be considered uncracked (Weimann and Li 2003) even when fully microcracked (Sahmaran et al. 2009).

Since most of the PVA-reinforced alkali-activated materials have been fly ash-based and, hence, fully polymerized geopolymers with an amorphous N-A-S-H type gel, the hydration mechanisms and probably the associated shrinkage behavior are likely even more complex than those in a C-A-S-H type gel; however, the compatibility with the base concrete for strengthening purposes is likely to be better because of the gel also filling the capillary pores as a "true gel", resulting in good bond to most materials (Provis and Van Deventer 2009, Hlavacek 2014). Shrinkage-optimized PVA-reinforced alkali activated materials could also be used in combination with technical fabrics or textiles, in a textile reinforced concrete-like manner. The high pH of the alkali-activated materials may have an adverse effect on the FRP reinforcement; the interaction needs to be investigated. The adhesion between e.g. carbon and alkali activated materials has been proven low by some authors; e.g. (Menna et al. 2013). If incorporating high amounts of slag, the (often too short) setting time may need to be also tailored for improved workability. Short setting time, however, can be an advantage; e.g., when using the strengthening material on vertical surfaces. The use of sodium carbonate as activator

in AAS may result in setting times and shrinkage properties comparable to OPC (Duran Atics et al. 2009).

7.2 Restrained shrinkage and compatibility issues

The importance to assess restrained shrinkage for strengthening purposes has been emphasized by (Torgal et al. 2015). One way to reduce shrinkage might be adding active magnesia; some research has already been done on the shrinkage-mitigating effects of added MgO on AAS (Fang et al. 2011). The chemical compatibility and absorption properties of alkali activated materials might need to be improved in order to prevent debonding from the concrete substrate.

7.3 Hydration mechanisms

For truly high performance materials with high fractions of SCM (such as repair mortars, like ECC), and alkali activated materials with hydration (or geopolymerization) mechanisms different from those in OPC, first the existence and nature of autogenous expansion should be confirmed and investigated, as it is *likely* to appear in a prominent way under certain curing conditions, as indicated by PCC and AASC tests performed in this PhD work – especially *if* heat cured. The mechanisms behind expansion (if found) should be clarified by performing XRD analysis to determine the exact hydration products that cause it. For example, in AAS systems with a moderate to high (over 5%) fraction of MgO and activated with sodium carbonate, (expansive) hydrotalcite has been shown to form (Bernal 2016) while calcium hydroxide ($Ca(OH)_2$) has typically not been found in AAS (Guerrieri et al. 2009) unless expansive admixtures are used, e.g., (Yuan et al. 2014). The effect of different activator – SCM combinations could result in an array of crystalline phases generated.

7.4 Modeling approaches

In order to predict shrinkage behavior even in "plain" OPC, it has been shown necessary to calibrate the thermal expansion/contraction coefficient. A calibrated coefficient may result in more reasonable decoupled deformations; however, it likely does not target the core issue with models based on the maturity concept, which has been identified as the unsystematic nature (Bjøntegaard 1999)

of the deformations (crossover effects). Other modeling approaches, e.g., micromechanical models based on capillary tension or activation energy have been suggested for pastes and concrete, e.g., (Chu et al. 2012, Zhang et al. 2012) which the author believes to be a more viable approach.

8 REFERENCES

Bakharev T, Sanjayan J, Cheng Y-B. 2000. Effect of admixtures on properties of alkali-activated slag concrete. Cement and Concrete Research. 30:1367–1374.

Bentur A, Kovler K. 2003. Evaluation of early age cracking characteristics in cementitious systems. Materials and Structures. 36:183–190.

Bentz DP, Jensen OM, Hansen KK, Olesen JF, Stang H, Haecker C-J. 2001. Influence of Cement Particle-Size Distribution on Early Age Autogenous Strains and Stresses in Cement-Based Materials. Journal of the American Ceramic Society. 84:129–135.

Bentz DP, Jones SZ, Peltz MA, Stutzman PE. 2015. Mitigation of autogenous shrinkage in repair mortars via internal curing. Concrete in Australia. 41:35–39.

Bernal SA. 2016. Advances in near-neutral salts activation of blast furnace slags. RILEM Technical Letters. 1:39–44.

Bernal SA, Provis JL. 2014. Durability of Alkali-Activated Materials: Progress and Perspectives. Journal of the American Ceramic Society. 97:997–1references008.

Bissonnette B, Courard L, Garbacz A, Vaysburd A, Fay K von. 2014. Concrete repair bond: evaluation and factors of influence. In: Proc Concrete Solutions-5th Int Conf on Concrete Repair. pp. 51–57.

Bjøntegaard Ø. 1999. Thermal Dilation and Autogenous Deformation as Driving Forces to Self-Induced Stresses in High Performance Concrete. PhD Thesis, The Norwegian University of Science and Technology, Trondheim, Norway.

Bjøntegaard Ø, Sellevold EJ. 2001. Interaction between thermal dilation and autogenous deformation in high performance concrete. Materials and Structures. 34:266–272.

Blanksvärd T. 2007. Strengthening of concrete structures by the use of mineral based composites. Department of Civil and Environmental Engineering. Licentiate Thesis, Luleå University of Technology, Luleå, Sweden.

Blanksvärd T. 2009. Strengthening of concrete structures by the use of mineral-based composites: System and design models for flexure and shear. Luleå University of Technology. PhD Thesis, Luleå University of Technology, Luleå, Sweden.

Blanksvärd T, Carolin A, Täljsten B. 2008. Shear crack propagation in MBC strengthened concrete beams. In: Proceeding of the Fourth International Conference on FRP Composites in Civil Engineering, Zurich, Switzerland. pp. 22–24.

Blanksvärd T, Täljsten B, Carolin A. 2009. Shear strengthening of concrete structures with the use of mineral-based composites. Journal of Composites for Construction. 13:25–34.

Brühwiler E, H. WF. 1990. The wedge splitting test: A method of performing stable fracture mechanics tests. Engineering Fracture Mechanics. 35:117–125.

Cartwright C, Rajabipour F, Radlińska A. 2015. Shrinkage Characteristics of Alkali-Activated Slag Cements. Journal of Materials in Civil Engineering. 27.

Chen L, Wang Z, Wang Y, Feng J. 2016. Preparation and Properties of Alkali Activated Metakaolin-Based Geopolymer. Materials. 9:767.

Chen W, Brouwers H. 2007. The hydration of slag, part 1: reaction models for alkali-activated slag. Journal of Materials Science. 42:428–443.

Choi J-I, Song K-I, Song J-K, Lee BY. 2016. Composite properties of high-strength polyethylene fiber-reinforced cement and cementless composites. Composite Structures. 138:116–121.

Chu I, Kwon SH, Amin MN, Kim J-K. 2012. Estimation of temperature effects on autogenous shrinkage of concrete by a new prediction model. Construction and Building Materials. 35:171–182.

Collins F, Sanjayan J. 2000. Effect of pore size distribution on drying shrinking of alkali-activated slag concrete. Cement and Concrete Research. 30:1401–1406.

Colombo I, Colombo M, Magri A, Zani G, Prisco M di. 2012. Tensile Behavior of Textile: Influence of Multilayer Reinforcement. In: High Performance Fiber Reinforced Cement Composites 6. RILEM. pp. 463–470.

Contamine R, Si Larbi A, Hamelin P. 2010. Matrix and Fabric Impregnation Influence on Textile Reinforcement Concrete Behaviour. In: The 5th International Conference on FRP Composites in Civil Engineering [CICE 2010]. Beijing, China.

Control of Cracking in Concrete - State of the Art. 2006. Washington, USA: Transportation Research Board.

Courard L, Bissonnette B, Garbacz A. 2015. Fundamental approach for the concept of concrete repair compatibility. Concrete Repair, Rehabilitation and Retrofitting IV. 164.

Cusson D, Hoogeveen T. 2006. Measuring early-age coefficient of thermal expansion in high-performance concrete. In: International RILEM Conference on Volume Changes of Hardening Concrete: Testing and Mitigation RILEM Publication, Lyngby, Denmark.

Cusson D, Hoogeveen T. 2008. Internal curing of high-performance concrete with pre-soaked fine lightweight aggregate for prevention of autogenous shrinkage cracking. Cement and Concrete Research. 38:757–765.

Dai JG, Wang B, Xu SL. 2009. Textile reinforced engineered cementitious composites (TR-ECC) overlays for the strengthening of RC beams. In: The Second Asia-Pacific Conference on FRP in Structures [APFIS 2009]. Seoul, Korea. pp. 75–80.

Duran Atics C, Bilim C, Çelik Ö, Karahan O. 2009. Influence of activator on the strength and drying shrinkage of alkali-activated slag mortar. Construction and Building Materials. 23:548–555.

Emborg M. 1989. Thermal stresses in concrete structures at early age. PhD Thesis, Luleå University of Technology, Luleå, Sweden.

Fang Y, Liu J, Chen Y. 2011. Effect of magnesia on properties and microstructure of alkali-activated slag cement. Water Science and Engineering. 4:463–469.

Fernández-Jiménez A, Puertas F, Sobrados I, Sanz J. 2003. Structure of calcium silicate hydrates formed in alkaline-activated slag: influence of the type of alkaline activator. Journal of the American Ceramic Society. 86:1389–1394.

Fischer G, Li VC. 2002. Influence of matrix ductility on tension stiffening behavior of steel reinforced engineered cementitious composites (ECC). ACI Structural Journal. 99:104–111.

Fjellström P. 2013. Measurement and modelling of young concrete properties. LicentiateThesis, Luleå University of Technology, Luleå, Sweden.

Funke H, Gelbrich S, Kroll L. 2016. The Durability and Performance of Short Fibers for a Newly Developed Alkali-Activated Binder. Fibers. 4:11.

Garbacz A, Courard L, Bissonnette B. 2013. A surface engineering approach applicable to concrete repair engineering. Bulletin of the Polish Academy of Sciences: Technical Sciences. 61:73–84.

Garcia-Lodeiro I, Palomo A, Fernández-Jiménez A, Macphee D. 2011. Compatibility studies between NASH and CASH gels. Study in the ternary diagram Na_2O-CaO-Al_2O_3-SiO_2-H_2O. Cement and Concrete Research. 41:923–931.

Grasley ZC, Lange DA. 2007. Thermal dilation and internal relative humidity of hardened cement paste. Materials and Structures. 40:311–317.

Gruskovnjak A. 2006. Hydration Mechanisms of Activated Blast Furnace Slag.

Gu K, Jin F, Al-Tabbaa A, Shi B, Liu J. 2014. Mechanical and hydration properties of ground granulated blastfurnace slag pastes activated with MgO-CaO mixtures. Construction and Building Materials. 69:101–108.

Guerrieri M, Sanjayan JG, Collins F. 2009. Residual compressive behavior of alkali-activated concrete exposed to elevated temperatures. Fire and Materials. 33:51–62.

Haha MB, Lothenbach B, Saout G Le, Winnefeld F. 2012. Influence of slag chemistry on the hydration of alkali-activated blast-furnace slag—Part II: Effect of Al2O3. Cement and Concrete Research. 42:74–83.

Haha MB, Saout G Le, Winnefeld F, Lothenbach B. 2011. Influence of activator type on hydration kinetics, hydrate assemblage and microstructural development of alkali activated blast-furnace slags. Cement and Concrete Research. 41:301–310.

Hai Y, Zhu Y. 2009. Mesocosmic study on autogenous shrinkage of concrete with consideration of effects of temperature and humidity. Water Science and Engineering. 2:85–94.

Hassan KE, Brooks JJ, Al-Alawi L. 2001. Compatibility of repair mortars with concrete in a hot-dry environment. Cement and Concrete Composites. 23:93–101.

Hedlund H. 2000. Hardening Concrete: Measurements and Evaluation of Non-Elastic Deformation and Associated Restraint Stresses. PhD Thesis, Luleå University of Technology, Luleå, Sweden.

Hedlund H, Jonasson J-E. 2000. Effect on stress development of restrained thermal and moisture deformation. Proceedings of Shrinkage. 355–375.

Hillerborg A, Modéer M, Petersson PE. 1976. Analysis of crack formation and crack growth in concrete by means of fracture mechanics and finite elements. Cement and Concrete Research. 6:773–781.

Hlavacek P. 2014. Engineering properties of alkali activated composites. PhD Thesis, Czech Technical University in Prague, Prague, Czech Republic.

Holt E, Leivo M. 2004. Cracking risks associated with early age shrinkage. Cement and Concrete Composites. 26:521–530.

Holt EE. 2001. Early age autogenous shrinkage of concrete. PhD Thesis, University of Washington, USA. Published by the Technical Research Centre of Finland (VTT).

Häußler-Combe U, Jesse F, Curbach M. 2004. Textile reinforced concrete-overview, experimental and theoretical investigations. In: Fracture Mechanics of Concrete Structures Proceedings of the Fifth International Conference on Fracture Mechanics of Concrete and Concrete Structures, Ia-FraMCos, Vail, CO, USA. pp. 12–16.

Jensen OM, Hansen PF. 1999. Influence of temperature on autogenous deformation and relative humidity change in hardening cement paste. Cement and Concrete Research. 29:567–575.

Jesse F, Will N, Curbach M, Hegger J. 2008. Load-bearing behavior of textile-reinforced concrete. ACI Special Publication. 250.

Kanda T, Saito T, Sakata N, Hiraishi M. 2003. Tensile and anti-spalling properties of direct sprayed ECC. Journal of Advanced Concrete Technology. 1:269–282.

Ke X, Bernal SA, Provis JL. 2016. Controlling the reaction kinetics of sodium carbonate-activated slag cements using calcined layered double hydroxides. Cement and Concrete Research. 81:24–37.

Klausen AB. 2016. Early age crack assessment of concrete structures: Experimental investigation of decisive parameters. PhD Thesis, Norwegian University of Science and Technology, Trondheim, Norway

Kramar S, Sajna A, Ducman V. 2016. Assessment of alkali activated mortars based on different precursors with regard to their suitability for concrete repair. Construction and Building Materials. 124:937–944.

Lee NK, Jang JG, Lee HK. 2014. Shrinkage characteristics of alkali-activated fly ash/slag paste and mortar at early ages. Cement and Concrete Composites. 53:239–248.

Li G, Wang Z. 2017. A Mesoscopic Simulation for the Early-Age Shrinkage Cracking Process of High Performance Concrete in Bridge Engineering. Advances in Materials Science and Engineering. 2017.

Li M, Li VC. 2011. High-Early-Strength Engineered Cementitious Composites for Fast, Durable Concrete Repair-Material Properties. ACI Materials Journal. 108:3–12.

Li VC. 1998. Repair and retrofit with engineered cementitious composites. In: Fracture Mechanics of Concrete Structures [FRAMCOS-3]. Gifu, Japan: AEDIFICATIO Publishers, Germany.

Li VC. 2008. Engineered Cementitious Composite (ECC): Material, Structural and Durability Performance. In: Concrete Construction Engineering Handbook. Taylor & Francis Group, LLC.

Li VC, Fischer G, Lepech MD. 2009. Shotcreting with ECC. In: Kusterle, Wolfgang, ed. Spritzbeton-Tagung. Alpbach, Austria.

Li VC, Horii H, Kabele P, Kanda T, Lim YM. 2000. Repair and retrofit with engineered cementitious composites. Engineering Fracture Mechanics. 65:317–334.

Li VC, Wang S, Wu C. 2001. Tensile Strain-Hardening Behavior of Polivinyl Alcohol Engineered Cementitious Composite (PVA-ECC). ACI Materials Journal. 98:483–492.

Li VC, Wu C, Wang S, Ogawa A, Saito T. 2002. Interface tailoring for strain-hardening polyvinyl alcohol-engineered cementitious composite (PVA-ECC). Materials Journal. 99:463–472.

Lim YM, Li VC. 1997. Durable repair of aged infrastructures using trapping mechanism of engineered cementitious composites. Cement and Concrete Composites. 19:373–385.

Linsbauer HN, Tschegg EK. 1986. Fracture energy determination of concrete with cube-shaped specimens. Zement Und Beton. 31:38–40.

Lodeiro IG, Macphee D, Palomo A, Fernández-Jiménez A. 2009. Effect of alkalis on fresh C-S-H gels. FTIR analysis. Cement and Concrete Research. 39:147–153.

Long WJ, Khayat KH, Xing F. 2011. Prediction on autogenous shrinkage of self-consolidating concrete. In: Advanced Materials Research. pp. 288–292.

Loser R, Münch B, Lura P. 2010. A volumetric technique for measuring the coefficient of thermal expansion of hardening cement paste and mortar. Cement and Concrete Research. 40:1138–1147.

Loukili A, Chopin D, Khelidj A, Touzo J-Y Le. 2000. A new approach to determine autogenous shrinkage of mortar at an early age considering temperature history. Cement and Concrete Research. 30:915–922.

Lura P, Breugel K van, Maruyama I. 2001. Effect of curing temperature and type of cement on early-age shrinkage of high-performance concrete. Cement and Concrete Research. 31:1867–1872.

Lura P, Jensen OM. 2005. On the measurement of free deformation of early age cement paste and concrete [Bjøntegaard Ø, Hammer TA, Sellevold EJ. Cement & Concrete Composites 2004; 26: 427-435]. Cement and Concrete Composites. 27:854–856.

Maalej M. 2012. Structural Applications of Hybrid Fiber Engineered Cementitious Composites-A Review. In: High Performance Fiber Reinforced Cement Composites 6. Springer. pp. 197–204.

Maruyama I, Teramoto A. 2011. Impact of time-dependant thermal expansion coefficient on the early-age volume changes in cement pastes. Cement and Concrete Research. 41:380–391.

Maruyama I, Teramoto A. 2013. Temperature dependence of autogenous shrinkage of silica fume cement pastes with a very low water–binder ratio. Cement and Concrete Research. 50:41–50.

Matsumoto T, Mihashi H. 2003. DFRCC Terminology and Application Concepts - JCI-DFRCC Committee Report. Journal of Advanced Concrete Technology. 1:335–340.

Menna C, Asprone D, Ferone C, Colangelo F, Balsamo A, Prota A, Cioffi R, Manfredi G. 2013. Use of geopolymers for composite external reinforcement of RC members. Composites Part B: Engineering. 45:1667–1676.

Mihashi H, Leite JP de B. 2004. State-of-the-art report on control of cracking in early age concrete. Journal of Advanced Concrete Technology. 2:141–154.

Mobasher B, Peled A, Pahilajani J. 2004. Pultrusion of fabric reinforced high flyash blended cement composites. In: RILEM Technical Meeting, BEFIB. pp. 1473–1482.

Myers RJ, Bernal SA, Provis JL. 2017. Phase diagrams for alkali-activated slag binders. Cement and Concrete Research. 95:30–38.

Naaman AE, Reinhardt HW. 1995. Characterization of high performance fiber reinforced cement composites-HPFRCC. In: Proceedings of High Performance Fiber Reinforced Cement Composites 2 [HPFRCC 2]. pp. 1–23.

Nematollahi B, Sanjayan J, Ahmed Shaikh FU. 2015a. Tensile strain hardening behavior of PVA fiber-reinforced engineered geopolymer composite. Journal of Materials in Civil Engineering. 27:04015001.

Nematollahi B, Sanjayan J, Qiu J, Yang E-H. 2017. Micromechanics-based investigation of a sustainable ambient temperature cured one-part strain hardening geopolymer composite. Construction and Building Materials. 131:552–563.

Nematollahi B, Sanjayan J, Shaikh FUA. 2015b. Strain hardening behavior of engineered geopolymer composites: effects of the activator combination. Journal of The Australian Ceramic Society Volume. 51:54–60.

Nematollahi B, Sanjayan J, Shaikh FUA. 2016. Matrix design of strain hardening fiber reinforced engineered geopolymer composite. Composites Part B: Engineering. 89:253–265.

Neto AAM, Cincotto MA, Repette W. 2008. Drying and autogenous shrinkage of pastes and mortars with activated slag cement. Cement and Concrete Research. 38:565–574.

Ohno M, Li VC. 2014. A feasibility study of strain hardening fiber reinforced fly ash-based geopolymer composites. Construction and Building Materials. 57:163–168.

Orosz K. 2013. Tensile behaviour of mineral-based composites. Department of Civil, Environmental and Natural Resources Engineering Structural and Construction Engineering. Licentiate Thesis, Luleå University of Technology, Luleå, Sweden.

Orosz K, Fjellström P, Jonasson J-E, Emborg M, Hedlund H. 2014. Evaluation of Thermal Dilation and Autogenous Shrinkage at Sealed Conditions. Nordic Concrete Research: Proceedings of the XXII Nordic Concrete Research Symposia. 50:299–302.

Palacios M, Puertas F. 2007. Effect of shrinkage-reducing admixtures on the properties of alkali-activated slag mortars and pastes. Cement and Concrete Research. 37:691–702.

Persson B. 1997. Self-desiccation and its importance in concrete technology. Materials and Structures. 30:293–305.

Provis JL, Deventer JSJ Van. 2009. Geopolymers: structures, processing, properties and industrial applications. Elsevier.

Puertas F, Palacios M, Manzano H, Dolado J, Rico A, Rodr'\iguez J. 2011. A model for the CASH gel formed in alkali-activated slag cements. Journal of the European Ceramic Society. 31:2043–2056.

Rokugo K, Kanda T, Yokota H, Sakata N. 2009. Applications and recommendations of high performance fiber reinforced cement composites with multiple fine cracking (HPFRCC) in Japan. Materials and Structures. 42:1197–1208.

Sahmaran M, Lachemi M, Hossain KM, Li VC. 2009. Internal curing of engineered cementitious composites for prevention of early age autogenous shrinkage cracking. Cement and Concrete Research. 39:893–901.

Sahmaran M, Li VC. 2010. Engineered Cementitious Composites: Can Composites Be Accepted as Crack-Free Concrete? Washington, USA: Transportation Research Board of the National Academies.

Sellevold E, Bjøntegaard Ø. 2006. Coefficient of thermal expansion of cement paste and concrete: mechanisms of moisture interaction. Materials and Structures. 39:809–815.

Sellevold EJ, Bjøntegaard Ø. 2004. Coefficient of Thermal Expansion (CTE) of Hardening Concrete. Nordic Concrete Research 1(31).

Sellevold EJ., Bjøntegaard Ø, Hammer TA. 2005. Response to discussion of the paper "On the measurement of free deformation of early age cement paste and concrete"[Bjøntegaard Ø, Hammer TA, Sellevold EJ. Cement and Concrete Composites 2004; 26: 427-435]. Cement and Concrete Composites. 27:857–858.

Shaikh F, Lu YY, Maalej M. 2013. Development of ductile fibre reinforced geopolymer composites. In: 8th International Conference on Fracture Mechanics of Concrete and Concrete Structures.

Shaikh FUA. 2013a. Deflection hardening behaviour of short fibre reinforced fly ash based geopolymer composites. Materials & Design. 50:674–682.

Shaikh FUA. 2013b. Review of mechanical properties of short fibre reinforced geopolymer composites. Construction and Building Materials. 43:37–49.

Shaikh FUA, Lu Y. 2013. Development of deflection-hardening geopolymer-based ductile fibre reinforced cementitious composites. Journal of the Chinese Advanced Materials Society. 1:7–20.

Shaikh FUA, Zammar R. 2017. Ductile behavior of polyethylene fibre reinforced geopolymer composite. In: MATEC Web of Conferences. p. 01047.

Tazawa E, Sato R, Sakai E and MS. 2000. Work of JCI committee on autogenous shrinkage. In: Proc Shrinkage 2000-Int RILEM Workshop on Shrinkage of Concrete. pp. 21–40.

Termkhajornkit P, Nawa T, Nakai M, Saito T. 2005. Effect of fly ash on autogenous shrinkage. Cement and Concrete Research. 35:473–482.

Timakul P, Rattanaprasit W, Aungkavattana P. 2016. Improving compressive strength of fly ash-based geopolymer composites by basalt fibers addition. Ceramics International. 42:6288–6295.

Tongaroonsri S. 2009. Prediction of autogenous shrinkage, drying shrinkage and shrinkage cracking in concrete. PhD Thesis, Thammasat University, Pathum Thani, Thailand

Torgal FP, Aguiar J, Ding Y, Tahri W, Baklouti S. 2015. Performance of alkali-activated mortars for the repair and strengthening of OPC concrete. Handbook of Alkali-Activated Cements, Mortars and Concretes. 627–641.

Turcry P, Loukili A, Barcelo L, Casabonne JM. 2002. Can the maturity concept be used to separate the autogenous shrinkage and thermal deformation of a cement paste at early age? Cement and Concrete Research. 32:1443–1450.

Täljsten B, Blanksvärd T. 2007. Mineral-Based Bonding of Carbon FRP to Strengthen Concrete Structures. Journal of Composites for Construction. 11:120–128.

Umbreen-Us-Sahar. 2015. Micromechanical modelling for deformational behavior of strain hardening cement-based composites. PhD Thesis, Yokohama National University, Japan

Vasconcelos E, Fernandes S, Aguiar JB de, Pacheco-Torgal F. 2011. Concrete retrofitting using metakaolin geopolymer mortars and CFRP. Construction and Building Materials. 25:3213–3221.

Vaysburd AM, Bissonnette B, Fay KF von. 2014. Compatibility Issues in Design and Implementation of Concrete Repairs and Overlays. Technical Report, U.S. Department of the Interior Bureau of Reclamation Technical Service Center.

Vilaplana J, Baeza F, Galao O, Alcocel E, Zornoza E, Garcés P. 2016. Mechanical properties of alkali activated blast furnace slag pastes reinforced with carbon fibers. Construction and Building Materials. 116:63–71.

Viviani M, Glisic B, Smith IFC. 2007. Separation of thermal and autogenous deformation at varying temperatures using optical fiber sensors. Cement and Concrete Composites. 29:435–447.

Wang K, Jansen DC, Shah SP, Karr AF. 1997. Permeability study of cracked concrete. Cement and Concrete Research. 27:381–393.

Wang S, Li VC. 2003. Tailoring of PVA Fibre/Matrix Interface for Engineered Cementitious Composites (ECC). In: Symposium in Advanced Flexible Materials and Structures: Engineering with Fibre. Loughborough, UK. pp. 91–92.

Wang S, Li VC. 2005. Polyvinyl alcohol fiber reinforced engineered cementitious composites: material design and performances. In: Proc, Int'l Workshop on HPFRCC Structural Applications, Hawaii.

Weimann MB, Li VC. 2003. Drying shrinkage and crack width of ECC. In: Proceedings of the Iternational Symposiumon Brittle Matrix Composites 7.

Yang E-H. 2008. Designing added functions in engineered cementitious composites. PhD Thesis, University of Michigan, Ann Arbor, Michigan, USA.

Ye H, Radlinska A. 2016. Quantitative analysis of phase assemblage and chemical shrinkage of alkali-activated slag. Journal of Advanced Concrete Technology. 14:245–260.

Yliniemi J, Kinnunen P, Karinkanta P, Illikainen M. 2016. Utilization of Mineral Wools as Alkali-Activated Material Precursor. Materials. 9:312.

Yoshitake I, Rajabipour F, Mimura Y, Scanlon A. 2012. A prediction method of tensile Young's modulus of concrete at early age. Advances in Civil Engineering. 2012.

Yuan X, Chen W, Lu Z, Chen H. 2014. Shrinkage compensation of alkali-activated slag concrete and microstructural analysis. Construction and Building Materials. 66:422–428.

Yuan Y, Wan ZL. 2002. Prediction of cracking within early-age concrete due to thermal, drying and creep behavior. Cement and Concrete Research. 32:1053–1059.

Zeng Q, Li K, Fen-Chong T, Dangla P. 2012. Effect of porosity on thermal expansion coefficient of cement pastes and mortars. Construction and Building Materials. 28:468–475.

Zhang J, Gong C, Guo Z, Zhang M. 2009. Engineered cementitious composite with characteristic of low drying shrinkage. Cement and Concrete Research. 39:303–312.

Zhang J, Hou D, Han Y. 2012. Micromechanical modeling on autogenous and drying shrinkages of concrete. Construction and Building Materials. 29:230–240.

Zhang J, Leng B. 2008. Transition from Multiple Macro-Cracking to Multiple Micro-Cracking in Cementitious Composites. Tsinghua Science & Technology. 13:669–673.

Zhou J. 2011. Performance of engineered cementitious composites for concrete repairs. PhD Thesis, Delft University of Technology, Delft, the Netherlands.

Østergaard L, Lange D, Stang H. 2004. Early-age stress–crack opening relationships for high performance concrete. Cement and Concrete Composites. 26:563–572.

2003. Advanced Concrete Technology. Butterworth-Heinemann. ISBN 978-0750656863

DOCTORAL AND LICENTIATE THESES

Luleå University of Technology, Division of Structural Engineering

Doctoral theses

1980 Ulf Arne Girhammar: Dynamic fail-safe behaviour of steel structures. Doctoral Thesis 1980:060D. 309 pp.

1983 Kent Gylltoft: Fracture mechanics models for fatigue in concrete structures. Doctoral Thesis 1983:25D. 210 pp.

1985 Thomas Olofsson: Mathematical modelling of jointed rock masses. Doctoral Thesis 1985:42D. 143 pp. (In collaboration with the Division of Rock Mechanics).

1988 Lennart Fransson: Thermal ice pressure on structures in ice covers. Doctoral Thesis 1988:67D. 161 pp.

1989 Mats Emborg: Thermal stresses in concrete structures at early ages. Doctoral Thesis 1989:73D. 285 pp.

1993 Lars Stehn: Tensile fracture of ice. Test methods and fracture mechanics analysis. Doctoral Thesis 1993:129D, September 1993. 136 pp.

1994 Björn Täljsten: Plate bonding. Strengthening of existing concrete structures with epoxy bonded plates of steel or fibre reinforced plastics. Doctoral Thesis 1994:152D, August 1994. 283 pp.

1994 Jan-Erik Jonasson: Modelling of temperature, moisture and stresses in young concrete. Doctoral Thesis 1994:153D, August 1994. 227 pp.

1995 Ulf Ohlsson: Fracture mechanics analysis of concrete structures. Doctoral Thesis 1995:179D, December 1995. 98 pp.

1998 Keivan Noghabai: Effect of tension softening on the performance of concrete structures. Doctoral Thesis 1998:21, August 1998. 150 pp.

1999 Gustaf Westman: Concrete creep and thermal stresses. New creep models and their effects on stress development. Doctoral Thesis 1999:10, May 1999. 301 pp.

1999 Henrik Gabrielsson: Ductility in high performance concrete structures. An experimental investigation and a theoretical study of prestressed hollow core slabs and prestressed cylindrical pole elements. Doctoral Thesis 1999:15, May 1999. 283 pp.

2000 Patrik Groth: Fibre reinforced concrete – Fracture mechanics methods applied on self-compacting concrete and energetically modified binders. Doctoral Thesis 2000:04, January 2000. 214 pp. ISBN 978-91-85685-00-4.

2000 Hans Hedlund: Hardening concrete. Measurements and evaluation of non-elastic deformation and associated restraint stresses. Doctoral Thesis 2000:25, December 2000. 394 pp. ISBN 91-89580-00-1.

2003 Anders Carolin: Carbon fibre reinforced polymers for strengthening of structural members. Doctoral Thesis 2003:18, June 2003. 190 pp. ISBN 91-89580-04-4.

2003 Martin Nilsson: Restraint factors and partial coefficients for crack risk analyses of early age concrete structures. Doctoral Thesis 2003:19, June 2003. 170 pp. ISBN: 91-89580-05-2.

2003 Mårten Larson: Thermal crack estimation in early age concrete – Models and methods for practical application. Doctoral Thesis 2003:20, June 2003. 190 pp. ISBN 91-86580-06-0.

2005 Erik Nordström: Durability of sprayed concrete. Steel fibre corrosion in cracks. Doctoral Thesis 2005:02, January 2005. 151 pp. ISBN 978-91-85685-01-1.

2006 Rogier Jongeling: A process model for work-flow management in construction. Combined use of location-based scheduling and 4D CAD. Doctoral Thesis 2006:47, October 2006. 191 pp. ISBN 978-91-85685-02-8.

2006 Jonas Carlswärd: Shrinkage cracking of steel fibre reinforced self compacting concrete overlays – Test methods and theoretical modelling. Doctoral Thesis 2006:55, December 2006. 250 pp. ISBN 978-91-85685-04-2.

2006 Håkan Thun: Assessment of fatigue resistance and strength in existing concrete structures. Doctoral Thesis 2006:65, December 2006. 169 pp. ISBN 978-91-85685-03-5.

2007 Lundqvist Joakim: Numerical analysis of concrete elements strengthened with carbon fiber reinforced polymers. Doctoral Thesis 2007:07, March 2007. 50 pp. ISBN 978-91-85685-06-6.

2007 Arvid Hejll: Civil structural health monitoring – Strategies, methods and applications. Doctoral Thesis 2007:10, March 2007. 189 pp. ISBN 978-91-85685-08-0.

2007 Stefan Woksepp: Virtual reality in construction: Tools, methods and processes. Doctoral Thesis 2007:49, November 2007. 191 pp. ISBN 978-91-85685-09-7.

2007 Romuald Rwamamara: Planning the healthy construction workplace through risk assessment and design methods. Doctoral Thesis 2007:74, November 2007. 179 pp. ISBN 978-91-85685-11-0.

2008 Björnar Sand: Nonlinear finite element simulations of ice forces on offshore structures. Doctoral Thesis 2008:39, September 2008. 241 pp.

2008 Bengt Toolanen: Lean contracting: relational contracting influenced by lean thinking. Doctoral Thesis 2008:41, October 2008. 190 pp.

2008 Sofia Utsi: Performance based concrete mix-design: Aggregate and micro mortar optimization applied on self-compacting concrete containing fly ash. Doctoral Thesis 2008:49, November 2008. 190 pp.

2009 Markus Bergström: Assessment of existing concrete bridges: Bending stiffness as a performance indicator. Doctoral Thesis, March 2009. 241 pp. ISBN 978-91-86233-11-2.

2009 Tobias Larsson: Fatigue assessment of riveted bridges. Doctoral Thesis, March 2009. 165 pp. ISBN 978-91-86233-13-6.

2009 Thomas Blanksvärd: Strengthening of concrete structures by the use of mineral based composites: System and design models for flexure and shear. Doctoral Thesis, April 2009. 156 pp. ISBN 978-91-86233-23-5.

2011 Anders Bennitz: Externally unbonded post-tensioned CFRP tendons – A system solution. Doctoral Thesis, February 2011. 68 pp. ISBN 978-91-7439-206-7.

2011 Gabriel Sas: FRP shear strengthening of reinforced concrete beams. Doctoral Thesis, April 2011. 97 pp. ISBN 978-91-7439-239-5.

2011 Peter Simonsson: Buildability of concrete structures: processes, methods and material. Doctoral Thesis, April 2011. 64 pp. ISBN 978-91-7439-243-2.

2011 Stig Bernander: Progressive landslides in long natural slopes. Formation, potential extension and configuration of finished slides in strain-softening soils. Doctoral

Thesis, May 2011, rev. August 2011 and April 2012. 250 pp. ISBN 978-91-7439-238-8. (In collaboration with the Division of Soil Mechanics and Foundation Engineering).

2012 Arto Puurula: Load carrying capacity of a strengthened reinforced concrete bridge: non-linear finite element modeling of a test to failure. Assessment of train load capacity of a two span railway trough bridge in Örnsköldsvik strengthened with bars of carbon fibre reinforced polymers (CFRP). Doctoral Thesis, May 2012. 100 pp. ISBN 978-91-7439-433-7.

2015 Mohammed Salih Mohammed Mahal: Fatigue behaviour of RC beams strengthened with CFRP. Analytical and experimental investigations. Doctoral Thesis, March 2015. 138 pp. ISBN 978-91-7583-234-0.

2015 Jonny Nilimaa: Concrete bridges: Improved load capacity. Doctoral Thesis, June 2015. 180 pp. ISBN 978-91-7583-344-6.

2015 Tarek Edrees Saaed: Structural control and identification of civil engineering structures. Doctoral Thesis, June 2015. 314 pp. ISBN 978-91-7583-241-8.

2015 Majid Al-Gburi: Restraint effect in early age concrete structures. Doctoral Thesis, September 2015. 190 pp. ISBN 978-91-7583-374-3.

2017 Cosmin Popescu: CFRP strengthening of cut-out openings in concrete walls – Analysis and laboratory tests. Doctoral Thesis, February 2017, 159 pp. ISBN 978-91-7583-794-9.

Licentiate theses

1984 Lennart Fransson: Bärförmåga hos ett flytande istäcke. Beräkningsmodeller och experimentella studier av naturlig is och av is förstärkt med armering. Licentiate Thesis 1984:012L. 137 pp. (In Swedish).

1985 Mats Emborg: Temperature stresses in massive concrete structures. Viscoelastic models and laboratory tests. Licentiate Thesis 1985:011L, May 1985. rev. November 1985. 163 pp.

1987 Christer Hjalmarsson: Effektbehov i bostadshus. Experimentell bestämning av effektbehov i små- och flerbostadshus. Licentiate Thesis 1987:009L, October 1987. 72 pp. (In Swedish).

1990 Björn Täljsten: Förstärkning av betongkonstruktioner genom pålimning av stålplåtar. Licentiate Thesis 1990:06L, May 1990. 205 pp. (In Swedish).

1990 Ulf Ohlsson: Fracture mechanics studies of concrete structures. Licentiate Thesis 1990:07L, May 1990. 66 pp.

1990 Lars Stehn: Fracture toughness of sea ice. Development of a test system based on chevron notched specimens. Licentiate Thesis 1990:11L, September 1990. 88 pp.

1992 Per Anders Daerga: Some experimental fracture mechanics studies in mode I of concrete and wood. Licentiate Thesis 1992:12L, April 1992, rev. June 1992. 81 pp.

1993 Henrik Gabrielsson: Shear capacity of beams of reinforced high performance concrete. Licentiate Thesis 1993:21L, May 1993. 109 pp.

1995 Keivan Noghabai: Splitting of concrete in the anchoring zone of deformed bars. A fracture mechanics approach to bond. Licentiate Thesis 1995:26L, May 1995. 123 pp.

1995 Gustaf Westman: Thermal cracking in high performance concrete. Viscoelastic models and laboratory tests. Licentiate Thesis 1995:27L, May 1995. 125 pp.

1995 Katarina Ekerfors: Mognadsutveckling i ung betong. Temperaturkänslighet, hållfasthet och värmeutveckling. Licentiate Thesis 1995:34L, October 1995. 137 pp. (In Swedish).

1996 Patrik Groth: Cracking in concrete. Crack prevention with air-cooling and crack distribution with steel fibre reinforcement. Licentiate Thesis 1996:37L, October 1996. 128 pp.

1996 Hans Hedlund: Stresses in high performance concrete due to temperature and moisture variations at early ages. Licentiate Thesis 1996:38L, October 1996. 240 pp.

2000 Mårten Larson: Estimation of crack risk in early age concrete. Simplified methods for practical use. Licentiate Thesis 2000:10, April 2000. 170 pp.

2000 Stig Bernander: Progressive landslides in long natural slopes. Formation, potential extension and configuration of finished slides in strain-softening soils. Licentiate Thesis 2000:16, May 2000. 137 pp. (In collaboration with the Division of Soil Mechanics and Foundation Engineering).

2000 Martin Nilsson: Thermal cracking of young concrete. Partial coefficients, restraint effects and influences of casting joints. Licentiate Thesis 2000:27, October 2000. 267 pp.

2000 Erik Nordström: Steel fibre corrosion in cracks. Durability of sprayed concrete. Licentiate Thesis 2000:49, December 2000. 103 pp.

2001 Anders Carolin: Strengthening of concrete structures with CFRP – Shear strengthening and full-scale applications. Licentiate thesis 2001:01, June 2001. 120 pp. ISBN 91-89580-01-X.

2001 Håkan Thun: Evaluation of concrete structures. Strength development and fatigue capacity. Licentiate Thesis 2001:25, June 2001. 164 pp. ISBN 91-89580-08-2.

2002 Patrice Godonue: Preliminary design and analysis of pedestrian FRP bridge deck. Licentiate Thesis 2002:18. 203 pp.

2002 Jonas Carlswärd: Steel fibre reinforced concrete toppings exposed to shrinkage and temperature deformations. Licentiate Thesis 2002:33, August 2002. 112 pp.

2003 Sofia Utsi: Self-compacting concrete – Properties of fresh and hardening concrete for civil engineering applications. Licentiate Thesis 2003:19, June 2003. 185 pp.

2003 Anders Rönneblad: Product models for concrete structures – Standards, applications and implementations. Licentiate Thesis 2003:22, June 2003. 104 pp.

2003 Håkan Nordin: Strengthening of concrete structures with pre-stressed CFRP. Licentiate Thesis 2003:25, June 2003. 125 pp.

2004 Arto Puurula: Assessment of prestressed concrete bridges loaded in combined shear, torsion and bending. Licentiate Thesis 2004:43, November 2004. 212 pp.

2004 Arvid Hejll: Structural health monitoring of bridges. Monitor, assess and retrofit. Licentiate Thesis 2004:46, November 2004. 128 pp.

2005 Ola Enochsson: CFRP strengthening of concrete slabs, with and without openings. Experiment, analysis, design and field application. Licentiate Thesis 2005:87, November 2005. 154 pp.

2006 Markus Bergström: Life cycle behaviour of concrete structures – Laboratory test and probabilistic evaluation. Licentiate Thesis 2006:59, December 2006. 173 pp. ISBN 978-91-85685-05-9.

2007 Thomas Blanksvärd: Strengthening of concrete structures by mineral based composites. Licentiate Thesis 2007:15, March 2007. 300 pp. ISBN 978-91-85685-07-3.

2008 Peter Simonsson: Industrial bridge construction with cast in place concrete: New production methods and lean construction philosophies. Licentiate Thesis 2008:17, May 2008. 164 pp. ISBN 978-91-85685-12-7.

2008 Anders Stenlund: Load carrying capacity of bridges: Three case studies of bridges in northern Sweden where probabilistic methods have been used to study effects of monitoring and strengthening. Licentiate Thesis 2008:18, May 2008. 306 pp. ISBN 978-91-85685-13-4.

2008 Anders Bennitz: Mechanical anchorage of prestressed CFRP tendons – Theory and tests. Licentiate Thesis 2008:32, November 2008. 319 pp.

2008 Gabriel Sas: FRP shear strengthening of RC beams and walls. Licentiate Thesis 2008:39, December 2008. 107 pp.

2010 Tomas Sandström: Durability of concrete hydropower structures when repaired with concrete overlays. Licentiate Thesis, February 2010. 179 pp. ISBN 978-91-7439-074-2.

2013 Johan Larsson: Mapping the concept of industrialized bridge construction: Potentials and obstacles. Licentiate Thesis, January 2013. 66 pp. ISBN 978-91-7439-543-3.

2013 Jonny Nilimaa: Upgrading concrete bridges: Post-tensioning for higher loads. Licentiate Thesis, January 2013. 300 pp. ISBN 978-91-7439-546-4.

2013 Katalin Orosz: Tensile behaviour of mineral-based composites. Licentiate Thesis, May 2013. 92 pp. ISBN 978-91-7439-663-8.

2013 Peter Fjellström: Measurement and modelling of young concrete properties. Licentiate Thesis, May 2013. 121 pp. ISBN 978-91-7439-644-7.

2014 Majid Al-Gburi: Restraint in structures with young concrete: Tools and estimations for practical use. Licentiate Thesis, September 2014. 106 pp. ISBN 978-91-7439-977-6.

2014 Tarek Edrees Saaed: Structural identification of civil engineering structures. Licentiate Thesis, November 2014. 135 pp. ISBN 978-91-7583-053-7.

2015 Cosmin Popescu: FRP strengthening of concrete walls with openings. Licentiate Thesis, December 2015. 134 pp. ISBN 978-91-7583-453-5.

2016 Faez Sayahi: Plastic Shrinkage Cracking in Concrete. Licentiate Thesis, December 2015. 134 pp. ISBN: 978-91-7583-678-2.

2016 Jens Häggström: Evaluation of the load carrying capacity of a steel truss railway bridge: testing, theory and evaluation. Licentiate Thesis, December 2016. 139 pp. ISBN: 978-91-7583-739-0.

2017 Yahya Ghasemi: Aggregates in concrete mix design. Licentiate Thesis, Mars 2017. 60 pp. ISBN: 978-91-7583-801-4.

Paper I

Orosz K, Blanksvärd T, Täljsten B and Fischer G

From material level to structural use of mineral-based composites - an overview

Published in:

Advances in Civil Engineering Vol. 2010
Article ID 985843.

Hindawi Publishing Corporation
Advances in Civil Engineering
Volume 2010, Article ID 985843, 19 pages
doi:10.1155/2010/985843

Review Article

From Material Level to Structural Use of Mineral-Based Composites—An Overview

Katalin Orosz,[1,2] Thomas Blanksvärd,[3] Björn Täljsten,[1,3] and Gregor Fischer[1]

[1] *Department of Civil Engineering, Technical University of Denmark, Brovej, Building 18, 2800 Kgs. Lyngby, Denmark*
[2] *Group Material Technology, Norut Narvik Ltd, P.O. Box 250, 8504 Narvik, Norway*
[3] *Division of Structural Engineering, Luleå University of Technology, 97187 Luleå, Sweden*

Correspondence should be addressed to Katalin Orosz, katalinorosz01@gmail.com

Received 22 April 2009; Revised 17 January 2010; Accepted 4 March 2010

Academic Editor: Tarun Kant

This paper surveys different material combinations and applications in the field of mineral-based strengthening of concrete structures. Focus is placed on mechanical behaviour on material and component levels in different cementitious composites; with the intention of systematically maping the applicable materials and material combinations for mineral-based strengthening. A comprehensive description of a particular strengthening system developed in Sweden and Denmark, denominated as Mineral-based Composites (MBCs), together with tests from composite material properties to structural elements is given. From tests and survey it can be concluded that the use of mineral-based strengthening system can be effectively used to increase the load bearing capacity of the strengthened structure. The paper concludes with suggestions on further development in the field of mineral-based strengthening.

1. Introduction

The existing civil engineering infrastructure is a very important element of the economical potential of a majority of the countries worldwide. A large number of today's buildings, transportation systems, and utility facilities are built with reinforced concrete and many of these systems are currently reaching the end of their expected service life. Additionally, increased loads and traffic flows, reuse, and ongoing deterioration even affect the durability of structures that are less than 20 years old.

There exist several repair and strengthening methods that can be applied to existing concrete structures for this purpose, such as cross section enlargement of critical elements, span shortening with additional supports, external/internal post tensioning, and steel plate bonding or strengthening with fibre-reinforced polymer (FRP) composites. Since the end of the 1980s, the use of FRP has been researched and applied increasingly for the rehabilitation of existing concrete structures. Externally epoxy-bonded FRP systems have been proven to be an effective strengthening method in repairing or strengthening structures and a large amount of literature is published on this topic; see, for example, [1–7]. FRP reinforcements can be used in numerous ways to strengthen a structure, For example, by bonding plates or sheets with a high-quality epoxy to the surface of concrete, timber, or even steel structures. There are also methods to wrap columns for enhanced ductility and strengthening systems where FRP rods are embedded in the concrete surface. Systems replacing the epoxy with polymer-modified mortars have been recently developed. For example, continuous fibre sheets can be embedded in a layer of mortar to provide, for example, confinement to a column; however, lately these sheets have been replaced by textiles due to bond issues related to difficulties with penetration as described in [8]. Biaxial or multidimensional FRP textiles are used in Textile-Reinforced concrete (TRC) [9, 10] systems or Textile-Reinforced mortar (TRM) jacketing, see; for example, [11].

In this paper a state-of-the-art report using mineral-based FRP strengthening systems is presented together with information about recent research at Luleå University of Technology (LTU), Sweden, and Technical University of Denmark (DTU). The literature survey is selective to published applications in which a fibre component has been

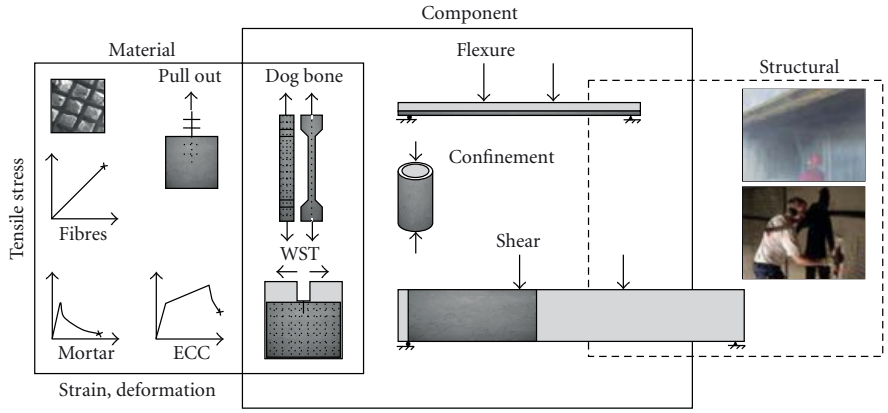

Figure 1: From material to structural level.

used together with a cementitious bonding agent, referred to as "mineral-based strengthening" in general. The authors also involved research and results from the field of ductile cementitious mortars which could be used together with an FRP component resulting in a high-performance strengthening material. The research significance within this paper is the mapping of possible design of different mineral-based strengthening systems. In addition, a systematic mapping of the novel strengthening system named mineral-based composites (MBCs), developed at LTU and DTU, going from material science to composite behaviour and some outlines for applications to existing structures are presented.

2. Definition and Development of Mineral-Based Strengthening Systems

"Mineral-based strengthening" in a broader perspective may be referred to any kind of a strengthening system in which a fibre component is embedded into a mineral-based binder to repair or strengthen existing concrete structures. Mineral-based strengthening in this context would include applications as surveyed in Section 3 from textile-reinforced mortar/concrete through fibre-reinforced cement to FRP grid applications.

Mineral-based strengthening systems are originally derived from other externally bonded FRP systems. The most commonly used adhesive to bond the FRP element to the surface of the structure (mainly concrete) is the epoxy adhesive. The use of epoxy has proven to give excellent force transfer. It bonds to the majority of surfaces (concrete, steel, timber, etc.) and shows to be durable and resistant to many different environments. However, some drawbacks can be identified. Firstly, epoxy as a bonding agent may create problem in the working environment, secondly, epoxy is recommended to have a minimum application temperature, often above 10°C, and thirdly, epoxy creates diffusion-closed (sealed) surfaces which may imply moisture and freeze/thaw problems for concrete structures. There might also be bond problems applying epoxy to wet or humid surfaces. To avoid some of these problems alternative strengthening systems have been researched and are currently being developed.

In mineral-based strengthening systems, the traditional epoxy bonding agent to adhere the FRP to the concrete surface is being replaced by cementitious matrices to bond the fibre material to the concrete surface. Mineral-based strengthening systems are made by replacing part of the cement hydrate binder of conventional mortar with polymers which, with the addition of fibre composites, become a high-performance external strengthening system for existing concrete structures.

3. Concept of Mineral-Based Strengthening

Mineral-based strengthening systems are dealt within three different levels. At the material level, the raw materials used in a mineral-based composite system such as binders (different quasibrittle or strain hardening mortars), FRP reinforcement (dry fibres, textiles, grids) and the most important properties of those are defined (Figure 1). At the component level, larger strengthened elements are discussed, for example, beams strengthened in flexure and shear. At the level of structural behaviour, field applications can be mentioned.

The intersection between material and component level would contain the different interactions between constituents and the effects of those on the structural behaviour (bond transfer mechanisms, fibre bridging and strain hardening).

3.1. Materials for Mineral-Based Strengthening. A list of requirements is proposed in [11] which should be met for a successful and efficient mineral-based strengthening. The mortar phase should have very low shrinkage deformations, high workability (application should be possible using a trowel, or shotcreted), high viscosity (application should not be problematic on vertical or overhead surfaces), low rate of workability loss (application of each mortar layer should be possible while the previous one is still in a fresh state), and sufficient shear (hence tensile) strength, in order to avoid premature debonding. In case E-glass fibre textiles are used, the mortar-based matrix should be of low alkalinity. Li [12], also adds a few requirements on

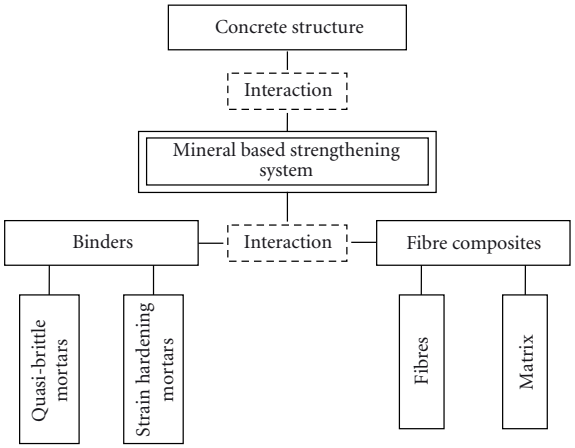

Figure 2: Overview of the constituents and possible interaction in mineral-based strengthening systems.

the "future concrete" which the authors feel relevant for a concrete-like repair and strengthening material as well: the "concrete" should be highly ductile with the ability of "yield" like a metal when overloaded to prevent unpredictable and sudden failure, highly durable and sustainable. These justify involving ductile mortars into the MBC system.

Mapping of the materials that have been or are promising to be used in mineral-based strengthening systems is shown in Figure 2. The integrated materials in the mineral-based strengthening systems can be divided in two main groups, binders and fibre composites. The components used in practical applications are detailed in the following.

3.1.1. Binders. Binders in practical applications are either quasibrittle, conventional polymer-modified or more ductile, strain hardening mortars.

Quasibrittle Mortars. Polymer-modified mortar (PMM) is the most widely used [13], suitable mortar in a mineral-based strengthening system. Polymeric admixture, or cement modifier, is defined as an admixture which consists of a polymeric compound that acts as a main ingredient when modifying or improving the properties such as strength, deformation, bond strength, or durability of mortars and concretes. The polymer-modified mortars or concretes therefore contain two types of binder, the hydraulic cement and the polymeric admixture. Polymeric admixtures can be latexes, powdered emulsions, water soluble polymers and liquid resins. Adding polymeric compounds to the fine-grained mortar phase is also common to enhance mechanical properties of Textile-Reinforced concrete (TRC) or mortar. In [14], improved interfacial bond is achieved by a secondary polymeric cohesive matrix within the mortar phase. In general, the properties of a polymer-modified mortar (or concrete) depend significantly on the polymer content or polymer-cement (P/C) ratio rather than the water-cement ratio compared with ordinary cement mortar [15].

Increasing the P/C ratio to about 10%–15% by weight has shown to increase the flexural strength. A P/C ratio higher than 15% by weight decreases the mechanical strength [15, 16]. Another source, [17] states that an addition of polymeric dispersion up to even 20% by weight results in a higher tensile strength of the (Textile-Reinforced) concrete.

To further enhance the properties of a PMM, for example, workability, flowability, mechanical properties, and so forth, of the mortars, superplasticizers, silica fume, fly ash and reinforcing fibres can be used.

Fibres in the matrix can be chopped or milled fibres. The fibres must be easily dispersed in the mixture, must have suitable mechanical properties, and must be durable in the highly alkaline cement matrix. They are randomly (in a good mix, uniformly) distributed throughout the mortar/concrete. Continuous fibres are more effective in increasing strength in a certain direction compared to randomly distributed short fibres, but they are not easily mixed into the cement matrix and their high cost does not allow them to be widely used. Different types of fibres are currently used such as steel, glass, carbon, polyvinyl-alcohol (PVA), polypropylene, nylon and natural fibres depending on the structural needs. Using a small percentage of carbon fibre addition (~0.5%), a considerable increase in flexural strength is achieved relative to unreinforced mortar [18]. Other researchers have investigated new type of fibres, such as ceramic fibres [19]. The results show that the flexural strength of mortar can be increased and also the durability of this ceramic fibre-reinforced mortar is much better than that of alkali-resistant (AR) glass fibre. The use of steel fibres is the most common solution to enhance toughness of a steel fibre-reinforced concrete (conventional FRC). For enhanced ductility, first cracking strength or ultimate tensile strength, other types of fibres may be more suitable. The addition of small volume fractions of synthetic fibres (up to 2%) to the mortar can improve the toughness of the mortar [20]. Among these fibres, the polypropylene fibres are very popular in concrete and the nylon fibres are recently becoming more widely used [21]. The propylene fibres reinforce the concrete performance under flexure, tension, impact blows and plastic shrinkage cracking. On the other hand, the nylon fibres improve the performance after the presence of cracks and sustained high stresses. In [22], both types of fibres were compared and the results showed a better improvement of the properties when using the nylon fibres than the polypropylene fibres. Other researches [23, 24] are focusing on the use of recycled PET (polyethylene terephthalate). PET fibres made from beverage bottles were used successfully up to 3% in (normal) concrete [23]. Another study on the durability in aggressive environments of a PET-reinforced concrete [24] emphasizes the sustainability and environmentally friendliness of such concretes since the PET fibre has a long decomposition time (over 100 years to completely degrade).

Some supplementary materials should be used for counteracting the insufficiencies brought about by the addition of fibres, such as increase in porosity or decrease in compressive strength. For example, substituting a part of the cement (20%) by silica fume increases the compressive strength of the resulting mortar and provides a reduction of porosity, which leads to an increase of the flexural strength. Adding

silica fume in concretes also increase the interfacial bond strength and interfacial fracture energy by about 100% due to its smaller particle size and thereby the ability to increase the density of the microstructure of a mix [25, 26].

In concrete prepared with ordinary Portland cement, the interfaces between the hydrated cement matrix and the aggregates are the weakest link [27]. The incorporation of industrial by-products such as fly ash in concretes can significantly enhance basic properties in both the fresh and hardened states [28, 29]. It is well known that blending cement with fly ash or other supplementary cementing materials improves the rheological properties of the fresh concrete and the engineering properties of hardened concrete [30–32]. Fly ash in Textile-Reinforced concrete is widely used to densify the grain structure [33] resulting in an improved bond between textile and concrete. Superplasticizers can also be used to improve consistency and workability.

Strain Hardening Mortars. Engineered Cementitious Composites (ECCs) are another type of binder which can be used together with an FRP component [34]. Both in the case of repair and strengthening, the failure mechanisms that lead to the need for repair/retrofit of a structure often involve fracture. This can be overcome by materials with improved toughness, ultimate tensile strength and ductility, which justifies involving ECC into the FRP strengthening. This micromechanically designed material invented in the early 1990s represents a particular class of HPFRCC (High-Performance Fibre-reinforced Cementitious Composites), exhibiting strain hardening behaviour and multiple cracking during the inelastic deformation process [35]. Since its introduction, ECC has undergone major evolution in both material development and the range of applications. Recently, it is often referred to as SHCC (strain hardening cementitious composites) due to its tensile (pseudo) strain hardening effect of (steel reinforced) ECC, see more in detail later, which has been previously documented by Fischer and Li [36].

Besides common ingredients of cementitious composites such as cement, sand, fly ash, water and additives, ECC utilizes short, randomly oriented polymeric fibres (e.g., polyethylene, polyvinyl alcohol) at moderate volume fractions (1.5%–2%). In contrast to some other types of fibres, there is a strong chemical bond between PVA and mortar which needs to be reduced [37]. This is done by a chemical coating applied on the fibre surface and additional fly ash in the mix in order to prevent premature PVA fibre rupture and thus achieve a more ductile failure mode, characterized by pull-out from the cement matrix.

The tensile strain capacity of ECC is several hundred times that of normal concrete [12] and the fracture toughness of ECC is similar to that of aluminium alloys [38]. Furthermore, the material remains ductile even when subject to high shear stresses [39]. The compressive strength of ECC ranges from 40 to 80 MPa depending on mix composition, the high end similar to that of high strength concrete. ECC has typically an ultimate tensile strength of 5–8 MPa and a strain capacity ranging from 3% to 5%.

There are a number of characteristics of ECC that make it attractive as a repair material. According to Li [40], the unique feature of ECC is its ultra high ductility. This implies that structural failure by fracture is less likely in comparison to normal concrete or steel fibre-reinforced concrete (FRCs). As a consequence, ECC has been used in a wide range of applications where ductility and/or energy absorption performance or damage tolerance of the material is an important criterion (seismic and nonseismic structural applications, see, e.g., [41–45]. In contrast to quasibrittle repair materials, ECC can eliminate premature delamination of the strengthening layer or surface spalling in an ECC/concrete repaired system [46]. Spall resistance of ECC in the surroundings of a corroded rebar in slabs has been investigated by Kanda et al. [47], where ECC accommodated the expansion by a "plastic yielding" process through radial microcracking [12]. Interface defects can be absorbed into the ECC layer and arrested without forming spalls, thus extending the service life [38]. Suthiwarapirak et al. [48] showed that ECC has significantly higher fatigue resistance than that of commonly used repair materials such as polymer mortars. It also has a good freeze-thaw resistance and restrained shrinkage crack control [41]. ECC-reinforced shear beams behaved in a ductile manner even without additional (steel) shear reinforcement and remained ductile even for short span shear elements which typically fail in a brittle manner with normal concrete [49]. Under shear, ECC develops multiple cracking with cracks aligned normal to the principal tensile direction. Because the tensile behaviour of ECC is ductile, the shear response is correspondingly ductile. ECC as a strengthening material also offers excellent crack control. When an ECC structural element is loaded in flexure or shear beyond the elastic range, the inelastic deformation is associated with microcracking with continued load carrying capacity across these cracks [40]. The microcrack width is dependent on the type of fibre and interface properties (generally less than 100 micron when PVA fibre is used). The tight crack width in ECC has advantageous implications on structural durability [12]. When used as strengthening or repair material, fine cracks also prevent penetration of substances [50]. The spacing between multiple cracks in a typical ECC is on the order of several mm, while the crack widths are limited to the order of 200 μm. In standalone applications, maximum crack width in ECC is a material property independent of the embedded reinforcement, unlike in RC or conventional FRC in which cracks widths are influenced by the steel reinforcement [12]. However, crack distribution of ECC as repair material is more concentrated adjacent to an existing crack in the base substrate [12].

"Flowability" or "self-compactability" of ECC refers to the ability of the material that it can flow under its own weight and fill the formwork properly. Despite the presence of (short, chopped, randomly oriented, typically PVA or PE) fibres, a self-compacting ECC is able to fill in each corner of the formwork without external vibration required [51]. This would also ensure a good bond to the embedded reinforcement (such as steel or FRP).

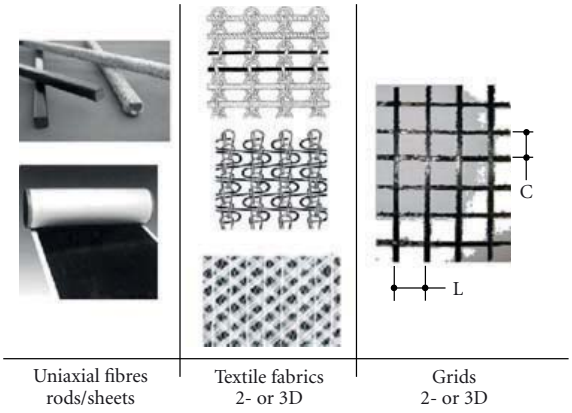

Figure 3: Different types of fibre composites.

3.1.2. Fibre Composites. Commonly used FRP reinforcements are shown in Figure 3. FRP rods are typically used as internal reinforcement or for near-surface mounted reinforcement (NSMR). Other pultruded profiles used are thin composite plates with a typical cross section of 1.4 × 80 mm; however none of these systems will be detailed within this paper. Uniaxial fibres or fibre sheets, textiles and grids used together with mineral-based bonding agents are other types of FRP reinforcement systems, these systems are described more in detail below.

Fabrics and Textiles (Knitted, Woven, or Unwoven). Different kinds of fibres used as FRP reinforcement and their mechanical properties are detailed, for example, in [52, 53]. There exist a few continuous long fibre applications, where nonimpregnated unidirectional fibres may be embedded in a mortar phase [21], but the impregnation of continuous fibre sheets with mortars is very difficult resulting in a poor bond between fibre and mortar [8]. Fibres used in most mineral-based strengthening systems usually come in the form of a textile or fabric (woven or knitted) or grid (with rigid joints), where the latter is impregnated and held together by an epoxy resin which also shapes the composite.

Fabrics are unidirectional or multidirectional FRP composites. They are widely used in Textile-Reinforced concrete systems. The most commonly used textiles are the bidirectional woven fabrics, in which the yarns are woven together crossing them orthogonally, having a width of 300–600 mm, in large spools cut at the workplace. The density of the yarns directly affects the penetrability of the adhesive into the fabric, higher density leads to lower penetrability as the mechanical interlock acts through the fabric openings [11]. Woven fabrics are easy to adapt to any surface which makes them very suitable for wrapping (U-warp or full wrap) or confinement. The flexible shape also represents some disadvantages. The reinforcing efficiency is lower than that in straight yarns due to the crimped geometry of the woven fibres; however, this crimped geometry is advantageous in providing mechanical anchoring between the woven fabric and the cement matrix in a polymer-modified mortar. Fabrics having relatively complicated yarn shapes may enhance the bonding and improve the composite performance [11]. However, very complex textile geometries may cause premature failure of some of the yarns resulting in lower strength than the nominal strength of the fibrous phase would be, as reported in [54].

Bi- and Triaxial Grids with Rigid Joints. An FRP grid is a multidirectional prefabricated composite. For externally bonded reinforcement, grids are made of continuous fibres alternating in two directions and impregnated with a resin to form a 2D-cross laminate grid structure with rigid joints. The resin is usually epoxy and its role is to hold the fibres together and shaping the composite. The fibre amount and grid spacing often vary in the two perpendicular directions. FRP grids are typically produced in large rolls and then cut into the required dimensions. Compared to woven fabrics, FRP grids have improved mechanical properties and in general, have more rigid connection points. The improved performance is due to the aligned fibres in a certain (predefined) direction and that there are no unpenetrated fibres or fibre bundles with would prematurely fail (further discussed in Section 4.2 under TRC). Thinner grids are flexible and can be adapted to curved surfaces.

4. Existing Mineral-Based Strengthening Systems

4.1. Continuous Dry Fibres. The use of continuous dry fibres is published in [55] where a pretreatment with silica fume and high amounts of polymers improved the bond between carbon fibres and cementitious matrices. It was found that a pretreatment with silica fume and relatively high amounts of polymers improved the bond behaviour of carbon fibre to the cement. Another report [56] has been published on large-scale tests of ordinary concrete beams strengthened with a cementitious fibre composite where the strengthening composite consisted of a unidirectional sheet of continuous dry carbon fibres and a polymer-modified mortar, applied by hand lay-up method. Both flexural and shear strengthening were investigated. From the tests it was concluded that the method works and that considerable strengthening effects can be achieved. However, in comparison with epoxy-bonded carbon fibre sheets using the same amount of carbon fibre, the strengthening effect for the mineral-based composite strengthening system was approximately half. The reason for this is most likely due to the reduced interfacial bond strength between the mortar and the carbon fibre-reinforcement. This is also emphasized by [57], where it was found that the loading capacity of the cementitious carbon fibre composite is influenced by the amount of fibres in the tow. If the cementitious matrix penetrated into the interior of the carbon fibre tow, a higher number of filaments would be active during loading, leading to the increase in load carrying capacity.

Another way of using continuous dry fibres, usually in the form of sheets is the fibre-reinforced composites (FRCs) strengthening system (which may also use dry fabrics), as described by, for example, [58]. Depending on the geometry of the fibres and the strengthening purpose, the composite

plates can be made as thin as 2 mm. The sheet or fabric is cut into chosen dimensions and the fibre geometry is submerged into cement slurry (matrix) for a better penetration. The impregnated sheet or fabric is then removed from the slurry and immediately bonded to the concrete surface. An improved penetration of the matrix into the fibres can be achieved by using multiple layers of continuous carbon fibres where all single layers were impregnated in cementitious slurry before bonded to the concrete surface. This procedure was also suggested in [51]; however not executed.

4.2. Textile-Reinforced Mortar (TRM) or Textile-Reinforced Concrete (TRC). Textile-Reinforced Concrete (TRC) is made from a cementitious matrix and layers of oriented, continuous fibres (technical textiles) as for reinforcement. Here TRC is only discussed as a strengthening material and not as a material also suitable for stand-alone applications such as thin shells. The most commonly used bonding agent for applying the textile on the structure is the fine grained concrete or mineral-based mortar which has a grain size of less than 1 mm and provides high strength and flowable consistencies. Less than 2 mm of concrete or mortar thickness is needed between textile layers due to the small maximum aggregate size of the concrete mix [9]. Alkali-resistant glass (AR-glass) or carbon is used most often as the fibrous material. The fibres can be in the form of a woven textile or be unidirectional and held together by a yarn in the perpendicular direction in order to make the material easier to work with. The fabrics can be manufactured with a maximum number of four reinforcing directions depending on the load direction [9] and can therefore be tailored (the filaments are intentionally aligned in the direction of the tensile stresses leading to an increase in their effectiveness). There are several designs of textile fabrics depending on the load case and the positioning of the fabrics. Most fabrics are bi- or multiaxial warp knits and woven fabrics since they offer a great flexibility of properties and are suited for many cases.

In a TRC strengthening system, the transfer of the bond forces from one layer to another through the bonding joint must be guaranteed to ensure a full composite action. The bond behaviour of TRC is a complex property that depends on both the textile and the matrix. Due to the reinforcement geometry, only the outer filaments are directly in contact with the concrete, hence the load bearing capacity of a TRC depends mainly on the proportion of the outer to the inner filaments, and just a certain part of the tensile strength of the concrete can be activated due to the limited contact surface [14, 59]. Significant improvement in load capacity can be achieved if the textile is previously penetrated with liquid polymers [17, 59] or epoxy- resins [17]. However, there is a risk that in an impregnated textile, a higher number of activated filaments would lead to abrupt failure of all filaments when the tensile strength of those is exceeded [17]. The same study also highlights that the tensile strength of a TRC (dogbone) specimen can be increased most effectively by both impregnating the textiles with polymers and adding polymer modifiers to the concrete.

TRC systems exhibiting mechanisms of distributed cracking and strain hardening behaviour (see Section 5) have been used for stand-alone structural applications such as extremely thin and slender structures [60], or for repair and strengthening of existing structural members [9, 10]. Confinement strengthening of short columns both with epoxy and cement-based mortars has been investigated by [8]. Effectiveness of the TRM jacketing compared to the epoxy-impregnated counterparts resulted in a reduced effectiveness (80% for strength and 50% for ultimate strain). The strengthening effect increased with the number of confining layers and was highly dependent on the tensile strength of the applied cement mortar. Failure was more ductile in case of the TRM jacketing than in the epoxy-bonded jackets due to the slowly progressing fracture of individual fibre bundles. Shear strengthening of concrete beams has been examined in [61] on six identical RC beams with different bonding agents (epoxy and cement matrix), one or two layers of textile in different arrangements (conventional wrapping and spirally applied textiles). Two layers of mortar-impregnated Textile-Reinforcement in the form of either conventional jackets or spirally applied strips were sufficient to increase the shear capacity of the beams tested more than 100% over the unstrengthened beam, preventing sudden shear failures and allowing activation of flexural yielding (as was the case with the resin-based jacket). The TRM system; however, was found to be about 50% less effective than the FRP-strengthened beam. Other experiments [9, 10, 62] have been carried out on T-beams which were designed with minimum shear reinforcement but a great amount of longitudinal flexural reinforcement in order to prevent flexural failure. The strengthening fabric was a multiaxial textile applied as a U-wrap in an angle of 45° to the load direction, aligned with the principal stresses in the web of the T-beam to be strengthened. Varying parameters were the number of textile layers (2–6) placed with or without mechanical anchorage in the compression zone. The adhesive tensile load carrying capacity is crucial in the performance of the system—this determines how many layers can be anchored to the web without any additional mechanical anchorage. Tests revealed the importance of mechanically anchoring of the reinforcement. A load increase could be achieved with a few layers of textile even without anchorage to the compressive zone; however, when the adhesive tensile bond between the web and the reinforcement was exceeded, the TRC layers peeled away and therefore the reinforcement fails.

4.3. Mineral-Based Composites (MBCs). MBCs (mineral-based composites) are defined as a system in which a FRP grid is applied onto the surface of the structure to be strengthened with a cement-based mortar as bonding matrix. MBC "inherits" the properties and behaviour of its constituents, for example, brittleness or tension softening behaviour when the linear elastic fibre material is used together with quasibrittle cementitious binders. However, its behaviour can significantly be changed/altered and the material can be enforced to exhibit more ductility, multiple cracking or strain hardening in tension in a modified

MBC where the mortar is a PVA-reinforced engineered cementitious composite (ECC) [63, 64]. In the recent development of MBC, two strengthening approaches meet and result in a high-performance hybrid strengthening material. One is finding the most suitable combinations of a FRP reinforcement and an existing mortar (which, depending on the application may be ordinary or polymer-modified mortar), and the other one is to strengthen/develop the mortar itself with different short fibres (in practice, mostly PVA) or involve existing, ductile mortars in order to improve the interaction between grid and mortar, tensile properties of the composite, crack spacing and crack widths, ductility and also if possible, fracture energy.

The FRP in MBC applications is normally a two-dimensional carbon fibre grid. As matrix, polymer-modified quasibrittle mortars (PMMs) are typically used. Between the two components little or no chemical bond exists. Therefore the bond strongly relies on mechanical bond, contrary to epoxy-based FRP systems. The precut CFRP grid with varying grid spacing and thickness is embedded between two relatively thin layers of mortar.

To achieve a good bond between the base concrete and the mortar, the surface of the base concrete needs to be roughened, for example, by sandblasting or water jetting, in order to remove the cement laitance. The surface preparation method normally is sandblasting. The strengthening layers can be applied by hand (hand lay-up) or shotcreting when strengthening large surfaces. The hand lay-up method includes prewetting the base concrete with water for 1–3 days depending on the conditions of the base concrete and the surrounding climate. The moisture conditions in the transition zone between the base concrete and mortar are further discussed in [65], where it is found that the best bond is obtained when the base concrete has just dried back from a saturated surface. Prior to mounting the MBC system the base concrete surface has to be primed using a silt-up product (primer) to prevent moisture transport from the wet mortar to the base concrete. A first layer of mortar is immediately applied to the primed surface. Next, the CFRP grid is placed on the first layer of mortar followed by an additional layer of mortar being applied on top of the grid. The thickness of the mortar depends on the maximum grain size in the mortar.

Reliability of the system highly depends on the bond in two interface layers, between the concrete substrate and the first layer of mortar and in the between the grid in the mortar; see [66].

5. Mineral-Based Strengthening at Material Level

On the interface between the base concrete and the strengthening layer interface, such as between the fibre composite and the mortar, bond is crucial for the performance of the strengthening system. In a TRC or MBC system, bond between FRP and mortar relies mostly on mechanical interlocking (physical bond). If the mortar contains PVA fibres, a chemical bond is also being built up within the mortar phase. Good (but not overly strong) bond together with the deformation compatibility of the mortar and PVA fibres, results in fibre bridging and as a consequence, multiple cracking and overall strain hardening, resulting in a "stronger" and more ductile mortar. These mechanisms are detailed below.

5.1. Bond between Base Concrete and Strengthening Layer. When an existing RC element is to be strengthened, the tensile force developed in the strengthening layer must be introduced into the original concrete of the member by bond forces. Failure can initiate from an interfacial defect causing delamination of the whole strengthening layer in the case of a "weak" bond and spalling in the case of an overly "strong" bond [35].

Bond strength in a mineral-based system generally depends on the adhesion in the interface, friction, aggregate interlocking and possibly, time-dependent factors [52].

The sensitivity of a structure to bond strength depends highly on what kind of load it is subjected to. The force transmission into the original concrete when strengthening for flexure occurs over a relatively large length (surface). In contrast, the force transmission via shear strengthening takes place only in the range behind the last shear crack [9]. As a result, significantly shorter anchorage lengths and "better bond", and in some cases, additional anchoring is required for shear strengthening. An example is a TRC-reinforced T-beam strengthened for shear [9] where if the U-wrap around its web is not anchored into the slab via an L-shaped steel section the TRC reinforcement has a tendency to peel away from the web.

Incompatibility between the base concrete and the repair material in repair and/or strengthening systems can lead to the same bond problem and render the system ineffective resulting in debonding or spalling of the strengthening layer especially if the load is applied parallel to the bond line of the combined system. If there is an incompatibility in the elastic modulus of the base concrete and the mortar, it will result in the incompatibility of the deformations on the interface as the "weaker" material will have larger deformations [67]. If the load bearing capacity of the material or the bond at the transition zone is exceeded by the transferred load, failure will occur. Recommendations for the modulus of elasticity of the repair or strengthening material suggest a modulus at least 30% larger than the modulus of elasticity for the base concrete [68]. When the bonding agent tensile load bearing capacity is exceeded in the interface between the base concrete and the strengthening layer, the strengthening would peel off the structure. To prevent debonding, it is usual to prescribe a minimum adhesive tensile strength of the original concrete substrate which, for example, in German codes is 1.5 N/mm^2 [9]. If the surface is roughened adequately, by means of removing the deteriorated parts and sandblasting, a good bond can be guaranteed. Another parameter that influences the compatibility of the combined repair or strengthening system is the drying shrinkage. As the fresh repair or strengthening material has a tendency to shrink, the more or less older base concrete acts as a rigid foundation that restrains these movements. These differential movements cause tensile stresses in the repair or strengthening material and compressive stresses in the base

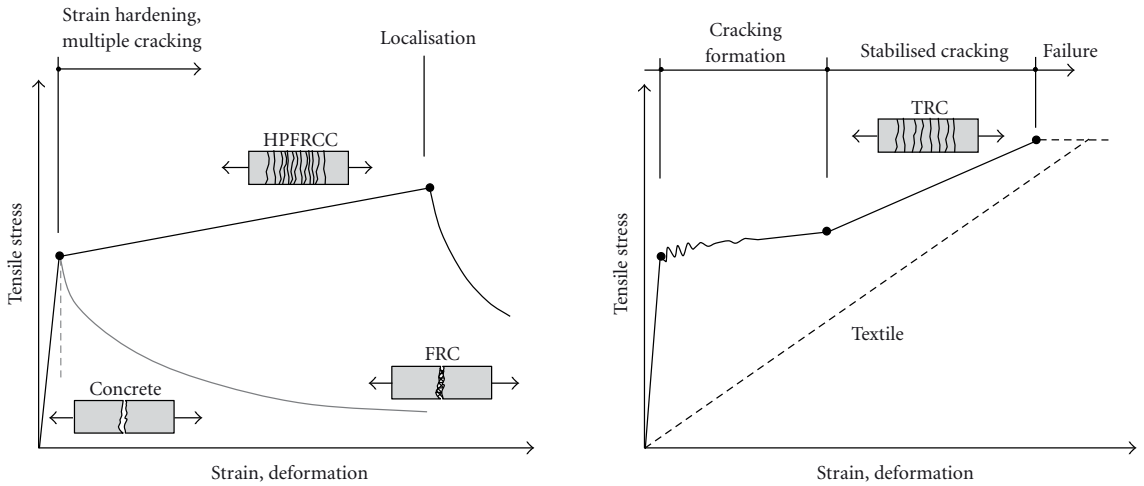

Figure 4: (a) Strain hardening and strain softening mortars. (b) Tensile behaviour of TRC.

concrete. Creep in this context can be an advantage since it releases parts of these stresses. Shrinkage incompatibility is more associated with cement-based mortars while the polymer-modified mortars (PMC) show better shrinkage compatibility and epoxy mortars proved to have the best shrinkage compatibility [68].

5.2. Bond of FRP in a Mortar. The mineral-based strengthening systems are strongly dependent on the bond between fibre composite and mineral-based binder. Using a non-impregnated textile fabric with a high density (high fibre filament amount) will make it hard for the mineral-based binder to penetrate. This type of inferior bond or penetration of textile fabrics has been the focus for researchers developing the TRC system [8, 11, 14]. Using an epoxy-impregnated CFRP grid, as in the MBC system, relies on *physical bond* between CFRP and mortar. This physical bond can originate from direct mechanical anchorage (joints in the grid, transversal tows of the grid), frictional forces on the interface, aggregate or fibre interlock (if the mortar contains longer fibres) but there is no chemical bond between the FRP and the mortar as in an epoxy-bonded system there would be.

When using strain hardening mortars, there is a chemical bond between the mortar fine-grain aggregates and the PVA fibres which affects bonding of the embedded FRP reinforcement in the mortar. PVA has a high chemical bond and reaches its peak load at relatively small pullout length. During the extraction process, it has a tendency to break instead of pulling out from the mortar. In order to increase the opening of an individual crack and enhance the composite stress-strain behaviour of PVA-ECC, the chemical and frictional bond of the PVA fibre is to be decreased, for example, by means of particular surface treatment (coating) [38] or by modification of the fibre/matrix interface transition zone. Bond can be lessened, for example, by adding fly ash to the mix.

Bond characteristics influence the mechanism of load transfer between reinforcement and concrete, and therefore control the concrete (or mortar) crack spacing, crack width, required concrete cover to the reinforcement, and the reinforcement development length. The behaviour of strengthened concrete structures thus depends on the integrity of the bond. Most literature to date has been published about bond of FRP bars in concrete or other cementitious matrices. Very little literature is found on the bond of FRP grids to a cementitious material which is more complex because of the geometry of the grid, including the formation of the joints.

5.3. Multiple Cracking—Crack Control through Strain hardening Materials. The deformation behaviour of cementitious composites (concrete, fibre-reinforced concrete) and high performance fibre-reinforced cement composites (HPFRCCs) is typically distinguished according to their tensile stress-strain characteristics and postcracking response [69]. In [70], it is shown that brittle matrices, such as plain mortar and concrete, lose their tensile load-carrying capacity almost immediately after formation of the first crack as illustrated in Figure 4.

The addition of fibres in conventional fibre-reinforced concrete (FRCs) can increase the toughness of cementitious matrices significantly; however, their tensile strength and especially strain capacity and ductility beyond first cracking are not enhanced [71]. FRC is therefore considered to be a quasibrittle material with tension softening behaviour, that is, a decaying load and immediate localization of composite deformation at first cracking in the FRC matrix. In contrast, strain hardening fibre-reinforced cementitious composites (SHCCs), which is a particular class of HPFRCC (high performance fibre-reinforced cementitious composites), are defined by an ultimate strength higher than their first cracking strength and the formation of multiple cracking

during the inelastic deformation process. Under tension, it initially exhibits *multiple cracking with associated overall hardening*, which later changes to softening as fracture localizes [72]. The crack continues to open, and the embedded fibres are pulled out of the matrix (or break, depending on what matrix/fibre composition is used), which still generates some resistance against crack opening within the tensile softening regime. When all fibres are completely pulled out (or broken), no resistance is left, that is, the tensile stress is equal to zero.

The contribution of a cementitious matrix to the load-deformation response of reinforced concrete or ECC is the so-called "strain hardening" or "plastic hardening". Tensile softening versus tensile hardening behaviour is illustrated in Figure 4(a). Textile-Reinforced concrete exhibits a similar hardening behaviour [73, 74]; however the cracking process is clearly not as uniform as in an ECC (Figure 4(b)). In the precracking regime (Stage I), the stresses are distributed until the first cracking strength of the concrete is reached. First cracking occurs at the point where the ultimate tensile strength of the concrete is reached and the FRP reinforcement will carry the entire applied load in the vicinity of the transverse crack location. The load carried by the concrete in the uncracked segments is transferred to the FRP reinforcement at the crack location via interfacial bond. After first crack formation (Stage IIa, "cracking formation"), the load-deformation curve shows a small increase in loading capacity as compared to that in Stage I due to the formation of additional transverse cracking. The member is softened by the formation of additional crack(s) and the load increase per deformation increment is decreasing with each crack until Stage IIb when a stabilized crack pattern is reached (postcracking regime). When the final crack pattern is being formed, the slope of the stress strain relationship becomes steeper again, which mainly results from the Young's modulus of the fibre-reinforcement. Crack widths are also governed by the FRP reinforcement and the bond characteristics to the surrounding concrete matrix. At this stage of a stabilized crack pattern (Stage III) no further cracking occurs. Here, mainly the FRPs determine the stiffness of the member. Stage III is characterized either by slippage in the fibre tows instead of yielding of steel reinforcement, or by linear elastic deformations until the FRP ruptures in a brittle manner upon reaching its tensile failure strain, as detailed in [75]. In practice, final failure normally is a combination of fibre slippage and rupture [73].

Due to the more homogeneous nature (as a consequence of randomly distributed, well mixed short fibres) of ECC, there is a gradually increasing part of the curve smoother than for TRC because of the fibre bridging characteristics of the PVA fibres compared to those of a textile mesh. In ECC, there is no definite distinction between stages IIa and IIb (crack saturation) [36]. The (pseudo)strain-hardening behaviour in ECC is achieved by sequential development of matrix multiple cracking [76]. "Multiple cracking" means that under tension, cracks are consecutively formed after first cracking, and become evenly and closely spaced. Deformation then is often expressed in terms of strain instead of crack opening displacement. Multiple cracking results in the improvement in "ductility, toughness, fracture energy, strain hardening, strain capacity and deformation capacity under tension, compression or bending" [77].

The strain hardening ensures that a structural element made of such a composite material will maintain its stability also after cracking. This is a significant difference between all conventional FRC and SHCC materials as shown in Figure 4. Deformation of ECC is uniform on a macroscale and considered as pseudostrain, which is a *material property* [36], in contrast to other reinforced concrete-like materials such as conventional FRC. As a consequence of the strain hardening, the tensile strain capacity and ultimate strength *in the cracked state of ECC* are much higher than that of conventional (steel) fibre-reinforced concrete.

5.4. Fibre Bridging. Since the overall hardening behaviour highly relies on fibre bridging, it is important to know how high bridging stresses arise in the fibres. This would also limit and determine which materials are usable as reinforcing fibres. For very flexible fibres which have a high strain capacity (polymeric fibres), a snubbing effect (fibre dowel action arising when a fibre is not loaded in the direction of the initial straight fibre) may occur reducing the fibre critical length leading to premature failure. For elastoplastic fibres (steel), local yielding can happen, as for elastic-brittle fibres (carbon, glass) fibre failure may happen due to bending of fibres [39]. The fibre bridging analysis is about relating the single fibre bridging stress to the crack opening which is a function of fibre and interface properties and mode of failure [78]. Fibre properties may include the fibre modulus, ultimate tensile strength, fibre length, diameter, and the interface properties are the cohesive strength, fracture properties and frictional properties. The micromechanics of fibre bridging is described more in detail by [79]. In a composite, the embedded fibres in the mortar would often bridge a crack at an angle. Inclined fibre pullout would depend on a greater number of parameters, involving the inclination angle of the fibre to the matrix crack plane, local fibre/matrix interaction properties and possible aging effects (interfacial properties and fibre/matrix interaction changing with time) [79].

Fibre bridging after first cracking of the cement matrix is well detectable in PVA-reinforced mortars. For MBC systems, the mechanism is important because with adequately chosen mortars, a MBC system can be altered/improved resulting in a more efficient strengthening material under tension or shear.

6. Testing MBC Systems

As previously shown in Figure 1, the three (material, component and structural) levels of mineral-based strengthening must be linked together. It is not within the scope of this paper to generalize about all existing mineral-based strengthening systems; however linking can be done and is presented for mineral-based composites through experimental investigations carried out at LTU and DTU.

Mineral-based composites are, as defined earlier, a particular instance of mineral-based strengthening in which

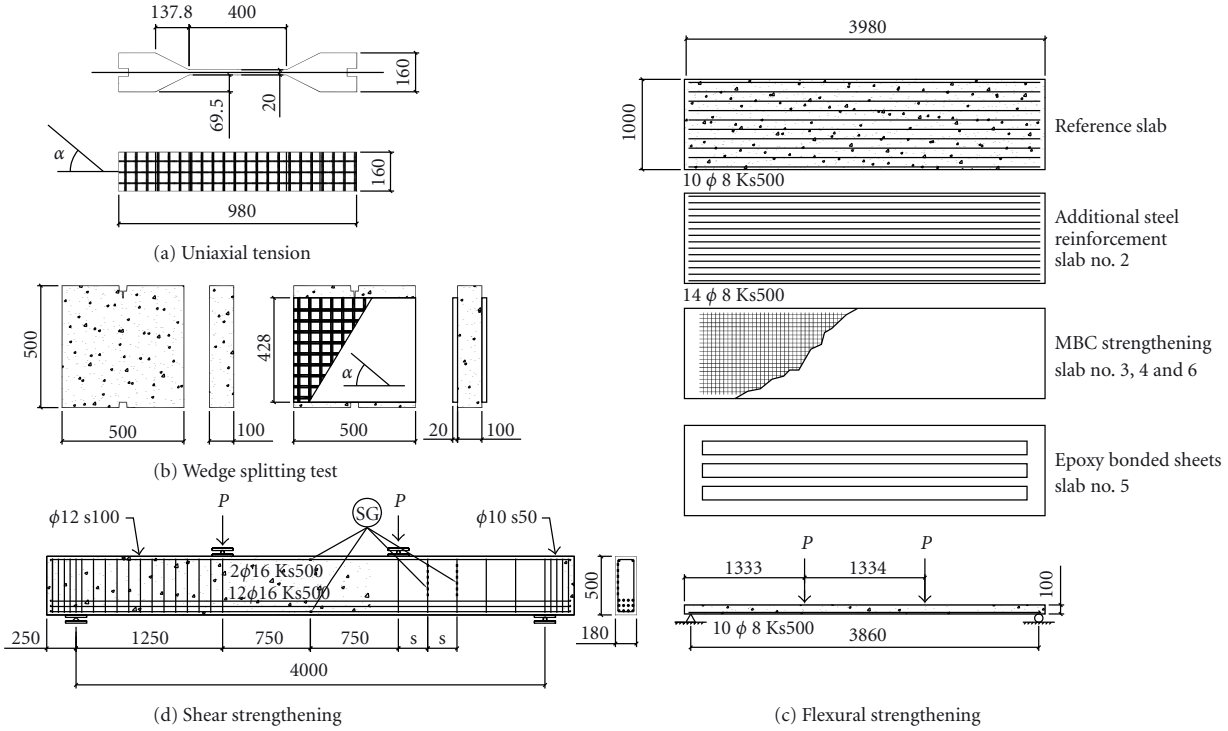

Figure 5: Experimental tests for tensile and fracture behaviour: (a) uniaxial tensile test on dogbones. (b) wedge-splitting test, (c) flexural beams, and (d) shear beams.

FRP grids are adhered to the concrete substrate by means of (quasibrittle or strain hardening) mortars. By using ECC as the mortar phase in MBC, different force transfer mechanisms come into play which did not exist in the initial phase of MBC research where the mortar was a quasibrittle PMM. In addition to that, MBC research has mostly focused on beams strengthened in flexure and shear, and much less attention has been paid to repairing structural members in which significant tensile forces may emerge. Before applying the MBC as a strengthening material in conditions where the structural member is subject to tensional or splitting forces (or bending combined with axial forces), it is necessary to properly characterize the tensile behaviour. Knowledge of related parameters such as the tensile strain-crack opening curve makes possible estimations, for example, about brittleness in compression and tension or shear capacity. Suitable test methods are being searched, which quantify the tensile properties of MBC directly (dogbone tests) or indirectly (WST, giving the splitting tensile strength).

This section will give insight in the MBC behaviour for tension, flexure and shear. Tests have been performed on the tensile behaviour of the MBC system, dogbone and wedge splitting tests (WST), along with flexural and shear strengthening, see Figure 5 where all tests are shown.

6.1. Experimental Set-Up. A summary of tests conducted at LTU and DTU is shown in Figure 5. Uniaxial tensile and wedge-splitting tests aim to characterize the tensile and fracture properties of the strengthening material. Shear and flexural strengthening (Figure 8) involving MBC lead towards the structural level and applications as outlined in Figure 1. Short descriptions of each test are summarized below, and further references are given to a more detailed description of each.

6.2. Material Properties. All the material properties for the materials used in the four different tests are summarized in Table 1 for the CFRP grids and Table 2 for the binders.

6.3. Linking Material and Component Levels

6.3.1. Uniaxial Tensile Tests. New test method and test specimens have been developed for testing MBC under uniaxial tension in [64]. The bare strengthening material was tested, without considering the interaction with a real structure to be strengthened. Quasibrittle polymer-modified mortars and ECC have been investigated together with an embedded CFRP grid in the mid-plane of the dogbone-shaped specimens, focusing on crack development and the influence of the applied mortar's ductility on the behaviour in tension.

Dimensions of the dogbone-shaped test specimens were $160 \times 160 \times 980$ mm, with a representative test section of $400 \times 160 \times 20$ mm. Two different grids with different grid spacings and three chosen grid orientations (0°—longitudinally placed grid, 90°—transversally placed grid, 15°—rotated grid) were tested in different combinations, more in detail presented in [64]. The number of the CFRP tows in the representative test section, tensile direction, were

Table 1: Mechanical properties for the fibres in each tow of the CFRP grids used in experimental tests [53].

Material	Direction	Tow spacing [mm]	Tensile strength [MPa]	E modulus [GPa]	Failure strain [‰]
Grid S	Transverse	25	5214	366	14.0
Grid S	Longitudinal	24	3546	278	12.5
Grid M	Transverse	43	4620	389	11.9
Grid M	Longitudinal	42	4219	404	10.5
Grid L	Transverse	72	3772	423	8.6
Grid L	Longitudinal	70	3877	320	12.8

Table 2: Material properties for binders used in experimental tests.

Material	Description	Tensile strength [MPa]	Compressive strength [MPa]
PMM	Polymer-modified mortar	2.4	53.2
ECC	Engineered cementitious composite	3.0	60.0

7 (small grid) and 4 (medium grid). The specimens were fixed in self-centering, custom-made clamps.

In Figure 6(a), quasibrittle and ductile mortars are compared and related to the linear elastic behaviour of the pure CFRP grid. Behaviour of all specimens was nearly identical up to first cracking irrespective of which mortar is used. After first cracking, ECC specimens show a significant strain hardening behaviour with both small (S) and medium (M) grids which is represented as the contribution of the mortar compared to the shifted lines of the pure grid. The ECC specimens, after the first crack, show a further load increase until the peak load. These curves are smooth due to the fibre-bridging characteristics of the cracks in ECC. Curves of quasibrittle mortars are more jagged and have a significant drop in load carrying capacity right after the first crack (and after further crack formation). This fact shows that the increased ductility of the ECC mortar has a positive effect on the interaction with the CFRP through the fibre bridging effect. It seems to prevent premature failure of the CFRP grid which was observed in the specimens with brittle mortars, with significantly reduced axial tensile strength.

Figure 6(b) illustrates the effect of the grid orientation. The apparent better performance of the grid when rotated transversally may be due to an epoxy surplus on the transversal tows resulting in improved mechanical anchorage or, more likely, due to the joint shape (between longitudinal and transversal tows of the grid) and associated deformation capacity of the grid joints when loaded in a certain direction.

6.3.2. Wedge Splitting Tests. Brittleness of concrete-like materials is usually evaluated by means of the post failure behaviour in tension governed by the stress versus crack width relation (σ-w), the so-called softening behaviour which is a basic property of a (conventional) concrete described by the tensile strength, the maximum crack width and the fracture energy, which corresponds to the area under the stress versus crack width curve. WST (wedge splitting test), originally introduced by [80] and further improved by [81] is a suitable method, traditionally used for brittle materials, for obtaining the splitting tensile strength along with the postpeak behaviour, and an estimation on the fracture energy.

WST is an extension of the uniaxial test because the MBC-strengthening is applied on a concrete surface. In a recently published study [63], behaviour of a CFRP grid reinforcement in two different directions (0° and 45°, resp.) together with quasibrittle and ductile mortars has been investigated and evaluated through recording and comparing crack widths, crack patterns, splitting load versus crack opening displacement curves and fracture energy values for the MBC-strengthened concrete specimens. External dimensions of the plain concrete test specimen were 500 × 500 × 100 mm, after strengthening with a representative test section of 400 × 420 × 140 mm where 140 mm is the total thickness after strengthening on both sides. The length of the starter notch together with the groove is 50 mm. The bottom groove served to ease proper vertical positioning and acted as a line support for the heavy specimens. The CFRP grid was applied on both sides (ten tows bridging the crack on both sides, in the nonrotated position), placed between two 10 mm thick layers of mortar, applied on the concrete surface roughened with sandblasting and treated with a primer to enhance bond on the concrete-mortar interface. Tests were run deformation-controlled, that is, through the crack opening displacement kept constant at 0.3 mm/min, by a clip gauge mounted at the tip of the notch in the midplane of the specimen. During the test, vertical load and crack opening displacement (COD) are recorded, hence the splitting load can be calculated.

The resulting splitting force versus crack opening displacement plots show that the splitting tensile strength of concrete can be significantly improved with MBC-strengthening, resulting in an increase of 30–110% in peak splitting load compared to the unstrengthened reference specimen (Figure 7). ECC has given significantly higher failure loads and similarly to the uniaxial tests, it prevented pronounced drops in load capacity. Ductility is significantly

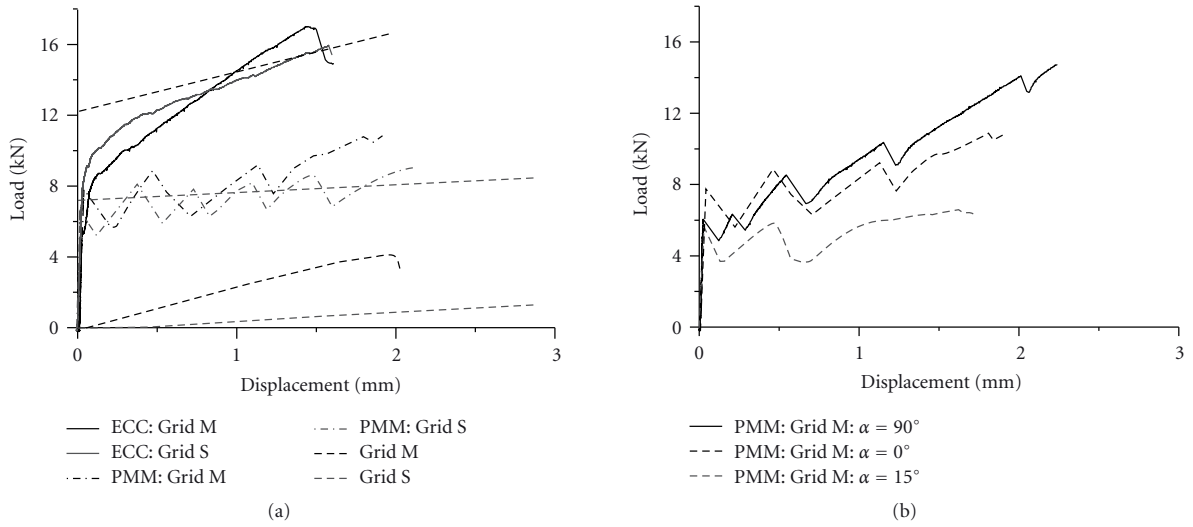

Figure 6: (a) All dogbone specimens with grid S and M placed in longitudinal (0°) direction. (b) Effect of grid orientation (transverse (90°), longitudinal (0°) and rotated in 15°).

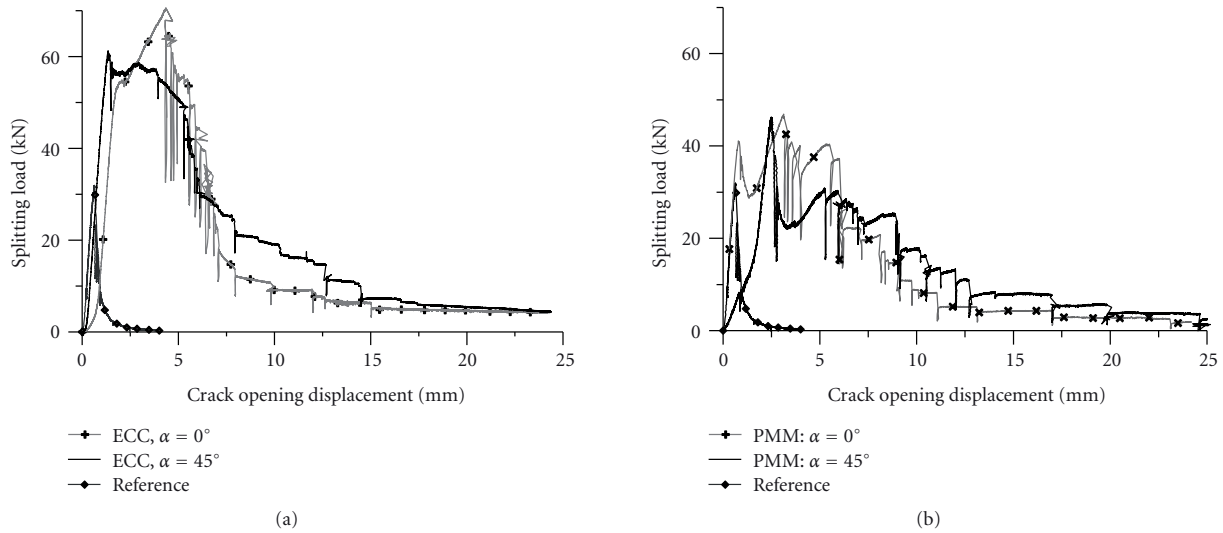

Figure 7: Splitting force versus COD curves for specimens with highest peak load per series, against reference specimen (plain concrete).

enhanced by all grid-mortar combinations resulting in an extreme increase of fracture energy which is directly proportional to the area under the curves.

Bond provided by both mortars was excellent leading to CFRP rupture. By applying PVA-reinforced ductile ECC as bonding agent, improved performance, significantly higher fracture energy, multiple cracking and enhanced ductility were observed, caused by improved bond between grid and mortar due to the refined grain structure, the bridging effect of the embedded fibres working against crack opening and via direct mechanical interlock with the grid.

Compared to a uniaxial tensile test, WST also has provided information on the softening part of the curve after peak load, revealing tendencies in how fast or how gradually load capacity decreases until all crack bridging fibre tows and embedded fibres in the mortar are broken. The slopes of the F_s versus COD curves reveal that the tensile ductility (recorded peak load and its tendency to decrease to zero) depends more on the grid orientation than on the mortar quality, unlike the increase in the energy absorption/fracture energy which seems to be "mortar-dependent" and is significantly higher for the ECC specimens.

6.4. Linking Component and Structural Levels

6.4.1. Slabs Strengthened in Flexure. The test set-up and geometry for the slab specimens is shown in Figure 5 and a more detailed overview and results are also published in [82, 83]. Three of the slabs were strengthened using the MBC system, one specimen with one CFRP grid, one specimens

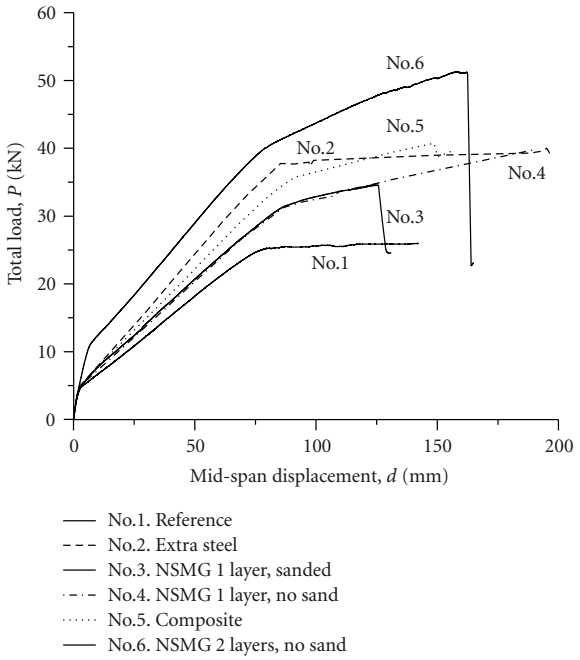

Figure 8: Load versus mid-span displacement of flexural strengthened specimens.

with a sanded CFRP for better mechanical anchorage and one specimen with double CFRP grid. In addition one specimen was strengthened using epoxy-bonded carbon fibre sheets and yet one specimen containing four extra flexural steel reinforcement bars, the extra reinforcement was calculated to correspond to the strengthening. Thus, all of the specimens were designed to have similar failure loads, except the specimen with dual CFRP grid. The thickness of the strengthening layer was approximately 10 mm and a quasibrittle mortar was used as binder. In all MBC-strengthened specimens the CFRP grid had a fibre content of 159 g/m^2 (Grid M). For the epoxy-based strengthening, the carbon fibre sheets had a fibre content of 200 g/m^2. The total carbon fibre amount in the tensile direction of the specimens corresponded to 20 mm^2/m (CFRP grid) and 62 mm^2/m (carbon fibre sheet) respectively.

All of the strengthened slabs increased the ultimate bearing capacity in comparison to the nonstrengthened reference beam. Strengthened specimens using one layer of CFRP grid failed at a total load of 35 kN and specimen with epoxy-bonded sheet failed at 41 kN while showing a stiffer behaviour compared to the latter. The specimen containing four extra flexural bars failed at a load of 38 kN, similar loads to the specimens with only one grid. However, the specimen with extra steel reinforcement showed stiffer response compared to both the specimens strengthened with sheets and one CFRP grid. It is also noted that sanding the surface of the grid (specimen No. 3) led to premature rupture of the CFRP grid. Strengthening the specimen with dual layer of CFRP grid will have a positive effect on the load bearing capacity. Thus this specimen (No. 6) had the highest ultimate load capacity of 51 kN. All of the specimens with the MBC system failed by fibre rupture while the epoxy-based strengthening system failed by a mix mode of debonding and fibre rupture. Comparative load-displacement curves are plotted in Figure 8.

6.4.2. Beams Strengthened in Shear. Beams strengthened in shear had a rectangular cross section and were 4.5 m long and had a height of 0.5 m. Again, these results are described in more detail in [53, 66]. Note, in Figure 8, that the beams were heavily shear reinforced in one shear span and had inferior to no shear reinforcement in the other shear span. Thus, only the shear span containing no or little shear reinforcement was strengthened. In these experiments, the influence of different grids and internal steel shear reinforcement ratios were studied. In all test the quasibrittle PMM was used as a binder of the strengthening system. The PMM was also used in the dogbone and WST tensile test. For testing the influence of different CFRP grids, the carbon fibre amount was varied from 66, 98, to 159 g/m^2 (Grid S, L, and M). All of these specimens had no internal shear reinforcement in the strengthened shear span. For specimens with different internal shear reinforcement the different distances was s = 350 mm and s = 250 mm, see also Figure 5. The internal shear reinforcement was monitored by six strain gauges mounted on both two stirrups closest to the load, see Figure 5. In addition, six strain gauges were mounted on the vertical CFRP tows in the grid at the same locations as the strain gauges mounted on the stirrups.

All of the specimens with no internal shear reinforcement and strengthened with the MBC system failed by fibre rupture of the vertical tows. For strengthened specimens with different internal reinforcement amounts the failure mode changed from a brittle shear failure to a more ductile compressive/crushing failure. The ultimate loads for all specimens are summed in Table 3 together with compressive- and tensile strength of the concrete, and failure modes (S-shear failure and C-compression/crushing). From the results of the specimens strengthened with different grids it was clear that the specimens with highest carbon fibre amount had the highest load bearing capacity. Since the specimens containing internal shear reinforcement were heavily monitored by strain gauges, the shear behaviour and strain development from initial load stages could be measured. Here, the strain development in the stirrups was reduced for beams strengthened with the MBC system. The strains monitored in the CFRP grid indicated that high strain concentrations were apparent in the vicinity of cracks.

Typical strain readings from internal shear reinforcement and CFRP grid are shown in Figure 9 for specimens with and without strengthening corresponding to specimens with concrete compressive strength of 47–52 MPa and internal stirrup distance of 350 mm (Specimens C35s3 and C35s3-Grid M in Table 3). Figures 9(a) and 9(b) shows that strains in the (steel) stirrups are reduced in all MBC-strengthened beams even at relatively low load levels (100–200 kN) when compared to the nonstrengthened ones. As the shear load increases, the favourable strain reduction of the MBC system is more pronounced for a strengthened specimen compared to a non strengthened specimen.

Table 3: Ultimate shear loads and failure modes, along with description of tested shear beams.

Beam	Binder	CFRP	Stirrup distance [mm]	Failure load [kN]	Failure mode	Compressive strength [MPa]	Tensile strength [MPa]
C40s0	—	—	—	123.5	S	44.8	2.9
C40s0*	—	—	—	126.7	S	36.3	2.5
C40s0-M	PMM	—	—	141.9	S	53.6	2.8
C40s0-Grid M	PMM	Grid M	—	244.9	S	53.6	2.8
C40s0-Grid M	PMM	Grid M	—	241.9	S	53.6	2.8
C40s0-Grid S*	PMM	Grid S	—	208.1	S	32.5	2.7
C40s0-Grid M*	PMM	Grid M	—	251.9	S	35.1	3.0
C40s0-Grid L*	PMM	Grid L	—	206.4	S	44.8	2.5
C35s0	—	—	—	130.6	S	47.0	2.7
C35s3	—	—	350	346.0	C+S	47.6	3.1
C35s3-Grid M	PMM	Grid M	350	336.9	C	52.4	3.0

* Tests were run not deformation-controlled but load-controlled at 10 kN/sec.

In the vertical CFRP tows, a significantly uneven strain distribution is visible, with locally high strains in the vicinity of forming shear cracks. These strains are increasing rapidly as the shear crack is opening.

6.5. Field Implementations. The MBC-strengthening system should be able to be implemented in various field strengthening applications such as, harbour structures (less sensitive to moisture compared to epoxy-bonded strengthening systems), large structures that requires higher compatibility of the strengthening system to the base concrete structure, low temperature applications, applications that demand diffusion openness and for concrete applications that excludes the use of epoxies. In addition, the MBC system can be used in tunnelling or mining applications instead of using steel fibre-reinforced shotcrete. In the latter, the combination of using ECC as a binder should further improve the ductility and crack bridging ability of the MBC system. Pilot studies for in-situ production techniques of the MBC system using quasibrittle mortars as binders have been investigated in [82]. The results from this study clearly show that spraying the MBC system can be made in an easy and efficient manner. The application technique is done by mounting the CFRP grid on preattached studs and then the binder is being sprayed. The thickness of the MBC system is controlled by the chosen length of the studs.

6.6. Discussion and Conclusions. Uniaxial tests have revealed that the most commonly used grid (medium-sized, M-grid) performs better when placed in transversal direction. This leads to the need of studying the effect of grid joint formations (i.e., the grid is "woven" out of two perpendicular tows of CFRP and the grid joint looks differently depending on the direction). The uneven distribution of the residual epoxy on the grid surface in the two perpendicular directions could also contribute to the direction-dependent performance.

Flexural specimens strengthened with MBC had higher ultimate load compared to the epoxy-bonded sheets of comparing the fibre amount in the tensile direction. However, the failure mode for the MBC was fibre rupture while the epoxy-bonded carbon fibres failed by a mix mode of debonding and fibre rupture. However, trying to improve the bond between the mineral-based binder and the CFRP grid by the use of sand-coated grids has negative effects on ultimate load bearing capacity. It appears that sanding the surface creates discrete increases in strain and leading to premature failure, this was however not monitored. But as shown in the shear strengthening in Figure 9(b), by the use of monitoring strains in the grid, discrete high strains occur in the vicinity of cracks.

All MBC-strengthened shear beams, which had no internal shear reinforcement, failed by rupture of the vertical tows in the grid. From this series of specimens it was concluded that increasing the fibre amount will also increase the ultimate failure load, to what extent is not within the scope of this paper. But increasing the fibre to a certain level should imply failure in the intermediate transition zone between binder and fibre composite. For beams withinternal reinforcement the failure mode changed from a brittle shear failure to a more ductile compressive failure. For the specimens withinternal reinforcement it could be seen from strain gauge monitoring that the MBC-strengthening system reduced strains in the steel reinforcement even for low shear loads. Thus, this indicates that the MBC-strengthening system can be used for crack width reduction in the service limit state.

MBC tests have shown that strain hardening mortars can be successfully used together with embedded FRP reinforcement and the fibre bridging behaviour of ECC "compensates" for the brittleness of the grid and prevents premature failure of it by retaining fast and rigid deformations in the grid joints. This may enable a better utilization of the grid.

To the authors' knowledge, ECC has been implemented into the MBC system for the first time. Due to its fibre bridging mechanisms and strain hardening behaviour, ECC shall further be tested as a bonding agent for mineral-based strengthening systems. Preliminary results from pullout tests carried out by the authors have shown that if the application

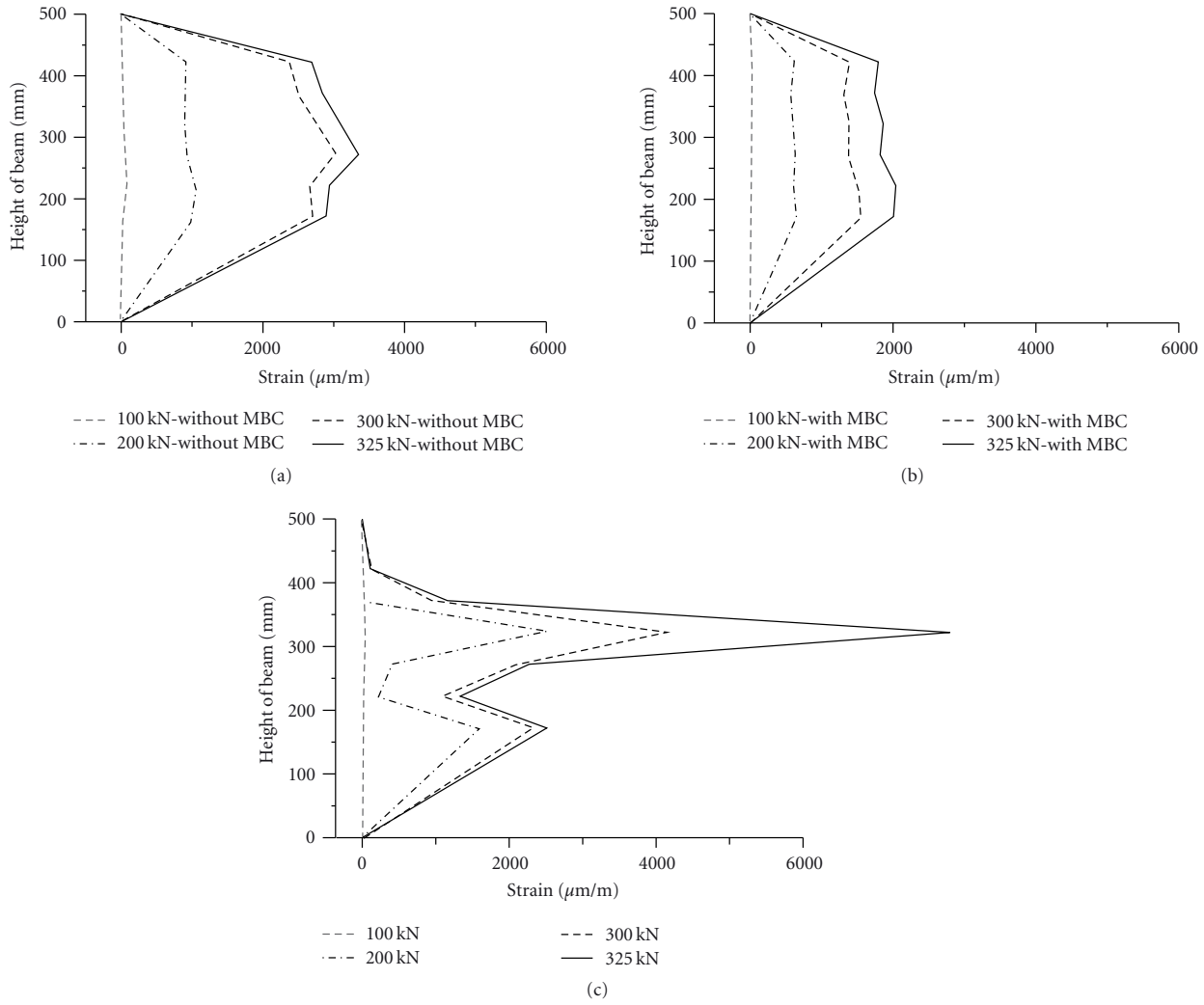

Figure 9: Strain development at different shear loads. (a) in stirrups without MBC and (b) in stirrups with MBC and (c) strains in vertical CFRP tows.

method is correct and the mix is properly compacted around the CFRP grid, there is a nearly perfect bond on the interface even at short embedment lengths (45 mm) using both polymer-modified quasibrittle mortars and ECC. Therefore in a real structural element, the failure mode is expected to be fibre rupture.

Traditionally, ECC has been used up to its maximum strain or deformation capacity (especially where energy dissipation is the major concern). In an ECC-based MBC, the FRP component is fully used up to its maximum potential; however the ECC is not because the FRP reinforcement fails prior to that the ECC would reach its maximum strain capacity. In a structural member made from pure ECC, the maximum strain capacity would be characterized by the highest yet sustainable crack density with evenly distributed fine cracks.

Despite the fact that when combined with FRP, the maximum strain capacity of the ECC is not fully utilized, ECC improves the MBC system significantly. Its main advantages are that it accommodates larger elongations than FRP therefore it will not be the weak link in strengthening, it enforces the failure mode to be more ductile [49] and prevents or reduces sudden brittle deformations. Its documented spalling resistance [46, 47] is also very attractive when designing externally bonded strengthening systems.

6.7. Future Research for MBC

6.7.1. Materials. Strain hardening mortars together with FRP grids should be further tested especially in shear beams or other shear sensitive structures where it should yield a more predictable and ductile failure mode.

Tri- or other multiaxial grids could also be effectively used, in particular for shear strengthening. More flexible grids, in which the joints are not rigid using a more elastic matrix for impregnating the fibres, would most likely

accommodate larger deformability of the grids for the use of, for example, wrapping. Also investigations of incorporating higher fibre amount in the CFRP grid should be made for further increasing the load bearing capacity.

When using ECC as binder, further investigation is needed on whether (and to what extent) the large improvement in load capacity is due to a direct tensile contribution from the ECC or the fact that it is capable to retain grid joints from fast and brittle deformations breaking the grid or to slow down this process, hence preventing premature failure in the grid.

6.7.2. Structural Behaviour and Future Applications. Influences on the bond in the transition zone between fibre composite and binder should be investigated when increasing the fibre amount in the FRP grids. The investigations done so far on the MBC system has shown no problems concerning the bond to the base concrete structure, future applications involving enhancing the load bearing capacity should be followed by an experimental program involving the bond to the base concrete.

For field applications the influence of shrinkage should also be investigated, especially when incorporating ECC as a binder. However, traditional precautions can be taken when commercially available PMM is used as binders.

Regarding future applications, stay-in-place formwork could be one new approach, especially for the combination of using concrete with low-quality as a core material and then using high-quality binders together with a FRP grid as a protective outer layer of remaining formwork.

To incorporate the MBC system for the use in civil engineering structures design guidelines should be developed for estimating the load bearing capacity.

7. Discussion and General Conclusions in Mineral-Based Strengthening

7.1. Guidelines. One of the most important aspects for implementing these mineral-based systems for the use in real structures is that there exist engineering design methods for calculating the load bearing capacity. To the authors' knowledge, there exists no general and commonly accepted design for the mineral-based system. These guidelines should be made on a sound physical basis dealing with both the favourable aspects at the service limit state (crack bridging and crack reducing effects) together with the load bearing increase in the ultimate limit state.

7.2. Production Methods and Procedures. For strengthening larger surfaces, sprayed ECC together with FRP grid reinforcement may be a solution. Although this paper has not dealt with sprayable ECC there has been publications about the topic, see, for example, [84]. As the tensile strength of the pure ECC is not significantly different from that of a concrete, combining it with FRP would be useful when the tensile stresses significantly exceed the upper load bearing capacity of an additional pure ECC strengthening layer.

7.3. Suitable Materials. Perhaps it is an advantage to strengthen a structure using a textile for increasing the ductility at ultimate failure load due to the relatively poor bond between binder and fibre composite. However, for service limit state a full utilization of interfacial bond between FRP and mortar is desirable to maintain economy. This justifies the applicability of grid-type reinforcement if the shape of the cross-section allows a grid to be used. It is important to emphasize that epoxy coating, compared to the textiles used in TRC, significantly improves the interaction between mortar and FRP because of the difficulties of the mortar to penetrate dry fibre bundles.

An alternative to TRC when ductility is an issue is strain-hardening mortars together with grids as published in [63, 64]. Strain-hardening mortars also offer the advantage of a more ductile and predictable failure mode which would be beneficial for strengthening shear sensitive structures.

It is assumed that ECC, when combined with grids, would be able to ensure a more even stress distribution among the grid tows along a crack line because of its fibre bridging effect. Then the peak strains in the adjacent grid tows (as shown, e.g., in Figure 9(b)) would be reduced and redistributed to the neighbouring tows hence making the failure more predictable.

New matrices could also be introduced for impregnating the FRP component. A common method for strengthening columns or beams is wrapping with textiles or continuous sheets/dry fibres. However, wrapping is not possible when using an epoxy-impregnated carbon fibre grid due to the rigidness and brittleness of the matrix. Using textiles makes wrapping around corners much easier [83]. Using a semielastic matrix, for example, latex, which still ensures rigid connection points but allows wrapping around corners, could be a beneficial solution for ensuring rigidity, anchorage and effectiveness of the fibres.

7.4. Interactions. Further research should be directed to the influence of bonding, both between base concrete and binder along with the transition zone and between binder and fibre composite. In MBC, having perfect bond between fibre composite and quasibrittle binder could lead to premature failure in the FRP. In TRC, bond between textile and mortar is significantly weaker and there is a limitation of how many layers of textile can be used effectively without anchorage problems (if there is no additional mechanical anchorage) and debonding. This also limits the maximum fibre amount applicable in a certain direction and therefore the maximum strengthening effect achievable by a TRC system.

Penetration of the FRP component has been a problematic issue with several existing systems (e.g., dry fibres/sheets, TRC). Using nonimpregnated sheets, grids or textiles will generate larger slips and inferior effective strain over the roving cross section with possibly overloaded yarns. Using impregnated fibres (fibres imbedded in an epoxy matrix) will create a more effective strain distribution in the FRP tow such as in case of FRP grids.

7.5. Other Issues. Further research should also be directed to the durability and fatigue aspects of mineral-based strengthening. In seismic regions, ductility and energy dissipation capacity is of importance, in this regard ECC-based systems

which use additional fibre composites as reinforcement could be further developed and investigated.

Acknowledgments

The research work presented in this paper was performed at the Technical University of Denmark and Luleå University of Technology, financed by the Norwegian Research Council through the strategic institute program RECON at Norut Narvik Ltd, the Swedish road administration, and the development fund of the Swedish construction industry. Sto Scandinavia should also be acknowledged for supplying materials in the experimental studies.

References

[1] A. Carolin, *Carbon fibre reinforced polymers for strengthening of structural elements*, Doctoral thesis, Luleå University of Technology, Luleå, Sweden, 2003.

[2] B. Täljsten, "FRP strengthening of existing concrete structures," in *Design Guideline*, Luleå University of Technology, Luleå, Sweden, 2006.

[3] U. Meier, "Bridge repair with high performance composite materials," *Material und Technik*, vol. 4, pp. 125–128, 1987.

[4] T. C. Triantafillou, "Shear strengthening of reinforced concrete beams using epoxy-bonded FRP composites," *ACI Structural Journal*, vol. 95, no. 2, pp. 107–115, 1998.

[5] A. Nanni, "Concrete repair with externally bonded FRP reinforcement," *Concrete International*, vol. 17, no. 6, pp. 22–26, 1995.

[6] H. Ohuchi, S. Ohno, H. Katsumata, et al., "Seismic strengthening design technique for existing bridge columns with CFRP," in *Proceedings of the 2nd International Workshop on Seismic Design and Retrofitting of Reinforced Concrete Bridges*, R. Park, Ed., pp. 495–514, Queenstown, New Zealand, 1994.

[7] M. J. Chajes, T. F. Januszka, D. R. Mertz, T. A. Thomson Jr., and W. W. Finch Jr., "Shear strengthening of reinforced concrete beams using externally applied composite fabrics," *ACI Structural Journal*, vol. 92, no. 3, pp. 295–303, 1995.

[8] T. C. Triantafillou, C. G. Papanicolaou, P. Zissimopoulos, and T. Laourdekis, "Concrete confinement with textile-reinforced mortar jackets," *ACI Structural Journal*, vol. 103, no. 1, pp. 28–37, 2006.

[9] A. Brückner, R. Ortlepp, and M. Curbach, "Anchoring of shear strengthening for T-beams made of textile reinforced concrete (TRC)," *Materials and Structures*, vol. 41, no. 2, pp. 407–418, 2008.

[10] A. Brückner, R. Ortlepp, S. Weiland, and M. Curbach, "Shear strengthening with textile reinforced concrete," in *Proceedings of the 3rd International Conference on Composites in Construction*, pp. 1307–1314, Lyon, France, 2005.

[11] T. C. Triantafillou and C. G. Papanicolaou, "Textile Reinforced Mortars (TRM) versus Fibre Reinforced Polymers (FRP) as strengthening materials of concrete structures," in *Proceedings of the 7th ACI International Symposium on Fibre-Reinforced (FRP) Polymer Reinforcement for Concrete Structures*, C. K. Shield, J. P. Busel, S. L. Walkup, and D. D. Gremel, Eds., pp. 99–118, American Concrete Institute, 2005, SP-230.

[12] V. C. Li, "Engineered cementitious composites," in *Proceedings of the 3rd International Conference on Construction Materials (ConMat '05)*, Vancouver, Canada, August 2005.

[13] J. Mirza, M. S. Mirza, and R. Lapointe, "Laboratory and field performance of polymer modified cement-based repair mortars in cold climates," *Construction and Building Materials*, vol. 16, pp. 365–374, 2002.

[14] M. Raupach, J. Orlowsky, T. Büttner, and A. Keil, "Recent developments of the usage of polymers in textile reinforced concrete," in *Proceedings of the 5th Asian Symposium on Polymers in Concrete*, pp. 53–60, Taramani, India, 2006.

[15] D. Van Gemert, L. Czarnecki, M. Maultzsch, et al., "Cement concrete and concrete-polymer composites: two merging worlds: a report from 11th ICPIC Congress in Berlin, 2004," *Cement and Concrete Composites*, vol. 27, no. 9-10, pp. 926–933, 2005.

[16] S. Pascal, A. Alliche, and Ph. Pilvin, "Mechanical behaviour of polymer modified mortars," *Materials Science and Engineering A*, vol. 380, no. 1, pp. 1–8, 2004.

[17] M. Schleser, B. Walk-Lauffer, M. Raupach, and U. Dilthey, "Application of polymers to textile-reinforced concrete," *Journal of Materials in Civil Engineering*, vol. 18, no. 5, pp. 670–676, 2006.

[18] P. Garcés, J. Fraile, E. Vilaplana-Ortego, D. Cazorla-Amorós, E. G. Alcocel, and L. G. Andión, "Effect of carbon fibres on the mechanical properties and corrosion levels of reinforced Portland cement mortars," *Cement and Concrete Research*, vol. 35, no. 2, pp. 324–331, 2005.

[19] A. Peled and A. Bentur, "Geometrical characteristics and efficiency of textile fabrics for reinforcing cement composites," *Cement and Concrete Research*, vol. 30, no. 5, pp. 781–790, 2000.

[20] Y. Wang, H. C. Wu, and V. C. Li, "Concrete reinforcement with recycled fibres," *Journal of Materials in Civil Engineering*, vol. 12, pp. 314–319, 2000.

[21] P. S. Song, S. Hwang, and B. C. Sheu, "Strength properties of nylon and polypropylene-fibre-reinforced concretes," *Cement and Concrete Research*, vol. 35, pp. 1546–1550, 2005.

[22] D. A. Silva, A. M. Betioli, P. J. P. Gleize, H. R. Roman, L. A. Gómez, and J. L. D. Ribeiro, "Degradation of recycled PET fibres in Portland cement-based materials," *Cement and Concrete Research*, vol. 35, pp. 1741–1746, 2005.

[23] T. Ochi, S. Okubo, and K. Fukui, "Development of recycled PET fiber and its application as concrete-reinforcing fiber," *Cement and Concrete Composites*, vol. 29, no. 6, pp. 448–455, 2007.

[24] A. M. Betioli and D. A. Silva, "Evaluation of durability of PET fibers under diverse aggressive environments," in *Proceedings of the 10th International Conference on Durability of Building Materials and Components (DBMC '05)*, pp. 1–7, Lyon, France, 2005.

[25] K. Wu and J. Zhou, "The influence of the matrix-aggregate bond on the strength and brittleness of concrete," in *Bonding in Cementitious Composites*, S. Mindess and S. P. Shah, Eds., vol. 114 of *Symposium Proceedings*, pp. 29–34, Materials Research Society, Pittsburgh, Pa, USA, 1988.

[26] K. Mitsui, Z. Li, D. A. Lange, and S. P. Shah, "Relationship between microstructure and mechanical properties of the paste-interface," *ACI Materials Journal*, vol. 91, pp. 30–39, 1994.

[27] Y. L. Wong, L. Lam, C. S. Poon, and F. P. Zhou, "Properties of fly ash-modified cement mortar-aggregate interfaces," *Cement and Concrete Research*, vol. 29, no. 12, pp. 1905–1913, 1999.

[28] I. Ahmed, *Use of Waste Materials in Highway Constructions*, Noyes Data Corporation, Westwood, NJ, USA, 1993.

[29] S. Chandra, *Waste Materials Used in Concrete Manufacturing*, Noyes, Westwood, NJ, USA, 1997.

[30] M. Urban, "Properties of hardened self-compacting concrete with fly ash," in *Proceedings of the 3rd International Scientific*

Conference on Quality and Reliability in Building Industry, pp. 533–538, Levoča, Slovak Republic, 2003.

[31] R. F. Feldman, G. G. Carette, and V. M. Malhotra, "Studies on mechanics of development of physical and mechanical properties of high-volume fly ash-cement pastes," *Cement and Concrete Composites*, vol. 12, no. 4, pp. 245–251, 1990.

[32] Z. Rudzionis and E. Ivanauskas, "Investigations in properties of self-compacting concrete modified by fly ash admixture," in *Proceedings of the 8th International Conference on Modern Building Materials, Structures and Techniques*, E. K. Zavadskas, P. Vainiunas, and F. M. Mazzolani, Eds., pp. 151–156, Vilnius, Lithuania, 2004.

[33] B. Mobasher, A. Peled, and J. Pahilajani, "Pultrusion of fabric reinforced high flyash blended cement composites," in *Proceedings of the 6th International RILEM Symposium on Fibre-Reinforced Concretes (BEFIB '04)*, pp. 1473–1482, 2004.

[34] S. Xu and Q. Li, "An experimental study on bending behavior of cementitious composites reinforced in combination with carbon textile and short-cut PVA fiber," in *Advances in Construction Materials*, C. U. Grosse, Ed., pp. 237–254, 2007.

[35] V. C. Li, "Repair and retrofit with Engineered Cementitious Composites," in *Proceedings of the 3rd International Conference on Fracture Mechanics of Concrete and Concrete Structures (FraMCoS '98)*, pp. 1715–1726, AEDIFICATIO, Freiburg, Germany, 1998.

[36] G. Fischer and V. C. Li, "Influence of matrix ductility on tension-stiffening behavior of steel reinforced Engineered Cementitious Composites (ECC)," *ACI Structural Journal*, vol. 99, no. 1, pp. 104–111, 2002.

[37] S. Wang and V. C. Li, "Tailoring of PVA fibre/matrix interface for Engineered Cementitious Composites (ECC)," in *Proceedings of the Fibre Society Symposium on Advanced Flexible Materials and Structures: Engineering with Fibre*, pp. 91–92, Loughborough, UK, 2003.

[38] M. Maalej, T. Hashida, and V. C. Li, "Effect of fibre volume fraction on the off-crack plane energy in strain hardening Engineered Cementitious Composites," *Journal of American Ceramics Society*, vol. 78, no. 12, p. 3375, 1995.

[39] V. C. Li and Y. W. Chan, "Determination of interfacial debond mode for fibre reinforced cementitious composites," *ASCE Journal of Engineering Mechanics*, vol. 120, no. 4, pp. 707–719, 1994.

[40] V. C. Li, "Reflections on the research and development of Engineered Cementitious Composites (ECC)," in *Proceedings of the JCI International Workshop on Ductile Fibre Reinforced Cementitious Composites (DFRCC)—Application and Evaluation (DRFCC '02)*, pp. 1–21, Takayama, Japan, 2002.

[41] V. C. Li, G. Fischer, Y. Kim, et al., "Durable link slabs for jointless bridge decks based on strain hardening cementitious composites," Research Progress Report, Michigan Department of Transportation, Ann Arbor, Mich, USA, 2003.

[42] H. Fukuyama, Y. Matsuzaki, K. Nakano, and Y. Sato, "Structural performance of beam elements with PVA-ECC," in *Proceedings of the 3rd International Workshop on High Performance Fibre Reinforced Cement Composites (HPFRCC '99)*, H. W. Reinhardt and A. Naaman, Eds., pp. 531–542, Chapman & Hull, 1999.

[43] G. Parra-Montesinos and J. K. Wight, "Seismic response of exterior RC column-to-steel beam connections," *Journal of Structural Engineering*, vol. 126, no. 10, pp. 1113–1121, 2000.

[44] S. L. Billington and J. K. Yoon, "Cyclic response of unbonded posttensioned precast columns with ductile fiber-reinforced concrete," *Journal of Bridge Engineering*, vol. 9, no. 4, pp. 353–363, 2004.

[45] G. Fischer and V. C. Li, "Intrinsic response control of moment-resisting frames utilizing advanced composite materials and structural elements," *ACI Structural Journal*, vol. 100, no. 2, pp. 166–176, 2003.

[46] Y. M. Lim and V. C. Li, "Durable repair of aged infrastructures using trapping mechanism of Engineered Cementitious Composites," *Cement and Concrete Composites*, vol. 19, no. 4, pp. 373–385, 1997.

[47] T. Kanda, T. Saito, and N. Sakata, "Tensile and anti-spalling properties of direct sprayed ECC," *Journal of Advanced Concrete Technology*, vol. 1, no. 3, pp. 269–282, 2003.

[48] P. Suthiwarapirak, T. Matsumoto, and T. Kanda, "Flexural fatigue failure characteristics of an engineered cementitious composite and polymer cement mortars," *JSCE Journal of Materials, Concrete Structures and Pavements*, vol. 718, no. 57, pp. 121–134, 2002.

[49] V. C. Li, "Large volume, high-performance applications if fibres in civil engineering," *Journal of Applied Polymer Science*, no. 83, pp. 660–686, 2002.

[50] A. Kamal, M. Kunieda, N. Ueda, and H. Nakamura, "Evaluation of crack opening performance of a repair material with strain hardening behavior," *Cement and Concrete Composites*, vol. 30, no. 10, pp. 863–871, 2008.

[51] V. C. Li and J. Kong, "Self-compacting Engineered Cementitious Composites (Self-compacting ECC)," January 2009, http://ace-mrl.engin.umich.edu/NewFiles/invention/sc_abstract.html.

[52] "Guide for the design and construction of externally bonded FRP systems for strengthening concrete structures," Tech. Rep. ACI 440.2R-02, ACI Committee, 2002.

[53] T. Blanksvärd, *Strengthening of concrete structures by the use of mineral based composites*, Licentiate thesis, Luleå University of Technology, Luleå, Sweden, 2007.

[54] A. Peled, A. Bentur, and D. Yankelevsky, "Effects of woven fabric geometry on the bonding performance of cementitious composites: mechanical performance," *Advanced Cement Based Materials*, vol. 7, no. 1, pp. 20–27, 1998.

[55] A. Badanoiu, "Improvement of the bond between carbon fibres and cementitious matrices," Tech. Rep., Royal Institute of Technology, Stockholm, Sweden, 2001.

[56] A. Wiberg, *Strengthening of concrete beams using cementitious carbon fibre composites*, Doctoral thesis, Royal Institute of Technology, Stockholm, Sweden, 2003.

[57] A. Badanoiu and J. Holmgren, "Cementitious composites reinforced with continuous carbon fibres for strengthening of concrete structures," *Cement and Concrete Composites*, vol. 25, no. 3, pp. 387–394, 2003.

[58] H. C. Wu and P. Sun, "Fibre reinforced cement based composite sheets for structural retrofit," in *Proceedings of the International Symposium on Bond Behavior of FRP in Structures (BBFS '05)*, J. F. Chen and J. G. Teng, Eds., pp. 351–356, Hong Kong, 2005.

[59] A. Keil and M. Raupach, "Improvement of the load-bearing capacity of textile reinforced concrete by the use of polymers," in *Proceedings of the 12th International Congress on Polymers in Concrete (ICPIC '07)*, pp. 873–881, Chuncheon, Korea, 2007.

[60] T. Brockmann and W. Brameshuber, "Matrix development for the production technology of Textile Reinforced Concrete (TRC) structural elements," in *Proceedings of the 3rd International Conference on Composites in Construction*, pp. 1165–1172, Lyon, France, 2005.

[61] T. C. Triantafillou and C. G. Papanicolau, "Shear strengthening of RC members with textile reinforced mortar (TRM)

jackets," *RILEM Journal of Materials and Structures*, vol. 39, pp. 1–9, 2006.

[62] M. Curbach, "Verstärkung von Balken und Plattenbalken mit textilbewehrtem Beton," in *SFB 528 Textile Bewehrungen zur Bautechnischen Verstärkung und Instandsetzung*, pp. 433–462, 2005.

[63] K. Orosz and B. Täljsten, "Development of a new test method for Mineral Based Composites—wedge splitting test," in *Proceedings of the 2nd International Conference on Concrete Repair, Rehabilitation and Retrofitting (ICCRRR '08)*, Cape Town, South Africa, 2008.

[64] B. Täljsten, K. Orosz, and G. Fischer, "Crack development in CFRP reinforced mortar—an experimental study," in *Proceedings of the Asia-Pacific Conference on FRP in Structures (APFIS '07)*, S. T. Smith, Ed., pp. 671–676, 2007.

[65] J. Carlsvärd, *Shrinkage cracking of steel fibre reinforced self compacting concrete overlays—test methods and theoretical modelling*, Doctoral thesis, Luleå University of Technology, Luleå, Sweden, 2006.

[66] T. Blanksvärd, B. Täljsten, and A. Carolin, "Shear strengthening of concrete structures with the use of mineral-based composites (MBC)," *Journal of Composites for Construction*, vol. 13, no. 1, pp. 25–34, 2009.

[67] P. S. Mangat and F. J. O'Flaherty, "Influence of elastic modulus on stress redistribution and cracking in repair patches," *Cement and Concrete Research*, vol. 30, no. 1, pp. 125–136, 2000.

[68] K. E. Hassan, J. J. Brooks, and L. Al-Alawi, "Compatibility of repair mortars with concrete in a hot-dry environment," *Cement and Concrete Composites*, vol. 23, no. 1, pp. 93–101, 2001.

[69] ACI Committee 224, "Cracking of concrete members in direct tension," Tech. Rep. ACI 224.2R-92, American Concrete Institute, Farmington Hills, Mich, USA, 1992.

[70] G. Fischer and V. C. Li, "Effect of fiber reinforcement on the response of structural members," *Engineering Fracture Mechanics*, vol. 74, no. 1-2, pp. 258–272, 2007.

[71] V. C. Li, "Performance driven design of fibre reinforced cementitious composites," in *Proceedings of the 4th RILEM International Symposium on Fibre Reinforced Concrete*, R. N. Swamy, Ed., pp. 12–30, Chapman and Hall, 1992.

[72] P. Kabele, S. Takeuchi, K. Inaba, and H. Horii, "Performance of Engineered Cementitious Composites in repair and retrofit: analytical estimates," in *Proceedings of the 3rd International RILEM Workshop on High Performance Fiber Reinforced Cement Composites (HPFRCC '99)*, pp. 617–627, RILEM, Cachan, France, 1999.

[73] J. Hegger and S. Voss, "Textile reinforced concrete under biaxial loading," in *Proceedings of the 6th RILEM Symposium on Fibre Reinforced Concrete (FRC) (BEFIB '04)*, pp. 1463–1472, Varenna, Italy, 2004.

[74] J. Hartig, U. Häußler-Combe, and K. Schicktanz, "Influence of bond properties on the tensile behaviour of Textile Reinforced Concrete," *Cement and Concrete Composites*, vol. 30, no. 10, pp. 898–906, 2008.

[75] W. Brameshuber, "Textile reinforced concrete: state-of-the-art report of RILEM technical committee 201-TRC," Tech. Rep., RILEM, Bagneux, France, 2006.

[76] E. H. Yang, *Designing added functions in Engineered Cementitious Composites*, Doctoral thesis, University of Michigan, Ann Arbor, Mich, USA, 2008.

[77] JCI-DFRCC Committee, "DFRCC terminology and application concepts," *Journal of Advanced Concrete Technology*, vol. 1, no. 3, pp. 335–340, 2003.

[78] V. C. Li, "From micromechanics to structural engineering—the design of cementitious composites for civil engineering applications," *Journal of Structural Mechanics and Earthquake Engineering*, vol. 10, no. 2, pp. 37–48, 1993.

[79] V. C. Li, "Post-crack scaling relations for fibre reinforced cementitious composites," *ASCE Journal of Materials in Civil Engineering*, vol. 4, no. 1, pp. 41–57, 1997.

[80] H. N. Linsbauer and E. K. Tschegg, "Fracture energy determination of concrete with cube-shaped specimens," *Zement und Beton*, vol. 31, pp. 38–40, 1986.

[81] E. Brühwiler and F. H. Wittmann, "The wedge splitting test, a new method of performing stable fracture mechanics tests," *Engineering Fracture Mechanics*, vol. 35, no. 1–3, pp. 117–125, 1990.

[82] T. Blanksvärd and B. Täljsten, "Strengthening of concrete structures with cement based bonded composites," *Journal of Nordic Concrete Research*, vol. 38, pp. 133–153, 2008.

[83] B. Täljsten and T. Blanksvärd, "Mineral-based bonding of carbon FRP to strengthen concrete structures," *Journal of Composites for Construction*, vol. 11, no. 2, pp. 120–128, 2007.

[84] Y. Y. Kim, H.-J. Kong, and V. C. Li, "Design of Engineered Cementitious Composite suitable for wet-mixture shotcreting," *ACI Materials Journal*, vol. 100, no. 6, pp. 511–518, 2003.

Paper II

Orosz K, Blanksvärd T, Täljsten B and Fischer G

Crack development and deformation behaviour of CFRP-reinforced mortars

Published in:

Nordic Concrete Research Vol. 48
pp 49-69.

Crack development and deformation behaviour of CFRP-reinforced mortars

Katalin Orosz
M.Sc., Ph.D. student
Luleå University of Technology
971 87 Luleå, Sweden
katalin.orosz@ltu.se

Thomas Blanksvärd
Ph.D., Senior Assistant Lecturer
Luleå University of Technology
971 87 Luleå, Sweden
thomas.blanksvärd@ltu.se

Björn Täljsten
Ph.D., Professor
Luleå University of Technology
971 87 Luleå, Sweden
bjorn.taljsten@ltu.se

Gregor Fischer
Ph.D., Associate Professor
Technical University of Denmark
2800 Kgs. Lyngby
gf@byg.dtu.dk

ABSTRACT

This paper reports on a research study investigating CFRP-reinforced mortars in uniaxial tension, as a strengthening material for concrete structures. The bare strengthening material was tested on dogbone specimens. Crack formation, crack development and the interaction between the grid and the mortar phase with varying geometrical parameters and mortar compositions have been investigated and evaluated. The use of engineered cementitious composites, exhibiting multiple cracking and enhanced pseudo-ductility in uniaxial tension, was found to result in an improved overall performance.

Keywords: concrete, strengthening, carbon fibre reinforced polymers (CFRP), mortar, mineral based composites (MBC), strain-hardening cementitious composites (SHCC), tensile tests, strain hardening, cracking, pseudo-ductility

1. INTRODUCTION

Fibre-reinforced polymers (FRP) have become a popular material for strengthening and/or retrofitting of existing concrete structures. Externally epoxy-bonded FRP systems have been proven to be an effective strengthening method in repairing or strengthening structures and there has been a large amount of literature published on the topic; see for example [1-4].

Despite their advantages over traditional strengthening methods, the use of epoxy-bonded systems is not entirely problem-free [2]. The epoxy resin creates sealed surfaces. Furthermore, it has poor thermal compatibility with the concrete substrate, it is sensitive to moisture at the time of application, and it creates a hazardous working environment. In cold climates, the use of epoxy is limited because of the minimum temperature of application (typically, 10°C or 50°F) [2]. Therefore, it is of interest to develop alternative strengthening systems where the epoxy bonding agent can be replaced with cementitious materials, for example a polymer-modified or purely cementitious mortar with similar properties to those of the concrete substrate and applicable in a more environmentally friendly and possibly also cost-effective way.

Mortars can be combined with FRP textiles or 2D grids to form an effective strengthening system. This kind of strengthening system has already been tested by [5, 6] on flexural and shear beams.

In the research presented, conventional, quasi-brittle, and “ductile” binders have been combined with CFRP grids. The quasi-brittle binders used are commercially available, pre-mixed, polymer-modified mortars. The ductile binder is strain-hardening cementitious composite (SHCC), namely, a polyvinyl alcohol-reinforced engineered cementitious composite (PVA-ECC), that exhibits strain hardening along with enhanced tensile ductility. The uniaxial tensile tests aimed at obtaining better understanding of the tensional behaviour of the FRP grid-reinforced cementitious composite material.

Only the bare strengthening material is tested here, not considering the interaction with the concrete structure to be strengthened. The main reasons for replacing the conventional mortar with strain-hardening mortars, in a few specimens, were to 1) enhance the loading capacity, 2) enhance the deformation capacity, and 3) prevent brittle failure in the FRP.

2. RESEARCH SIGNIFICANCE

By substituting the traditionally quasi-brittle mortar with a strain-hardening cementitious mortar in an externally bonded strengthening system, the interaction between the cementitious mortar and the FRP reinforcement can be significantly altered and improved, (potentially) leading to a more effective use of the FRP reinforcement. Such cement-based systems may in certain conditions, replace the conventional epoxy-based systems. It is also shown how the behaviour of a strain-hardening cementitious mortar can improve the mechanical properties of a mineral-based strengthening system.

3. RESEARCH QUESTIONS

The study aimed to answer the following questions:

1. Which is the best material combination/orientation leading to the optimal utilization of the FRP?
2. How do the failure modes and the load- and deformation capacity compare, depending on the mortar type? Can a strain-hardening effect be shown in specimens cast with tensile strain-hardening mortars?
3. Can the brittle and/or premature failure of the FRP grid be prevented by applying a ductile matrix?
4. Prove whether the dogbone test setup is a suitable test method for testing MBC in tension.

4. STRENGTHENING WITH CEMENTITIOUS COMPOSITES

The mechanics and design of different FRP reinforcements together with cementitious bonding agents have been extensively researched. The short overview here is selective to applications, which have led to strengthening with grid-reinforced mortars. A more detailed "state-of-the-art" can be found in [7].

Embedded continuous (dry) fibres, fibre reinforced cementitious mortars, textile-reinforced mortar (TRM) or textile-reinforced concrete (TRC) make use of the tensile strength of the FRP reinforcement which is significantly higher than that of the mortar phase. The FRP component in these applications is intentionally aligned accordingly to the principal stresses expected during the lifespan of the structure. In TRC, the load capacity is heavily dependent on the proper penetration of the textile by the mortar, as emphasized by e.g. [8]. If instead of a textile, the FRP is a grid, it offers the advantage of an improved mechanical anchorage due to the rigid joints of FRP in fine-grain mortars and it ensures that all fibre filaments will work together. The pre-cut grid, available with different grid spacing and thickness, can be embedded between two layers of polymer-modified mortar, resulting in a strengthening layer of about 5-10 mm of total thickness [5].

In a cementitious strengthening system, the bond between base concrete (structure to be strengthened) and first layer of polymeric mortar is enhanced by a primer. Several tests have been carried out with grid-reinforced mortars, mainly focusing on flexural [5, 9], and shear strengthening [5, 10]. These tests have shown that that it is possible to achieve a near-perfect bond between the grid and the cementitious matrix so that the composite material will fail with FRP rupture. However, failure of the grid is often premature because of local stress concentrations.

In the mortar phase, mix designs that introduce fly ash and/or silica fume partly replacing the cement in order to densify the microstructure result in higher bond strength between FRP (textiles) and matrix [11]. Mortars can also contain chopped or milled fibres of different kinds. If such a mortar is used together with an embedded reinforcement, improved bond is expected because of the fibre interlock mechanism.

In recent years, micromechanically designed strain-hardening materials have been developed, in which a tensile stress-strain behaviour analogous to that of metals has been achieved. Strain-hardening cementitious composites (SHCC) are defined by an ultimate strength higher than their first cracking strength and the formation of multiple cracking during the inelastic deformation process [12]. However, the inelastic deformation behaviour of SHCC is based on the sequential development of matrix multiple cracking while undergoing strain-hardening [13]. It is more

accurate to refer to the mechanism as *pseudo* strain hardening in order to differentiate it from the "real" strain hardening observed in metals, that is based on dislocation micromechanics in the plastic deformation regime.

The most typically used SHCC, the engineered composite (ECC) utilizes short, randomly oriented polymeric fibres (e.g. polyethylene, polyvinyl alcohol) at moderate volume fractions - typically less than 2% [13, 14]. ECC has been used in standalone and strengthening applications where ductility is an important criterion. The pseudo strain-hardening behaviour of ECC has been utilized as a mechanism to redistribute concentrated loading and thus prevent sudden failure at critical structural connections where steel and concrete come into contact, i.e., shear studs, fasteners or joints, where a steel beam meets an RC column in a hybrid structure [15]. The high damage tolerance of ECC is valuable to the performance of a structure in terms of collapse resistance, extension of service life, and minimization of repair after an extreme event [15] or strengthening purposes. When used in combination with (steel) reinforcement, the tensile ductility of the ECC matrix can on a macro scale, eliminate the strain difference between reinforcement and matrix material [13].

5. LOAD-DEFORMATION RESPONSE OF CEMENTITIOUS COMPOSITES

5.1. Tensile response of cementitious materials

Cement-based composites can be conveniently classified according to their tensile response [12]. The authors have compared the tensile behaviour of steel fibre reinforced concrete, textile reinforced concrete (TRC), engineered cementitious composites (ECC), and steel-reinforced ECC more in detail, based on the existing literature. Only a comparative figure is being presented here (Figure 1) with brief explanations. The different stages are named in a way that they mean the same for the different materials, so not all stages exist for all materials.

Quasi-brittle and ECC mortars used in the tests behave identical to the mortar components shown in Figures 1a and 1c, respectively. During the formation of multiple, evenly distributed, closely spaced, small cracks (Figure 1c), the ECC matrix shows an overall strain-hardening behaviour, without definitely distinctive parts in the curve from σ_{cc} to σ_{pc}. After localization, there is a gradually decreasing, softening range due to the fibre pullout mechanism.

ECC works well with regular steel reinforcement [16]. The hardening part of the load-deformation curve of the steel reinforced ECC (R/ECC) is not as uniform as in plain ECC but has a steeper and a gradually raising part, in accordance with the elastic stage/yielding of the steel. In the inelastic deformation regime, where both components are yielding, cracking of the ECC and yielding of the reinforcement are uniformly distributed over the length of the specimen, until rupture of the steel. The hatched area in Figure 1d represents the contribution of the ductile matrix compared to steel.

Finally, in TRC [17] where the FRP is linear elastic up to failure and the mortar (typically) is quasi-brittle, the hardening part can be divided in two distinct parts as shown in Figure 1e. After first crack formation, the load-deformation curve shows a small increase in loading capacity due to the formation of additional transverse cracking. The member is softened by the formation of additional crack(s) and the load increase per deformation increment is decreasing with each crack until the stabilized crack pattern (II/b) is reached which is nearly linear.

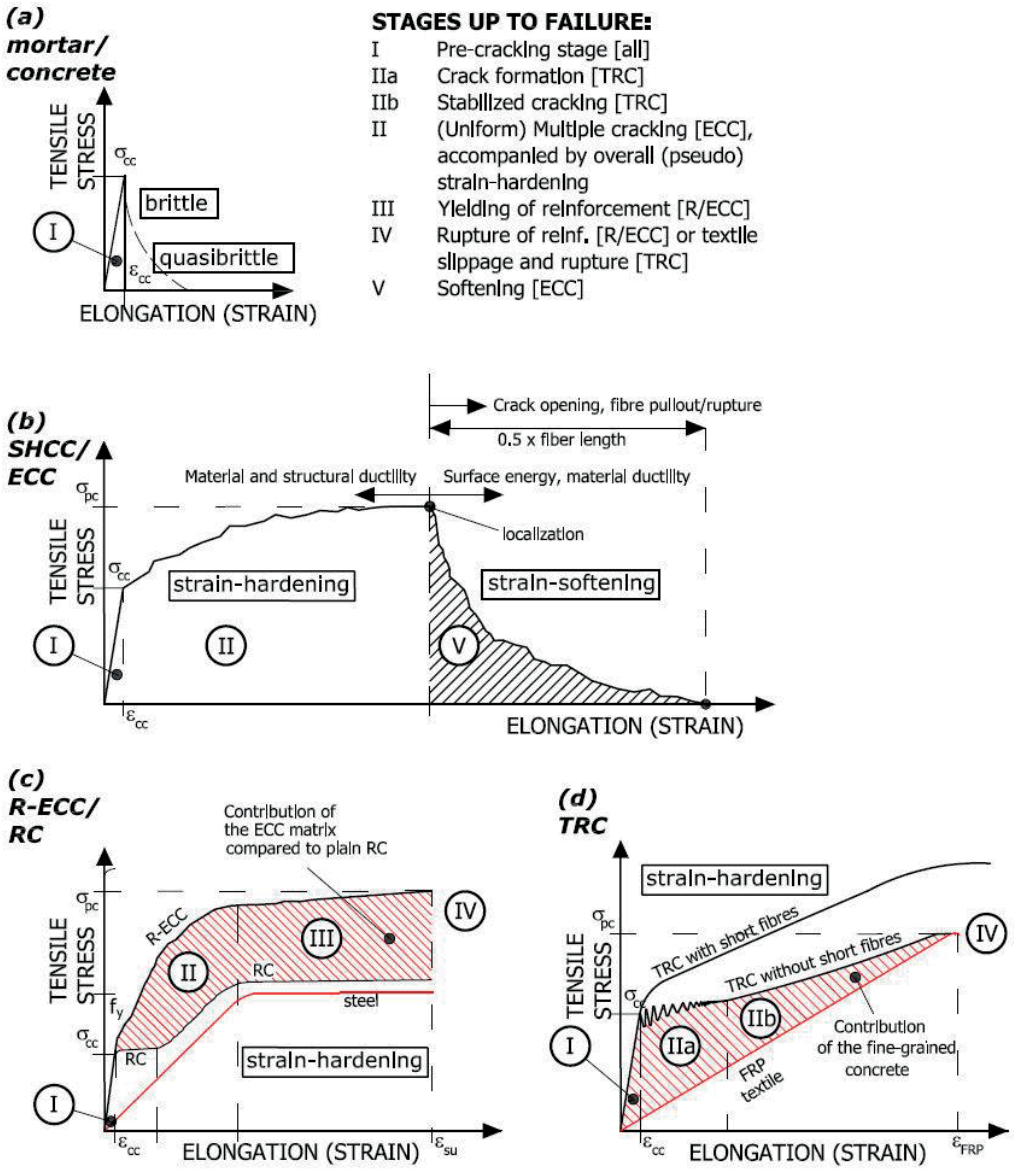

Figure 1 – Tensile response of cementitious materials, based on and [12, 13, 18, 19].
(a) Conventional mortar and concrete, (b) strain-hardening cementitious composites, (c) steel vs. reinforced concrete vs. steel-reinforced engineered cementitious composite, (d) textile-reinforced concrete.

Crack widths here are governed by the FRP reinforcement and the bond characteristics to the surrounding concrete matrix, and *mainly* the FRP determines the stiffness of the member. However, the uncracked segments between the cracks still increase the stiffness of the member, as long as they are not debonded from the FRP reinforcement. Since the FRP reinforcement has no inelastic deformation capacity, failure of a TRC is characterized either by slippage in the fibre tows or by linear elastic deformations until the FRP ruptures in a brittle manner upon reaching its tensile failure strain [17]. In practice, final failure normally is a combination of both fibre slippage and rupture [19].

If the TRC matrix contains short fibres, after first cracking the hardening part becomes uniform, similar to that of the ECC [18].

5.2. Tension stiffening effect

The contribution of a cementitious matrix to the load–deformation response in uniaxial tension is generally described as tension-stiffening effect [20]. The response of the reinforced cementitious composite is compared to that of the bare strengthening material (steel or FRP) and the difference in load capacity is attributed to the tensile load carried by the cementitious matrix between transverse cracks. The matrix contribution is most emphasized in steel reinforced ECC (Figure1d), but also significant in textile reinforced concretes (Figure 1e).

6. EXPERIMENTAL PROGRAM

6.1. Materials

In the experimental program, two different CFRP grids and three types of mortars were used. Material properties are listed in Table 1 (grids) and Table 2 (mortars).

Table 1 – Material properties of the grids used

FRP *tested* values	Spacing L x T [mm]	E_{Lt} [GPa]	E_{Tt} [GPa]	f_{Lt} [GPa]	f_{Tt} [MPa]	ε_{Lt} [‰]	ε_{Tt} [‰]
small	24 x 25	79	51	988	740	12.5	14.0
medium	42 x 43	85.4	45	944	500	11.1	11.1
FRP *supplier* data	Spacing L x T [mm]	E_{Lm} [GPa]	E_{Tm} [GPa]	f_{Lm} [GPa]	f_{Tm} [MPa]	ε_{Lt} [‰]	ε_{Tt} [‰]
small	24 x 25	262	289	4300	3950	15.0	14.9
medium	42 x 43	284	253	3800	3800	13.4	15.0

Table 2 – Material properties of the mortars used

Material	E_c [GPa]	f_{cc} [MPa]	f_{ct} [MPa]	w/c	notes
M1 (from supplier)	26.5	53.2	9	0.16	-
M2 (from supplier)	35	77	2.8		-
ECC (from earlier tests)	19	60	3	0.88	Fly ash 45 mass %; PVA 0.01 mass %

The utilized grids are the C3000 A X1 grid (referred to as “medium grid”) and the C5500 A X1 grid (“small grid”) from Chomarat, U.S. Both grids are epoxy-coated with a fibre volume percentage of 20-25%. We used two pre-mixed, commercially available mortars; StoCrete GM1 (M1) and StoCrete TS100 (M2), from Sto Scandinavia AB. These mortars are one-component, high-strength, polymer-modified, quasi-brittle mortars with tensile strengths of 53.2 MPa (M1) and 77.0 MPa (M2). M1 also has low fibre reinforcement content. The exact mortar compositions or information on the fibrous component is not provided by the manufacturer.

The used primer (Table 3) is a one-component, cement-based and polymer-reinforced powder mixed with water. It is used as a silt-up product on the roughened (sandblasted) concrete surface. Its function is to enhance the bond in the transition zone.

***Table 3** – Material properties and mixing ratio for the primer*

	Density [kg/m^3]	d_{max} [mm]	Mixing ratio, primer:water
Primer	2020	2	1:0.22

The third mortar tested is an ECC mix ("DTU ECO-3 M9 Melflux") containing PVA fibres (1% by weight, or 2% by volume) and a large portion (44% by weight) fly ash. Its tensile strength is 60 MPa. The exact mix composition is given in Table 4.

Table 4 – Mix composition of the ECC used

Material	Fraction [mass %]
Cement (basic Portland)	22
Fly ash	44
Sand (<0.15mm)	8
Quartz powder 100/22	8
Water	18
Superplasticizer (Melflux)	0.02
PVA fibre (oiled)	1

6.2. Test matrix

With the three different mortars (M1, M2, ECC), two different grids (medium and small) and three chosen grid configurations (0°, 90°, and 15° with respect to the applied tensile force), the final test matrix consists of 13 different combinations, 3 specimens per each series, in total 44 specimens. The first five are dummies (2 x M1 without reinforcement, 2 x M1 with medium grid longitudinal direction, and 1 x ECC medium grid longitudinal direction), followed by the 3x13 reinforced specimens. The tested combinations are summarized in Table 5.

Table 5 – Test matrix

Series nr.	Mortar	Grid spacing	Grid config.	Test specimen	No. of specimens
1	M1	---	---	Dummy	2
2	M1	medium	0°	Dummy	2
3	ECC	medium	0°	Dummy	1
4	M1	---	---	M1 reference	3
5	M2	---	---	M2 reference	3
6	M1	medium	0°	M1-0-M	3
7	M1	small	0°	M1-0-S	3
8	ECC	medium	0°	ECC-0-M	3
9	ECC	small	0°	ECC-0-S	3
10	M2	medium	0°	M2-0-M	3
11	M1	medium	15°	M1-15-M	3
12	M2	medium	15°	M2-15-M	3
13	M2	small	15°	M2-15-S	3
14	M1	medium	90°	M1-90-M	3
15	M1	small	90°	M1-90-S	3
16	M2	small	90°	M2-90-S	3

6.3. Specimens

Earlier "dogbone" tests with textile reinforced concrete and a large-scale experiment were described by [21], on 900 x 100 x 60 mm specimens with a 10mm thick web. Based on those sizes, but considering that a typical MBC strengthening layer consists of two 10 mm thick layers and a grid, new specimens were designed, as illustrated in Figure 2.

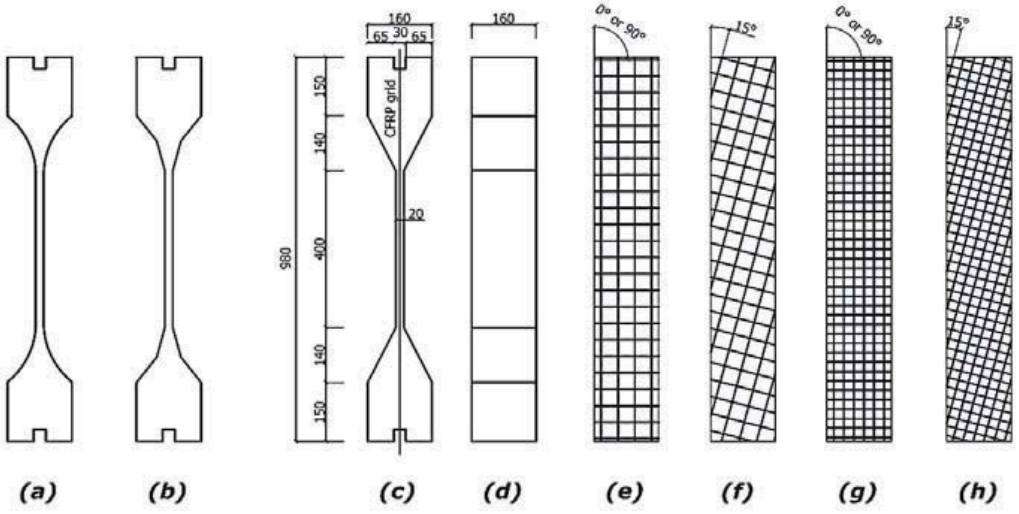

Figure 2 – Test specimen and reinforcement configuration

For brittle or quasi-brittle materials, the uniaxial tests are very sensitive, as an uncontrolled deformation at cracking occurs despite the displacement control. In addition to that, the dogbone geometry is very sensitive to cracks initiating towards the ends of the test field, where the thin web meets the bulk end of the specimen. To prevent cracking in these areas, the optimal solution would be a concave slant surface (a) or a specimen with 2-step slant surface (b) to minimize this risk. Due to resources, simpler dogbone geometry was decided upon (c and d), with a total length of 980 mm, and a web thickness of 20 mm.

The length of the test field was set to the longest possible so that it has a high crack potential; yet short enough to be able to de-mould and handle the specimens without breaking them apart. The final dimensions were set to 160 x 160 x 980 mm in order to meet the geometry of the existing moulds, with a representative test section of 400 x 160 x 20 mm. The CFRP grid was placed in the mid-plane of the specimen (Figure 2b) into the slits at the ends. Figure2e through Figure 2h shows the different reinforcement orientations. The 30 x 30 mm wedged slits at the end of each bulk can be used to glue some additional CFRP material to the reinforcement with epoxy as extra anchorage in the case that bond slippage occurs prematurely. The end slits were wedged, to ease the de-molding process. All specimens were de-molded after 24 hours except for the unreinforced reference specimens and the ECC specimens, which were de-molded after 48 hours. All specimens were water cured for at least 28 days prior to testing.

6.4. Anchor clamp

The uniaxial test requires special devices for loading. The anchor clamp is the fixating mechanism between the test machine and the test specimen. Its main purpose is to hold the specimen fixed and centred, and to transfer the tensile force form the test machine evenly into the specimen. It has joints in both planes parallel to the tensile force, to avoid any shear forces in the specimens.

The clamps were designed based on combining multiple clamp designs detailed in [22], shown in Figure 3. A combination of (b) and (d) has been chosen and custom-welded for this experiment. From (b), the concept of two crossbars, transferring the force through a slant surface, and from (d), the double joints were taken, in order to nullify any shear forces in the web. However, in order to save space, the custom device had both joints working in the same plane.

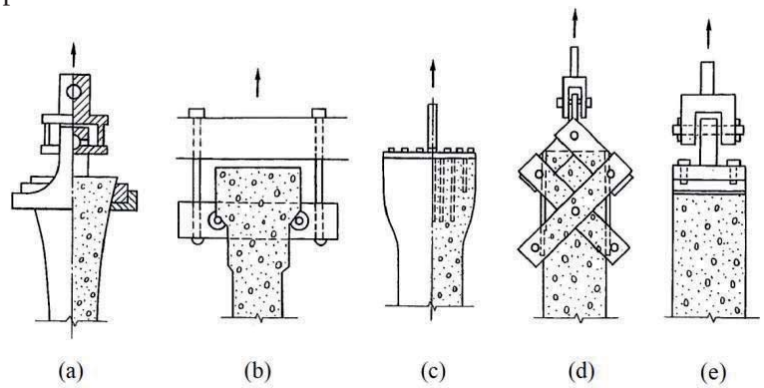

Figure 3 – Various tensile clamps for direct tensile testing [22]

Between the crossbars and the specimen, neoprene was used to distribute the forces evenly. The main bulk of the specimen is in compression at all times during testing, which means that the

connection between the clamp and the specimen is less vulnerable to fracture. The clamp is self-centring, since the crossbars are rotate-able and automatically wedge the specimen into the right position. The side plates are also able to rotate, to help the easy mounting and demounting of the specimens. The anchor clamps are shown in Figure 4.

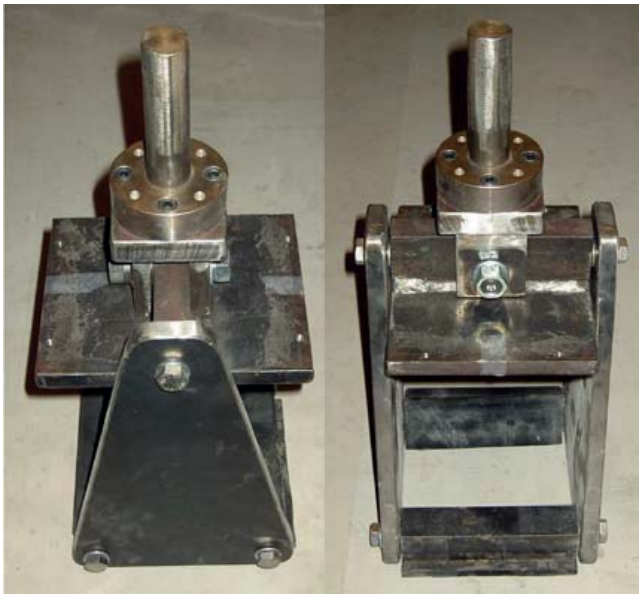

Figure 4 – Custom-welded self-centring anchor clamps

6.5. Measurements and monitoring

The dogbone tests were run under displacement control at a rate of 0.6 mm/s. The load-deformation behaviour was monitored within the representative test section, and recorded by a data logger connected to the test machine. A digital image correlation system (ARAMIS from GOM Optical Measuring Techniques, Germany) was also used to monitor deformations in the test field. ARAMIS is a non-contact and material independent 3D optical measuring system, which analyzes, calculates, and documents material deformations by means of recording and calculating relative displacements of discrete points on a patterned surface. The ARAMIS measurements were conducted primarily to monitor and analyze crack development and crack widths. In addition, strain overlay photos were taken for illustrating crack development within the test field.

7. EXPERIMENTAL RESULTS

7.1. Evaluation and presentation of test data

The specimens were compared by their load-deformation behaviour, first cracking strength, failure load, mean number of cracks developed within the test field and average crack width. The ARAMIS documentation consists of plots illustrating crack development (crack widths, crack density) and elongations within the test field.

7.2. Load-deformation response

The un-strengthened mortar specimens failed in a brittle manner as expected for plain mortar. Average failure loads were 8.7 kN and 8.3 kN for M1 and M2, respectively.

Three quasi-brittle specimens had small cracks on them close to the end of the test field after de-molding; these are excluded from the results. For the remaining specimens, the tensile response is plotted in Figures 5-15. Here we did not include the plain mortar specimens to save space (the response was linear elastic). Additionally, part of the curves we plotted against the *measured* properties of the bare grid on Figures 5-9, and 13 [23], which is the straight line starting at first cracking.

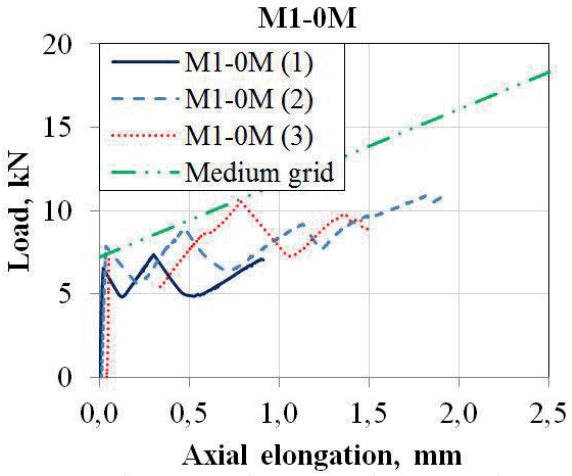

Figure 5 – M1-0-M

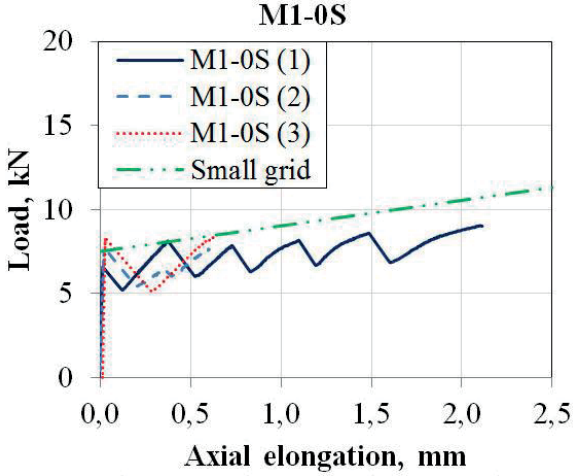

Figure 6 – M1-0-S

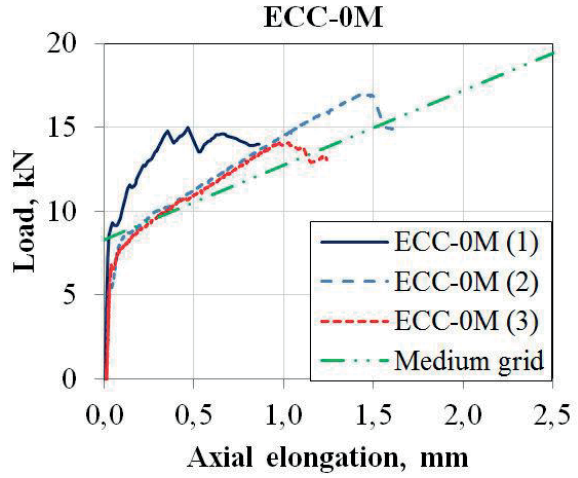

Figure 7 – ECC-0-M

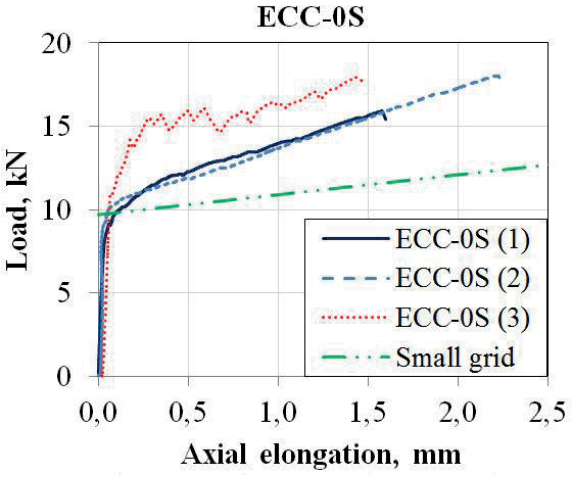

Figure 8 – ECC-0-S

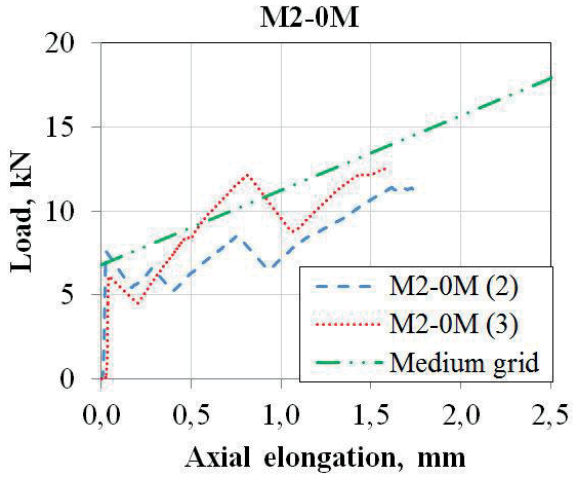

Figure 9 – M2-0-M

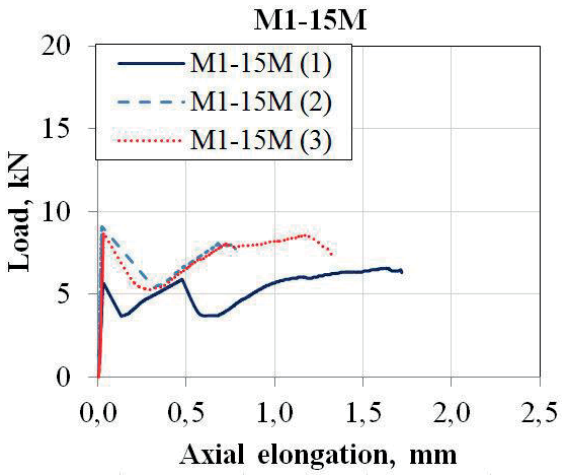

Figure 10 – M1-15-M

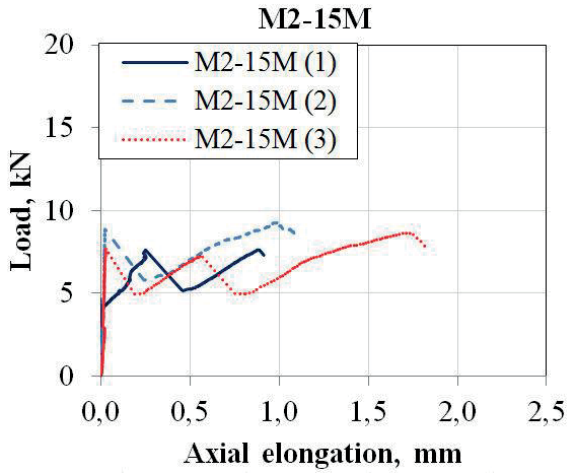

Figure 11 – M2-15-M

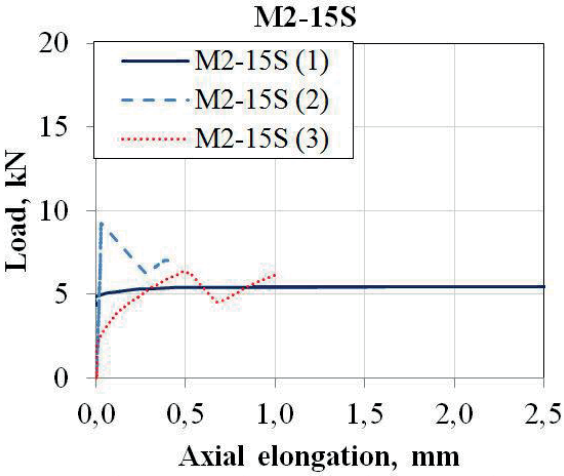

Figure 12 – M2-15-S

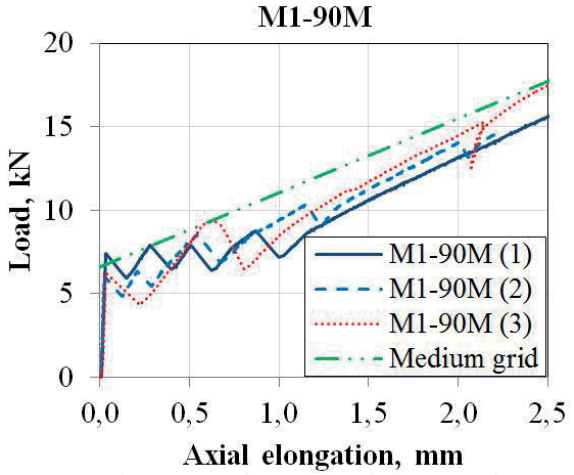

Figure 13 – M1-90-M

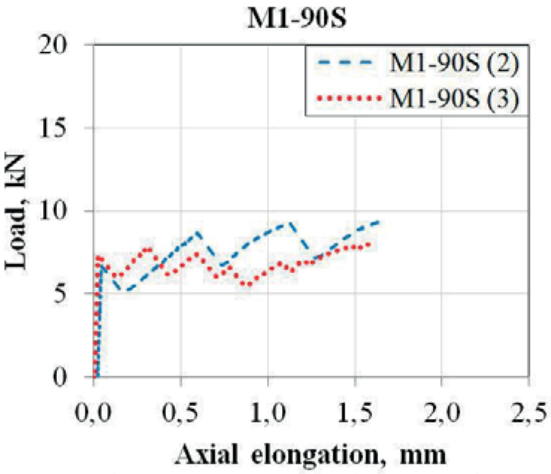

Figure 14 – M1-90-S

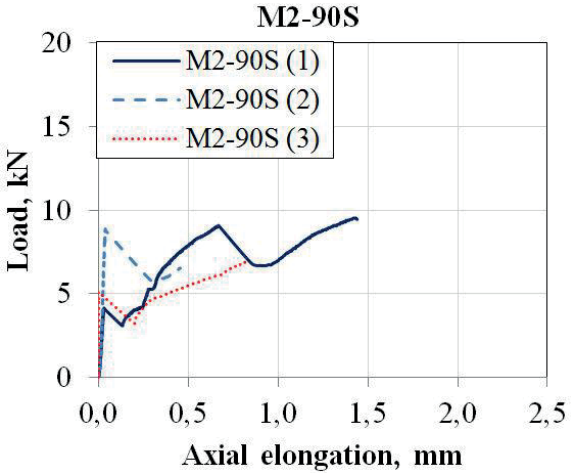

Figure 15 – M2-90-S

Parallel to the plots, Table 6 summarizes first cracking and failure loads, also including the plain mortar specimens.

Table 6 – Results

Test specimen	Failure load [kN]	First cracking load [kN]	Mean nr. of cracks	Average crack width [mm]	Min. expected load capacity (grid only) [kN] theoretical/measured
M1 reference	8.7	8.7	1	N/A	N/A
M2 reference	8.3	8.3	1	N/A	N/A
M1-0-M	9.2	7.2	2.3	N/A	14/22
M1-0-S	8.3	7.5	2.7	0.7	7/8.8
ECC-0-M	15.0	8.3	6.7	0.3	14/22
ECC-0-S	17.3	9.7	7.0	0.2	7/8.8
M2-0-M	11.9	6.8	2.3	0.7	14/22
M1-15-M	7.7	5.7	1.3	N/A	N/A
M2-15-M	8.5	7.1	1.7	N/A	N/A
M2-15-S	6.6	N/A	N/A	N/A	N/A
M1-90-M	15.9	6.6	4.0	N/A	14/22
M1-90-S	8.9	7.4	4.3	0.6	9.8/8.1
M2-90-S	9.0	5.9	6.0	N/A	9.8/8.1

As a general remark, we can conclude that the there is a significant difference in the behaviour of the quasi-brittle and "ductile" specimens after first cracking. Curves of quasi-brittle mortars M1 and M2 are jagged and have a significant drop in load carrying capacity right after the first crack (and after every further crack developing). Contrary to the quasi-brittle ones, the ECC specimens after the first crack show a further load increase until the peak load. These curves are smooth due to the fibre-bridging characteristics of the ECC. However, it has to be noted that only a total number of six ECC specimens were tested, so our results are not conclusive.

First cracking strengths are slightly higher in the ECC specimens (8.3-9.7 kN) compared to the quasi-brittle specimens (5.7-7.5 kN). In case of the ECC, it was difficult to determine, even from the test data, when exactly the actual cracks form, because of the smooth transition between the un-cracked and the cracked stage. Studying the load-deformation graphs of the ECC specimens and applying tendency lines between the pre- and post-cracking stages, we approximated the first cracking loads. It revealed that the initial cracking of the ECC does in fact occur at a later stage than for the M1 and M2 specimens.

The most consistent behaviour we could observe in the M1-90-medium and M1-90-small specimens. Interestingly, in both of the ECC series, we had one specimen behaving very differently both in terms of first cracking load and stiffness (see discussion).

7.3. Comparative load-deformation plots

Specimens with similar grid size, and/or orientation have been paired and plotted in Figures. 16-19. Figure 16 shows all medium grids when placed longitudinally, in different mortars. Figure 17 compares all transversally placed grids. Figure 18 shows the small grid placed longitudinally. Finally, Figure 19 illustrates the effects of the (medium) grid orientation from 0° to 90° for one quasi-brittle mortar (M1).

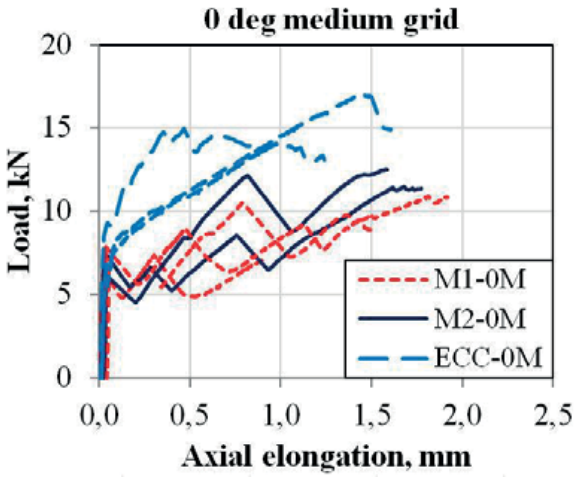

Figure 16 – Medium grid 0°

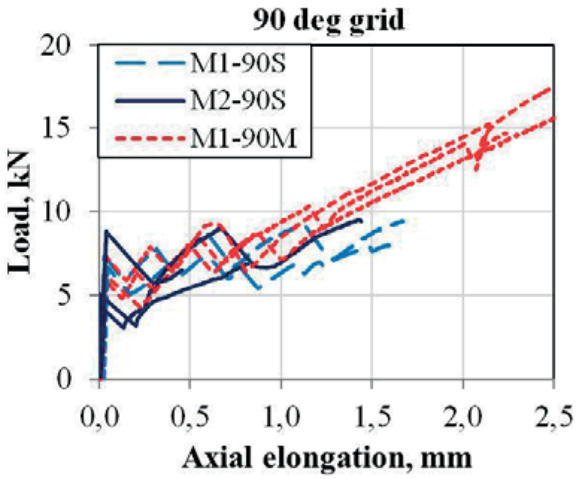

Figure 17 – All 90° grids

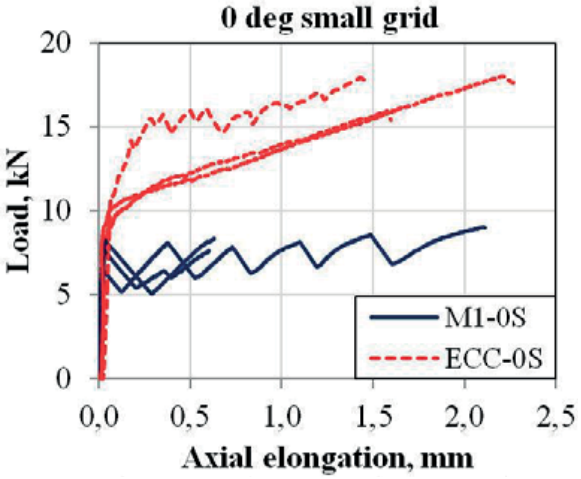

Figure 18 – Small grid 0°

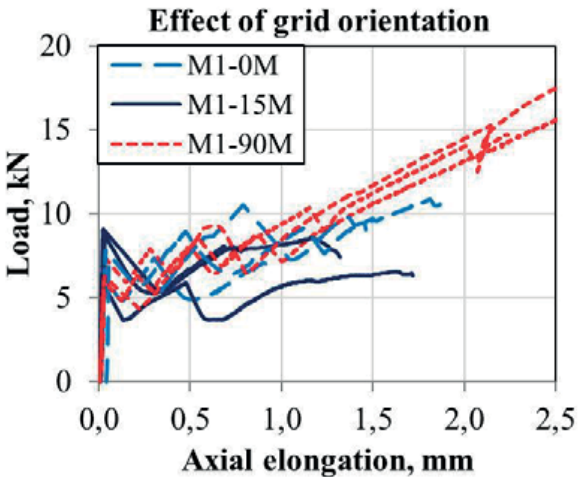

Figure 19 – Medium grid 0°-15°-90°

From Figures 16-19 along with the individual plots against the bare grid (Figures 5-9) it can be concluded that a significant and consistent tension-stiffening effect can only be shown for the ECC, while there is only a slight to moderate increase in load capacity with the quasi-brittle mortars. First cracking in ECC happens slightly later than in M1 and M2. In case of the small grid (Figure 18), after first cracking, the load capacity does not increase significantly if we use quasi-brittle mortars, while it does in the ECC-based specimens.

All 90° grids are plotted in Figure 17. The M1 mortar gave the most concise results, highest failure loads, and largest deformations, while the most brittle mortar, M2 yielded the most jagged and least concise results allowing very little deformations compared to any other combinations.

Finally, Figure 19 illustrates the changes in stiffness and load capacity with the grid orientation for the medium grid with the M1 mortar. Unexpectedly (and against the material data given in Table 1), the transversally rotated grid showed to be the strongest, while the 15° grid the weakest. In addition, the 90° medium grid combinations accommodated the largest elongations.

7.4. Crack widths, crack patterns

Figures 20-21 show two ARAMIS plots for the specimens M1-90-small and ECC-0-small. The crack widths of the ECC specimens are very small, ranging from 0.20 mm to 0.40 mm of the medium grid, and 0.08 mm to 0.50 mm for the small grid and they are not fully developed. In addition to that, the cracks are more evenly distributed in the ECC. In contrast, the crack widths determined by ARAMIS are ranging from 0.20 mm to 0.80 mm of the M1-90-small and between 0.75mm and 1 mm for the M2-0-medium. “Average crack widths”, defined as the sum of crack widths divided by the number of the cracks within the test field, are also given in Table 6, where available.

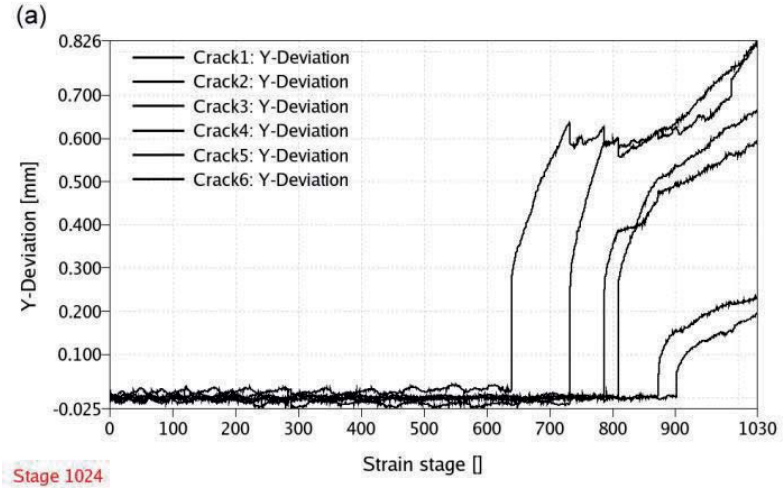

Figure 20 – Crack widths recorded by ARAMIS, M1-90-small

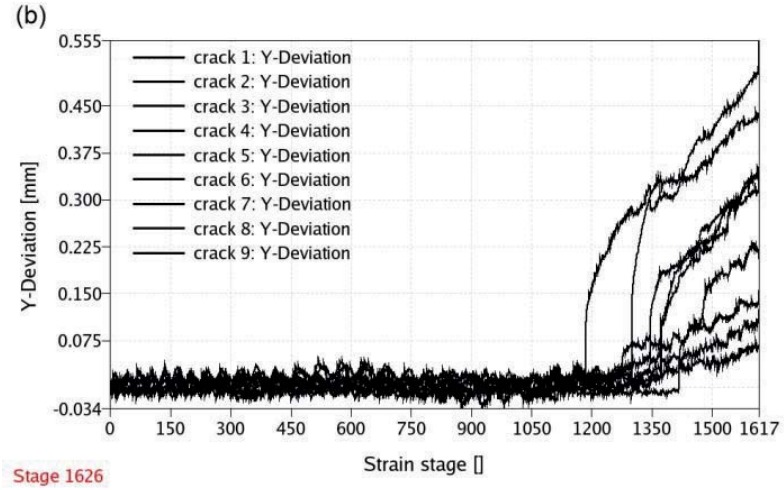

Figure 21 – Crack widths recorded by ARAMIS, ECC-0-small

7.5. ARAMIS "strain images"

The crack development was monitored by ARAMIS. The strain overlay images taken at the moment of failure confirm the characteristic ductile behaviour of the ECC as it shows more numerous, finer and more evenly distributed crack patterns compared to the quasi-brittle (M1 and M2) mortars. Where no strain images were available (Figure 22a, f, g and h), failure photos are given. The cracks in all specimens developed in line with the grid tows.

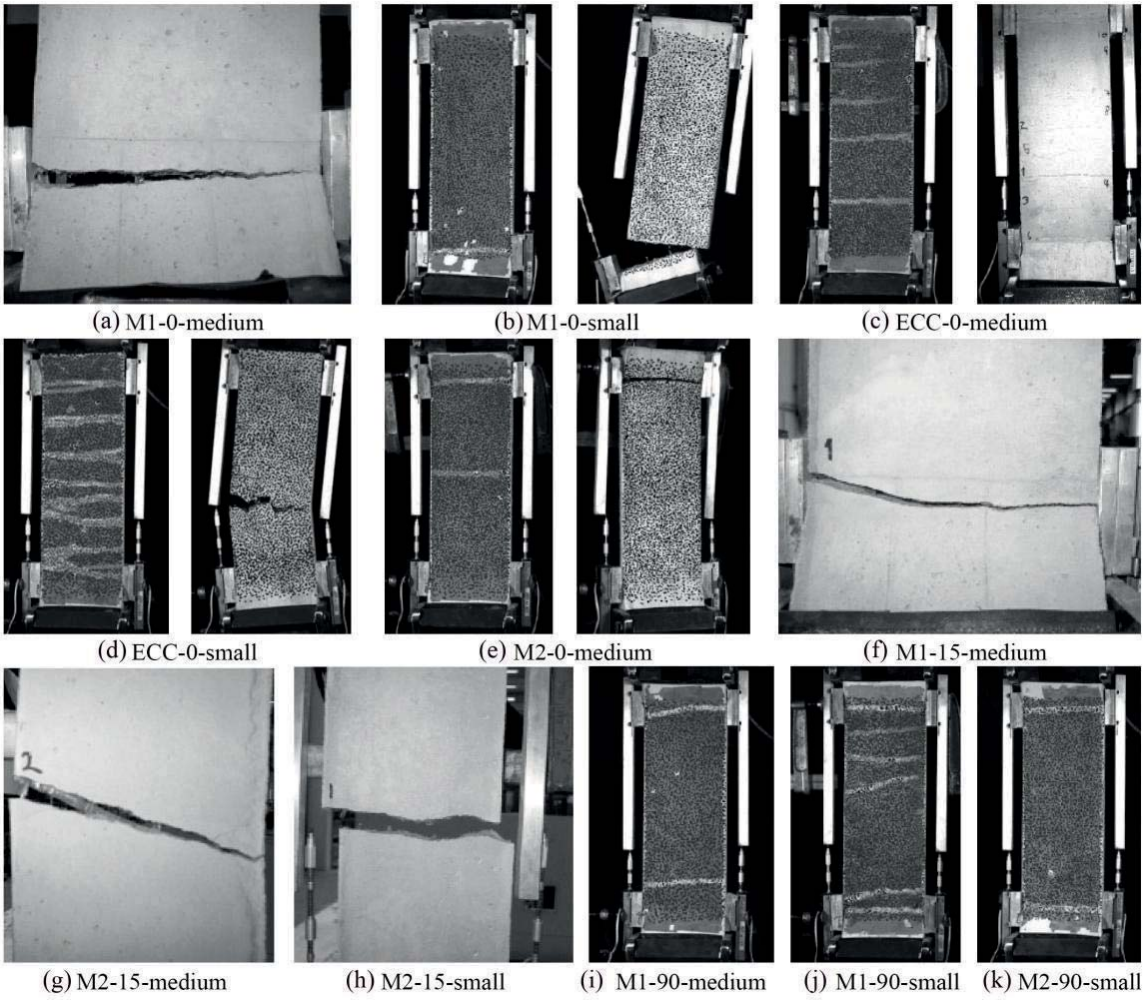

Figure 22 – Crack development as documented by ARAMIS.

8. DISCUSSION

We can compare the behaviour of the composite with the tensile properties of the bare grid. The specimens with the medium or small grid have 4 or 7 tows in the test section, respectively. The load capacity of the bare grid can be calculated based on manufacturer data. For the medium grid, it is 3.5 kN/tow in both directions, while for the small grid it is 1.4 kN/tow and 1.0 kN/tow in longitudinal and transversal direction, respectively. Test data from Blanksvärd gave much higher values [23]. Compared to these, the failure loads of the composite should be higher. Examining the failure loads, however, we can conclude that with quasi-brittle mortars we get significantly lower values (we do not even reach the nominal capacity of the grid) in all cases except for the transversally placed medium grid. The ECC specimens exceed the manufacturer-given grid failure loads, but still fall behind the tested values, suggesting premature failure of the grid.

The most concise, and homogenous test series were M1-90-medium and M1-90-small, with quasi-brittle, but fibre-reinforced mortars while the most scattered ones are the M2-series. The significant differences within the same test series (in particular, M2-15-small and M2-90-small)

are attributed to micro-cracks developing during the de-molding process, due to the very fragile geometry.

In case of the ECC, there is one specimen in both series showing a very different behaviour. One possible explanation to this could be the way we mixed the mortars. We could only mix a very small quantity in one batch because we used a dedicated mortar mixer with a limited capacity. It is possible that there were some very slight changes in the fibre content (2 vol. %) and/or water-to-cement ratios in the two separate mixes. Based on the known behaviour of the bare ECC (Figure 1), we believe that ECC-0-medium (3) and ECC-0-small (3) should be cancelled out of the results. The remaining specimens show a similar behaviour in terms of first cracking strength and stiffness.

It was observed that the medium grid performs very differently depending on its orientation. Two possible reasons for the "over-performance" of the medium grid when transversally placed are (1) that the joints can deform more without fibre breakage in that direction. The grid joints look and behave differently depending on the grid orientation; this is due to the "woven" nature of the grid. (2) Another possible explanation is the additional anchorage provided by the epoxy surplus, which for some reason is only present on the transversal fibre tows. In earlier tests by [5] however, it was shown that sanding the grid (giving increased bond) creates stress concentrations and premature rupture, therefore it cannot be stated that the additional anchorage equals to increased load capacity. Further research is needed in this regard.

The 15° orientated specimens, compared to the longitudinally placed reinforcement, do not develop as many cracks, and have a slightly reduced tensile strength. Cracks developing here tend to follow the grid tows. Finally, the behaviour of the small is less direction-dependent than that of the medium grid.

Some specimens initiated cracks near the ends of the test field. We attributed this to the fact that the dogbone geometry is prone to initiating cracks near sharp changes in cross section because of possible local stress concentrations. Using improved (curved) dogbone geometry, however, would have made the testing procedure far more time consuming and expensive. The test setup showed to be particularly sensitive to de-moulding, handling, and testing because of the very thin test field.

In addition to the possibly too low curing time before de-molding, there is an initial curvature in the grid strips because of the factory shape (roll). The grids were tensioned in the slits at both ends before casting in order to reduce the curvature. Yet in such a thin cross-section, the effect of the slightest curvature may be significant, and it might result in reduced performance. This effect has not been investigated more in detail.

9. CONCLUSIONS

The goals of the experimental program have been fulfilled in great part. A wide scale of material combinations has been tested, yet not all possible combinations. Adaptation of the dogbone geometry to testing large MBC-specimens has been successful with some limitations. Most of the specimens have been able to initiate cracks within the pre-defined test field, but an improved geometry would yield results that are more concise.

Multiple cracking and a significant tension stiffening behaviour were observed when applying a ductile, PVA-reinforced ECC as bonding agent, which, based on the two only test series, has

proven to be superior to quasi-brittle mortars. ECC has given significantly higher failure loads and prevented pronounced drops in load capacity by its increased ductility. Recorded peak values in the load-displacement curves show a more balanced behaviour for the ECC specimens. The same plots for the quasi-brittle mortars are jagged indicating a more uneven stress distribution and possible local failures in the grid joints. Typical brittle failure and corresponding crack patterns were recorded in case of the quasi-brittle M1 and M2 mortars.

10. FURTHER RESEARCH

Quasi-brittle mortars rely on high bond strength between CFRP reinforcement and the mortar, to accommodate the high internal stresses. Therefore, bond slip or local high stress concentrations may result in failure of the grid joints. Using a mortar with improved ductile deformation capabilities, where the CFRP reinforcement and the cementitious matrix deform close to identically, results in a composite material where apparently high mechanical bond stresses in local areas, as the grid intersections between the longitudinal and transversal tows are significantly reduced, thereby preventing bond slip damage to the CFRP-reinforcement.

The high fly ash content of ECC results in a refined and densified grain structure. This may improve the bond strength between the grid and the mortar, as confirmed by [11] for yarns/textiles embedded in cementitious matrices. The apparently better bond characteristics of ECC are also partly due to the compatible deformation behaviour between FRP reinforcement and ECC, which makes ECC very attractive for further investigation in combination with FRP grids.

Due to its pseudo strain hardening and fibre bridging properties, and for the additional mechanical anchorage it provides for the FRP grid, ECC will be tested further as a bonding agent for mineral-based strengthening. The different geometry (and associated rigidity, and deformation capacity) of the grid joints in the two perpendicular directions could also be further investigated, as this may have caused the significant “over-performance” of the medium grid in transversal direction.

Finite element modelling of the interaction between grid and mortar would give a better understanding of structural applications where mineral-based strengthening systems are subject to tensional/splitting forces, or axial forces combined with bending.

ACKNOWLEDGEMENTS

The research work presented in this paper was performed at the Technical University of Denmark and financed by the Norwegian Research Council through the strategic institute program RECON at Norut Narvik Ltd. The ARAMIS equipment was acquired with support from the Villum Kann Rasmussen Foundation. Sto Scandinavia should also be acknowledged for supplying most of the strengthening material.

REFERENCES

1. Carolin, A., Carbon Fibre Reinforced Polymers for Strengthening of Structural Elements, in Department of Civil and Mining Engineering2003, Luleå University of Technology: Luleå, Sweden.

2. Täljsten, B., FRP Strengthening of Existing Concrete Structures. Design Guideline, 4th Edition. 3rd Edition ed. 2006, Luleå, Sweden.
3. Triantafillou, T.C., Shear strengthening of reinforced concrete beams using epoxy-bonded FRP composites. ACI Structural Journal, 1998. 95(2): p. 107-115.
4. Ohuchi, H., et al., Seismic strengthening design technique for existing bridge columns with CFRP, in Proceedings of the Second International Workshop on Seismic Design and Retrofitting of Reinforced Concrete Bridges1994: Queenstown, Nerw Zealand. p. 495-514.
5. Blanksvärd, T., Strengthening of concrete structures by the use of mineral based composites, in Department of Civil and Environmental Engineering2007, Luleå University of Technology: Luleå, Sweden.
6. Blanksvärd, T., B. Täljsten, and A. Carolin, Shear Strengthening of Concrete Structures with the Use of Mineral-Based Composites. Journal of Composites for Construction, 2009. 13(1): p. 25-34.
7. Orosz, K., et al., From material level to structural use of mineral based composites – An overview. Advances in Civil Engineering, 2010. 2010.
8. Hegger, J., et al., Load–bearing behaviour and simulation of textile reinforced concrete. Materials and Structures, 2006. 39(8): p. 765-776.
9. Becker, D., Betongplattor förstärkta med kolfibrekomposit (in Swedish), in Division of Structural Engineering2003, Luleå University of Technology: Luleå, Sweden.
10. Blanksvärd, T. and B. Täljsten, Strengthening of concrete structures with cement based bonded composites. Journal of Nordic Concrete Research, 2008. 38: p. 133-153.
11. Soranakom, C. and B. Mobasher, Geometrical and mechanical aspects of fabric bonding and pullout in cement composites. Materials and Structures, 2008. 42(6): p. 765-777.
12. Naaman, A.E. and H.W. Reinhardt, Characterization of high performance fiber reinforced cement composites-HPFRCC, in Proceedings of High Performance Fiber Reinforced Cement Composites 2 [HPFRCC 2]1995. p. 1-23.
13. Li, V.C. and G. Fischer. Reinforced ECC - An Evolution from Materials to Structures. in Proceedings of the 1st FIB Congress. 2002. Osaka, Japan.
14. Kim, Y.Y., B.Y. Lee, and J.K. Kim, Evaluation of fiber dispersion of PVA-ECC, 2008, ICCES. p. 167-172.
15. Stang, H. and V.C. Li, Classification of fibre reinforced cementitious materials for structural applications, in 6th RILEM Symposium on Fibre-Reinforced Concretes (FRC) - BEFIB 20042004: Varenna, Italy. p. 197-218.
16. Fischer, G. and V.C. Li, Influence of matrix ductility on tension-stiffening behavior of steel reinforced engineered cementitious composites (ECC). ACI Structural Journal, 2002. 99(1): p. 104-111.
17. Brameshuber, W., Textile Reinforced Concrete: State-of-the-art report of RILEM technical committee 201-TC, 2006, RILEM Publications.
18. Hinzen, M. and W. Brameshuber, Improvement of Serviceability and Strength of Textile Reinforced Concrete by using Short Fibres, in 4th Colloquium on Textile Reinforced Structures (CTRS4)2009: Dresden, Germany. p. 261-272.
19. Hegger, J. and S. Voss, Textile reinforced concrete under biaxial loading, in 6th Rilem Symposium on Fibre Reinforced Concrete (FRC), BEFIB 20042004: Varenna, Italy. p. 1463-1472.
20. ACI 224.2R-92, 1992, American Concrete Institute.
21. Hegger, J., et al., Decentralized Wastewater Treatment Plants Made of Textile Reinforced Concrete, in 12th International Techtextil Symposium for Technical Textiles, Nonwovens and Textile Reinforced Materials 2003: Frankfurt, Germany. p. CD-ROM nr. 4.28, 38pp.

22. Kanakubo, T., Tensile Characteristics Evaluation Method for Ductile Fibre-Reinforced Cementitious Composites. Journal of Advanced Concrete Technology, 2006. 4(1): p. 3-17.
23. Blanksvärd, T., Mechanical properties of different geometries of CFRP grid: tensile evaluation of material properties, 2006, Luleå University of Technology: Luleå, Sweden.

Paper III

Orosz K, Hedlund H, and Cwirzen A

Effects of variable curing temperatures on autogenous deformation of blended cement concretes

Accepted for publication in May 2017

Journal of Construction & Building Materials

JCBM 10489
20 May 2017
ARTICLE IN PRESS
No. of Pages 7, Model 5G

Construction and Building Materials xxx (2017) xxx–xxx

Contents lists available at ScienceDirect

Construction and Building Materials

journal homepage: www.elsevier.com/locate/conbuildmat

Effects of variable curing temperatures on autogenous deformation of blended cement concretes

Katalin Orosz [a,*], Hans Hedlund [b], Andrzej Cwirzen [a]

[a] Department of Civil, Environmental and Natural Resources Engineering, Luleå University of Technology, SE-971 87 Luleå, Sweden
[b] Skanska Sverige AB, SE-405 18 Gothenburg, Sweden

HIGHLIGHTS

- Autogenous shrinkage under variable temperature curing investigated.
- Concretes with blended cement (fly ash) tested.
- Prominent expansive behavior found in high temperature curing.
- Expansion could not be linked to fly ash content.
- Different curing paths likely result in different thermal coefficient developments.

GRAPHICAL ABSTRACT

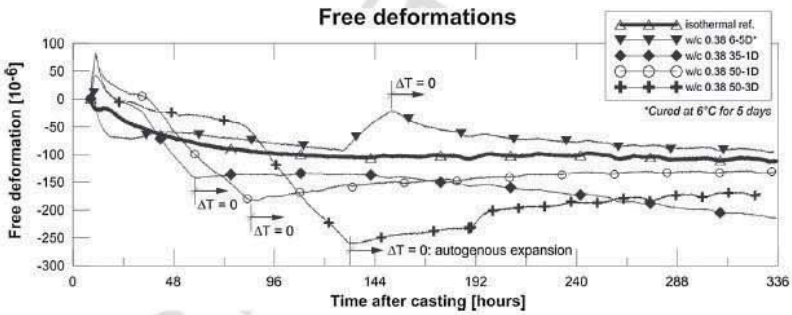

ARTICLE INFO

Article history:
Received 30 January 2017
Received in revised form 15 May 2017
Accepted 15 May 2017
Available online xxxx

Keywords:
Autogenous deformation
Autogenous expansion
Swelling
Blended cement
Variable temperature curing
Early-age concrete
Free deformation

ABSTRACT

Shrinkage tests have been performed on blended Portland cement based early-age concrete with different w/c ratios, undergoing variable temperature curing. Results showed presence of induced non-negligible autogenous swelling which could mitigate part of the stresses related to shrinkage at very young concrete age. Recorded swelling was higher at higher curing temperatures and longer duration, especially pronounced for the low w/c mix. The swelling continued for several days after the temperature stabilized. Although not investigated directly, evidence to the nonlinear nature of the thermal expansion coefficient in young concrete has also been provided.

1. Introduction

1.1. Autogenous deformation and cracking risk

The young concrete is at an increased risk of cracking due to the combination of differential shrinkage and internal restraints. In mass concrete, differential shrinkage results from inability of the structure to dissipate quickly the heat generated, resulting in larger temperature gradients and corresponding larger autogenous shrinkage (AS) in the center, while the aggregates act as restraint [1]. In thin structures with large surfaces drying out, combined autogenous and drying shrinkage can generate high enough stresses that lead to early-age cracking.

Autogenous, or self-desiccation shrinkage is an inherent part of the total deformation that is unavoidable [2–4], because it is a

* Corresponding author.
E-mail address: katalin.orosz@ltu.se (K. Orosz).

http://dx.doi.org/10.1016/j.conbuildmat.2017.05.143
0950-0618/

Effects of variable curing temperatures on autogenous deformation of blended cement concretes

Katalin Orosz[a], Hans Hedlund[b], Andrzej Cwirzen[a]
[a]Department of Civil, Environmental and Natural Resources Engineering, Luleå University of Technology, SE-971 87 Luleå, Sweden
[b]Skanska Sverige AB, SE-405 18 Gothenburg, Sweden

HIGHLIGHTS

- Autogenous shrinkage under variable temperature curing investigated.
- Concretes with blended cement (fly ash) tested.
- Prominent expansive behavior found in high temperature curing.
- Expansion could not be linked to fly ash content.
- Different curing paths likely result in different thermal coefficient developments.

ABSTRACT

Shrinkage tests have been performed on blended Portland cement based early-age concrete with different w/c ratios, undergoing variable temperature curing. Results showed presence of induced non-negligible autogenous swelling which could mitigate part of the stresses related to shrinkage at very young concrete age. Recorded swelling was higher at higher curing temperatures and longer duration, especially pronounced for the low w/c mix. The swelling continued for several days after the temperature stabilized. Although not investigated directly, evidence to the nonlinear nature of the thermal expansion coefficient in young concrete has also been provided.

Graphical abstract

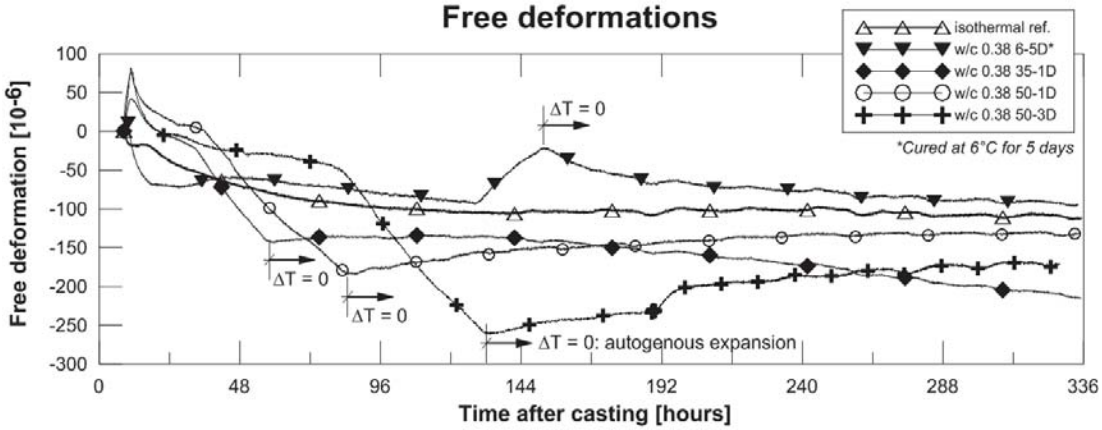

Keywords:
Autogenous deformation
Autogenous expansion
Swelling
Blended cement
Variable temperature curing
Early-age concrete
Free deformation

1. Introduction

1.1 Autogenous deformation and cracking risk

The young concrete is at an increased risk of cracking due to the combination of differential shrinkage and internal restraints. In mass concrete, differential shrinkage results from inability of the structure to dissipate quickly the heat generated, resulting in larger temperature gradients and corresponding larger autogenous shrinkage (AS) in the center, while the aggregates act as restraint [1]. In thin structures with large surfaces drying out, combined autogenous and drying shrinkage can generate high enough stresses that lead to early-age cracking.

Autogenous, or self-desiccation shrinkage is an inherent part of the total deformation that is unavoidable [2–4], because it is a direct consequence of chemical shrinkage that happens after the final set of concrete [4–8]. With the recent increased use of high early strength-, high performance-, and/or blended binder concretes, with low water/cement ratio the AS makes up for a substantially larger part of the total shrinkage [9–12]. It is significant enough to induce micro- or macro cracking due to the increased paste volume and higher binder content per unit volume. In a high performance concrete sample, AS reached 240 x 10^{-6} by 24 hours of age [9] this presents a significant cracking risk if movements are restrained.

1.2 Autogenous expansion

Typically, autogenous deformation (AD) manifests as shrinkage. Recent research, however, has reported on cases where a substantial autogenous expansion or "AD swelling", as commonly referred to, has occurred; e.g., [10,13–18]. This expansion may be beneficial since it has the potential to partially mitigate tensile stresses when the young concrete has a very low modulus of elasticity. For estimating cracking risk in young concrete undergoing early expansion, however, it has been recommended that the conservative estimation of using the net shrinkage (occurring after early-age expansion) be used, instead of the total deformation after first setting [9], thereby ignoring the possible shrinkage-mitigating effects of the early-age expansion.

Autogenous expansion in early age concrete/mortar typically takes place after the cooling down stage. Earlier studies showed that the natural cooling down phase from temperatures exceeding 50^0C was characterized by a reduced rate of AS and was followed by autogenous expansion. The expansion started at about 4 days of age and was attributed to thermally induced swelling [10]. Heating-cooling curing regime has been observed to cause AD swelling during the cooling off phase, lasting until the temperature levels off [19]. The AD swelling is likely to appear in concrete having w/c ratios over 0.40.

Recently, slow expansion of over 10 days in fly ash concretes was observed [13]. The onset of swelling about coincides with the maximum temperature and continues throughout the cooling down phase. Swelling is prominent when $\Delta T \leq 20°C$, regardless of fly ash content (17—45%). The Type I OPC reference sample, however, exhibits swelling despite that it has undergone a 30°C temperature change. AD swelling was also observed in both OPC cement paste and OPC with 30% and 45% blast furnace slag (w/c 0.40) [16]. In that case, the curing temperature of 60°C was applied 50 hours after casting. The AD swelling was observed for the entire duration of the cooling down phase [16]. Smaller but steady swelling was also observed in the OPC sample cured at 40°C. AD swelling in OPC concrete with 50% fly ash w/c 0.30,

under 20°C isothermal conditions has been reported by others, [15]. The expansion occurred well after the concrete has cooled down; the temperature in the sample did not reach 25°C at any point. The swelling was prominent at around day five and lasted for another 7-8 days. The authors attributed the swelling to a possible ettringite formation. No swelling was observed in mixes with only 25% fly ash. Finally, AD swelling has been also linked to possible ettringite formation in mixes made with coarser cements by [17].

1.3 Thermal dilation

During hydration, fully coupled autogenous deformation (AD) and thermal deformation (TD) are recorded as free deformations. For a generalized model capable to describe any conceivable temperature history and to calculate shrinkage-induced stresses, it is fundamental to have a robust, generalized model for both AD and TD [10]. Assuming that the development of CTE over time is known for the young concrete, the total deformation could be split into AD and TD to determine the relative importance of each mechanism separately. However, for young concrete, the thermal dilation coefficient CTE(t) is highly nonlinear, depending heavily on the moisture content [20,21], since water has a CTE about 7 times that of hardened concrete. The development of CTE appears to be less affected by the curing regime history than the AD and may also be influenced be the pore structure in the concrete body [21]. After casting, the CTE decreases sharply during the first hours due to large amounts of unbound water (above $20x10^{-6}$/°C) [22–24], to a minimum value around setting time (~$6\text{-}7x10^{-6}$/°C), and thereafter it slowly increases with time due to self-desiccation [20], converging to the value characteristic of hardened concrete (9…12 $x10^{-6}$/°C). The reduction around setting time is due to the fact that before setting, the free water is continuous while as a solid skeleton is being built up, this continuity gets disrupted. Ranges of CTE (typically for hardened concrete) are available in literature, but data for early-age concrete are rather limited and inconsistent.

It was beyond the scope of this study to determine the development of CTE for the specific concrete mixes. However, if splitting of the total (free) deformations is attempted to characterize the autogenous deformation separately, it is crucial to use proper CTE values.

1.4 Variable temperature curing

It has been well known and implemented in early models [25,26] that the magnitude of AS depends on the maximum temperature reached throughout the curing process. Variable temperature curing where the length of the curing certain temperature level varies, has not been taken into account when modeling AS.

Recent data reveals that different imposed temperature paths result in substantially different AD developments, even despite the same degree of hydration; and that the AD can manifest as expansion in certain circumstances. Measuring AD directly, at *constant* temperature levels, and deducing AD from these for other temperature levels does not appear to be possible due to both the magnitude and the development rate of AD showing strong temperature history dependence [5,10,13,14,27,27]. Others also emphasized that higher temperature does not necessarily lead to higher AS. As a result, AD in a real structure cannot be predicted from isothermal test results because the fundamental behavior (contraction or expansion) depends on the specific imposed temperature history [28].

This study has been focusing on providing experimental data for the modeling of AD under variable temperature curing, for later incorporation into existing AD models, in order to address the knowledge gap regarding variable temperature curing.

2. Experimental procedure

2.1 Materials

Tests have been performed on ordinary concrete with w/c ratios of 0.38 and 0.55. The mix designs are tabulated in Table 1.

***Table 1**. Concrete mix designs used in the project; BAS and ANL mixes provided by Cementa.*

	BAS 0.38		BAS 0.55		ANL 0.55		ANLFA 0.38	
	kg/m^3	L/m^3	kg/m^3	L/m^3	kg/m^3	L/m^3	kg/m^3	L/m^3
cement	470	157	360	120	340	106	294	92
fly ash	-	-	-	-	-	-	126	N/A*
0/8	975	361	1067	395	1072	397	928	343
8/16	790	298	733	277	398	150	844	318
16/27	-	-	-	-	401	150	-	-
water, eff.	179	179	198	198	187	187	168	168
air content		5		5		10		10

**N/A: replaced by weight fraction; density of fly ash not tested.*

As binder, two different kinds of Portland cement, both produced by Cementa, Sweden were used. The BAS cement, type II/A-V 52.5N, according to EN 197-1, contains 16% fly ash and 4% limestone. The coarser ANL cement type CEM I 42.5 N - SR 3 MH/LA, according to EN 197-1, has low C_3A content. The physical and chemical properties of both cements are shown in Table 2.

Table 2
Physical and chemical properties of binders

Property/amount	BAS cement	ANL cement
Blaine-fineness	450 m^2/kg	310 m^2/kg
Setting time	150 min	160 min
Compact density	3000 kg/m^3	3200 kg/m^3
CaO	55.4%	64.1%
SiO_2	24.0%	22.4%
Al_2O_3	6.7%	3.7%
Fe_2O_3	N/A	4.5%

MgO	2.8%	1.2-1.5%
K_2O	1.3%	N/A
SO_3	3.4%	2.4%
Water-soluble Cr^{6+}	< 2 ppm	< 2 ppm
C_3A	5.2%	2.1%
C_3S	N/A	48%
C_2S	N/A	28%
C4AF	N/A	13.8%

Mix ANLFA 0.38 was made by replacing 30 wt% of the cement of a proven Cementa mix ("ANL 0.38"; not used here) with fly ash. In addition, the 16/27 aggregate was replaced by 8/16 in order to ensure a better d_{max} : sample diameter ratio. This mix was not optimized further. ANL is a much coarser cement, therefore, in the ANLFA mix, more prominent swelling could be expected for the same curing conditions than in any other tests since both the cement coarseness and the high fly ash content have been linked to expansion or delayed ettringite formation; [17] and [15], respectively.

2.2 Test set-up

The test set-up (Figure 1) is based on earlier research [26]. Free deformation was measured on sealed, Ø=80mm, h=300mm concrete cylinders by two symmetrically mounted LVDTs, mounted on composite bars made of carbon.

***Fig. 1**. Test set-up*

For every variable temperature regime/material combination, two specimens were cast; a heat-cured sample and a reference sample cured isothermally at 20^0C. The temperature of the specimens was controlled based on the temperature measurements in the water tank with ± 3^0C accuracy. The curing regimens consisted of the initial adiabatic rise, followed by a constant curing temperature; 6^0C, 35^0C and 50^0C, kept constant for 1, 3, and 5 days, Figure 2. In the last stage samples were cooled down to 20^0C. The steering for the cooled down sample has been inverted so that the rate of

cooling down/heating up to 20^0C corresponded to the rate applied for the heat-cured samples. The total duration of the tests was 14 days. The number of samples was 3 (BAS 0.38-50-3D), 2 (all other 50^0C and 35^0C levels for both BAS concretes), and 1 (6-5D samples and ANL/ANLFA control mixes).

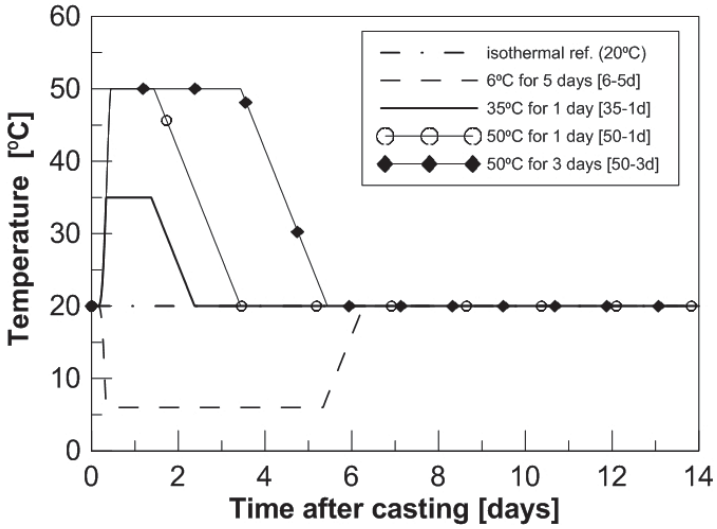

Fig. 2. *Curing regimes*

Specimens were allowed to develop their natural adiabatic temperature rise until the mounting of the LVDTs which was done at approximately 8 hours after casting. The sealed samples were submerged into the water bath with matching temperature to avoid thermal shock strains. The deformation values were zeroed at 8.5 hours. The logged data consisted of the coupled free deformations, the temperature of the controlling water bath and in the center of the samples, and room temperature versus time.

The same test setup and logging equipment have been used on a piece of steel pipe of the same geometry to show that the deformations recorded are “real”. Since steel has a constant and known thermal coefficient and all its deformations are purely thermal, the deformation measured is expected to closely follow the steering curve, consisting of straight lines during warming up and cooling down, and no deformation when the temperature is kept constant. The – not zeroed – deformations recorded on the steel pipe sample are shown in Figure 3, which proved the reliability of the used setup.

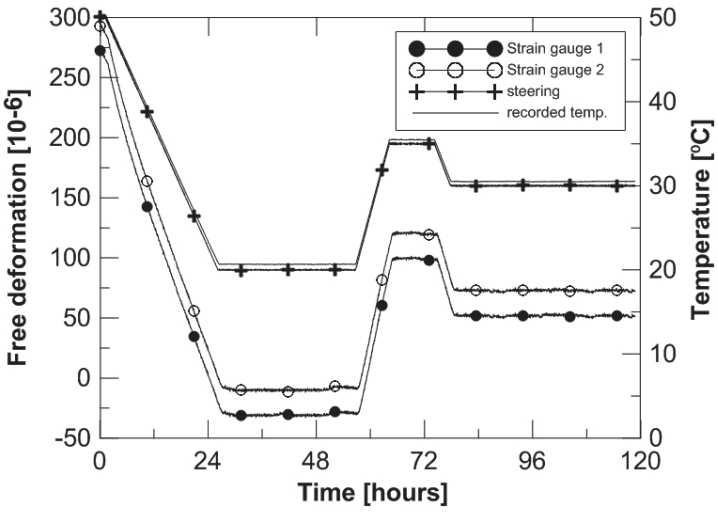

Fig. 3. *Deformation recorded on steel pipe*

3. Test results and discussion

The individual results for the BAS cement recipes are plotted as free deformation (AD+TD) vs. time after casting and are shown in Figures 4a—d and 5a—d. Negative values represent shrinkage while positive values correspond to expansion – AD swelling and/or thermal expansion. Each plot shows the coupled deformation of the heat-cured sample against the 20^0C isothermal reference, along with the steering and the recorded heat development in the center of the heat-cured sample. The deformations plotted represent the average of the two LVDT readings for each sample, averaged through the total number of samples per test, zeroed at 8.5 hours. The scatter was less than 10% in end value after 14 days.

The measured deformations of the two control mixes with ANL cement are shown in Figure 6a and 6b. The plots are only shown here in order to compare the past cooling off behavior. No deeper analysis has been performed on the ANL/ANLFA samples because of the small sample size. Reference sample data are not available for the ANL sample.

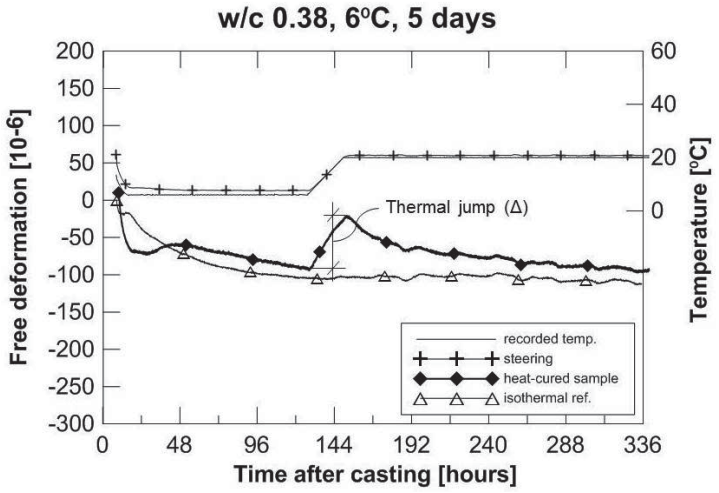
w/c 0.38, 6°C, 5 days
Free deformation [10-6]
Temperature [°C]
Time after casting [hours]
Thermal jump (Δ)
recorded temp.
steering
heat-cured sample
isothermal ref.

(a)

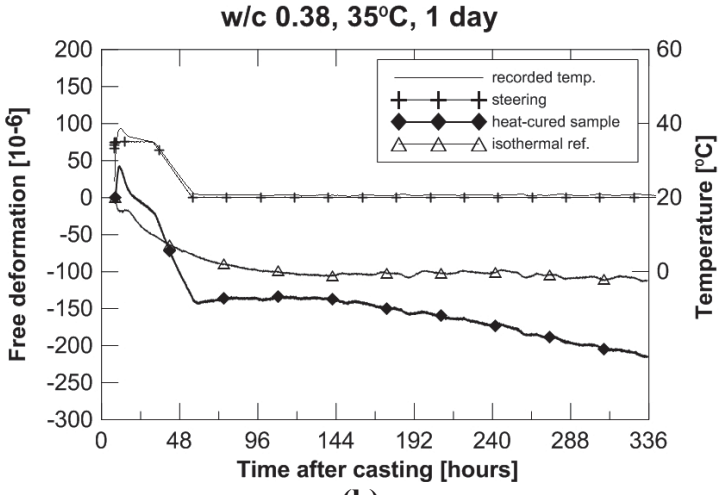
w/c 0.38, 35°C, 1 day
Free deformation [10-6]
Temperature [°C]
Time after casting [hours]
recorded temp.
steering
heat-cured sample
isothermal ref.

(b)

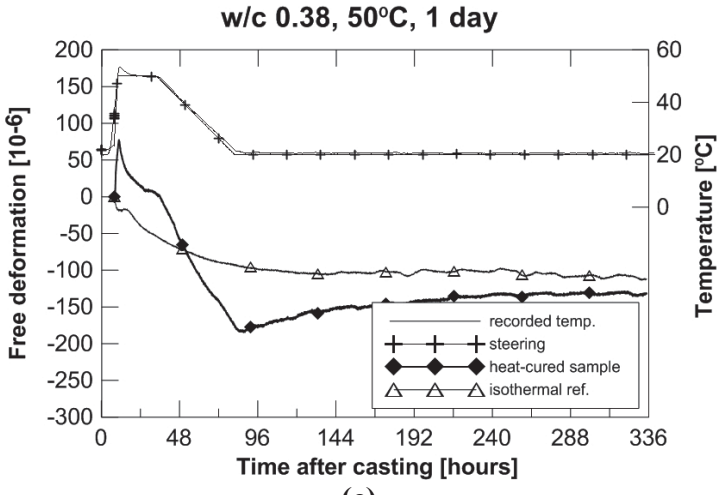
w/c 0.38, 50°C, 1 day
Free deformation [10-6]
Temperature [°C]
Time after casting [hours]
recorded temp.
steering
heat-cured sample
isothermal ref.

(c)

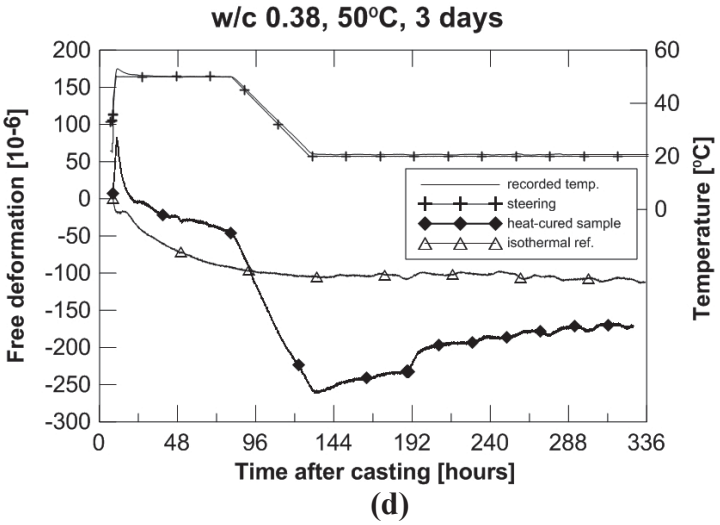

(d)

Fig. 4. *Individual free deformation plots for the BAS w/c 0.38 mixes. (a) 0.38 6-5D, (b) 0.38 35-1D, (c) 0.38 50-1D, (d) 0.38 50-3D*

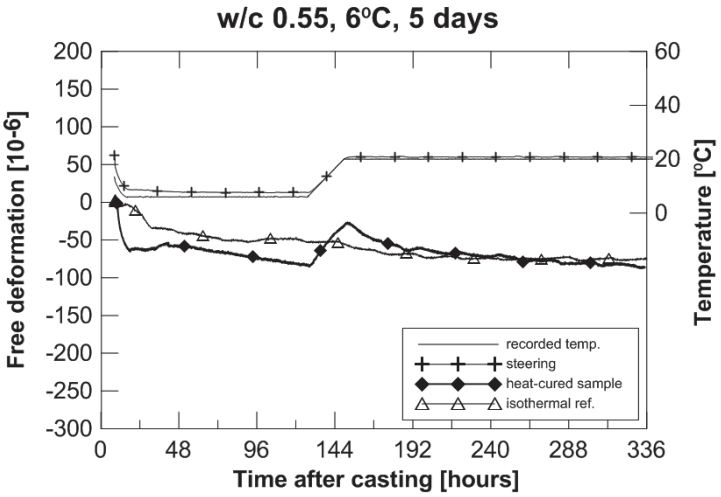

(a)

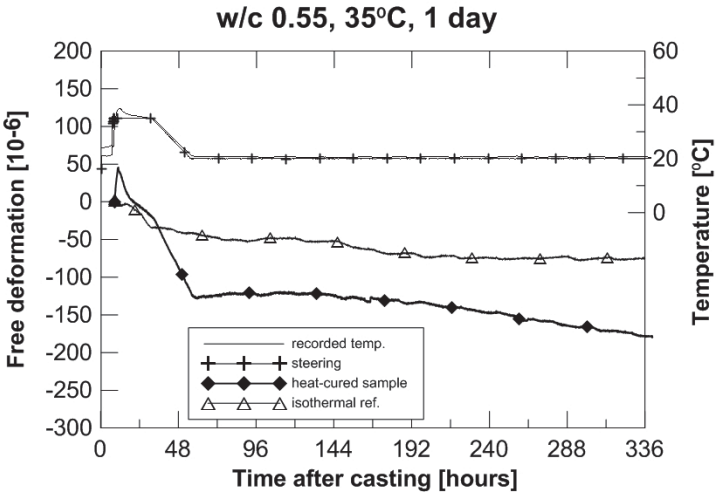

(b)

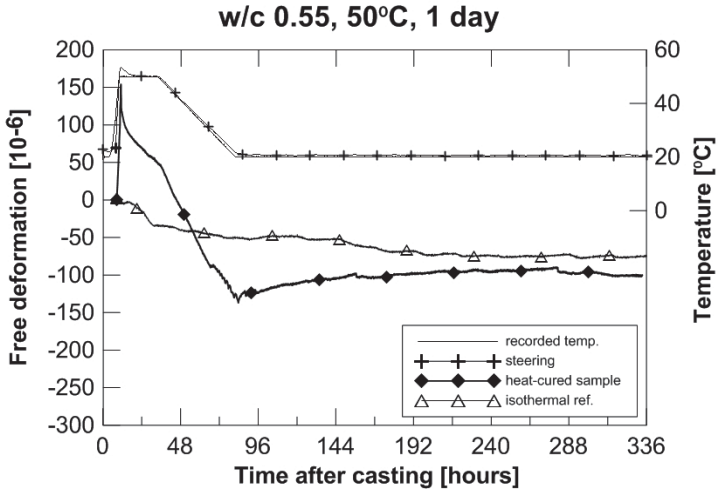

(c)

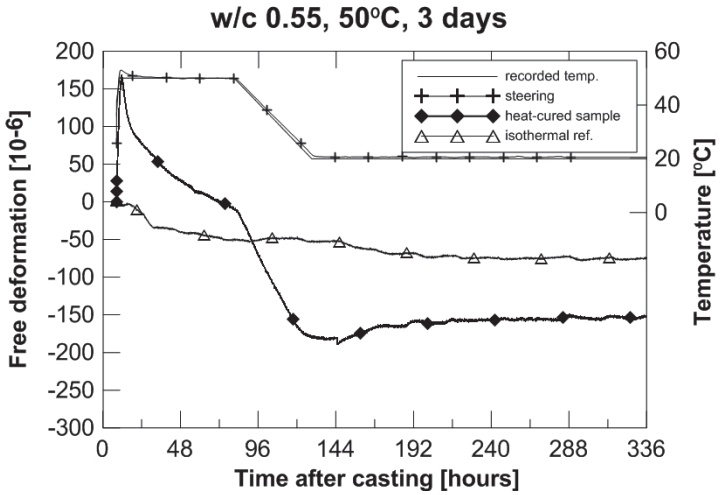

(d)

Fig. 5. *Individual free deformation plots for the BAS w/c 0.55 mixes. (a) 0.55 6-5D, (b) 0.55 35-1D, (c) 0.55 50-1D, (d) 0.55 50-3D*

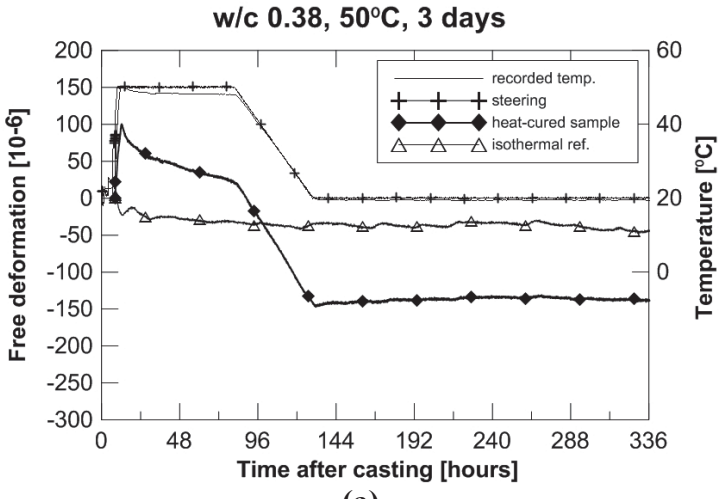

(a)

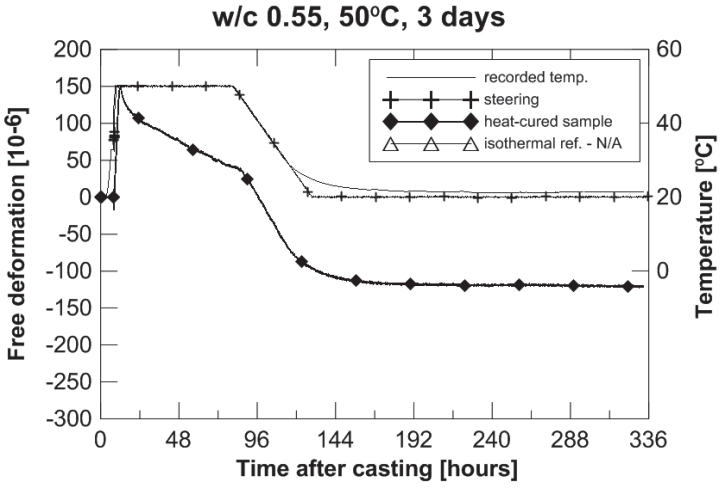

(b)

Fig. 6. *Individual free deformation plots for (a) ANLFA w/c 0.38 and (b) ANL w/c 0.55 mixes*

In the free deformation plots of the heat-cured samples, the following stages can be distinguished:

Initial expansion due to heat of hydration

For both w/c concretes, all deformation plots begin with a small initial expansion due to the hydration heat. Naturally, the thermal peak for the sample cured at 50^0C is larger than for the 35^0C sample since the latter is not allowed to develop the same heat of hydration peak due to the lower temperature bath.

Curing at constant temperatures

During constant temperature curing (1 or 3 days), rapid shrinkage was observed at a higher rate when cured at higher temperature levels, which is in agreement with common knowledge. Slope changes were observed matching the sharp changes in the temperature steering, indicated by the knick points in the steering plots.

Cooling off/warming up

The thermal jumps (as illustrated in Figure 4a) recorded during cool-off were not directly proportionate to the actual temperature drops, which supports earlier observations that the thermal expansion (or contraction) coefficient is time-, moisture content- [20,21], and likely temperature history dependent [21]. The thermal jumps are listed in Table 3. It is important to emphasize that during the cooling stages, AD was occurring parallel; the thermal jumps are also coupled deformations, not purely thermal.

Table 3
Thermal contraction/expansion jumps (Δ) during cooling down phase in w/c 0.38 samples. Positive values represent expansion; negative values indicate contraction.
** indicates a 22-hour long period during which the sample is being warmed up*

Sample	Δ [μstrain]	ΔT [^{0}C]	Occurrence; length [h]
0.38 6-5D	45	+14^{0}C (6→20^{0}C)	128-150 [22]*
0.38 35-1D	-120	-15^{0}C (35→20^{0}C)	32-56 [24]
0.38 50-1D	-180	-30^{0}C (50→20^{0}C)	35-83 [48]
0.38 50-3D	-210	-30^{0}C (50→20^{0}C)	83-131 [48]

The cool off of the 0.38 35-1D sample results in a 120 μstrain contraction over 24 hours. In contrast, cooling off the 50 degree samples generates only 1.5 times the deformation in double the time. This is inconsistent with earlier findings investigating the nature of CTE since the CTE of the younger concrete – in terms of maturity – should be lower. The thermal drop belonging to the same ΔT, but with a two-day offset in occurrence, increased from 180 to 210 microstrains when comparing the two 50^{0}C levels. This may suggest that the CTE(t) is increasing during this 2-day window. This is in line with earlier observations; i.e., that the CTE tends to gradually increase from a minimum value measured around setting time, slowly converging to the value characteristic for hardened concrete, [20]. Alternatively, it may imply that these two distinct curing paths result in the formation of substantially different binder matrices; likely with a different amount and distribution of gel-, meso-, and capillary pores and air voids, resulting in different CTEs.

Furthermore, a ~45 μstrain expansion during ~1 day was observed for the 0.38 6-5D sample while allowed to warm up to room temperature again. The hydration process of that sample was significantly delayed in comparison with other temperature levels.

The same trends can be observed for the w/c 0.55 samples as tabulated in Table 4 below. The thermal jumps are marginally smaller with the exception of the 0.55 6-5D sample.

Table 4
Thermal contraction/expansion during cooling down phase in w/c 0.55 samples.
** indicates a 22-hour long period during which the sample is being warmed up*

Sample	Δ [μstrain]	ΔT [^{0}C]	Occurrence; length [h]
6-5D	45	+14^{0}C (6→20^{0}C)	128-150 [22]*
35-1D	-100	-15^{0}C (35→20^{0}C)	32-56 [24]
50-1D	-175	-30^{0}C (50→20^{0}C)	35-83 [48]
50-3D	-165	-30^{0}C (50→20^{0}C)	83-131 [48]

Stabilized isothermal conditions

After the temperature has stabilized at 20^{0}C, delayed onset autogenous expansion was observed in samples cured at 50^{0}C. For both 35-1D samples, the expansion recorded between ~55 and ~140 hours of age lies within measurement error, but the

slope between ~50 and ~180 hours of age turning upward could indicate that some swelling may have started already during cooling down phase, which correlates well with results obtained by several others [13,16,19]. It is impossible to say whether the AD swelling begins during or after the cooling down phase without splitting the deformations by subtracting thermal deformations with a CTE(t) specific for concrete and curing. However, since the expansion is visible at constant temperature, it can be concluded that the observed swelling past the 131-hour mark (50-3D samples) and after 83 hours (50-1D samples) was an autogenous deformation. This swelling was referred to as "thermally induced swelling" [14] which would develop as a result of the type of the curing regime.

The sample cooled down to 6^0C (Figures 4a and 5a), during the first two days, shrank at a rate higher than the isothermal reference. Initially, this was assumed to be a measurement/logging error, since it is well known that lower temperatures tend to delay hydration of cement and thus decrease the associated shrinkage. The initially rapid shrinkage decreased significantly during the first day, and the 6-5D continued to shrink slightly less in comparison to the reference. After warming the sample to reach the room temperature again, the shrinkage increased and while the isothermal reference sample has nearly stabilized by this stage, the 6-5D produced nearly half of its total shrinkage during this interval.

The mix with ANL cement and 30% fly ash (ANLFA – Figure 6a) showed only minimal swelling the value of which barely exceeded the measurement error. The ANL mix (Figure 6b) did not exhibit any swelling past cooling down; however, the cooling down happened at a smoother rate than intended, due to the cooler unit not working properly for the particular test. It is possible that that the *rate* of cooling down would affect whether swelling develops or not. Cement type, especially its fines and tricalcium aluminate content, may be contributing factors affecting the extent of the autogenous swelling. While ANLFA had much higher fly ash content (the maximum allowed, according to Swedish regulations, 30%), the ANL cement has a low C_3A content of only 2.1%, which may explain the lack of swelling, despite the added fly ash. It is important to mention here that the exact chemical composition of the bulk fly ash is unknown. Moreover, according to the producer, the 16% fly ash content in the BAS cement may also exhibit certain chemical variability from batch to batch, depending on the sourcing; therefore, the exact hydration products that may cause swelling and the extent of swelling may also vary considerably.

4. Conclusions

Based on the results of this study the following conclusions can be formulated:

1. Heat curing at variable temperature levels in concretes based on blended cement has induced non-negligible autogenous swelling. This may mitigate some of the stresses arising from shrinkage when the concrete is very young. The higher the curing temperature and the longer the duration of heat curing the more prominent the swelling has been, in particular for the low w/c mix. The swelling continued for several days after the temperature stabilized. The expansion did not level off during the 2-week duration of the testing.
2. Cold curing (6^oC) which simulated cold weather casting has shown to delay, but not to mitigate the ultimate deformation. Cold curing also resulted in an increased shrinkage rate very early into the curing. No explanation to this behavior can be given without further investigation.

3. The swelling could not be traced back unequivocally to the fly ash content of the cement. The BAS cement (which contains 16% FA added by the manufacturer) exhibited swelling while the swelling recorded in the ANLFA control mix with 30% FA (Figure 6a) lies within measurement error.
4. While CTE itself has not been the focus of the study, the nonlinearity in free deformations observed during the cooling off stages (Tables 3 and 4) of the imposed temperature paths have supported evidence to the highly nonlinear nature of CTE in young concrete.

5. Further research

1. It appears to be necessary to calibrate the thermal expansion coefficient CTE(t) for the exact same conditions (concrete recipe *and* temperature history) to be able to deduce the "correct" AD.
2. The expansion – where observed – did not level off during the 2-week duration of the testing. Originally, the set-up and steering had been designed to provide input data for adapting existing AS models to variable curing temperatures for *early-age* concrete. AD swelling, at the stage of planning, was not expected in these mixes/tests. In order to predict the behavior past the first two weeks, it would be necessary to conduct longer tests to see if and when the expansion levels off.
3. SEM studies would prove useful to investigate the differences in pore structure due to different curing regimes. It is expected that higher curing temperatures would generate coarser pores and the distribution of capillary pores vs. air voids would be different depending on the curing regime.
4. SEM/XRD analysis would also be able to provide insight into what exact hydration products are causing the swelling as this has not been established *clearly* in earlier research.

6. Acknowledgements

The funding for this project was provided by Trafikverket (Swedish Transport Administration) and SBUF (Development Fund of the Swedish Construction Industry). The materials were supplied by Cementa Ltd., Sweden. Their support is greatly appreciated along with the technical help from the lab staff at LTU.

7. References

[1] P. Lura, Autogenous deformation and internal curing of concrete, 2003. PhD Thesis, Delft University of Technology, the Netherlands.

[2] B. Persson, Self-desiccation and its importance in concrete technology, Materials and Structures. 30 (1997) 293–305.

[3] O.M. Jensen, P.F. Hansen, Autogenous deformation and RH-change in perspective, Cement and Concrete Research. 31 (2001) 1859–1865.

[4] E. Tazawa, R. Sato, E. and M.S. Sakai, Work of JCI committee on autogenous shrinkage, in: Proc. Shrinkage 2000-Int. RILEM Workshop on Shrinkage of

Concrete, 2000: pp. 21–40.

[5] O.M. Jensen, P.F. Hansen, Influence of temperature on autogenous deformation and relative humidity change in hardening cement paste, Cement and Concrete Research. 29 (1999) 567–575.

[6] P. Lura, O.M. Jensen, K. van Breugel, Autogenous shrinkage in high-performance cement paste: an evaluation of basic mechanisms, Cement and Concrete Research. 33 (2003) 223–232.

[7] E.E. Holt, Early age autogenous shrinkage of concrete, 2001. PhD Thesis. University of Washington, USA. Published by the Technical Research Centre of Finland (VTT).

[8] K. Kovler, S. Zhutovsky, Overview and future trends of shrinkage research, Materials and Structures. 39 (2006) 827–847.

[9] D. Cusson, T. Hoogeveen, Internal curing of high-performance concrete with pre-soaked fine lightweight aggregate for prevention of autogenous shrinkage cracking, Cement and Concrete Research. 38 (2008) 757–765.

[10] Ø. Bjøntegaard, Thermal Dilation and Autogenous Deformation as Driving Forces to Self-Induced Stresses in High Performance Concrete, The Norwegian University of Science and Technology, 1999.

[11] H. Hedlund, J.-E. Jonasson, Effect on stress development of restrained thermal and moisture deformation, Proceedings of Shrinkage. (2000) 355–375.

[12] P. Turcry, A. Loukili, L. Barcelo, J.M. Casabonne, Can the maturity concept be used to separate the autogenous shrinkage and thermal deformation of a cement paste at early age?, Cement and Concrete Research. 32 (2002) 1443–1450.

[13] A.B. Klausen, Early age crack assessment of concrete structures: Experimental investigation of decisive parameters, 2016. PhD Thesis, Norwegian University of Science and Technology, Trondheim, Norway.

[14] Ø. Bjøntegaard, E.J. Sellevold, Interaction between thermal dilation and autogenous deformation in high performance concrete, Materials and Structures. 34 (2001) 266–272.

[15] P. Termkhajornkit, T. Nawa, M. Nakai, T. Saito, Effect of fly ash on autogenous shrinkage, Cement and Concrete Research. 35 (2005) 473–482.

[16] I. Maruyama, A. Teramoto, Impact of time-dependant thermal expansion coefficient on the early-age volume changes in cement pastes, Cement and Concrete Research. 41 (2011) 380–391.

[17] D.P. Bentz, O.M. Jensen, K.K. Hansen, J.F. Olesen, H. Stang, C.-J. Haecker, Influence of Cement Particle-Size Distribution on Early Age Autogenous

Strains and Stresses in Cement-Based Materials, Journal of the American Ceramic Society. 84 (2001) 129–135.

[18] Ø. Bjøntegaard, T.A. Hammer, E.J. Sellevold, On the measurement of free deformation of early age cement paste and concrete, Cement and Concrete Composites. 26 (2004) 427–435. http://www.sciencedirect.com/science/article/pii/S0958946503000659.

[19] M. Viviani, B. Glisic, I.F.C. Smith, Separation of thermal and autogenous deformation at varying temperatures using optical fiber sensors, Cement and Concrete Composites. 29 (2007) 435–447.

[20] E. Sellevold, O. Bjøntegaard, Coefficient of thermal expansion of cement paste and concrete: mechanisms of moisture interaction, Materials and Structures. 39 (2006) 809–815.

[21] Z.C. Grasley, D.A. Lange, Thermal dilation and internal relative humidity of hardened cement paste, Materials and Structures. 40 (2007) 311–317.

[22] D. Cusson, T. Hoogeveen, Measuring early-age coefficient of thermal expansion in high-performance concrete, in: International RILEM Conference on Volume Changes of Hardening Concrete: Testing and Mitigation. RILEM Publication, Lyngby, Denmark, 2006.

[23] R. Loser, B. Münch, P. Lura, A volumetric technique for measuring the coefficient of thermal expansion of hardening cement paste and mortar, Cement and Concrete Research. 40 (2010) 1138–1147.

[24] I. Chu, S.H. Kwon, M.N. Amin, J.-K. Kim, Estimation of temperature effects on autogenous shrinkage of concrete by a new prediction model, Construction and Building Materials. 35 (2012) 171–182.

[25] M. Emborg, Thermal stresses in concrete structures at early age, 1989. PhD Thesis, Luleå University of Technology, Sweden.

[26] H. Hedlund, Hardening Concrete: Measurements and Evaluation of Non-Elastic Deformation and Associated Restraint Stresses, 2000. PhD Thesis, Luleå University of Technology, Sweden.

[27] A. Loukili, D. Chopin, A. Khelidj, J.-Y. Le Touzo, A new approach to determine autogenous shrinkage of mortar at an early age considering temperature history, Cement and Concrete Research. 30 (2000) 915–922.

[28] P. Lura, K. van Breugel, I. Maruyama, Effect of curing temperature and type of cement on early-age shrinkage of high-performance concrete, Cement and Concrete Research. 31 (2001) 1867–1872.

Paper IV

Orosz K, Hedlund H, and Cwirzen A

Maturity concept vs. prediction of autogenous deformations

Submitted for

Materials and Structures

Maturity concept vs. prediction of autogenous deformations

Katalin Orosz
Department of Civil, Environmental and Natural Resources, Luleå University of Technology, SE-971 87 Luleå, Sweden
+46 920-493025
e-mail: katalin.orosz@ltu.se

Hans Hedlund
Skanska Sverige AB, SE-405 18 Gothenburg, Sweden

Andrzej Cwirzen
Department of Civil, Environmental and Natural Resources Engineering, Luleå University of Technology, SE-971 87 Luleå, Sweden

Abstract

This study has been focusing on evaluating the applicability of a prevalent, maturity concept-based model, originally developed for CEM I (EN 197-1) to predict early age autogenous deformations of concretes using CEM II type blended cements cured at variable temperatures. In the recorded free deformation significant autogenous expansion has been found, with a magnitude correlating to the heat curing temperature amplitude applied. Test results were evaluated both using the specific maturity concept-based model and by performing a manual decoupling of autogenous and thermal deformations, assuming a constant thermal expansion coefficient. It has been concluded that the type of autogenous deformation (contraction vs. expansion) depends on the specific imposed temperature history. Hence, it has not been possible to incorporate the "temperature effects" into the model because it can only accommodate monotonous shrinkage. Calibration of the thermal expansion coefficient, assumed constant in the model, has shown to be necessary. Results showed that higher curing temperature may result in lower shrinkage strains due to significant early-age expansion, alleviating part of the shrinkage. Due to the observed crossover effects, likely a new, non-maturity concept based model is needed for variable temperature curing to predict early age autogenous deformations.

Keywords: early age concrete, autogenous deformation, maturity concept, expansion, modeling, thermal dilation

1 INTRODUCTION

In recent years, there has been an increasing interest in characterizing the early-age behavior of concrete; in great part, due to the fact that with the increasing use of modern, low water/cement ratio, high early strength-, high performance concretes, and/or supplementary cementing materials, relatively high autogenous shrinkage (AS) develops compared to that observed in conventional concrete. Shrinkage develops rapidly because the already initially low water content is being drained from very fine capillary pores that result in development of high tensile stresses especially at early ages. The AS that develops is sufficient to induce micro- or macro cracking when the concrete is restrained (internally or externally), [1–4]. Moreover, recent research has reported on cases where a substantial autogenous expansion or "AD swelling", as commonly known, has occurred under certain conditions in early-age samples. Expansion has been observed past a heat curing period followed by cooling down [2,5,6], or in connection with fly ash concretes [6,7] or the addition of slag [8]. AD swelling has also been linked to possible ettringite or calcium hydroxide formation in mixes made with coarser cements [9], referred to as thermal shock; "probably … thermally induced swelling caused by relatively slow moisture redistribution in the pore system of the concrete"; [2], or attributed to the reabsorption of bleed water, e.g., [10].

During hydration, fully coupled autogenous deformation (AD) and thermal deformation (TD) are recorded as free deformations; Eq. 1 and Eq. 2.

$$\varepsilon_{tot} = \varepsilon_{SH} + \varepsilon_T \tag{1}$$

$$\varepsilon_T = \alpha \cdot \Delta T \tag{2}$$

Where ε_{tot} is the total deformation, ε_T is the thermal dilation, ε_{SH} is the autogenous deformation, α is the coefficient of thermal expansion (CTE) and ΔT is the temperature change. For a robust model capable to describe any conceivable temperature history and to calculate shrinkage-induced stresses in the concrete, it is fundamental to determine the relative importance of both AD and TD, and to be able to model satisfactorily both [2].

One of the most widely used shrinkage prediction model developed by Hedlund [4] in 1999 (Eqs. 3—6) has proven to work well for normal- and high strength ordinary Portland cement (CEM I according to EN 197-1) concretes, but has recently been shown to be inaccurate for certain newer types of blended cements for example containing fly ash, [11,12]. This model, further referred to as "HH model" is based on an ultimate reference autogenous shrinkage (Eq. 3) which is determined based on w/c ratio and altered to account for the temperature effects (Eq. 4). The effects of heat curing are incorporated into a factor $\beta_{ST}\left(T\right)$ denoted as temperature sensitivity factor (Eq. 5.) or the "temperature effect on autogenous shrinkage", [4]. This expression accounts for the temperature in the sample in relation to $T_c^{max}\left(t\right)$, the maximum temperature in the sample, up to the time of

interest. It does not, however, account for how long that $T_c^{max}(t)$ has been kept at a certain level. In essence, it accounts for the amplitude of temperature (T) but not the duration of it.

The following equations are used:

$$\varepsilon_{ref} = (-0.65 + 1.3 \cdot (w/c)) \cdot 10^{-3} \quad (3)$$

$$\varepsilon_{SH} = \varepsilon_{ref} \cdot \beta_{s0}(t_e) \cdot \beta_{ST}(T) \quad (4)$$

$$\beta_{ST}(T) = a_0 + a_1 \cdot \left(1 - \exp\left[-T_c^{max}(t)/T_1\right]^{b_1}\right) + a_2 \cdot \left(1 - \exp\left[-T_c^{max}(t)/T_2\right]^{b_2}\right) \quad (5)$$

$$\beta_{s0}(t_e) = \exp\left(-\left[t_{s0}/(t_e - t_{start})\right]^{\eta_{SH}}\right) \quad (6)$$

where ε_{ref} [-] = reference ultimate shrinkage, a fitting parameter determined by the least square method; ε_{SH} [-] = autogenous shrinkage; $\beta_{ST}(T)$ [-] = temperature sensitivity factor; $T_c^{max}(t)$ [°C] = maximum temperature in the concrete sample up to time t; t [s, h or d] = real time specified as time after mixing; a_0 [-], a_1 [-], a_2 [-], b_1 [-], b_2 [-], T_1 [°C], T_2 [°C] = fitting parameters; β_{s0} [-] = relative time development or time distribution of autogenous shrinkage; t_e [s, h or d] = equivalent time of maturity; t_{start} [s, h or d] = start time of autogenous shrinkage specified in real time after mixing; t_{s0} [s, h or d] and η_{SH} [-]= curvature parameter; a fitting parameter determined by least square method.

One of the known limitations of the HH model is that it only considers the w/c ratio as the primary influencing factor that determines the AS, which leads to underestimation of shrinkage and results in a large scatter for self-compacting concretes, [13]. Furthermore, the HH model operates with a constant thermal expansion/contraction coefficient (CTE). However, for young concrete, newer research indicates that the CTE is highly nonlinear, depending heavily on the moisture content [14], since CTE of water is about seven times higher in comparison with hardened concrete. The CTE decreases sharply during the first hours after casting due to large amounts of unbound water from 20x10^{-6}/°C to ~7x10^{-6}/°C at around the setting time [15–17]. Thereafter, it slowly increases due to self-desiccation [14], converging to the value characteristic of hardened concrete 9…12 x10^{-6}/°C. The reduction around setting time can be related to the fact that before setting, the free water is continuous while as a solid skeleton is being built up, this continuity is disrupted. CTE has been measured "stepwise", [2]. During the intervals where the temperature is kept constant, only AD is recorded as a function of the entire temperature history leading up to that point. Conversely, when an "instantaneous" thermal load is applied in steps, ideally, pure TD can be measured. A similar method was applied also for mortars [18] and pastes [19,20]. CTE values for hardened concrete are published in literature, but data for early-age concrete are rather limited and inconsistent.

There exist several other shrinkage prediction models; with the major driving forces contributing to AS having been identified as the surface tension, capillary depression, and capillary tension. The Tazawa and Miyazawa prediction model developed in 1997 takes into consideration both w/c ratio and cement type [13]. Another model, called the CEB-FIP model relates the AS to the compressive strength, cement type, and concrete age and is only applicable to normal strength concretes. It has also been shown to underestimate shrinkage [13]. However, despite the earliest observations of autogenous expansion dating back to the late 90s [2], to the authors' knowledge, no current model taking into account the possibility of autogenous expansion exists. Another significant gap in knowledge is the incorporation of variable temperature levels into prediction models. There is no clear agreement whether the maturity concept can be applied to describe AD development under variable temperature curing conditions, which is a prerequisite to successful decoupling of AD and TD. It was suggested that the maturity concept based on effective age could be used by addition of a temperature-correcting factor, [21]. It should be possible to separate AD and TD in cement pastes, based on the maturity concept, by offsetting the total deformation by thermal deformation part (TD) as long as the temperature range is between 10^0C and 40^0C, [22]. In contrast, others indicate that the maturity concept is unsuitable, [2,23]. Early models [3,4] took into account the effect of curing temperature as the maximum curing temperature only. However, according to new data, the AD development rate and its magnitude are strongly dependent on the curing temperature history, [2,6,23–25]. Furthermore, the AD behavior has been found to be unsystematic, even when assuming realistic CTEs; i.e., crossover effects are present, where a sample cured at a higher temperature level does not necessarily shrink more than a sample cured at a lower level. Others also emphasized that higher temperature does not necessarily lead to higher AS [26]. Therefore, AD in a real structure cannot be predicted from isothermal test results alone because the deformation depends on the specific imposed temperature history.

This study is focusing on the possibility to incorporate the effects of variable temperature curing into the HH model to describe the development of autogenous deformation in young concrete.

2 EXPERIMENTAL

2.1 Materials

The used ordinary concrete mix designs with two different w/c ratios are presented in Table 1. The BAS Portland cement Type CEM II/A-V 52.5N contains 16% fly ash and 4% limestone, produced by Cementa, Sweden. Sikament 5650 by Sika was used to achieve the required consistency (Class S4).The 28-day cube strengths of the two mixes were 70 MPa (BAS 0.38) and 45 MPa (BAS 0.55).

Table 1. Concrete mix designs with w/c ratios of 0.38 and 0.55

	BAS 0.38		BAS 0.55	
	kg/m^3	L/m^3	kg/m^3	L/m^3
cement	470	157	360	120
0/8	975	361	1067	395
8/16	790	298	733	277
water, eff.	179	179	198	198
air content		5		5

2.2 Test setup

The used test set-up was based on earlier work done at LTU by [4] and [12]. The set-up allows for testing beginning right after setting time, in a perfectly sealed environment. Free deformations were measured on Ø=80mm, h=300mm concrete cylinders by two symmetrically mounted strain gauges of type LVDT Schaevitz type 010 MRH, mounted on composite bars made of carbon to minimize unintended thermal deformations. For every (variable) temperature history/material combination, a heat-cured and a reference (20^0C isothermal) sample were cast. The temperature development of the specimens was controlled by the temperature in the water tank with $\pm$ 3^0C accuracy.

Curing regimes for the test duration of 14 days are presented in Fig. 1. An initial adiabatic temperature rise was followed by constant curing temperature levels of 6^0C, 35^0C and 50^0C kept for 1, 3 and 5 days, respectively. The adiabatic rise was calculated using the commercially available ConTest Pro software, which enables to calculate temperature developments and cracking risk in hardening concrete. The adiabatic rise was allowed to develop in the samples until mounting the gauges while the water bath was heated along the same path. This allowed for the sample in the waterproof encasing to be submerged in the water bath without any thermal shock on the concrete sample. After the constant temperature heat curing, a constant cooling rate was applied followed by a steady temperature of 20^0C. The steering for the cooled down sample has been inverted so that the rate of cooling down/heating up to 20^0C occur at the same rate as for the heat-cured samples.

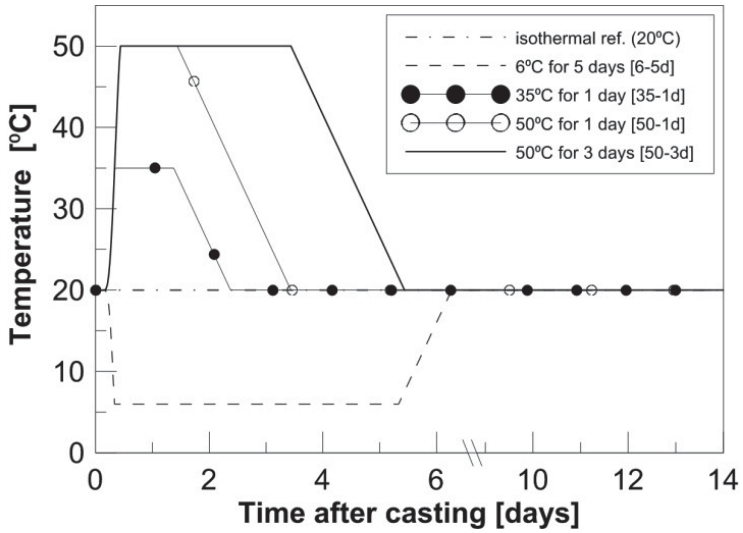

Fig. 1 Curing temperature profiles

The logged data consisted of the coupled free deformation, the temperature of the controlling water bath and in the center of the samples, and room temperature.

A steel pipe with known thermal behavior was used to validate the test setup and logging equipment. The deformations of the steel pipe, depicted on Fig. 2 are purely thermal, closely following the steering.

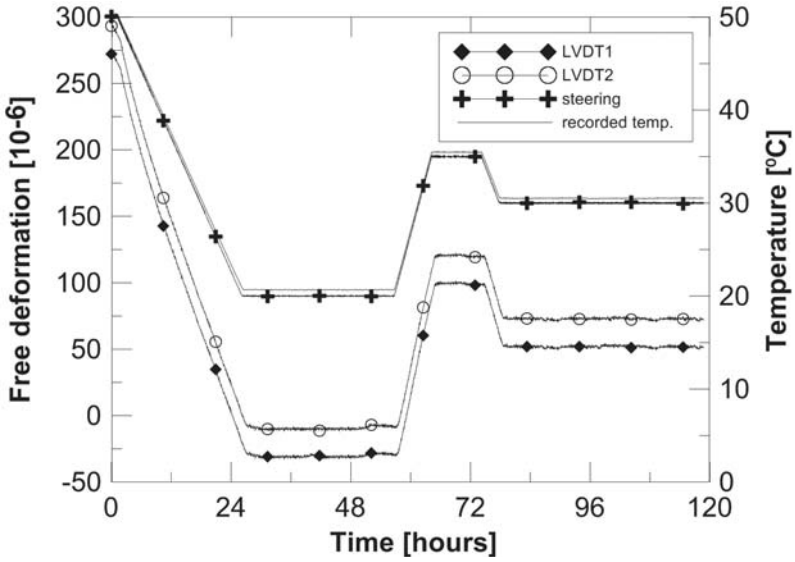

Fig. 2 Deformation recorded on steel pipe.

3 TEST RESULTS AND DISCUSSION

For the analysis of the induced stresses in case of restrained deformations, the deformation values have been zeroed at 8.5 hours after casting. The portion of the deformation prior to setting time has been removed. All timescales have been converted to equivalent time for direct comparison.

3.1 Individual best fit obtained with the HH model

In Figs 3-6, BAS1 (w/c 0.38) results are plotted. Figs 7-10 summarize the BAS2 (w/c 0.55) results. "Free def." denotes the measured free deformations for both the heat-cured and the isothermally cured reference sample, as indicated. "Calc." stands for the best fitting achieved with the HH model, for both samples. For the heat-cured sample, AD + TD splitting using the HH model has been performed marked with "heat-cured AD" and "heat-cured TD", respectively. Finally, manual splitting (marked as "AD manual split") has been performed by offsetting the recorded free deformation with $\varepsilon_{TD} = \alpha \cdot \Delta T$, assuming a constant CTE of 10×10^{-6} $1/^0$C.

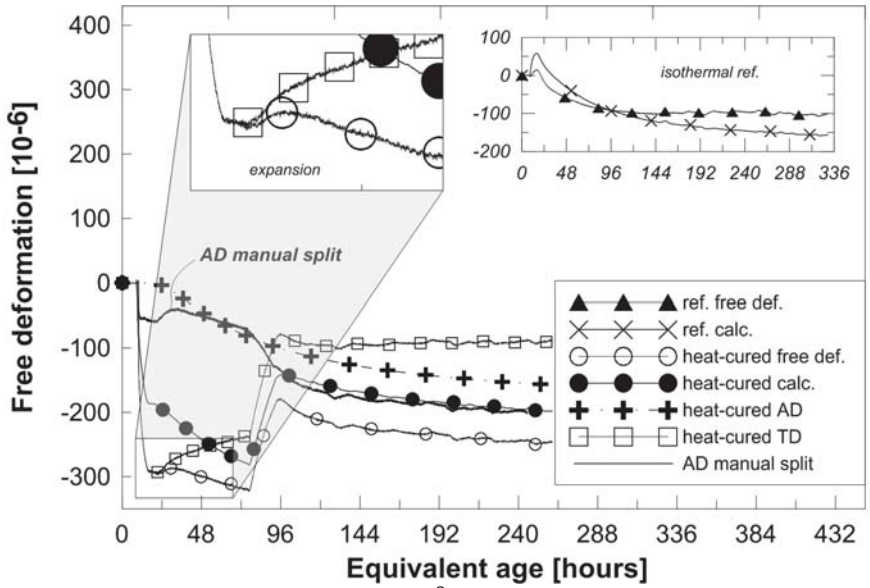

Fig. 3 BAS1 w/c 0.38 cured at 6^0C for 5 days vs. reference sample

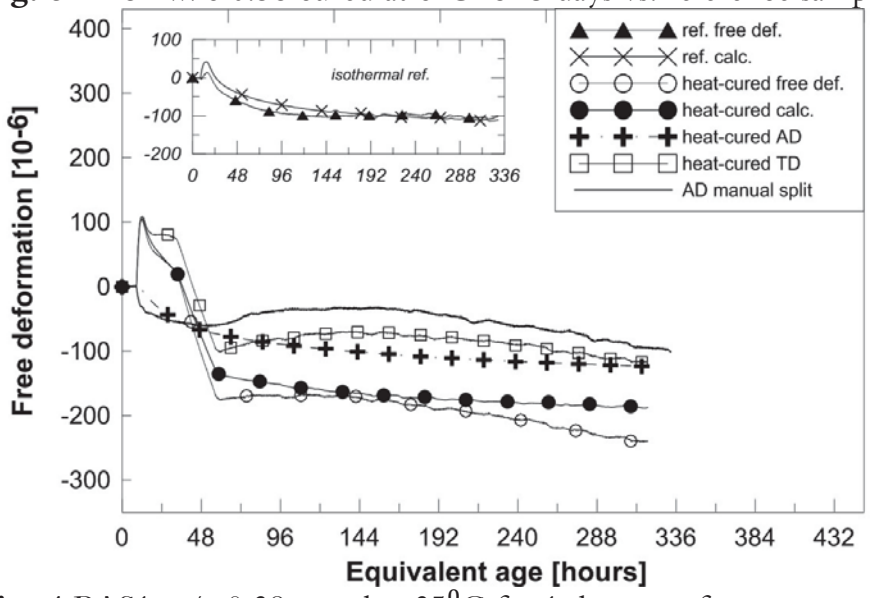

Fig. 4 BAS1 w/c 0.38 cured at 35^0C for 1 day vs. reference sample

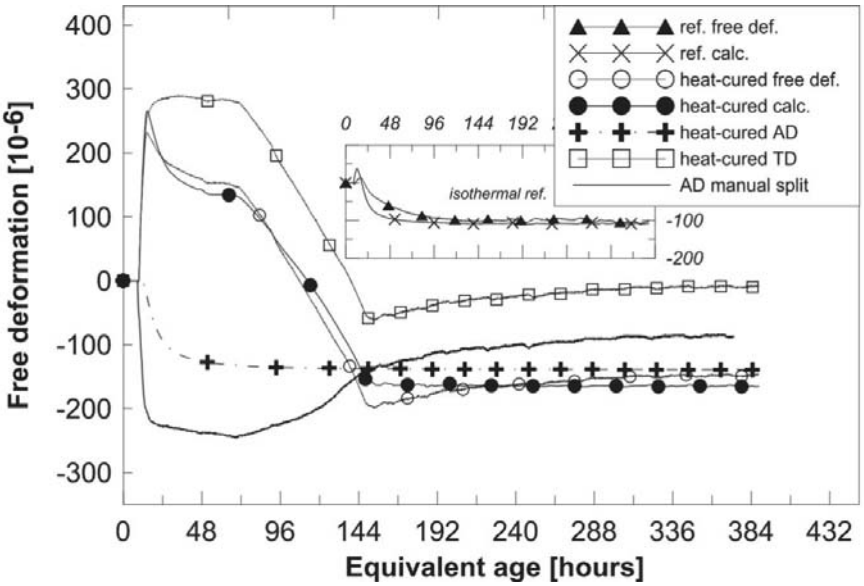

Fig. 5 BAS1 w/c 0.38 cured at 50^{0}C for 1 day vs. reference sample

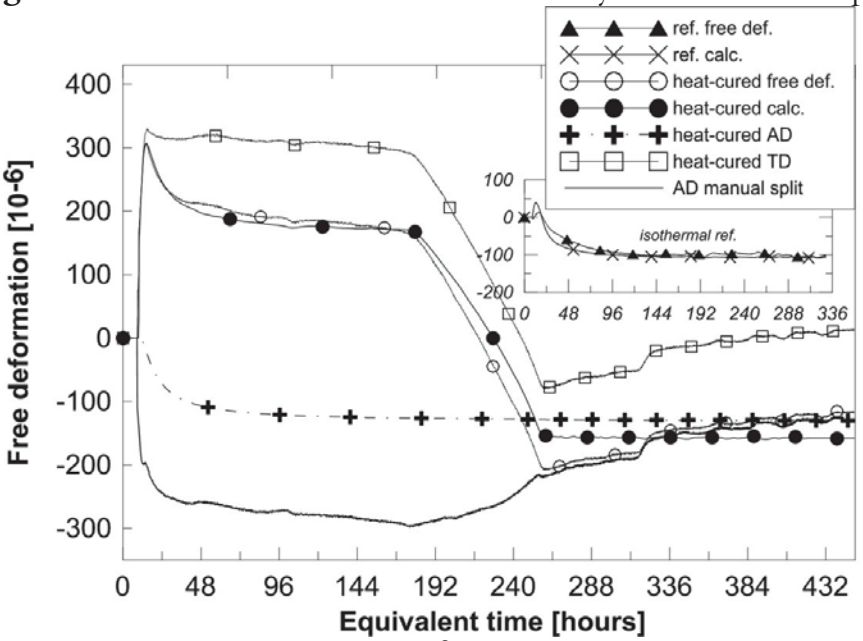

Fig. 6 BAS1 w/c 0.38 cured at 50^{0}C for 3 days vs. reference sample

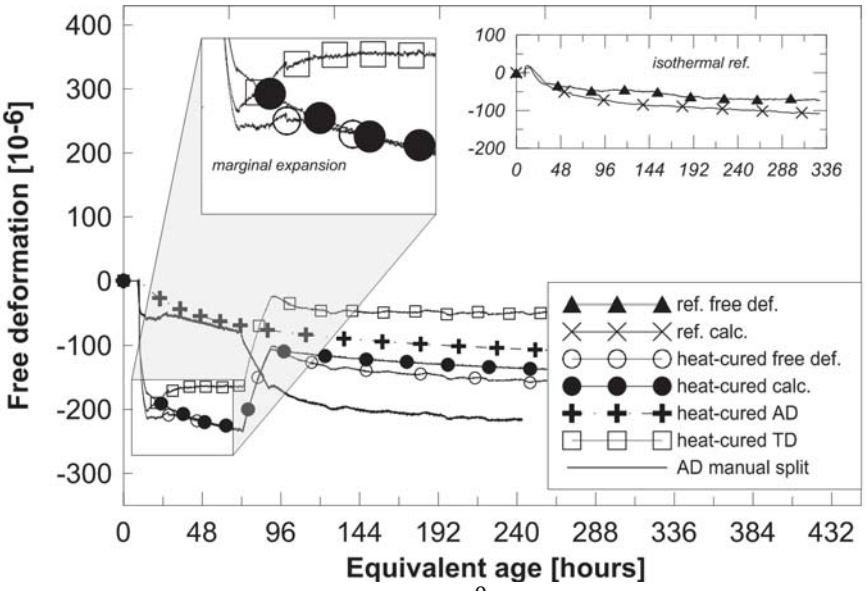

Fig. 7 BAS2 w/c 0.55 cured at 6^0C for 5 days vs. reference sample

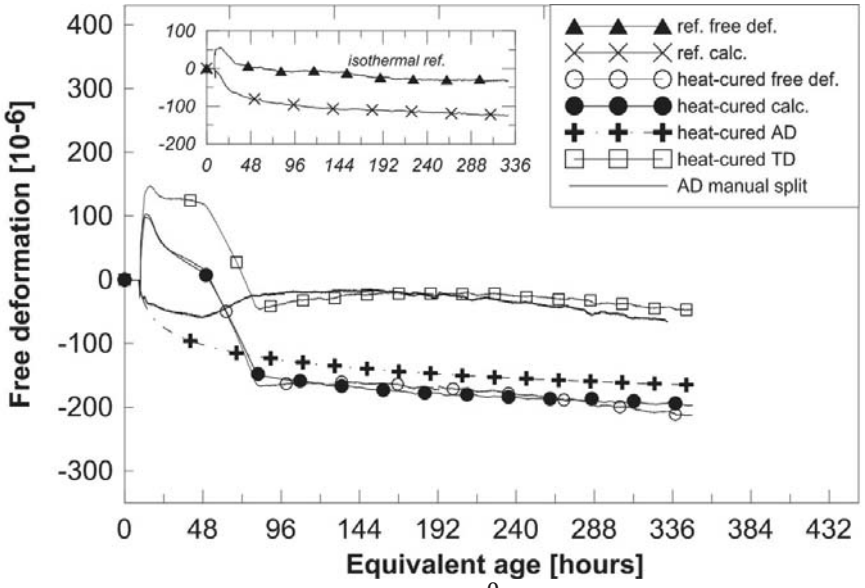

Fig. 8 BAS2 w/c 0.55 cured at 35^0C for 1 day vs. reference sample

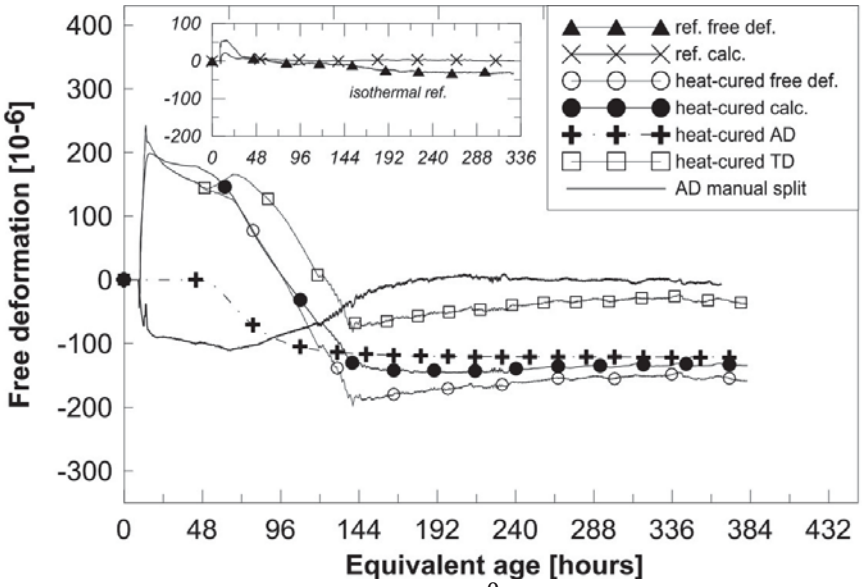

Fig. 9 BAS2 w/c 0.55 cured at 50^0C for 1 day vs. reference sample

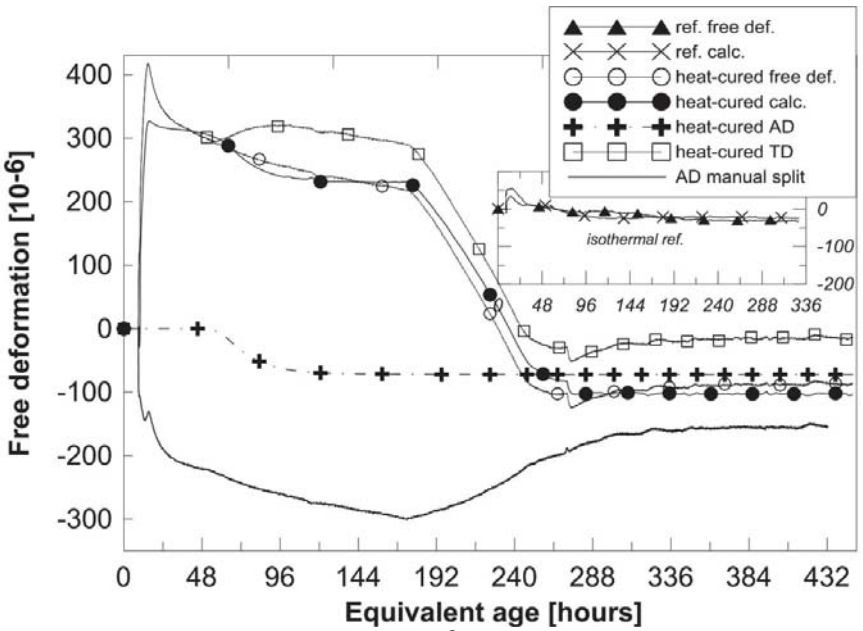

Fig. 10 BAS2 w/c 0.55 cured at 50^0C for 3 days vs. reference sample

3.1.1 Autogenous expansion

The free deformation plots represent coupled AD + TD; however, at stabilized temperature levels ($\Delta T = 0$), the deformation recorded is purely autogenous. Significant autogenous expansion has been detected for the two 50^0C temperature levels (Figs. 5, 6, 9, and 10) following the cooling down stage.

Due to the timescale conversion it can barely be detected, but there is a mild autogenous swelling and the cold curing while the samples are being cooled down at a high rate, Figs. 3 and 7.

3.1.2 Cold curing

The lower w/c sample cured at 6^0C (Fig. 3) resulted in the worst fit among all combinations tested. Common knowledge would suggest that cold curing would lower the rate of shrinkage; however, for some reason, extremely rapid shrinkage was observed for the first ~20 hours (in terms of equivalent time). The faster rate of shrinkage compared to the isothermally cured reference sample is rare, but not unheard of. Recently, [19] a study was published in which an increased magnitude of autogenous shrinkage in silica fume cement paste samples undergoing cooling down shortly after mixing, followed by a larger increase at higher temperature histories, was observed. The authors attributed the larger deformations to possible cracking within the concrete, and warned that this behavior may "pose problems for winter construction".

This initial rapidly shrinking part of the deformation plot cannot be modeled satisfactorily; the HH model underestimates the initial shrinkage by more than 30%. Acceptable results have only been obtained during the short period of the curing path when the sample is being warmed up from 6^0C to 20^0C. An overall better fit is achieved for the higher w/c concrete (Figure 7) where the entire curing path is modeled with acceptable precision. During the finishing stage at stabilized room temperature, shrinkage is underestimated for the cooled BAS1 sample but it appears to be well approximated for the higher w/c ratio BAS2.

3.1.3 Heat curing

When evaluating the results with the HH model, the overall best fit has been obtained for the BAS2 35^0C 1 day sample, Fig. 8. At 35^0C, no significant expansion has been detected past cooling down phase. In the case of the samples cured at 50^0C for 1 day, the initial peak due to heat of hydration is slightly underestimated by the HH model, Figs. 5 and 9, while significantly underestimated – by about 20% – for the BAS2 50^0C 3 days sample, Fig. 10. Most importantly, the autogenous expansion part past cooling down phase cannot be accurately modeled. The HH model can only calculate strict shrinkage for AD, and offset the total deformation with that to calculate TD. The calculated TD should be a flat line where the temperature is constant.

As it can be seen in all heat-cured samples, even in the case of best fitting, AD swelling cannot be predicted by the HH model. For AD, monotonous contraction can be calculated only due to the fact that the total deformation is calculated as a function of the shrinkage of the reference sample isothermally cured at 20^0C (i.e., applying the maturity concept), which is always contraction. TD is also calculated incorrectly since TD is calculated back from the incorrectly fitted total deformation. TD ($\varepsilon_T = \Delta T_c(t) \cdot \alpha$) should be constant where the curing temperature is kept constant (during curing plateau/after the cooling down phase), but the calculated TD ($\varepsilon_T = \varepsilon_{tot} - \varepsilon_{SH}$) suggests that the sample is being warmed up. This is, however, simply an artifact due to the AD part not being modeled properly; not a deficiency of the model per se.

3.2 Evaluated fitting parameters

Tables 3 and 4 contain the evaluated fitting parameters for the best fit, determined by the least square method according to Eqs. 3-6. All fitting is optimized for the heat-cured sample.

The parameter t_{s0} corresponds to the time at which the concrete shrinkage "begins" – which, in the model, is a fitting parameter. Before t_{s0}, the concrete autogenous shrinkage is assumed to be zero; i.e., no solid skeleton has been built yet – therefore, from a cracking risk viewpoint, no stresses are generated. Therefore, t_{s0} was chosen to correspond the beginning of the shrinkage measurements; i.e., 8.5 hours after casting.

Table 3. Fitting parameters

Mix	Curing	t_{s0} [h]	t_{start} [h]	ε_{ref} [10^{-6}]	η_{SH} [-]	α_T [$10^{-6}/^0$C]
BAS1	all	8.5				
(0.38)	6-5D		30	290	1.5	10
	35-1D		60	42	0.6	9.8
	50-1D		8.5	170	1	9.9
	50-3D		9.9	52	1.1	11.1
BAS2	all	8.5				
(0.55)	6-5D		60	-139	0.4	9.5
	35-1D		60	-186	0.2	10.1
	50-1D		60	-156	3.8	9.3
	50-3D		60	-120	5	11.5

Table 4. Fitting parameters vs. parameters proposed by Hedlund [4] for NSC and HSC

Mix	Curing	a_0 [-]	a_1 [-]	T_1 [°C]	b_1 [-]	a_2 [-]	T_2 [°C]	b_2 [-]
BAS1	6-5D	0.1	0.5	9	2.9	0.1	55	7.0
(0.38)	35-1D	2.2	1.9	9	2.9	0.9	55	6.5
	50-1D	2.0	-1.3	9	2.9	2.6	73	9.2
	50-3D	1	1.3	9	2.9	0.5	55	6.9
BAS2	6-5D	1.2	0.1	9	2.5	1.9	56	5.8
(0.55)	35-1D	-2.2	1.4	9	3.4	3.9	55	6.0
	50-1D	-1.0	1.0	9	5.3	1.2	50	5.0
	50-3D	0.2	0.2	9	0.2	0.7	55	7.0
NSC	-	0.4	0.6	9	2.9	1.3	55	7.0
HSC	-	0.4	0.6	9	2.9	0.1	55	7.0

All curve fitting has been optimized for the heat-cured samples instead of evaluating both the heat-cured and the isothermal reference samples in the same step. This results in a larger number of fitting parameters (see section 3.2), but gives a better fit for the heat-cured samples. Ideally, a bulk fitting across all temperature

levels per concrete mix would be attempted. This, however, has shown to be not feasible in this case.

In general, fitting parameters listed in Table 3 appear to be very unsystematic in the sense that the first two columns in particular (t_{start} and ε_{ref}) vary excessively across recipes and temperature levels. Most importantly, the calculated ε_{ref} values scatter, in particular for the BAS1 concrete. Given that ε_{ref}, according to the model, is a function of the w/c ratio *only* (Eq. 3), its value should not vary substantially within the same recipe. Part of the reason why the high variance has been obtained is due to the fact that it was not possible to optimize the fitting for each pair of heat-cured and reference sample simultaneously. Ideally, the iteration should be optimized for both samples simultaneously in order to determine the temperature effect in the heat-cured sample compared to the isothermal reference one. Here, the decision was made to optimize only for the heat-cured sample in order to improve the fit for the heat-cured sample.

3.3 Effects of CTE on AD

The manual splitting (denoted as "AD manual split" in Figs 3—10) reveals that autogenous expansion takes place following the cooling down stage for all samples, including the initial cooling down stage of the 6^0C sample and the entire cooling down stage of the 35^0C 1 day sample which, according to the HH model, expands only so minimally that it is considered to lie within measurement error.

Figs. 11 and 12 depict a series of possible AD curves that have been derived by offsetting the measured free deformation in the BAS2 concrete with the calculated thermal dilation ($\varepsilon_{SH} = \varepsilon_{tot} - \varepsilon_T$), assuming the two extreme values of CTE typically used for hardened concrete; $CTE_1=12x10^{-6}$ $1/^0$C and $CTE_2=8x10^{-6}$ $1/^0$C, respectively, in relation to the shrinkage of the isothermally cured reference sample.

It can be deduced that despite having chosen "realistic" – but constant – values of CTE, autogenous expansion at some stages of the curing path can be observed for most temperature levels. The splitting results in a set of parallel shifted AD curves, which are *all* morphologically different from the deformation of the isothermal reference sample. However, it is well-known that in a real concrete, CTE at early ages is not constant, as elaborated in the Introduction. In addition, the development of CTE is a product of the specific imposed temperature history. It is assumed that, to some extent, a more "realistic" splitting could be obtained with a more "realistic" (time-dependent) CTE, determined separately for each temperature history and concrete mix. This, however, has not been substantiated in the current research.

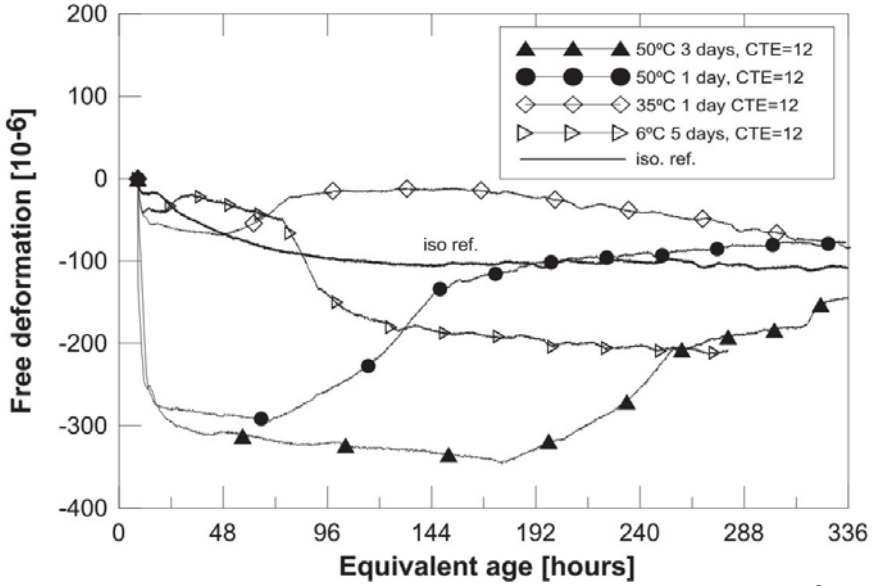

Fig. 11 Calculated AD with a constant CTE of $12x10^{-6}$ $1/^0C$

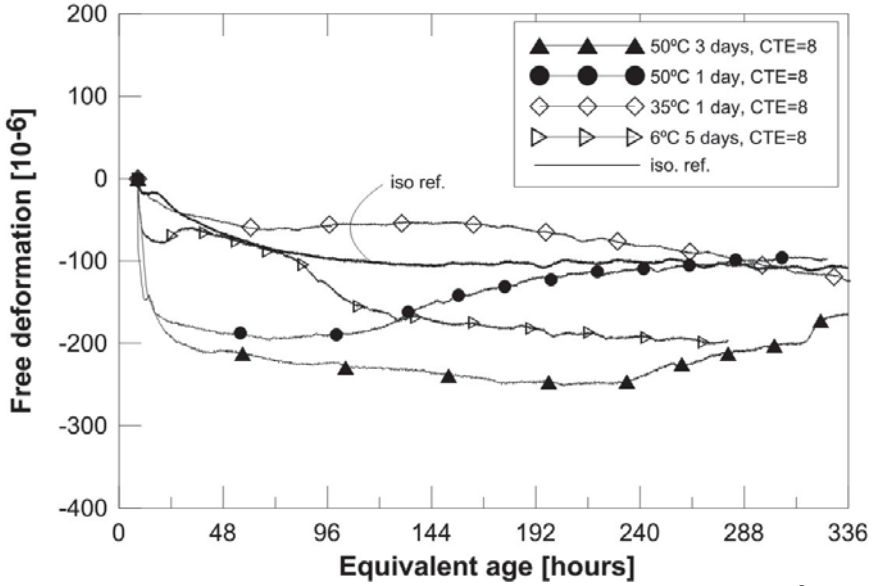

Fig. 12 Calculated AD with a constant CTE of $8x10^{-6}$ $1/^0C$

Depending on the choice of CTE, it can also be seen that certain crossover effects magnify; e.g., if the CTE is chosen a higher value then the 50^0C 1 day sample shrinkage at the 14-day (336 hours) mark will be less than that of the 35^0C 1 day sample, while the isothermal reference 14-day shrinkage exceeds the deformation of both the 35^0C 1 day or the 50^0C 1 day sample, due to the expansion observed in the heat-cured samples.

4 Concluding remarks and future research

1. The HH model gives an acceptable fit for *some* of the reference samples, but an unsatisfactory fit for all heat-cured samples after the cooling down stage

because it is not able to accommodate AD swelling. However, a robust model capable to predict early age AD must be able to accommodate expansion, which has been documented experimentally by several authors since the late 90s.

2. Determination of the development of CTE, with regard to the imposed temperature histories, appears to be necessary to be able to decouple AD and TD successfully. It was beyond the scope of this study to test the development of CTE. However, when splitting of the total (free) deformations is attempted, it is crucial to use the CTE values relevant for young concrete.

3. It appears to be necessary to incorporate factors other than w/c into the way ε_{ref} is calculated.

4. Based on the obtained tests results it can be concluded that a new non-maturity concept-based model should be developed to properly describe early-age AD.

5 Acknowledgements

The funding for this project was provided by the Swedish Road Administration (TRV) and the Development Fund of the Swedish Construction Industry (SBUF). The materials were supplied by Cementa Ltd., Sweden. Their support is greatly appreciated along with the technical help from the lab staff at Luleå University of Technology (LTU).

6 References

[1] D. Cusson, T. Hoogeveen, Internal curing of high-performance concrete with pre-soaked fine lightweight aggregate for prevention of autogenous shrinkage cracking, Cement and Concrete Research. 38 (2008) 757–765.

[2] Ø. Bjøntegaard, Thermal Dilation and Autogenous Deformation as Driving Forces to Self-Induced Stresses in High Performance Concrete, 1999. PhD Thesis, The Norwegian University of Science and Technology, Norway.

[3] M. Emborg, Thermal stresses in concrete structures at early age, 1989. PhD Thesis, Luleå University of Technology, Luleå, Sweden

[4] H. Hedlund, Hardening Concrete: Measurements and Evaluation of Non-Elastic Deformation and Associated Restraint Stresses, 2000. PhD Thesis, Luleå University of Technology, Luleå, Sweden

[5] M. Viviani, B. Glisic, I.F.C. Smith, Separation of thermal and autogenous deformation at varying temperatures using optical fiber sensors, Cement and Concrete Composites. 29 (2007) 435–447.

[6] A.B. Klausen, Early age crack assessment of concrete structures: Experimental investigation of decisive parameters, 2016. PhD Thesis, Norwegian University of Science and Technology, Trondheim, Norway.

[7] P. Termkhajornkit, T. Nawa, M. Nakai, T. Saito, Effect of fly ash on autogenous shrinkage, Cement and Concrete Research. 35 (2005) 473–482.

[8] I. Maruyama, A. Teramoto, Impact of time-dependant thermal expansion coefficient on the early-age volume changes in cement pastes, Cement and Concrete Research. 41 (2011) 380–391.

[9] D.P. Bentz, O.M. Jensen, K.K. Hansen, J.F. Olesen, H. Stang, C.-J. Haecker, Influence of Cement Particle-Size Distribution on Early Age Autogenous Strains and Stresses in Cement-Based Materials, Journal of the American Ceramic Society. 84 (2001) 129–135.

[10] S. Boivin, P. Acker, S. Rigaud, B. Clavaud, Experimental assessment of chemical shrinkage of hydrating cement pastes, Autogenous Shrinkage of Concrete. (1999) 81–92.

[11] K. Orosz, P. Fjellström, J.-E. Jonasson, M. Emborg, H. Hedlund, Evaluation of Thermal Dilation and Autogenous Shrinkage at Sealed Conditions, Nordic Concrete Research: Proceedings of the XXII Nordic Concrete Research Symposia. 50 (2014) 299–302.

[12] P. Fjellström, Measurement and modelling of young concrete properties, 2013. Licentiate Thesis, Luleå University of Technology, Luleå, Sweden.

[13] W.J. Long, K.H. Khayat, F. Xing, Prediction on autogenous shrinkage of self-consolidating concrete, in: Advanced Materials Research, 2011: pp. 288–292.

[14] E. Sellevold, O. Bjøntegaard, Coefficient of thermal expansion of cement paste and concrete: mechanisms of moisture interaction, Materials and Structures. 39 (2006) 809–815.

[15] I. Chu, S.H. Kwon, M.N. Amin, J.-K. Kim, Estimation of temperature effects on autogenous shrinkage of concrete by a new prediction model, Construction and Building Materials. 35 (2012) 171–182.

[16] R. Loser, B. Münch, P. Lura, A volumetric technique for measuring the coefficient of thermal expansion of hardening cement paste and mortar, Cement and Concrete Research. 40 (2010) 1138–1147.

[17] D. Cusson, T. Hoogeveen, Measuring early-age coefficient of thermal expansion in high-performance concrete, in: International RILEM

Conference on Volume Changes of Hardening Concrete: Testing and Mitigation. RILEM Publication, Lyngby, Denmark, 2006.

[18] A. Loukili, D. Chopin, A. Khelidj, J.-Y. Le Touzo, A new approach to determine autogenous shrinkage of mortar at an early age considering temperature history, Cement and Concrete Research. 30 (2000) 915–922.

[19] I. Maruyama, A. Teramoto, Temperature dependence of autogenous shrinkage of silica fume cement pastes with a very low water–binder ratio, Cement and Concrete Research. 50 (2013) 41–50.

[20] E.J.. Sellevold, Ø. Bjøntegaard, T.A. Hammer, Response to discussion of the paper:"On the measurement of free deformation of early age cement paste and concrete" [Bjøntegaard Ø, Hammer TA, Sellevold EJ; Cement and Concrete Composites 2004; 26: 427-435], Cement and Concrete Composites. 27 (2005) 857–858.

[21] H. Hedlund, J.-E. Jonasson, Effect on stress development of restrained thermal and moisture deformation, Proceedings of Shrinkage. (2000) 355–375.

[22] P. Turcry, A. Loukili, L. Barcelo, J.M. Casabonne, Can the maturity concept be used to separate the autogenous shrinkage and thermal deformation of a cement paste at early age?, Cement and Concrete Research. 32 (2002) 1443–1450.

[23] O.M. Jensen, P.F. Hansen, Influence of temperature on autogenous deformation and relative humidity change in hardening cement paste, Cement and Concrete Research. 29 (1999) 567–575.

[24] Ø. Bjøntegaard, E.J. Sellevold, Interaction between thermal dilation and autogenous deformation in high performance concrete, Materials and Structures. 34 (2001) 266–272.

[25] Y. Hai, Y. Zhu, Mesocosmic study on autogenous shrinkage of concrete with consideration of effects of temperature and humidity, Water Science and Engineering. 2 (2009) 85–94.

[26] P. Lura, K. van Breugel, I. Maruyama, Effect of curing temperature and type of cement on early-age shrinkage of high-performance concrete, Cement and Concrete Research. 31 (2001) 1867–1872.

Paper V

Orosz K, Humad A, Hedlund H, and Cwirzen A

Early-age autogenous deformation of heat-cured alkali activated blast furnace slag

Submitted for

Journal of Advanced Concrete Technology

Early-age autogenous deformation of heat-cured alkali activated blast furnace slag

Katalin Orosz[a], Abeer Humad[a], Hans Hedlund[b], Andrzej Cwirzen[a]
[a]Department of Civil, Environmental and Natural Resources Engineering, Luleå University of Technology, SE-971 87 Luleå, Sweden
[b]Skanska Sverige AB, SE-405 18 Gothenburg, Sweden

Abstract

Autogenous deformation behavior of alkali activated slag concrete (AASC) undergoing variable (realistic) temperature curing conditions has been evaluated and compared. The slag contained 6.6% MgO (moderately high) and 12.5% Al_2O_3 (moderate). Activator type (sodium silicate and sodium carbonate) and concentration were varied, and the results compared with a standard w/c 0.38 concrete mix. The type of the activator did not appear to make a major difference in the development or magnitude of shrinkage under heat curing. In all mixes, autogenous expansion was found at stabilized isothermal conditions past cooling down of the samples. This expansion did not level off for the duration of the tests. X-ray diffraction analysis performed shortly after cooling down the samples indicated the formation of hydrotalcite, a crystalline phase that may cause expansion. Higher amount of sodium silicate resulted in lesser expansion, likely due to the increased stiffness of the concrete body due to the accelerated rate of hydration and geopolymerization. Empirical evidence to the thermal expansion/contraction coefficient of AASC being different from OPC at early ages has also been provided.

1 Introduction

The development of alkali-activated materials (AAM) has been in the focus of interest over the last few decades (Palomo et al. 1999, Roy 1999, 2014, Provis and Bernal 2015, Provis et al. 2015). Alkali activated slag (AAS) and AASC (alkali activated slag concrete) are made by activating granulated blast furnace slag (GGBS) with alkali solutions, replacing the Portland cement entirely – thus offering a substantially reduced environmental impact over conventional concrete. Concretes made with GGBS are less sensitive to early age thermal cracking due to the lower heat of hydration generated (Turu'allo 2013). The workability is improved and the hardened concrete has an improved microstructure with smaller and fewer capillary pores, resulting in better ability to withstand chemical attacks (Heikal et al. 2014). The strength of AAS concretes is comparable or superior to ordinary Portland cement (OPC) concrete; compressive strengths as high as 100-130 MPa have been reported (Cartwright et al. 2015, Nedeljkovic et al. 2016).

GGBS is (most often) an amorphous, glassy material containing mainly calcium and aluminosilicates. In a high calcium system, alkali activation renders the aluminosilicates into a reactive form that, with the available water and the alkali and calcium ions, produce primarily calcium silicate hydrates (C–S–H), similar but to that observed in OPC but with a lower Ca/Si ratio (Gruskovnjak 2006) and a higher Al content (Haha et al. 2012), and calcium-aluminosilicate hydrates (C–A–S–H). Since the gel contains a certain amount of sodium (Na), it is often referred to as (C–(N)–A–S–H). The main difference between the two phases is that the C–A–S–H gel exhibits nanocrystallinity while a C–(N)–A–S–H type gel is amorphous (Gong and White 2016). The exact type of gel that forms depends on the calcium- and magnesium content of the system, the type and pH of the activator, and the curing conditions (Fernández-Jiménez et al. 2003, Lodeiro et al. 2009, Garcia-Lodeiro et al. 2011, Puertas et al. 2011, Bernal and Provis 2014). The mechanisms of hydration in AAS have been shown to be different (Bakharev et al. 2000, Gruskovnjak 2006).

Widespread industrial adoption, commercial scale production, and standardization of design procedures employing AAS, however, have been hindered by the lack of long-term performance/durability data and the limited understanding of shrinkage behavior and the driving mechanisms behind shrinkage. The shrinkage is considered as an important engineering property due to the risk of cracking when deformations in the material are restrained.

For cement-based materials, the autogenous shrinkage is closely related to the chemical shrinkage, microstructure development (pore size distribution) and the internal relative humidity of the material; e.g., (Tazawa et al. 1995, 2000, Baroghel-Bouny et al. 2006, Kovler and Zhutovsky 2006), while drying shrinkage is mainly influenced by the paste volume, the specimen size (surface area exposed to drying out), the relative humidity of the surroundings (Bissonnette et al. 1999) and the rate of capillary pressure development and the duration of dormant period (Sayahi 2016). In alkali-activated materials, both the autogenous and the drying shrinkage behavior appear to be more complex than in OPC. Both autogenous and drying shrinkage in AAS have shown to exceed that of comparable strength OPC (Collins and Sanjayan 2000, Neto et al. 2008, Cartwright et al. 2015). It has been found that chemical, autogenous and drying shrinkage increase with the addition of more slag and sodium silicate (Lee et al. 2014). Drying shrinkage of AAS paste activated by sodium silicate was about four times that of a comparable OPC mortar (Palacios and Puertas 2007). Drying shrinkage lower than that in OPC mortar was obtained in AAS when using sodium carbonate as activator, rather than sodium silicate (Duran Atics et al. 2009). Different activators generate coarser or finer capillary porosity (Haha et al. 2011) which is expected to influence the shrinkage behavior. Porosity is also affected by the amount of slag in the mix; an increase in slag content results in reduced total porosity and a denser microstructure (Lee et al. 2014). Higher Blaine fineness of slag resulted in greater reactivity and higher porosity (Pacheco-Torgal et al. 2008). Heat curing, besides

providing high early strength, reduced drying shrinkage in AAS (Bakharev et al. 1999). No clear relationship between drying shrinkage and moisture loss in AAS has been established. Despite the higher drying shrinkage observed in AAS, the actual moisture loss in AAS was less than in the comparable OPC samples (Collins and Sanjayan 2000). The authors attributed the greater drying shrinkage observed in AAS to the relatively large amount of mesopores and the pore radius which increases the capillary stresses. In contrary, consistently higher moisture loss compared to OPC was also observed in AAS (Ye et al. 2014). The authors reported on irregular drying shrinkage behavior where lower ambient humidity (faster rate of drying) did not necessarily translate into more rapid shrinkage development, indicating that (drying) shrinkage mechanisms in AAS are significantly more complex than in OPC.

Research focusing specifically on autogenous shrinkage in alkali-activated materials is limited to a very small number of studies, some of which are reviewed below. Alkali activation of slag by a sodium silicate solution may result in twice the chemical shrinkage of a comparable OPC paste (Thomas et al. 2012). Autogenous shrinkage of AAS mortars was tested by the corrugated tube method (Cartwright et al. 2015) under isothermal conditions and linear autogenous shrinkage strains reaching 2700-2800 με over ca. 8 months have been recorded for AASC mixes activated with both plain sodium hydroxide (NaOH) pellets or a combination of sodium hydroxide and aqueous sodium silicate or waterglass [$Na_2O(SiO_2)_n$], while about 400 με shrinkage strain was obtained in the OPC reference mix. The development of autogenous shrinkage did not slow down significantly over the observed period of 8 months while the OPC reference stabilized around the 3-month mark.

The driving mechanism behind the autogenous shrinkage in AAS is not clarified. On one hand, the chemical shrinkage is greater than that in OPC, while the AAS C-S-H has been found to have lower atomic packing density than the C-S-H in OPC, “thus the large chemical shrinkage associated with AAS hydration is likely related to the glassy nature of the slag itself, which results in a relatively low atomic packing density of the unhydrated material” (Thomas et al. 2012). Others concluded that the main driving mechanism behind autogenous shrinkage of alkali activated fly ash/slag (AFS) was accelerated self-desiccation due to the decreasing internal relative humidity in the mesopores in the hardened state rather than chemical shrinkage in the fresh state (Lee et al. 2014). In the same study, it was also found that the mesopores made up 60-80% of the total pore volume vs. 36% in OPC paste. Another study states that up to 90-95% of the total pore volume is mesopores in AAS (Neto et al. 2008). One study reported on shrinkage measurements in AAM samples kept at 99% RH (which can be considered autogenous conditions) where the introduction of polypropylenglycol-based shrinkage-reducing admixtures (SRA) in waterglass-activated slag mortars resulted in shrinkage reduction through induced expansion (Palacios and Puertas

2007). 1% SRA resulted in a ~200 με expansion over a period of 25 days, Figure 1. Increasing the amount of SRA to 2% led to lesser expansion. The authors also observed expansion in the OPC reference, and a minimal, but clearly detectable expansion in the AAS without SRA.

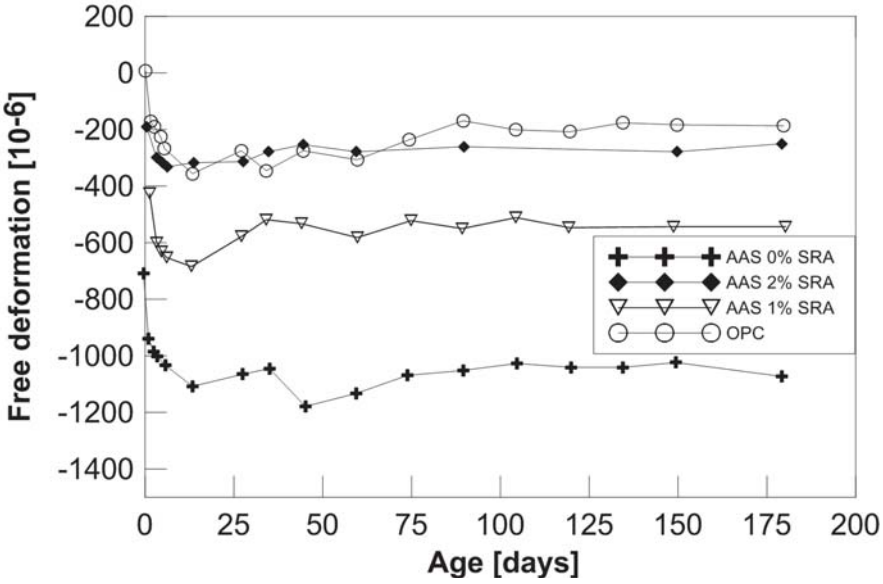

Figure 1. Deformation in waterglass-activated slag mortars with SRA; data from (Palacios and Puertas 2007)

It is clear that further research is needed to explain the experimentally observed large shrinkage deformations in AAS. There is no clear agreement in the literature whether autogenous or drying shrinkage is the dominant mechanism causing volumetric changes in AAS (Sakulich and Bentz 2013).

The autogenous shrinkage of concrete is generally a well-documented phenomenon, closely related to the self-desiccation process. However, certain curing conditions and/or materials (typically pozzolanic additives) have been found to occasionally produce delayed autogenous expansion several days into shrinkage tests. Often triggered by heat curing reaching 50^0C or higher followed by a cooling down period, autogenous expansion or "AD swelling" is a recurring phenomenon observed by several authors on an experimental level; yet the mechanisms or causes are still not fully understood. To give a few examples, the heating-cooling regime caused a steady period of autogenous expansion starting at around 4 days into the curing in OPC (Bjøntegaard 1999). Recently, expansion was documented in heat-cured fly ash concretes during the entire cooling down stage, regardless of the exact percentage of fly ash (17-45%) (Klausen 2016), and in OPC mixes made with 30-45% slag replacement (Maruyama and Teramoto 2011). In some cases, the temperature trigger appears to be missing: in concretes made with a very high percentage of fly ash (50%), w/c 0.30, a steady expansion – attributed to possible ettringite formation in large amounts – occurred, beginning around day 5 and lasting for another 7-8 days, despite the fact that the temperature

in the concrete at no point did exceed 25°C before the onset of swelling (Termkhajornkit et al. 2005). Ettringite formation has been identified in another study as well, as a possible swelling inducing mechanism in OPC mixes made with coarser cements (Bentz et al. 2001).

Finally, for practical applications, it is important that the materials be tested under realistic conditions in terms of curing. While most alkali activated materials benefit from heat curing and hence, are habitually heat cured in order to gain early compressive strength faster, and for fly ash geopolymers heat curing is required (Al-Majidi et al. 2016), shrinkage tests are typically performed under ambient temperature conditions, or past heat curing – by when most of the shrinkage has already developed. To the authors' knowledge, up to the date of publication, no studies on autogenous shrinkage of heat-cured AAS *while undergoing heat curing* exist. This paper presents experimental results comparing the autogenous deformation behavior of AAS to that of OPC undergoing variable temperature ("realistic") curing. Strictly speaking, the concrete mix used as baseline is a Portland composite cement (CEM II/A) mix; for simplicity, it will be referred to as OPC in this paper.

2 Experimental program

2.1 Materials

For the AASC mixes, ground granulated blast furnace slag (GGBS, Merit 5000) provided by MEROX, Sweden was used in this study. Its chemical composition, determined by XRF spectrometry, along with the known properties of the cement used for the ordinary Portland cement concrete mixes are listed in *Table 1*. The type II/A-V 52.5N Portland cement contains 16% fly ash and 4% limestone, provided by Cementa, Sweden.

The mix designs are summarized in *Table 2*. The PCC (composite Portland cement) mixes are normal strength concretes with a w/b of 0.38. The required consistency (S4) was achieved by using Sikament 5650 plasticizer from Sika, Sweden. No superplasticizers were used in any of the studied AASC mixes, which all contained 450 kg/m^3 of GGBS and had w/b ratio of 0.45. The only difference in the mixes is the type and the amount of activator used (10wt% and 14wt% of binder weight). Both sodium silicate (SS) and sodium carbonate (SC) were used as activator. The sodium carbonate was provided in dry powder form by CEICH S.A. in Poland. The aqueous solution of sodium silicate (SS) was provided by PQ Corporation. The SS had alkali modulus (SiO_2/Na_2O) = 2.2 with 34.37% SiO_2, 15.6% of Na_2O and a solid content of 49.97%. The alkali modulus of the liquid SS was adjusted to 1.00 by adding chemically 98% pure sodium hydroxide (NaOH) pellets.

Table 1. Physical and chemical properties of binders

Slag	CaO	SiO_2	Al_2O_3	Fe_2O_3	MgO	Na_2O	K_2O	TiO_2	MnO	P_2O_5	SO_3	Cl	others
Oxides [%]	48.91	24.24	7.89	0.76	6.56	0.08	0.97	5.95	1.21	0.41	2.51	0.017	0.502

Physical data	Specific surface [kg/m^2]	Particle density [kg/m^3]	Bulk density [kg/m^3]	Moisture content [%]	Glass content [%]
	500	2950	1100	0.1	97-98

Cement	CaO	SiO_2	Al_2O_3	Fe_2O_3	MgO	Na_2O	K_2O	TiO_2	MnO	P_2O_5	SO_3	Cl	others
Oxides [%]	55.4	24.0	6.7	N/A	2.8	N/A	1.3	N/A	N/A	N/A	3.4	N/A	N/A

Physical data	Specific surface (Blaine-fineness) [kg/m^2]	Compact density [kg/m^3]	Water-soluble Cr^{6+}
	450	3000	< 2 ppm

Table 2. Mix proportions and mix properties

Amount [kg/m^3]/mix	SC10	SS10	SS14	PCC
slag	450	450	450	-
0/4	1332	1332	1332	-
4/8	331	331	331	-
water, eff.	202.5	202.5	202.5	179
cement	-	-	-	470
0/8	-	-	-	975
8/16	-	-	-	790
activator	10% SC	10% SS	14% SS	-
alkali modulus		1.00	1.00	-
pH of activator	11.2	13.7	13.7	-
28-day cube strength [MPa]	48	50	77	70

The activator solution was prepared and put to rest for 24 hours prior to mixing. After mixing all dry ingredients for 3 minutes in a Hobart mixer, the activator was added and mixing continued for another 4 minutes. 28-day cube strength was determined on 100x100mm cubes. The PCC samples were prepared

in a standard concrete pan mixer. Immediately after casting, all samples were sealed in plastic bags.

2.2 Testing program

2.2.1 Free deformations

The test setup for measuring autogenous deformations had been used successfully at LTU in the past to evaluate early age free deformations of OPC (Hedlund 2000, Fjellström 2013). Fully coupled autogenous and thermal deformations were recorded on Ø=80mm, h=300mm concrete cylinders by means of two symmetrically mounted Schaevitz type 010 MRH linear variable deformation transducers. The gauge length was 100mm. Prior to the tests, the test setup and logging equipment were validated by recording the thermal deformations on a steel pipe. As evidenced in Figure 2, the deformations recorded closely follow the temperature steering, consisting of straight lines, with minimal noise.

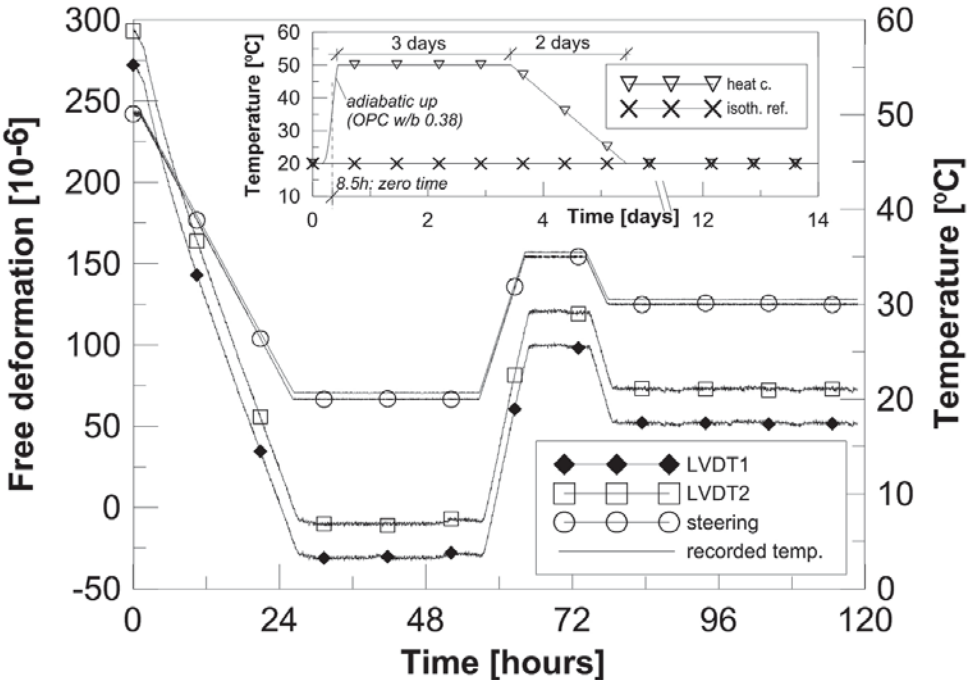

Figure 2 Deformation recorded on steel pipe (non-zeroed).

To facilitate demolding the AASC samples at 8 hours, the cylinder molds were lined with transparency foil before casting. The demolded cylindrical samples, with the LVDTs mounted on, placed inside a waterproof casing underwent heat curing while submerged in a water tank. The curing temperature was regulated with ± 3^0C accuracy. Initially, the forced temperature path – for all samples – followed the adiabatic temperature development of the w/b 0.38 PCC

sample. After reaching the prescribed curing temperature, the steering consisted of a constant temperature curing plateau, a steady-rate cooling down stage, and steady room temperature curing; Figure 2.

The total duration of the tests was 14 days. The recorded data consisted of the free deformation, the temperature in the center of the sample measured by a cast in thermocouple, the temperature of the water bath and the ambient temperature. LVDTs were mounted on the already hardened samples. This choice is arbitrary; the test setup is suitable for measuring free deformations as soon as the sample can be demolded without breaking it. Here, the samples were demolded at 8 hours of age and the deformations zeroed at 8.5 hours (after mounting the LVDTs) in order for the results to be comparable with the PCC results (performed earlier).

2.2.2 XRD analysis

For XRD analysis, AAS paste samples have been cast in Petri dishes, and then sealed. The samples underwent heat curing identical to the free deformation cylinders. After 168 hours, they have been first crushed then hand-grinded into a fine powder. The XRD analysis was performed within two hours after powdering the samples; therefore, no solvents were employed to stop the hydration.

3 Test results and discussion

3.1 Free deformations

The presented results represent the average of the two LVDT readings per sample, across all tested samples for the same temperature level (Heat-cured PCC – 3 samples; heat-cured SC10 and SS10 – 2-2 samples; heat-cured SS14 and all room temperature reference samples, 1 sample). The scatter across the measurements per material was less than 10%.

Recorded free deformations are presented in Figure 4 – Figure 3, along with the curing temperature path (in Figure 3) and recorded temperature development in the center of the heat-cured samples. While equivalent age would be a more suitable way to compare the different samples, the free deformation plots have been drawn in terms of real time after casting (in hours) because calculation of the equivalent age for AAS requires material parameters not available at the time of writing. These fitting parameters, θ_{ref} and κ_3, described in e.g., (Hedlund 2000, Nilsson 2003, Fjellström 2013), experimentally determined for each separate mix, are incorporated into an empirical expression for activation energy determined by (Jonasson 1984) and, henceforth, the maturity function. However, since all heat-cured samples have undergone the same temperature path, the use of real time is acceptable here for comparing the effects of heat curing in AAS vs. concrete.

On the deformation axis, positive values indicate expansion while negative values indicate contraction (shrinkage). Lab room temperature (20^0C) isothermal

reference samples are also plotted, with the exception of the SS14 sample where no data are available. *Figure 7* presents a comparison for all heat-cured samples.

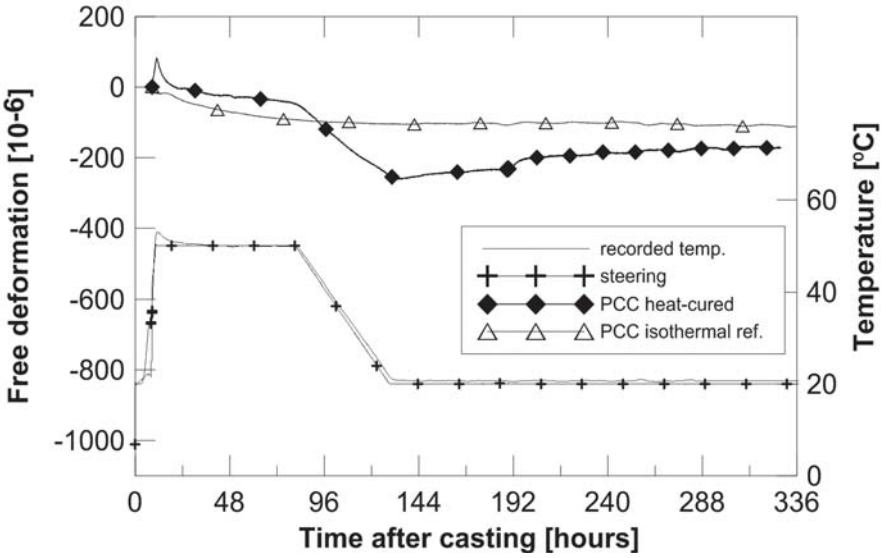

Figure 3. Free deformations and temperature development recorded on the PCC samples, along with the temperature steering used in all tests.

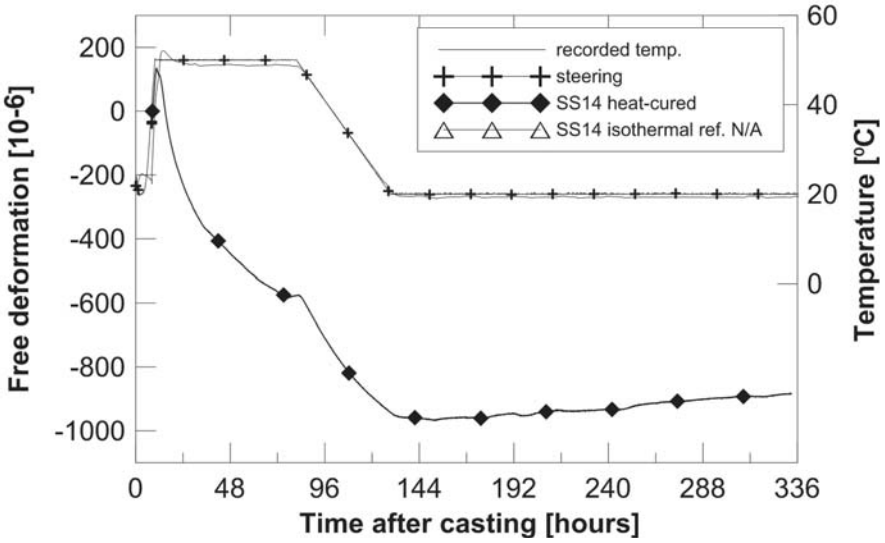

Figure 4. Free deformations and temperature development recorded on SS14 heat-cured sample.

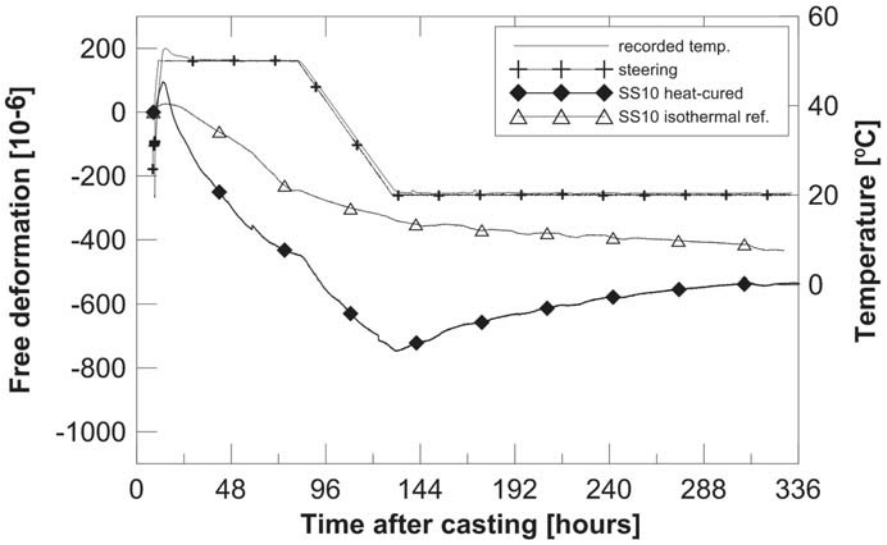

Figure 5. Free deformations and temperature development recorded on SS10 samples.

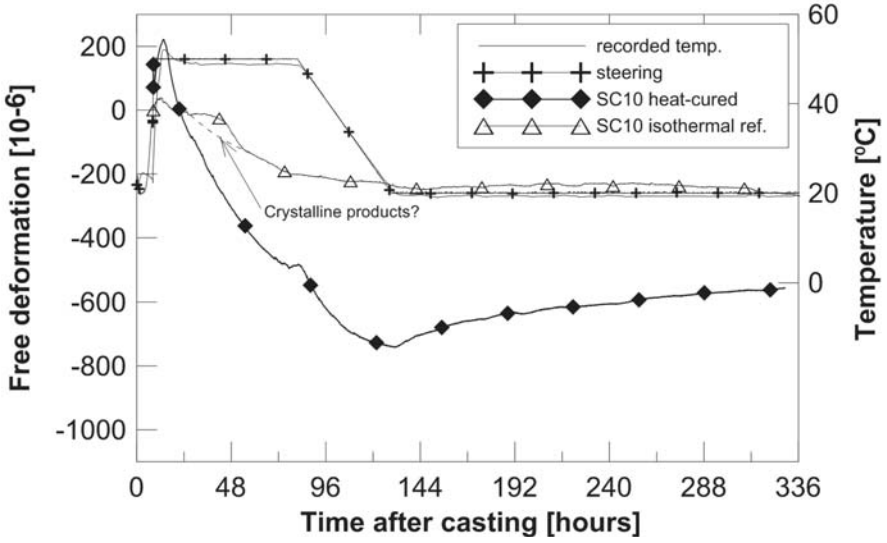

Figure 6. Free deformations and temperature development recorded on SC10 samples.

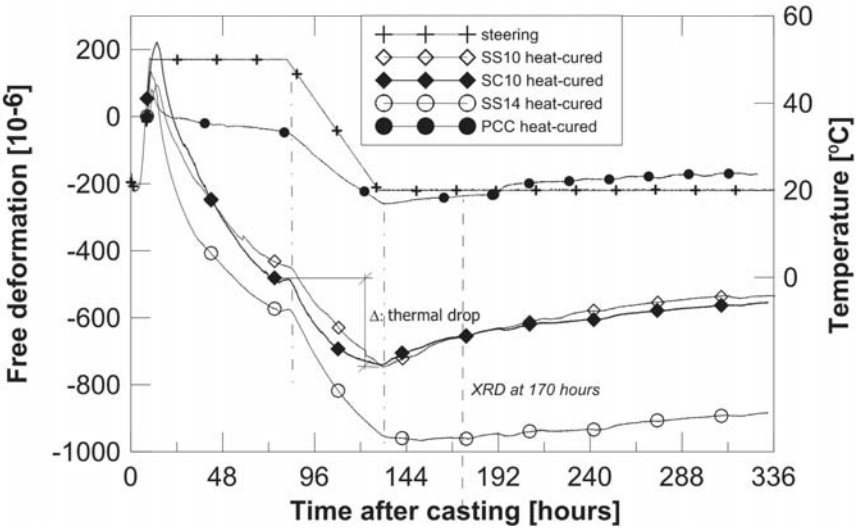

Figure 7. Free deformations on heat-cured samples, comparison.

The maximum aggregate size of the AASC mixes was 8 mm, while 16 mm for the PCC mix, while both contain about the same amount of binder per volume. Therefore, the AAS mixes had a higher paste volume per unit than the concrete counterpart. In addition, the w/b ratios of the AAS and PCC mixes were not the same due to the fact that the tests were carried out in two independent steps.

Isothermal reference samples

The total deformation of all AASC samples exceeded that of the comparable PCC sample significantly, which is in line with the literature. Monotonous shrinkage has been observed in all isothermal reference samples. The SS10 reference shrank about twice as much as the SC10. Data presented by, e.g., (Duran Atics et al. 2009) on AAS pastes suggested the preferred use of sodium carbonate as activator over sodium silicate because in resulted in reduced (drying) shrinkage of AAS, comparable to that of OPC mortars.

The activator dependence of the shrinkage behavior is prominent in the reference samples; the SC10 mix develops virtually no shrinkage (<20 με) for the first 32 hours of the heat curing at high temperature as evidenced by Figure 5. Since there is no singularity in the heat curing possibly causing the sharp change in the rate of shrinkage at around 40 hours, the shape of the curve suggest that expansive products may be forming already at that early stage in the form of a "hump". There was no such slope change observed in the SS10 reference sample. However, no XRD analysis has been performed on reference samples to confirm the possible early formation of crystalline products.

The results presented here show that sodium carbonate resulted in near triple the shrinkage of PCC and, as expected, sodium silicate would cause even more shrinkage. However, it is important to mention here that deformations during the first 8.5 hours were still not recorded due to the test setup. Therefore it is

impossible to tell how the 14-day shrinkage would compare if the measurements were started right after casting, such as with the corrugated tube method. For example, the difference between sodium silicate and carbonate could be even larger. These results correlate with earlier tests on AAS activated with a mix of sodium silicate and sodium hydroxide where autogenous shrinkage strains up to 7 times larger than in PCC were obtained (Bakharev et al. 2000).

Heat cured samples

The influence of the activator type (SC10 vs. SS10) on the magnitude and development rate of the shrinkage was minimal for the heat-cured samples. The "OPC-like" behavior of SC has not been substantiated. Sodium carbonate generated higher heat of hydration in the beginning which may increase the risk of very early age thermal cracking. Increasing the amount of the activator (SS14 vs. SS10) resulted in faster rate of shrinkage development initially, in agreement with earlier studies by, e.g., (Neto et al. 2008); however, after about 48 hours of age after casting, the shrinkage rates of the SS10 and SS14 are nearly identical. After 130 hours, the expansion in SS14 is noticeably slower than in the other two samples with lower amounts of activator; the rate at which the SC14 sample swelled was, in fact, lower than that of the PCC reference.

Autogenous expansion has been observed in all heat cured samples. The expansion is clearly identifiable after the 130-hour mark where the curing temperature was kept constant; however, based on the slope change during the cooling down stage, it is likely that the swelling begins already while the samples undergo cooling down. The expansion appears to have plateaued in the PCC mix but did not begin to level off yet in either AASC mix by Day 14 after casting. Such swelling – beginning during cooling down – is not uncommon to OPC; e.g., (Bjøntegaard 1999, Klausen 2016). The sodium carbonate sample appears to have started to swell earlier into the cooling down stage than the sodium silicate sample, as indicated by the slope of the free deformation curves shifting upward during the cooling down period. The differences in deformation behavior due to increasing the amount of activator could partly be ascribed to the differences in the developing pore structures. Larger amounts of silica increase the percentage of mesopores (Collins and Sanjayan 2000, Neto et al. 2008, Gu et al. 2015, Thomas et al. 2017), and generate a denser microstructure with the both the maximum pore size and the overall porosity reduced (Neto et al. 2008). It is a well-known fact that the volume of the mesopores is one of the governing factors that influence autogenous shrinkage in cementitious materials because it increases capillary tension.

The thermal drop (marked with Δ in Figure 7; listed in *Table 3*) indicates coupled autogenous and thermal deformation (AD + TD) during the cooling down stage, where TD is calculated as $\alpha*\Delta T$, where α is the thermal dilation coefficient and ΔT is the temperature change. The value of α in cement-based materials is closely connected to the internal RH of the sample (Sellevold and Bjøntegaard

2006), and may be also influenced by the pore structure in the concrete body (Grasley and Lange 2007). The development of the thermal coefficient in AAM lacks documentation; however, the variations in thermal drop indicate differences in the materials at that curing stage; i.e., different moisture content, hydration products, and/or pore structure (total porosity; amount of mesopores).

Table 3. Comparative deformation values

sample	Δ thermal drop [με]	early expansion due to heat of hydration [με]	shrinkage before cooling down [με]	expansion past 130 hours [με]
PCC	210	75	-125	90
SS10	290	90	-540	210
SC10	250	225	-730	190
SS14	380	150	-710	65

As it can be seen from the table, the contraction for SS14 during cooling down is about 30% larger than in the S10 sample. The contraction Δ is partly autogenous and partly thermal, related to the coefficient of thermal expansion, CTE. In ordinary concrete, the CTE decreases sharply right after casting due to large amounts of free water (above $20x10^{-6}$/°C) (Cusson and Hoogeveen 2006, Loser et al. 2010, Chu et al. 2012) to a minimum value around setting time (~$7x10^{-6}$/°C). Thereafter, it slowly increases due to self-desiccation (Sellevold and Bjøntegaard 2006), converging to the value characteristic of hardened concrete (9…12 $x10^{-6}$/°C). The reduction around setting time is due to the fact that while still plastic, the free water is continuous while during the formation of the solid skeleton this continuity gets disrupted. Considering that the hydration rate of the SS14 is faster, and the thermal coefficient is skewed by the water content, therefore, it should be lower in a material with accelerated hydration rate, it can be deduced that in AAS, the developing pore structure – as hypothesized for concrete by (Grasley and Lange 2007) – or the different proportions of hydration/geopolymerization products, or other, yet unknown factors have a significant impact on the CTE.

3.2 Hydration products

The slag has a relatively high MgO (6.6%) and CaO (48.9%) content (Table 1). AAM systems with high calcium and magnesium content tend to form C–(A)–S–H dominated gels which are less porous than the polymerized gel that forms in a system with low Ca (Bernal and Provis 2014, Bernal 2016). The structural differences (density, porosity, Ca/Si ratio) (Gruskovnjak 2006, Thomas et al. 2012) in the C–S–H forming in AAS and OPC and the larger paste volume

together account for the much larger deformations (contractions) observed in the AAS.

The formation of a predominantly C–(A)–S–H type gel has been confirmed by XRD diffraction analysis on all AAS samples (Figure 8), performed after one week of heat curing, at 170 hours of age. However, no XRD data on the PCC sample is available.

The dominant phases in AAS could be identified as C–(A)–S–H gel and calcite ($CaCO_3$), in alignment with e.g., (Ke et al. 2016). Neither ettringite ($Ca_6Al_2(SO_4)_3(OH)_{12}\cdot 26H_2O$) nor hydrogarnets have been detected in either AAS mix, contrary to the findings presented in, e.g., (Gruskovnjak 2006, Chen and Brouwers 2007). Higher Al_2O_3 content of slag has been related to larger amounts of ettringite forming (Gruskovnjak 2006). However, the slag used here had a moderate Al_2O_3 content ($Al_2O_3/(CaO+Al_2O_3+MgO)=12.5\%$). It is also known that available MgO in cementitious systems can precipitate as brucite (Lothenbach and Winnefeld 2006). Brucite peaks have not been detected at the stage when the XRD analysis was performed. It is also possible for brucite to have formed early on but later converting into hydrotalcite (Lothenbach and Winnefeld 2006, Gu et al. 2014).

Calcite peaks were detected only in the AAS mix activated with sodium carbonate. The use of sodium carbonate as activator has been associated with a prolonged hardening process (Ke et al. 2016) in which the alkalinity required to fully dissolve the slag develops slowly. Prior to the formation of C–(A)–S–H, Ca^{2+} ions from the dissolved slag react with CO_3^{2-} from the activator to form calcite ($CaCO_3$) which, in turn, will raise the alkalinity. The presence of calcite as a minor or trace reaction product in AAS activated with sodium carbonate has also been confirmed by (Myers et al. 2017).

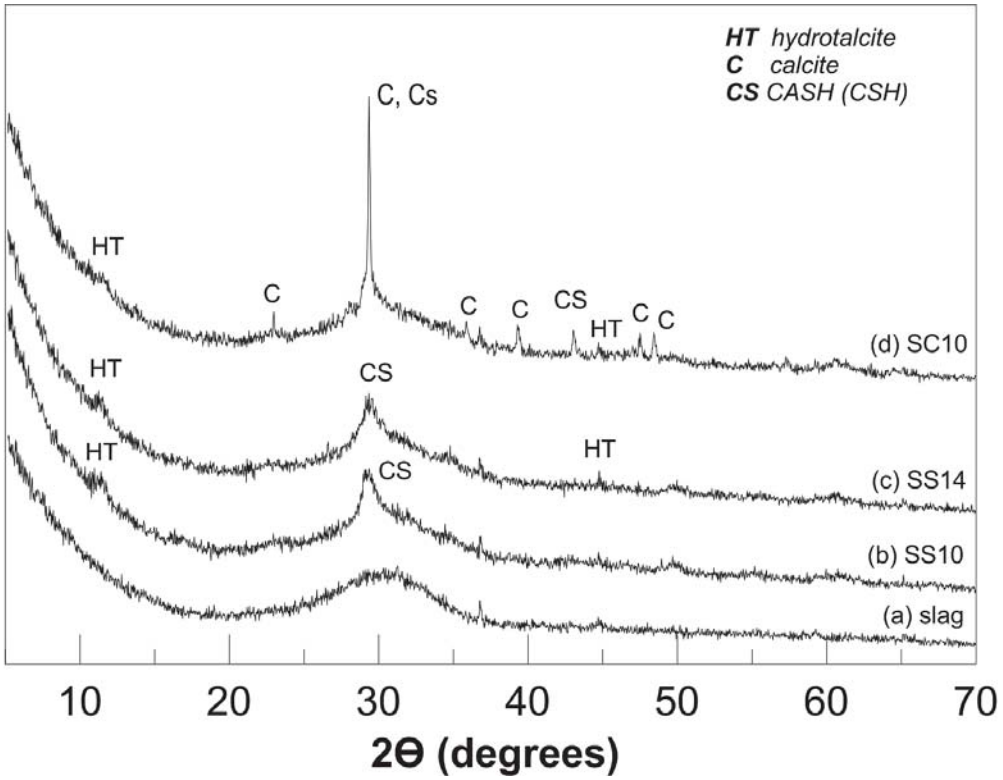

Figure 8. X-ray diffractograms at one week of age – (a) unreacted slag, (b) heat-cured SS10, (c) heat-cured SS14, and (d) heat-cured SC10.

A typical hydration product in AAS is hydrotalcite ($Mg_6Al_2(CO_3)(OH)16{\cdot}4(H_2O)$ – a magnesium aluminate hydrate) which has shown to be forming depending on the MgO content of the slag, activator type, and curing conditions; e.g., (Chen and Brouwers 2007, Haha et al. 2011, 2012, Gu et al. 2014, Ke et al. 2016, Ye and Radlinska 2016, Myers et al. 2017), often in the form of tiny crystals forming within the C–S–H (Wang and Scrivener 2003). Higher MgO contents have been linked to a denser microstructure and higher compressive strength because of additional hydrotalcite forming (Haha et al. 2012). The available Al_2O_3 first tends to form hydrotalcite (and hydrogarnets/ettringite), then into the C-(A)-S-H and AFm, depending on the Ca/Si ratio (Chen and Brouwers 2007, Li et al. 2010). Small, but detectable hydrotalcite peaks have been identified for all three heat-cured AAS mixes. Hydrotalcite forms small platelets, which is one possible reason for the swelling experienced. Two hydrotalcite peaks have been detected for the SS14 while only one for the SS10. It can be hypothesized that more hydrotalcite formed in the SS14 mix; yet, the expansion was less pronounced. One possible explanation for the lesser swelling in SS14 could be that the hydration– and strength development rate in the SS14 sample is accelerated; therefore, at the stage when swelling due to hydrotalcite formation occurs, a stiffer skeleton has been built already that resists deformations better.

The XRD analysis alone did not unequivocally clarify the differences in the magnitude of the observed expansion in AASC. It is only suspected that the hydration products causing the – compared to AASC, little – expansion in the PCC sample could be ettringite (Termkhajornkit et al. 2005) or possibly some brucite, although the MgO content of the cement is rather low for brucite formation. Swelling of the OPC sample could also be related to the condensation water inside the waterproof casing being absorbed back into the sample – a steep drop in temperature may cause sudden condensation in the air space between the sample and the casing. When opening the molds at the end of the testing, no condensation water was found inside. This may mean that the samples soaked up the condensation water (if any). This could be confirmed by performing regular internal RH measurements inside the samples. It is less likely, however, that the reason for the swelling would be condensation in the AAS samples because the hydration in an AASC is happening at an accelerated rate, therefore, the internal RH at the beginning of the cooling down should be lower than that in the PCC counterpart, needing a larger temperature gradient to cause condensation.

4 Concluding remarks and future research

The observed larger shrinkage in AASC is likely a combination of the higher paste volume, slightly lower w/b, different C–S–H and hydration- and/or geopolymerization products, and different pore size distribution – significantly larger amount of mesopores – in AASC vs. OPC.

Autogenous expansion has been detected in all AASC mixes. It is not possible to determine the exact onset of the expansion without decoupling the autogenous and thermal deformations; however, based on slope changes in the free deformation plots, expansion likely begins during the cooling down stage. The expansion did not level off during the duration of the tests. Hydrotalcite peaks have been detected by XRD in all AAS samples. Further SEM analysis could help in identifying the exact hydration products that cause expansion. Additionally, XRD analysis could be performed at different ages; for example, it could be used to detect hydration products that may convert into others later, such as brucite into hydrotalcite (Lothenbach and Winnefeld 2006, Gu et al. 2014).

Since larger amounts of slag have been associated with a more refined microstructure, it would be of interest to test autogenous deformation mixes with different amounts of slag. In such refined systems, autogenous shrinkage makes up for a larger part of the total deformation. In order to be able to quantify and model cracking risk in AASC, it is fundamental that more research be conducted on autogenous deformation. Increasing amounts of slag, however, result in an increased fraction of amorphous gel phase (Nedeljkovic et al. 2016) so the mechanisms causing shrinkage are expected to become even more complex.

Furthermore, it is important that shrinkage tests be performed under realistic curing conditions – conditions the AASC would undergo in a real structure. The

measurements should begin the latest at the time when the solid skeleton builds and restrained shrinkage stresses start to be generated. While heat curing is often impractical in field applications, *if* heat curing is performed, the deformation behavior of a (concrete) sample cured at ambient temperature vs. a heat-cured sample can be fundamentally – morphologically – different; e.g., (Bjøntegaard 1999). If heat curing is involved, decoupling of autogenous and thermal deformations is necessary in order to be able to quantify both mechanisms separately, and to evaluate their relative importance when assessing cracking risk. For successful decoupling it is crucial to use the correct thermal coefficient, in particular for early-age materials when it is expected to be highly nonlinear. In the current study, no decoupling has been attempted. It is likely that, due to the different hydration/geopolymerization processes in AAM, the thermal coefficients taken from literature for concrete would not be applicable. At the moment of writing, no data on the development of the thermal coefficient specific to early-age AAM exists.

Acknowledgements

The funding for this PCC part of this project was provided by Trafikverket (Swedish Road Administration) and SBUF (Development Fund of the Swedish Construction Industry). The materials were supplied by Cementa Ltd., Sweden. Their support is greatly appreciated along with the technical help from the lab staff at LTU. Further, the AASC research, to a great extent, was financed by the Government of Iraq.

References

Bakharev T, Sanjayan J, Cheng Y-B. 1999. Effect of elevated temperature curing on properties of alkali-activated slag concrete. Cement and Concrete Research. 29:1619–1625.

Bakharev T, Sanjayan J, Cheng Y-B. 2000. Effect of admixtures on properties of alkali-activated slag concrete. Cement and Concrete Research. 30:1367–1374.

Baroghel-Bouny V, Mounanga P, Khelidj A, Loukili A, Rafaï N. 2006. Autogenous deformations of cement pastes: Part II. W/C effects, micro–macro correlations, and threshold values. Cement and Concrete Research. 36:123–136.

Bentz DP, Jensen OM, Hansen KK, Olesen JF, Stang H, Haecker C-J. 2001. Influence of Cement Particle-Size Distribution on Early Age Autogenous Strains and Stresses in Cement-Based Materials. Journal of the American Ceramic Society. 84:129–135.

Bernal SA. 2016. Advances in near-neutral salts activation of blast furnace slags. RILEM Technical Letters. 1:39–44.

Bernal SA, Provis JL. 2014. Durability of Alkali-Activated Materials: Progress and Perspectives. Journal of the American Ceramic Society. 97:997–1008.

Bissonnette B, Pierre P, Pigeon M. 1999. Influence of key parameters on drying shrinkage of cementitious materials. Cement and Concrete Research. 29:1655–1662.

Bjøntegaard Ø. 1999. Thermal Dilation and Autogenous Deformation as Driving Forces to Self-Induced Stresses in High Performance Concrete. PhD Dissertation, The Norwegian University of Science and Technology.

Cartwright C, Rajabipour F, Radlińska A. 2015. Shrinkage Characteristics of Alkali-Activated Slag Cements. Journal of Materials in Civil Engineering. 27.

Chen W, Brouwers H. 2007. The hydration of slag, part 1: reaction models for alkali-activated slag. Journal of Materials Science. 42:428–443.

Chu I, Kwon SH, Amin MN, Kim J-K. 2012. Estimation of temperature effects on autogenous shrinkage of concrete by a new prediction model. Construction and Building Materials. 35:171–182.

Collins F, Sanjayan J. 2000. Effect of pore size distribution on drying shrinking of alkali-activated slag concrete. Cement and Concrete Research. 30:1401–1406.

Cusson D, Hoogeveen T. 2006. Measuring early-age coefficient of thermal expansion in high-performance concrete. In: International RILEM Conference on Volume Changes of Hardening Concrete: Testing and Mitigation RILEM Publication, Lyngby, Denmark.

Duran Atics C, Bilim C, Çelik Ö, Karahan O. 2009. Influence of activator on the strength and drying shrinkage of alkali-activated slag mortar. Construction and Building Materials. 23:548–555.

Fernández-Jiménez A, Puertas F, Sobrados I, Sanz J. 2003. Structure of calcium silicate hydrates formed in alkaline-activated slag: influence of the type of alkaline activator. Journal of the American Ceramic Society. 86:1389–1394.

Fjellström P. 2013. Measurement and modelling of young concrete properties. Licentiate Thesis, Luleå University of Technology, Luleå, Sweden

Garcia-Lodeiro I, Palomo A, Fernández-Jiménez A, Macphee D. 2011. Compatibility studies between NASH and CASH gels. Study in the ternary diagram Na_2O-CaO-Al_2O_3-SiO_2-H_2O. Cement and Concrete Research. 41:923–931.

Gong K, White CE. 2016. Impact of chemical variability of ground granulated blast-furnace slag on the phase formation in alkali-activated slag pastes. Cement and Concrete Research. 89:310–319.

Grasley ZC, Lange DA. 2007. Thermal dilation and internal relative humidity of hardened cement paste. Materials and Structures. 40:311–317.

Gruskovnjak A. 2006. Hydration Mechanisms of Activated Blast Furnace Slag. PhD Dissertation. University of Bern, Switzerland.

Gu K, Jin F, Al-Tabbaa A, Shi B, Liu J. 2014. Mechanical and hydration properties of ground granulated blastfurnace slag pastes activated with MgO-CaO mixtures. Construction and Building Materials. 69:101–108.

Gu Y, Fang Y, You D, Gong Y, Zhu C. 2015. Properties and microstructure of alkali-activated slag cement cured at below-and about-normal temperature. Construction and Building Materials. 79:1–8.

Haha MB, Lothenbach B, Saout G Le, Winnefeld F. 2012. Influence of slag chemistry on the hydration of alkali-activated blast-furnace slag—Part II: Effect of Al2O3. Cement and Concrete Research. 42:74–83.

Haha MB, Saout G Le, Winnefeld F, Lothenbach B. 2011. Influence of activator type on hydration kinetics, hydrate assemblage and microstructural development of alkali activated blast-furnace slags. Cement and Concrete Research. 41:301–310.

Hedlund H. 2000. Hardening Concrete: Measurements and Evaluation of Non-Elastic Deformation and Associated Restraint Stresses. PhD Dissertation. Luleå University of Technology, Luleå, Sweden.

Heikal M, Nassar M, El-Sayed G, Ibrahim S. 2014. Physico-chemical, mechanical, microstructure and durability characteristics of alkali activated Egyptian slag. Construction and Building Materials. 69:60–72.

Jonasson J-E. 1984. Slipform construction: calculations for assessing protection against early freezing. Technical Report, Swedish Cement and Concrete Research Institute

Ke X, Bernal SA, Provis JL. 2016. Controlling the reaction kinetics of sodium carbonate-activated slag cements using calcined layered double hydroxides. Cement and Concrete Research. 81:24–37.

Klausen AB. 2016. Early age crack assessment of concrete structures: Experimental investigation of decisive parameters. PhD Dissertation. Norwegian University of Science and Technology, Trondheim, Norway.

Kovler K, Zhutovsky S. 2006. Overview and future trends of shrinkage research. Materials and Structures. 39:827–847.

Lee NK, Jang JG, Lee HK. 2014. Shrinkage characteristics of alkali-activated fly ash/slag paste and mortar at early ages. Cement and Concrete Composites. 53:239–248.

Li C, Sun H, Li L. 2010. A review: The comparison between alkali-activated slag (Si+ Ca) and metakaolin (Si+ Al) cements. Cement and Concrete Research. 40:1341–1349.

Lodeiro IG, Macphee D, Palomo A, Fernández-Jiménez A. 2009. Effect of alkalis on fresh C-S-H gels. FTIR analysis. Cement and Concrete Research. 39:147–153.

Loser R, Münch B, Lura P. 2010. A volumetric technique for measuring the coefficient of thermal expansion of hardening cement paste and mortar. Cement and Concrete Research. 40:1138–1147.

Lothenbach B, Winnefeld F. 2006. Thermodynamic modelling of the hydration of Portland cement. Cement and Concrete Research. 36:209–226.

Al-Majidi MH, Lampropoulos A, Cundy A, Meikle S. 2016. Development of geopolymer mortar under ambient temperature for in situ applications. Construction and Building Materials. 120:198–211.

Maruyama I, Teramoto A. 2011. Impact of time-dependant thermal expansion coefficient on the early-age volume changes in cement pastes. Cement and Concrete Research. 41:380–391.

Myers RJ, Bernal SA, Provis JL. 2017. Phase diagrams for alkali-activated slag binders. Cement and Concrete Research. 95:30–38.

Nedeljkovic M, Arbi K, Zuo Y, Ye G. 2016. Microstructural and Mineralogical Analysis of Alkali Activated Fly Ash-Slag Pastes. In: 3rd International RILEM Conference on Microstructure Related Durability of Cementitious Composites: Nanjing, China. pp. 1–10.

Neto AAM, Cincotto MA, Repette W. 2008. Drying and autogenous shrinkage of pastes and mortars with activated slag cement. Cement and Concrete Research. 38:565–574.

Nilsson M. 2003. Restraint factors and partial coefficients for crack risk analyses of early age concrete structures. PhD Dissertation. Luleå University of Technology, Luleå, Sweden.

Pacheco-Torgal F, Castro-Gomes J, Jalali S. 2008. Alkali-activated binders: A review: Part 1. Historical background, terminology, reaction mechanisms and hydration products. Construction and Building Materials. 22:1305–1314.

Palacios M, Puertas F. 2007. Effect of shrinkage-reducing admixtures on the properties of alkali-activated slag mortars and pastes. Cement and Concrete Research. 37:691–702.

Palomo A, Grutzeck M, Blanco M. 1999. Alkali-activated fly ashes: a cement for the future. Cement and Concrete Research. 29:1323–1329.

Provis JL, Bernal SA. 2015. Milestones in the analysis of alkali-activated binders. Journal of Sustainable Cement-Based Materials. 4:74–84.

Provis JL, Palomo A, Shi C. 2015. Advances in understanding alkali-activated materials. Cement and Concrete Research. 78:110–125.

Puertas F, Palacios M, Manzano H, Dolado J, Rico A, Rodriguez J. 2011. A model for the CASH gel formed in alkali-activated slag cements. Journal of the European Ceramic Society. 31:2043–2056.

Roy DM. 1999. Alkali-activated cements opportunities and challenges. Cement and Concrete Research. 29:249–254.

Sakulich AR, Bentz DP. 2013. Mitigation of autogenous shrinkage in alkali activated slag mortars by internal curing. Materials and Structures. 46:1355–1367.

Sayahi F. 2016. Plastic Shrinkage Cracking in Concrete. Licentitate Thesis. Luleå University of Technology, Luleå, Sweden.

Sellevold E, Bjøntegaard O. 2006. Coefficient of thermal expansion of cement paste and concrete: mechanisms of moisture interaction. Materials and Structures. 39:809–815.

Tazawa E, Miyazawa S, Kasai T. 1995. Chemical shrinkage and autogenous shrinkage of hydrating cement paste. Cement and Concrete Research. 25:288–292.

Tazawa E, Sato R, Sakai E and MS. 2000. Work of JCI committee on autogenous shrinkage. In: Proc Shrinkage 2000-Int RILEM Workshop on Shrinkage of Concrete. pp. 21–40.

Termkhajornkit P, Nawa T, Nakai M, Saito T. 2005. Effect of fly ash on autogenous shrinkage. Cement and Concrete Research. 35:473–482.

Thomas JJ, Allen AJ, Jennings HM. 2012. Density and water content of nanoscale solid C-S-H formed in alkali-activated slag (AAS) paste and implications for chemical shrinkage. Cement and Concrete Research. 42:377–383.

Thomas R, Lezama D, Peethamparan S. 2017. On drying shrinkage in alkali-activated concrete: Improving dimensional stability by aging or heat-curing. Cement and Concrete Research. 91:13–23.

Turu'allo G. 2013. Early age strength development of GGBS concrete cured under different temperatures. PhD Thesis, University of Liverpool, Liverpool, England.

Wang S-D, Scrivener KL. 2003. 29 Si and 27 Al NMR study of alkali-activated slag. Cement and Concrete Research. 33:769–774.

Ye H, Cartwright C, Rajabipour F, Radlinska A. 2014. Effect of drying rate on shrinkage of alkali-activated slag cements. 4th International Conference on the Durability of Concrete Structures.

Ye H, Radlinska A. 2016. Quantitative analysis of phase assemblage and chemical shrinkage of alkali-activated slag. Journal of Advanced Concrete Technology. 14:245–260.

Alkali Activated materials: State-of-the-Art Report, RILEM TC 224-AAM. Springer, 2014.